Załącznik nr V do wniosku

Dr inż. Michał Gdula

Politechnika Rzeszowska im. Ignacego Łukasiewicza
Wydział Budowy Maszyn i Lotnictwa
Katedra Technik Wytwarzania i Automatyzacji

CYKL POWIĄZANYCH TEMATYCZNIE ARTYKUŁÓW WRAZ Z OŚWIADCZENIAMI WSPÓŁAUTORÓW I HABILITANTA

ARTYKUŁ
A1

dr inż. Michał Gdula
Politechnika Rzeszowska im. I. Łukasiewicza
Wydział Budowy Maszyn i Lotnictwa
Katedra Technik Wytwarzania i Automatyzacji

Rzeszów, dn. 05.05.2025 r.

OŚWIADCZENIE WSPÓŁAUTORA

Oświadczam, że w pracy:

lp.: A1

Gdula M., Nowotnik A., Mrówka-Nowotnik G.: *Analysis the surface integrity taking into account the tool wear stage in the multi-axis torus milling of a Ni-based superalloy using the active cutting edge segment change technique and new approach for machining aircraft engine blades.* WEAR, vol. 574-575, (2025), 206095. IF 5.3, MNiSW 200 pkt.;

mój wkład w powstanie tej pracy polegał na: analizie aktualnego stanu wiedzy w zakresie tematu pracy, opracowaniu modelu matematycznego odległości wierszowania, opracowaniu modelu zużycia narzędzia uwzględniającego rozkład maksymalnej grubości warstwy skrawanej w funkcji kąta obrotu narzędzia oraz mechanikę kontaktu ostrza z obrabianą powierzchnią, opracowaniu metodyki badań, przeprowadzeniu badań symulacyjnych i eksperymentalnych, przeprowadzeniu analizy zużycia narzędzia, przeprowadzeniu analizy morfologii obrobionych powierzchni, współudziale w analizie mikrostruktury obrobionych powierzchni, współudziale w analizie naprężeń resztkowych w technologicznej warstwie wierzchniej, opracowaniu nowego podejścia do obróbki mechanicznej łopatek turbin silników lotniczych, interpretacji wyników i opracowaniu wniosków, wykonaniu wykresów, rysunków oraz tabel, współudziale w opracowaniu manuskryptu, koordynowaniu procesu wydawniczego.

Gdula Michał

.....

Podpis
dr inż. Michał Gdula

dr hab. inż. Andrzej Nowotnik, prof. PRz
Politechnika Rzeszowska im. I. Łukasiewicza
Wydział Budowy Maszyn i Lotnictwa
Katedra Nauki o Materiałach

Rzeszów, dn. 05.05.2025 r.

OŚWIADCZENIE WSPÓŁAUTORA

Oświadczam, że w pracy:

lp.: ....A1.....

Gdula M., Nowotnik A., Mrówka-Nowotnik G.: *Analysis the surface integrity taking into account the tool wear stage in the multi-axis torus milling of a Ni-based superalloy using the active cutting edge segment change technique and new approach for machining aircraft engine blades.* WEAR, vol. 574-575, (2025), 206095. IF 5.3, MNiSW 200 pkt.;

mój wkład w powstanie tej pracy polegał na: przeprowadzeniu pomiarów rozkładu naprężeń w warstwie wierzchniej, współudziale w analizie tych naprężeń oraz współudziale w opracowaniu korekty wersji roboczej manuskryptu.

.....
Podpis
dr hab. inż. Andrzej Nowotnik, prof. PRz

dr hab. inż. Grażyna Mrówka-Nowotnik, prof. PRz
Politechnika Rzeszowska im. I. Łukasiewicza
Wydział Budowy Maszyn i Lotnictwa
Katedra Nauki o Materiałach

Rzeszów, dn. 05.05.2025 r.

OŚWIADCZENIE WSPÓŁAUTORA

Oświadczam, że w pracy:

lp.: A1

Gdula M., Nowotnik A., Mrówka-Nowotnik G.: *Analysis the surface integrity taking into account the tool wear stage in the multi-axis torus milling of a Ni-based superalloy using the active cutting edge segment change technique and new approach for machining aircraft engine blades.* WEAR, vol. 574-575, (2025), 206095. IF 5.3, MNiSW 200 pkt.;

mój wkład w powstanie tej pracy polegał na: przeprowadzeniu obserwacji i wykonaniu mikrofotografii powierzchni obrobionych oraz tekstury materiału obrabianego ze współudziałem w analizie tekstury, z zastosowaniem mikroskopu skaningowego (SEM) wyposażonego w układy EDS i WDS do analizy składu chemicznego oraz układ EBSD umożliwiającego wyznaczenie tekstury materiałów oraz identyfikację składników fazowych, współudziale w opracowaniu korekty wersji roboczej manuskryptu.

.....
Podpis
dr hab. inż. Grażyna Mrówka-Nowotnik, prof. PRz

Wear 574–575 (2025) 206095

Contents lists available at ScienceDirect

Wear

journal homepage: www.elsevier.com/locate/wear

Analysis the surface integrity taking into account the tool wear stage in the multi-axis torus milling of a Ni-based superalloy using the active cutting edge segment change technique and new approach for machining aircraft engine blades

Michał Gdula [a,*], Andrzej Nowotnik [b], Grażyna Mrówka-Nowotnik [b]

[a] Department of Manufacturing Techniques and Automation, Rzeszow University of Technology, Al. Powstańców Warszawy 12, 35-959, Rzeszow, Poland
[b] Department of Materials Science, Rzeszow University of Technology, Al. Powstańców Warszawy 12, 35-959, Rzeszow, Poland

ARTICLE INFO

Keywords:
Multi-axis milling
Ni-based superalloy
Active cutting edge segment
Tool wear
Technological surface layer
Ressidual stresses
Aircraft engine blade

ABSTRACT

This study aims to comprehensively investigate the state of the technological surface layer taking into account the tool wear stage in multi-axis torus milling of a Ni-based superalloy using the author's active cutting edge segment change (ACESC) technique. A mathematical model of the distance between tool paths as a function of the angle of inclination of the tool axis in relation to the active cutting edge segment change technique is established. Addition, a theoretical model of flank wear width is established, taking into account the elastic recovery effect of the material, with an average prediction error of 10 %. Analysis of the surface morphology revealed a scratch with a curved outline, arranged according to the surface velocity vector as a function of the tool rotation angle. This is the result of micro-chipping and adhesion of chips to the cutting edge of the round insert. At the same time, it has been observed that in the boundary zone of adjacent machining marks, adhesion occurs after the elastic recovery of the material. The deformation of the material grains and the distribution of residual stresses depend significantly on the stage of tool wear and the angle of inclination of the tool axis. Based on the results, a new approach for multi-axis torus milling of aircraft engine blades was proposed.

1. Introduction

Ni-based superalloys (e.g. Inconel 718) are widely used mainly in the aerospace industry but also in marine, automotive, medical and other industries because of their excellent strength in high-temperature environments. In addition, they are equally characterised by excellent creep and corrosion resistance, as well as the ability to maintain stable performance in terms of mechanical properties in high-temperature environments over long periods of exploitation [1,2]. However, Ni-based superalloys are difficult-to-cut materials because of their high strength at high temperatures, good ductility, high coefficient of friction, and low thermal conductivity [3,4]. As a result, the efficiency of the cutting process, especially precision multi-axis milling, is significantly hampered by high cutting forces, high temperatures in the cutting zone, and the deformations that occur [2,5]. All of this causes severe wear on cutting tools, and worn tools directly affect the integrity of state of the technological surface layer of the workpiece [2,6–9]. The integrity of state of the technological surface layer of the workpiece directly determines its properties, both physical and mechanical. These include fatigue properties, corrosion resistance due to vortices in the near-surface layer, as well as friction resistance, etc. [2,6,10]. Therefore, in order to improve the integrity of state of the technological surface layer and the fatigue resistance of the machined Ni-based superalloy workpiece, it is necessary to investigate the effects of tool wear, changes in Cutter-Workpiece Engagement (CWE) in the cutting zone [11], and changes in toolpath distances during multi-axis precision torus milling of the Inconel 718 superalloy by a new technique of changing the active segment of the cutting edge, on the integrity of state of the technological surface layer.

In industrial practice, multi-axis torus milling is increasingly being used to machine geometrically complex Ni-based superalloy parts (e.g. turbine blade). The process of precision multi-axis milling is currently being developed with new machining strategies [12] and techniques [13]. Current research and the development of new strategies for

* Corresponding author.
E-mail address: gdulam@prz.edu.pl (M. Gdula).

https://doi.org/10.1016/j.wear.2025.206095
Received 25 February 2025; Received in revised form 10 April 2025; Accepted 22 April 2025
Available online 25 April 2025
0043-1648/© 2025 Elsevier B.V. All rights are reserved, including those for text and data mining, AI training, and similar technologies.

multi-axis machining focusses mainly on the problem of tool wear. This is one of the main problems encountered in the machining of Ni-based superalloys. Tool wear affects both the mechanics of cutting and the integrity of state of the technological surface layer.

In the field of tool wear, many studies have been carried out to date in various areas. The first area concerns the modelling of tool wear. Zhu and Zhang [14] proposed and verified a general wear model with adjustable coefficients. In this model, they divided the three wear zones of the entire tool life according to the critical times, taking into account the nature of the different wear stages. The authors have developed a tool flank wear model with adjustable coefficients to accurately predict tool wear and cutting forces in ball-end mill machining. The model shows high agreement with experimental data and can be easily adapted to different machining conditions. The model makes it possible to monitor and predict tool life in real time. Zhang et al. [15] developed a tool wear model that takes into account the effective cutting distance, making it possible to predict the wear distribution along the side of the ball-end mill under machining sculptured surfaces. They conducted comparative experiments on tool wear under different feed directions during the machining of sculptured surfaces. The model achieves high accuracy (average prediction error ≈ 2 % at the point of maximum wear) and is experimentally validated. It takes into account complex changes in tool position when cutting curved surfaces, which makes it possible to predict the wear distribution. Mao et al. [16] presented a method and a model to predict tool wear, taking into account the diversity of wear rates and cutting lengths along the cutting edge. They conducted milling experiments on free-form surfaces to validate the proposed method. The wear model takes into account varying cutting speeds and assigns different wear rates for different blade heights. The model achieves a prediction error of 12.5 % when approaching the wear criterion. Zhang et al. [17] proposed and verified a general wear model with adjustable coefficients. Taking into account the intrinsic mechanisms of the different wear stages, they divided the whole life of the tool into three main wear zones according to the critical time, which correspond to the three main types of wear: lapping wear, adhesive wear, and abrasive wear. They verified the wear model against other known wear models on the basis of experimental data and further refined it to increase its adaptability. The model has high prediction accuracy (R^2 > 98 %) and good generality - it can be used with different cutting conditions and workpiece materials. It allows predicting tool life and assessing its condition in real time using a genetic algorithm. The second area concerns the modelling of tool temperature variation. Yan et al. [18] presented a thermal model that describes the temperature variation of a coated tool during the dry milling of a Ni-based superalloy turbine blade. The effect of flank wear was considered according to the rapid wear of the tool. In the proposed model, they calculated both the heat fluxes to the tool from the rake face and due to the flank face. They estimated the temperature distribution of the tool under different tool states and performed experimental verification. The temperature of the tool increases significantly with increasing feed rate and degree of lateral wear, and the effect of lateral wear can increase the temperature by more than 20–30 %. Bjerke et al. [19] attempted to develop a model to predict the phase composition and the driving force of degradation and the formation of protective interaction products in the cutting zone. They applied the modelling framework to investigate the interactions that occur in the cutting zone. They validated the modelling by examining tool wear and reaction products formed during machining with ceramics, PcBN, and coated carbide tools. The third area concerns the modelling of noth wear in the milling of Ni-based superalloys. The formation of stable protective layers such as $(Al,Fe,Cr)_2O_3$ and $(Al,Fe,Cr)_3O_4$ oxides, which slow down tool wear, has been predicted and confirmed. Kasim et al. [20] developed a tool wear model to determine the location of the occurrence of notch wear and flaking. They found that a large radial depth of the cut was the main factor. They showed that the dominant wear was located near the depth of the cut line. They obtained an error between the pitting prediction model and the actual notching/peeling of less than 6 %. Zeng et al. [21] developed a model to predict the wear of the notch. They compared the changes in the thickness of the undeformed chip under two different types of cutting. They attempted to explain the appearance of notch wear from the point of view of stress concentration. They conducted a series of cutting tests to validate the notch wear depth model, and the results indicate that the proposed model can be used to optimise the cutting process. The radial depth of cut is the major factor that affects notch wear depth. Notch wear depth increases first and then decreases with increasing the radial depth of cut. The most severe notch wear may occur when the immersion ratio is about 10 %. The fourth area concerns the tool wear, and chip and machined surface morphology analysis. Halim et al. [22] detailed an investigation into the performance of PVD-coated tungsten carbide ball-end mills under Inconel 718 using environmentally friendly cryogenic carbon dioxide (CO2) machining and dry machining conditions. They found that, compared to cryogenic cutting, the shape and colour of the chips were distorted and darker during dry cutting, confirming that they were thermally affected by the high cutting temperature. Cryogenic CO2 cooling managed to effectively reduce the cutting temperature at the cutting point to 80 %, compared to dry cutting, which significantly improved the chip morphology. An et al. [23] An et al. developed a theoretical model of flank wear width with an average prediction error of 15.87 %. They showed that supercritical carbon dioxide with oil-on-water based MQL reduces lateral wear by 67.2 % compared to supercritical carbon dioxide alone due to better lubricity. They characterised in detail the morphology of the machined surface using a continuous wavelet transform. The researchers in Refs. [5,13] demonstrated the strong influence of varying multi-axis cutting conditions and torus milling cutter wear patterns on the morphology and topography of the machined surface. They concluded that the orientation of the tool axis plays an important role in terms of tool life extension and surface shaping. It was pointed out, the importance of the morphology of the machined surface in terms of the integrity of state of the technological surface layer.

To date, many studies have been carried out on the integrity of state of the technological surface layer during the typical milling process [7, 24–31]. Yin et al. [2] compared tool life, tool wear forms, and wear mechanisms in different wear states in high-speed ultrasonic peening milling and conventional milling. They obtained a 32.5 % increase in tool life in ultrasonic peening milling owning to lower tool wear compared to that in conventional milling. Ultrasonic peening milling was significantly more effective in improving the surface integrity and fatigue life of the workpiece. Kasim et al. [3] investigated selected surface integrity parameters after face milling. The experiments involved the use of PVD coated with TiAlN/AlCrN ball nose tungsten carbide with varying of cutting speeds ranging between 100 and 140 m/min, a feed rate of 0.1–0.2 mm/tooth, and an axial depth of cut of 0.5–1.0 mm. They found that the surface roughness measured in the feed direction was lowered instead of picking a direction. Furthermore, they found that the widths of cut are causes the variation in surface roughness. Musfirah et al. [4] presents the experimental investigations conducted to assess the effectiveness of cryogenic cooling for the milling of Inconel 718 in comparison to the dry cutting process. They found, that the cryogenic cooling system is more effective than dry cutting for reducing tool flank wear, improving surface roughness and lessening deformation of microstructure changes at the sub-surface level. Tan et al. [8] conducted a study the effects of tool wear on the machined surface integrity characteristics in the ball-end milling process of Inconel 718. They found that, the higher tool flank wear width produces larger surface roughness and deteriorative surface topography, a high-amplitude and deep layer of compressive residual stress are induced by a worn tool with flank wear width of 0.3 mm, the surface microhardness induced by the new tool is larger than that induced by worn tool. Furthermore, plastic deformation and strain streamlines they observed within 10 μm depth beneath the top surface. Silva et al. [32] evaluated the machined surface integrity and wear resistance of cutting tools coated by physical vapour

deposition (PVD) of HiPIMS with TiAlYN in finish milling Inconel 718 by varying process parameters such as cutting speed, feed per tooth, and cutting length. They found that cutting length had the greatest effect on surface integrity. Sivalingam et al. [33] conducted surface integrity studies in an Atomized Spray Cutting Fluid environment, in turning Inconel 718. They observed a significant improvement in surface roughness between 17 and 34 % in Atomized Spray Cutting Fluid machining. In addition, Atomized Spray Cutting Fluid significantly reduced tool wear in terms of abrasion and notch wear. Iturbe et al. [34] carried out microstructural analysis and microhardness measurements of test samples to correlate the microstructural state with the mechanical properties of Inconel 718. Chen et al. [35] conducted a study of the multi-axis ball-end milling process in terms of surface integrity. They did not obtain conclusive results, and therefore gave recommendations for optimal tool axis orientation in conjunction with cutting parameters. Bloul et al. [36] carried out theoretical and experimental studies on the wear modelling and evaluation of the effect of flank wear on surface integrity after turning with a round cutting insert.

It can be seen from the above studies that the effect of tool wear in multi-axis milling on the integrity of state of the technological surface layer and the zonality of machining of the workpiece has not yet been investigated. In addition, the effect of changing the active cutting edge segment on torus milling cutter wear at high speeds in multi-axis milling requires further research. In this study, we evaluate the effect of high-speed multi-axis milling using the own Active Cutting Edge Segment Change Technique (ACESCT) on the integrity of the technological state of the surface layer at different stages of tool wear and, in view of integrity, on the possibility of introducing machining zoning on the workpiece. In the ACESCT technique, the orientation of the torus milling cutter axis, and thus the variation in cutter-workpiece engagement, is defined by the cutting blade working angle parameter. The basic results of the study can help to understand the effect of ACESCT on tool wear and its impact on the integrity of state of the technological surface layer of the workpiece and enable the definition of machining zones on the workpiece made of Inconel 718 superalloy, taking into account the aspect of increasing the workpiece exploitation parameters.

2. Multi-axis milling with the torus cutter

2.1. Simplified model of the contact point location of the cutter with the sculptured surface

In a multi-axis milling process, the torus milling cutter axis can, at least in theory, have any orientation in 3D space, relative to the adopted coordinate system (X_M, Y_M, Z_M) of the workpiece. Of course, the assumption is that there is no collision with other pieces of technological equipment on the machine tool or undercutting of the machined surface.

During movement along the programmed toolpath, the torus surface T of the cutter comes into contact with the workpiece (turbine blade) in a momentary lobe of the surface, which is called the cutter-workpiece engagement (CWE). Thus, an undeformed cut layer (chip) is delineated within the CWE. Taking into account the preceding machined strip and the inclination angle of the cutter axis, the CWE is usually located at a lower depth of cut, as defined in the work [12]. Alternatively, as proposed by the authors of this paper, the CWE is located in the process asymmetry relative to the feed plane. The asymmetry of the CWE will depend on the degree of inclination of the cutter axis defined by the inclination angle parameter δ, and thus on the distance between the toolpaths b_r. At any moment of cutting, the segments on the cutting edges that are contained in the CWE are called active cutting segments, i.e. they are involved in cutting at a given moment as a function of the instantaneous contact angle (working) of the tool φ. Because the cutter rotates at high speed around the axis itself, the CWE $s_{CWE,i}$ at the cutter position (CLData) CL_i forms the active cutting belt $s_{b,i}$. This is a distinguishing feature of our approach compared to conventional multi-axis milling techniques.

Another distinctive feature of our approach is the milling of the tangent plane with an inclined cutter with an inclination angle δ, where the tool paths are parallel to each other. This plane was assumed to be a simplified model of location of the CP_i contact point of the cutter with the sculptured surface based on the isoparametric curves U_{CPi}, V_{CPi}, and the vectors u_{CPi}, v_{CPi}. The point of contact CP_i is also the point of attachment of the normal vector n_{CPi} of this surface. Thus, this plane can be regarded as the plane tangent to the sculptured surface at a given point of contact resulting from CLData (see Fig. 1).

2.2. Toolpaths distance - theoretical modeling

In order to develop a model of the toolpaths distance b_r for the purpose of applying the uniform roughness distribution criterion in the own ACESCT technique, the case of constituting the kinematic roughness in the feed direction R_{thvf} was first considered by transforming the undeformed chip contours to the tool base plane. Next, the constitution of kinematic roughness in the step direction was considered. Both cases are schematically illustrated in Fig. 2.

In the multi-axis torus milling finishing process, both the feed per tooth and the nominal depth of cut have very small values. This configuration of the process parameters produces a low undeformed chip thickness. In this case, the kinematic surface roughness relative to the radius of the round cutting insert of the torus and the feed per tooth has poor agreement with the actual achieved surface roughness.

This is because the plastic side flow introduced by the radius of the round cutting insert and the feed per tooth, as well as the minimum undeformed chip thickness residual dependent on the radius of the cutting edge, and the recovery of elastic material under the influence of the radius of the round cutting insert, the radius of the cutting edge, and the rake angle, as shown in Fig. 2a, have reached the same magnitude of the residual height in kinematics [37]. Therefore, based on [36–39], for the surface after multi-axis torus milling, the final surface topography profile is pictorially described in Fig. 2b. In this figure, r_p, f_z, $r_p|_{\text{transform}}$, b_r and a_p denote the radius of the round cutting insert, the feed per tooth, the radius of the transformed round cutting insert, the distance between the toolpaths and the nominal depth of cut, respectively. The parameter R_{thvf} is the residual height in kinematics and R_{thvf}' is the overall height taking into account the influence of kinematics, plastic side flow, minimum undeformed chip thickness, and elastic recovery of material. The parameters $h_{\min}$ and $h_{\max}$ are the minimum and maximum undeformed chip thickness, respectively. It was noticed and therefore assumed that the peak points of the kinematic roughness and the overall roughness lie on the same line. Similar assumptions were used by other researchers [37,39,40]. These lines were assumed to be normal to the tangent plane in the vicinity of the contact point CP_i, as shown in Fig. 2. Therefore, in a similar manner, a cutting blade mapping system was adopted for the step direction in which the parameter $b_r \equiv a_e$ was set. As observed during our own research [13], the value of the b_r parameter does not change despite the tool flank wear, but as a result of the tool wear, the width of the machined strip is reduced. Moreover, the nature of the pulsating cutting forces, revealed in the cutting torque, is changed [13], which may influence the residual stresses in the surface layer.

Therefore, in order to develop the b_r parameter model, the kinematic mapping scheme of the cutting blade was adopted, as shown in Fig. 3.

For the multi-axis torus milling process, the theoretical or kinematic

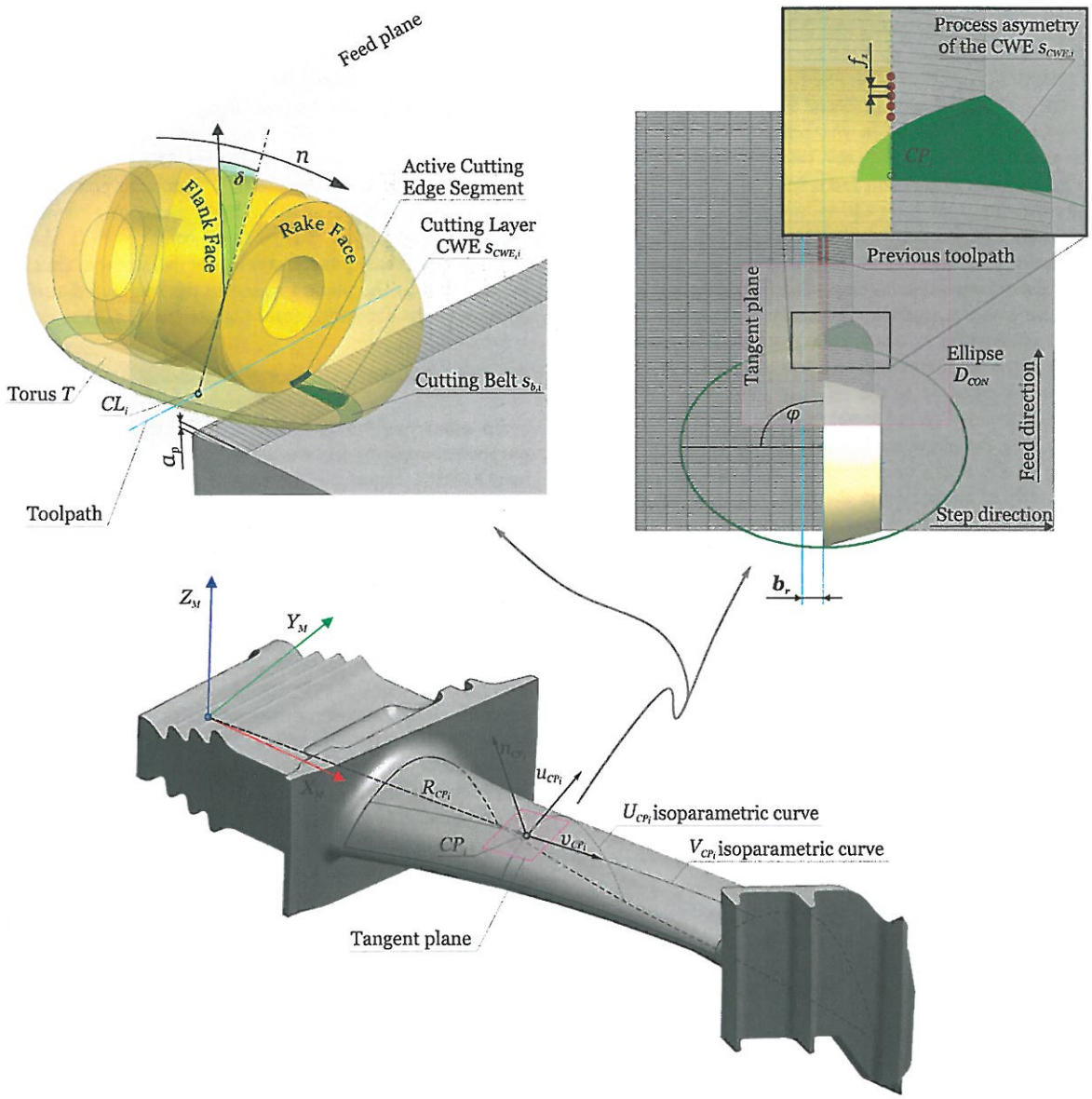

Fig. 1. Simplified model of the contact point location at multi-axis torus milling process.

ten-point height, i.e. surface roughness, can be written as:

$$R_{th} = R_{thvf} = \frac{r_p}{2} - \sqrt{\frac{r_p^2 - f_z^2}{4}} \tag{1}$$

The parameter R_{CON} is the radius of the contact curve, i.e. the curve lying on the torus and touching the machined surface at the point CP_i. The radius of the contact curve depends on the radius of the torus cutter R_T, the radius of the round cutting insert r_p, and the tool axis inclination angle δ [41]. Hence the contact radius can be written as:

$$R_{CON} = R_T + r_p \sin(\delta) \tag{2}$$

Therefore, based on the trigonometric relationships of the torus mapping in multi-axis milling using own ACESCT technique and after transformations, the model relationship of the distance between toolpaths finally takes the form:

$$b_r = 2\sqrt{2(R_T + r_p\sin(\delta))\cdot\frac{\frac{r_p}{2} - \sqrt{\frac{r_p^2 - f_z^2}{4}}}{\sin(\delta)} - \left(\frac{\frac{r_p}{2} - \sqrt{\frac{r_p^2 - f_z^2}{4}}}{\sin(\delta)}\right)^2} \tag{3}$$

$$\text{for } 0° < \delta < \left(90 - \left(\frac{90 - \sin^{-1}\left(1 - \frac{a_p}{r_p}\right)}{2}\right)\right)$$

Summarising the above considerations, it can be stated that the current methods and models predicting flank wear do not reflect the physical phenomenon and cutting mechanism in the multi-axis torus milling process. Therefore, in the next stage of the research, based on the

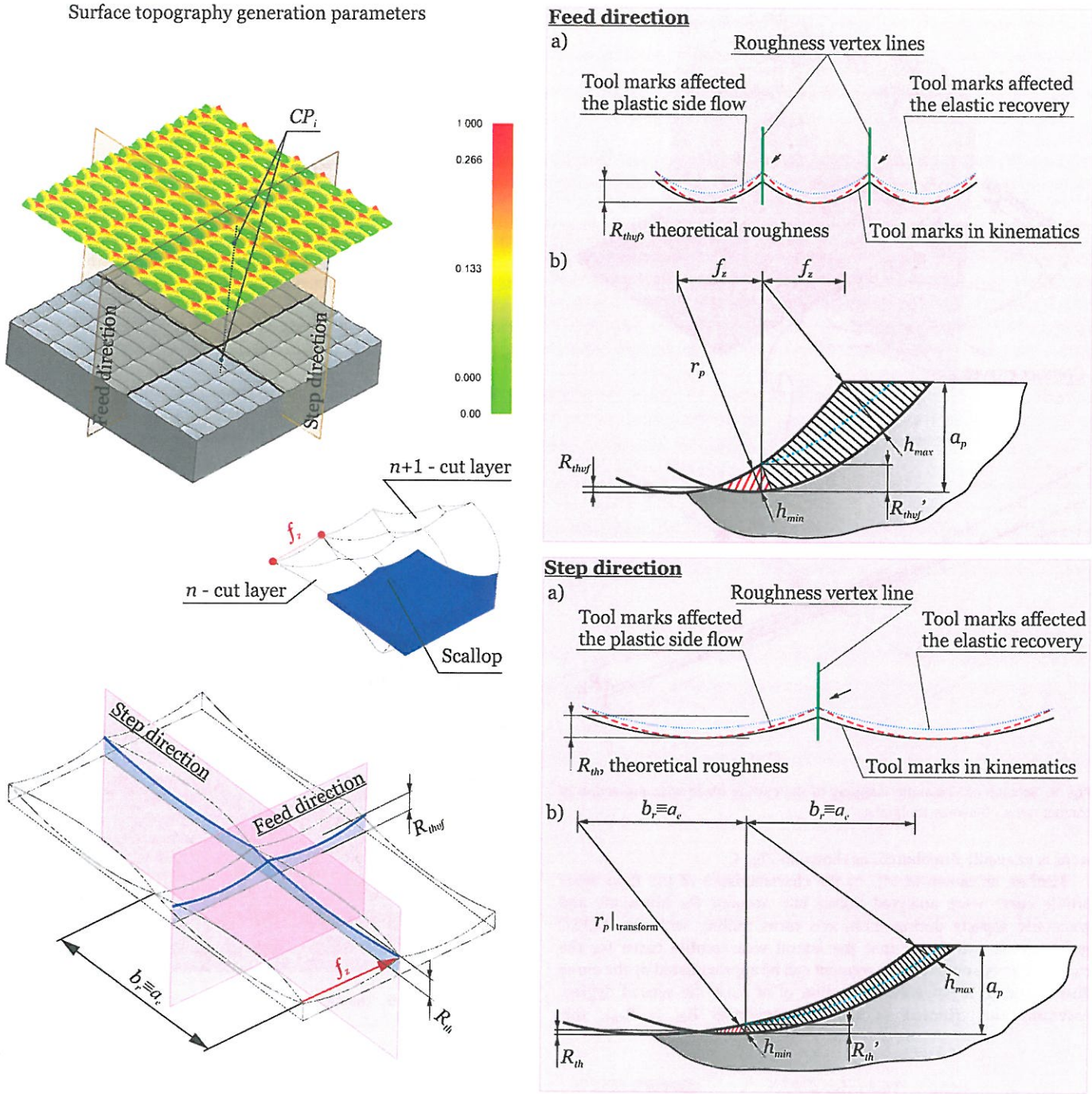

Fig. 2. Typical surface prediction with a round cutting insert: a) the effect of plastic side flow and elastic recovery, b) comprehensive height coupled with the effects of kinematics, minimum undeformed chip thickness, plastic side flow and elastic recovery.

contact characteristics of the torus cutting blade with the workpiece in the third deformation zone, a theoretical model of the maximum flank wear width VB_{Bmax} at different CWE in the own ACESCT technique was established, and then the wear profile area was determined as a function of the tool rotation angle Ω (see Fig. 4).

3. Tool wear modeling taking into account physical aspect of the multi-axis cutting process

3.1. Flank wear profile taking into account the distribution of the undeformed chip maximum thickness

The analysis of the conditions in the CWE zone that was carried out as part of our own research [13,42,43] shows that the cutting edge flank

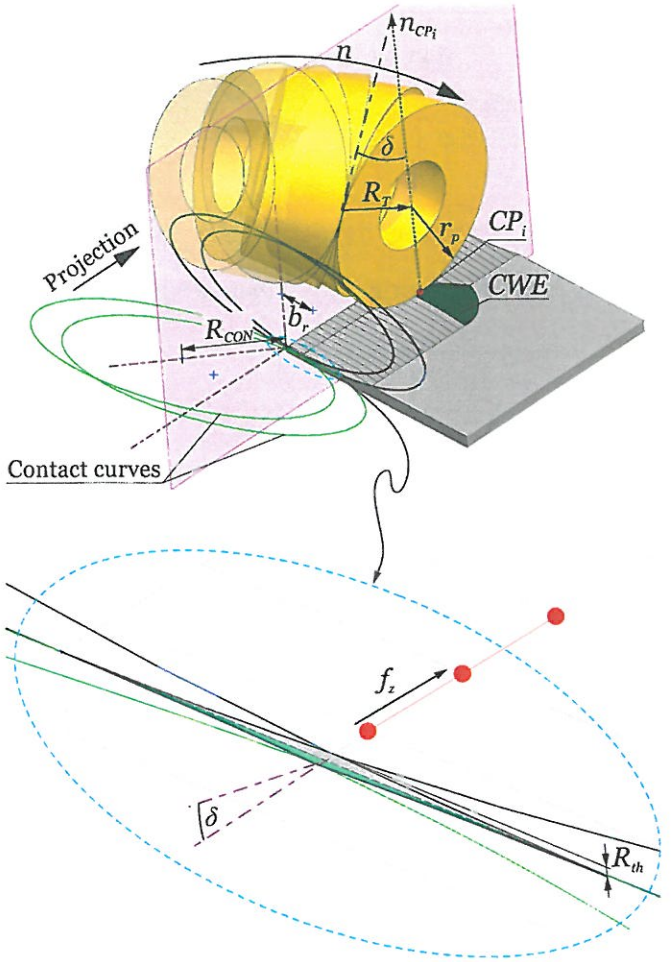

Fig. 3. Scheme of kinematic mapping of the cutting blade with projection of contact curves between toolpaths.

wear is unevenly distributed, as shown in Fig. 4.

Further, as shown in Fig. 5, the characteristics of the flank wear profile curve were analysed taking into account the kinematic and geometric aspects during multi-axis torus milling with the ACESC technique. It was found that the lateral wear profile curve for the currently active cutting edge segment can be approximated by the curve distribution of a polynomial function of at least the second degree. Assuming the criterion of uniform roughness $R_{th} = R_{thvf}$, this approximation is independent of the tool axis angle δ. Verification of the criterion of uniform roughness was carried out in the work [13].

For further considerations, the parameter $VB_{Bmax|mean}$ is introduced and it is assumed that the relationship between the wear width VB_i and $VB_{Bmax|mean}$ on the side wear profile curve of the cutting edge is as follows:

$$VB_i = \frac{4l_i(\Omega)}{d_{ACES}}\left(1 - \frac{l_i(\Omega)}{d_{ACES}}\right) VB_{Bmax|mean} \tag{4}$$

where: $l_i(\Omega)$ is the length of the cutting edge contact within the active cutting segment as a function of the tool rotation angle.

In relation (4), the d_{ACES} parameter denotes the length of the active arc of the cutting edge segment expressed by the relation:

$$d_{ACES} = 2\pi r_p \frac{\left[\frac{\pi}{2} + \sin^{-1}\left(\frac{f_z}{2r_p}\right) - \sin^{-1}\left(1 - \frac{a_p}{r_p}\right)\right]}{360} \tag{5}$$

Hence, after substituting the relations (5) into (4), the relation between the flank wear width VB_i and $VB_{Bmax|mean}$ on the wear profile curve of the side cutting edge finally takes the form:

$$VB_i = \frac{4l_i(\Omega)}{2\pi r_p \frac{\left[\frac{\pi}{2} + \sin^{-1}\left(\frac{f_z}{2r_p}\right) - \sin^{-1}\left(1 - \frac{a_p}{r_p}\right)\right]}{360}}$$

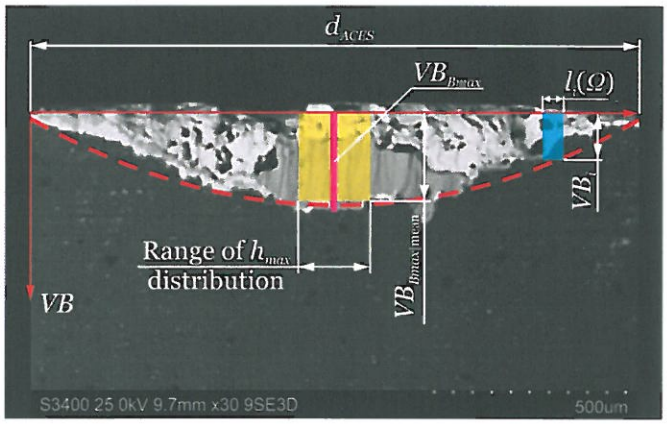

Fig. 5. The flank wear profile curve aproximation.

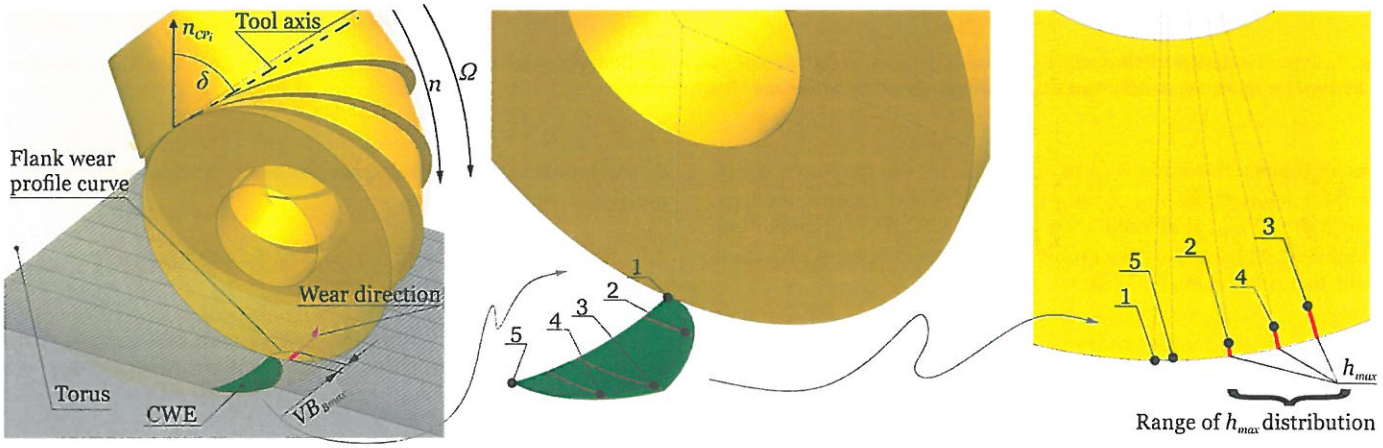

Fig. 4. Flank wear and h_{max} range distribution of torus milling cutter.

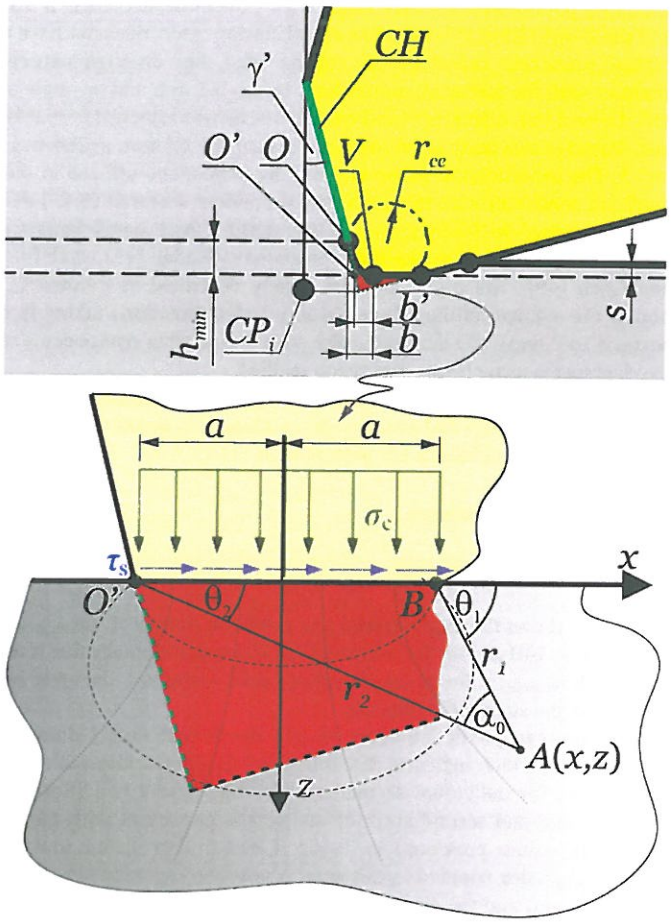

Fig. 8. Stresses in the wear zone [23,46].

expressed as:

$$\sigma_{x,s} = \frac{\tau_s}{2\pi}\left[4\ln\left(\frac{r_1}{r_2}\right) - (\cos 2\theta_1 - \cos 2\theta_2)\right]$$
$$\sigma_{z,s} = \frac{\tau_s}{2\pi}(\cos 2\theta_1 - \cos 2\theta_2) \tag{11}$$
$$\tau_{xz,s} = -\frac{\tau_s}{2\pi}[2(\theta_1 - \theta_2) - (\sin 2\theta_1 - \sin 2\theta_2)]$$

where: $r_{1,2} = \sqrt{(x \mp a)^2 + z^2}$.

τ_s was then assumed to be the shear stress, which is expressed by the formula:

$$\tau_s = \mu\sigma_c \tag{12}$$

where: μ is the friction coefficient.

$$\mu = \frac{K_{te}}{K_{ra_e}} \tag{13}$$

where: K_{te} is the tangent edge force coefficient. The K_{ra_e} parameter, on the other hand, is a proxy for the radial edge force coefficient. This parameter results from the resultant cutting force, determined from the assembly of radial force and axial force taking into account the inclined tool axis. This represents the author's original approach, which will be described in a separate paper. The coefficients described above represent the active edge force acting per unit length in the CWE zone.

Then, according to the mechanics of contact [47], the total state of stress in the technological surface layer of the workpiece was assumed, which is expressed by the relationship:

$$\sigma_x = \sigma_{x,c} + \sigma_{x,s}$$
$$\sigma_z = \sigma_{z,c} + \sigma_{z,s} \tag{14}$$
$$\tau_{xz} = \tau_{xz,c} + \tau_{xz,s}$$

After calculating the total stress state in the technological surface layer of the workpiece, the equivalent von Mises stress σv was determined according to the relationship:

$$\sigma_v = \sqrt{\sigma_x^2 - \sigma_x\sigma_z + \sigma_z^2 + 3\tau_{xz}^2} \tag{15}$$

In the next step, the depth of plastic deformation h_p was determined. This is also the depth at which the yield stress of Inconel 718 is reached. This depth is described by equation:

$$h_p = x \equiv max, \sigma_v(x,z) \geq \sigma_{lim} \tag{16}$$

The relationship (16) should be read as follows: the depth of plastic deformation h_p is equal to the maximum max value of the von Mises equivalent stress σ_v on the direction of the x-coordinate (see Fig. 8).

The elastic recovery height s of the material can be calculated from the formula:

$$s = \begin{cases} h_{min} - h_p, h_p < h_{min} \\ 0, \quad h_p \geq h_{min} \end{cases} \tag{17}$$

After calculating the elastic recovery height s of the material according to equation (17), it should be substituted in equation (9) taking into account the distribution of compression and shear stress in the material together with the schematic diagram of this distribution (see Fig. 8) and the relationship (12), and then equations (7)–(9) should be combined, and finally the mean maximum width of the flank wear $VB_{Bmax|mean}$ using the final equation:

$$VB_{Bmax|mean} = \frac{K_{re}}{k_o H_V \sqrt{\frac{H_V}{E}}}\left[\sqrt{r_{ce}^2 - (r_{ce} - h_{min})^2} - (h_{min}\tan\gamma')\right] - \frac{s}{\tan\alpha} \tag{18}$$

The above equation is an integral part of the own developed ACESC technique in multi-axis machining [13].

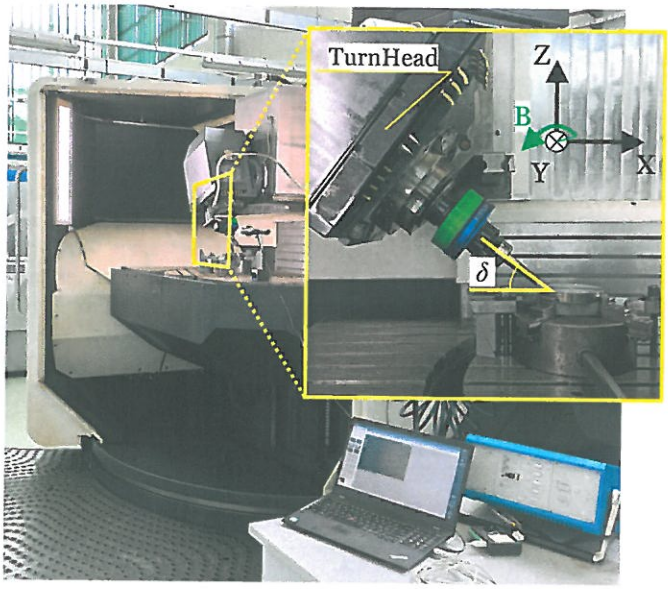

Fig. 9. Experimental set-up.

4. Experiment and methodology

4.1. Experimental set-up

The experimental set-up is shown in Fig. 9. A vertical 5-axis CNC machine tool is used to conduct the multiaxis milling tests. The primary workpiece was cylindrical in shape with a diameter of 110 mm and a height of 12 mm. The total number of workpieces was 18. On each one separately, the areas resulting from the stage of wear were recorded in terms of the adopted criterion of cutting blade life. Flood cooling was used in each experiment. The tool life was determined on the basis of the localized mean flank wear ($VB_{Bmax|mean}$) until it reached 0.2 mm, according to the developed torus cutter wear model.

In order to observe the changes in the microstructure after the multi-axis milling with ACESC technique, the microstructure of the Inconel 718 was observed using scanning electron microscope (SEM) Hitachi S-3400N with EDS system for X-ray microanalysis and transmission electron microscope (TEM) Jeol-2100 with STEM/EDS. Similarly, surfaces after treatment were investigated using the aforementioned Scanning Electron Microscope (SEM) for investigation on machined surface morphology.Metallographic specimens were prepared using standard methods. The samples were etched. Thin foils were prepared using a method based around double sided thinning by electrochemical polishing in a reagent using a Tenupol-3 device by Struers and ion beam milling device by Cressington.

The Hommel-Etamic T800 RC120-400 device was used to measure surface roughness and surface topography. A tip for standard surface roughness measurements, designated TKU300, was used, which has a diamond needle with a rounding radius of $r_k = 5$ μm. The area of the scanned surface was 4.8 x 4.8 mm. The rowing step was 20 μm, resulting in 241 paths for an area of 4.8 x 4.8 mm. The elementary stretch l_r was assumed to be numerically equal to the filter wavelength $\lambda_c = 0.8$ mm, and the measurement stretch $l_n = 4.8$ mm. After measurement, the surface topography was levelled and the shape error was removed using a 4th degree polynomial function.

Residual stress measurements were performed on a Proto LXRD diffractometer (Proto Manufacturing Ltd.) with *Mn-Kαα* radiation, focusing on the (311) crystallographic plane of Inconel 718 (FCC). The key parameters included a Bragg angle of 151.88°, an X-ray tube voltage of 30 kV, a current of 25 mA, an exposure time of 1 s for 10 exposures, and a 2 mm aperture. Data were collected and analysed using the sin2 ψ method. A Beta oscillation of 3° was applied to reduce surface effects, and each specimen was cleaned prior to measurement. This procedure allowed precise determination of near-surface residual stresses resulting from multi-axis milling of Inconel 718.

4.2. Multi-axis ACESCT torus milling experiment

The workpiece material is Ni-based superalloy IN718. The multi-axis torus milling process using the ACESCT was conducted by applying steel torus milling cutter body R300-016A20L-08L for indexable round cutting inserts R300-0828E-PL. The body of the torus milling cutter has a neutral geometry. Round cutting inserts are made of S30T cemented carbide grade. Grade S30T has fine-grain cemented carbide and a TiAlN PVD coating. The round cutting inserts used in the tests have the following parameters: the rake angle is 20°, the clearance angle is 15° and the insert radius is 4 mm. The round cutting insert does not have a typical roundness radius of the cutting edge, but an asymmetrical chamfer with the following dimensions: length 0.1 mm and an angle of 15°. These 8 mm diameter round cutting inserts was attached in to a 16 mm diameter tool body at an overhang measuring 65 mm, as shown in Fig. 9. The experimental set-up and milling parameters utilized in this work are consistent with the main author previous research [5,13] and are summarised in Tables 2 and 3. The cutting force coefficients are calibrated according to the methods proposed by Budak [45], Shah [48] and Chen [49]. The procedures are briefly described as follows: (1) obtain the average milling forces in *x*, *y* and *z* directions taking into account tool wear; (2) determine the edge and cutting components of average forces using linear regression method.

taking into account tool wear; (3) calculate force coefficients based on milling parameters and average forces taking into account tool wear. The edge force coefficients are presented in Tables 4 and 5.

5. Results and discussion

5.1. Torus milling cutter wear

Fig. 10 shows the experimental and predicted values of $VB_{Bmax|mean}$ for segments I-III and for the adopted CCs. The experimental value is the average $VB_{Bmax|mean}$ for all torus milling cutter teeth, and the error bar represents the standard deviation.

The average prediction error of this theoretical model does not exceed 10 %, which indicates that the model developed is reliable. The $VB_{Bmax|mean}$ for individual segments under the cutting conditions for both the first and second stage of the tests is consistent with the K_{re} coefficient values presented in Tables 4 and 5 This means that the $VB_{Bmax|mean}$ index adopted in this work is positively correlated with the K_{re} coefficient, and the flank wear of the round cutting insert will increase the edge forces.

Based on theresults obtained, it was found that despite the decrease in the distance between toolpaths due to the change in the inclination of the tool axis in the ACESC technique, the wear indicator does not show any significant fluctuations. However, it was noted that in the developed ACESC technique the wear rate closely depends on the cutting speed at the point of contact of the shaped surface. As the cutting speed increases, the $VB_{Bmax|mean}$ index also increases, whereas when the cutting speed is kept constant at the CP_i point, regardless of the inclination angle δ, the $VB_{Bmax|mean}$ index does not show any significant changes. This phenomenon is due to the following reasons: (1) The friction in the CWE zone, despite the change in the cutting layer width due to the change in b_r, is maintained at a very similar level, which is confirmed by the edge force coefficients, as shown in Table 4. (2) The ACESC multi-axis milling process is an intermittent cutting process, i.e. one or less than one cutting edge is active. In this case, the cutting edge is subjected to alternating thermal stresses [11]. However, when the cutting conditions are at the same level in each of the active segments in the ACESC technique, despite the alternating thermal stresses, their distribution is very similar on the individual segments and this causes a certain stability of these stresses (susceptibility to fatigue damage) regardless of the tool axis inclination. It should be noted that flood cooling was used for all

Table 2
Cutting Conditions (CCs) for I-st stage of the research.

	Inclination angle δ [°]	Total work angle of cutting blade ψ_{r_sum} [°]	Distance between toolpaths b_r [mm]	Axial depth of cut a_p [mm]	Feed per tooth f_t [mm/t]	Cutting speed (at p. C_D) v_c [m/min]	Cutting speed (at p. CP_i) v_c [m/min]	R_{th}=R_{thvf} [mm]
Segment I	1.10946	24.55056	1.6				71	
Segment II	24.55056	47.99167	0.411	0.3	0.1549	140	99	0.0015
Segment III	47.99167	71.43277	0.335				122	

Table 3
Cutting Conditions (CCs) for II-nd stage of the research.

	Inclination angleδ [°]	Total work angle of cutting blade ψr_sum [°]	Distance between toolpaths br [mm]	Axial depth of cut ap [mm]	Feed per tooth ft [mm/t]	Cutting speed (at p. CD) vc [m/min]	Cutting speed (at p. CPi) vc [m/min]	Criterion Rth = Rthvf [mm]
Segment I	1.10946	24.55056	1.6			274		
Segment II	24.55056	47.99167	0.411	0.3	0.1549	197	140	0.0015
Segment III	47.99167	71.43277	0.335			160		

Table 4
Edge force coefficients for CCs I.

Segment No.	K_{te} (N/mm)	K_{re} (N/mm)
I	66	25
II	64	28
III	77	29

Table 5
Edge force coefficients for CCs II.

Segment No.	K_{te} (N/mm)	K_{re} (N/mm)
I	70	30
II	74	30
III	79	31

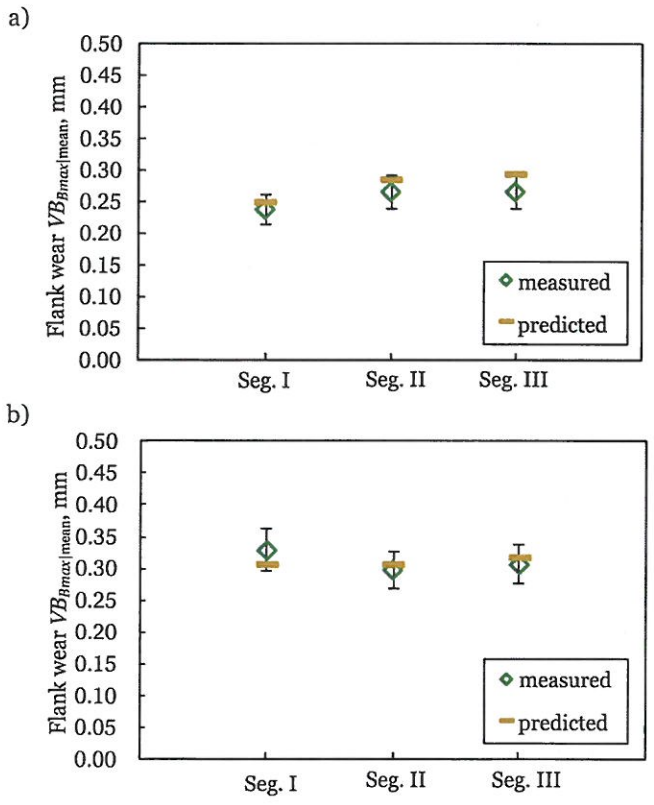

Fig. 10. Predicted and experimental values of $VB_{Bmax|mean}$ for segments from: a) first stage of CCs, b) second stage of CCs.

machining tests. In this context, it can be concluded from the above analysis that lubrication is even more important than cooling to reduce the wear of torus cutter in the process of precision multi-axis finish milling of Ni-based superalloys by ACESC technique.

The phenomenon of interrupted cutting and the resulting pulsating cutting forces observed during the above analyses may significantly affect the state of the technological surface layer. Therefore, an attempt at a comprehensive approach to this issue will also be undertaken in the further stages of the analysis of this work.

5.2. Morphology of machined surfaces

SEM micrographs of machined surface morphology are shown in Fig. 11. While observing the obtained micrographs of the machined surfaces, attention was first drawn to arc-shaped scratches arranged in accordance with the cutting speed vector as a function of the tool rotation angle. These scratches are observed independently of the CCs. This is the result of microchipping and chip adhesion to the cutting edge of the round cutting insert of the torus cutter [5]. However, it was noted that the mildest nature of the resulting scratches occurred in multi-axis machining with the use of the second active cutting edge segment. This primarily indicates a lower level of microchipping and, therefore, tool wear, and at the same time confirms the obtained service life of the torus cutter in machining with this active segment of the cutting edge [13,42]. Regardless of the CCs, clearly visible marks of the feed per tooth f_z are observed. These distances are not identical, which is caused by the run-out of the cutting blades and the resulting slightly uneven wear of one blade relative to the other [5]. No traces generated by tool vibration were observed. In addition, a few sticky chips were observed. This is because the friction of the tool-chip interface deteriorates locally as a result of the hardening of the Ni-based superalloy, and the chips are then easily weldable and adhere to the machined surface during interrupted tool operation. However, these are rare cases and result in a better surface finish at the contact point regardless of CCs. At the same time, it was noticed that in the zone of the boundaries of adjacent machining marks, adhesive deposits of the material plough appeared. This is because the thickness of the cutting layer is less than h_{min} in these places. Mostly plastic deformation and initial crushing of the material occur before physical cutting is initiated. This phenomenon intensifies with the increase of the inclination angle δ of the torus cutter axis, which is positively correlated with the results of our own research on the distribution of the cutting layer thickness.

In further considerations in this article, the 3D topography analysis of machined surfaces was omitted because this analysis was carried out in Ref. [13].

5.3. Microstructure of machined surfaces

Images of the surface microstructure after milling with a multi-axis torus cutter using its own ACESC technique are shown in Fig. 12. The analysis of the microstructures obtained showed that the plastic deformation that occurs near the machined surface layer was more visible in milling at higher cutting speeds and with higher values of the edge force coefficients K_{te} and K_{re}. This caused a deformation of the grain structure near the machined surface. During multi-axis milling with ACESC techniqe, the microstructure changes due to the interactions between the strain hardening and thermal softening. It was observed that with an increase of the inclination angle δ of the torus cutter axis (that is,

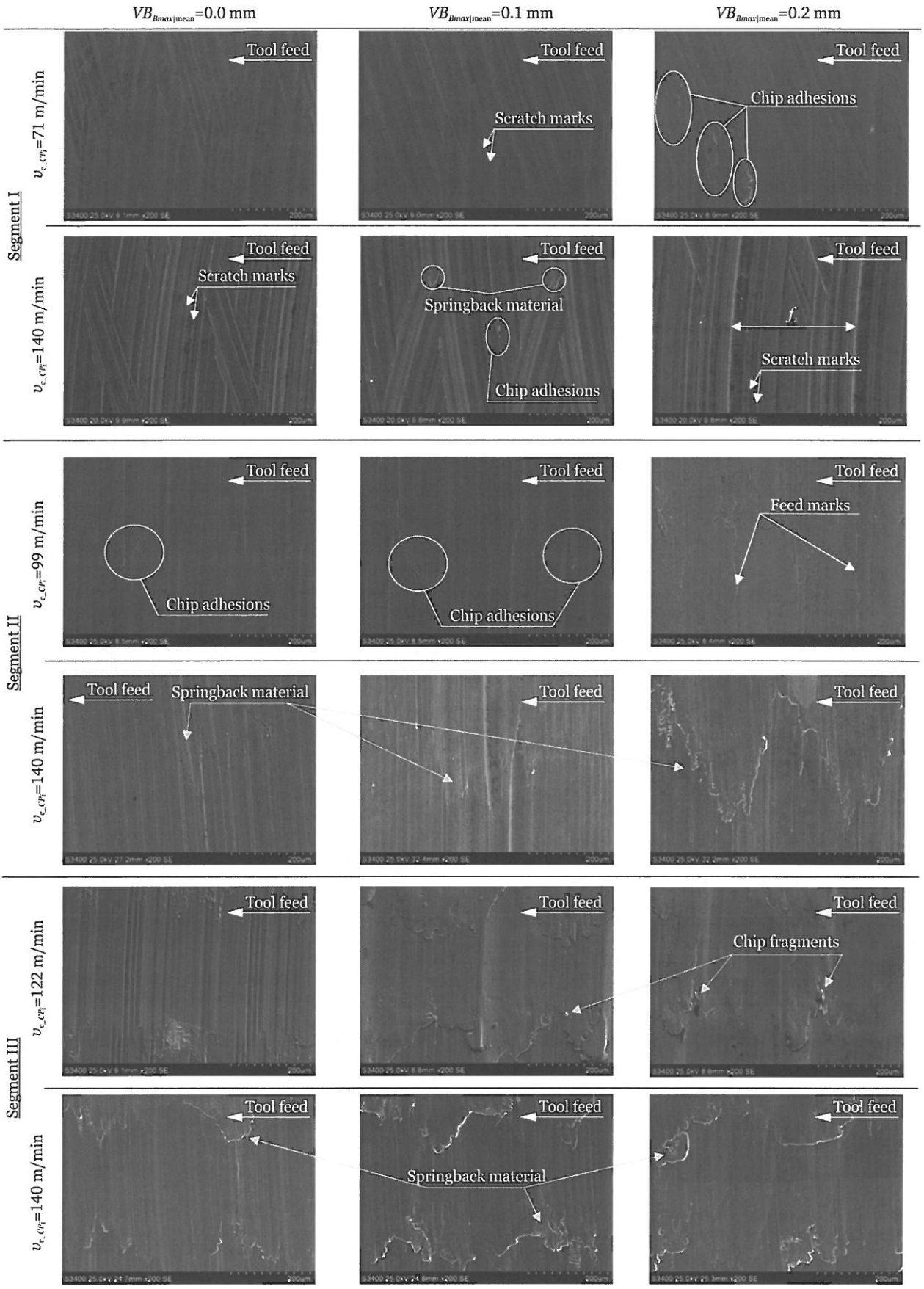

Fig. 11. SEM micrographs of machined surface.

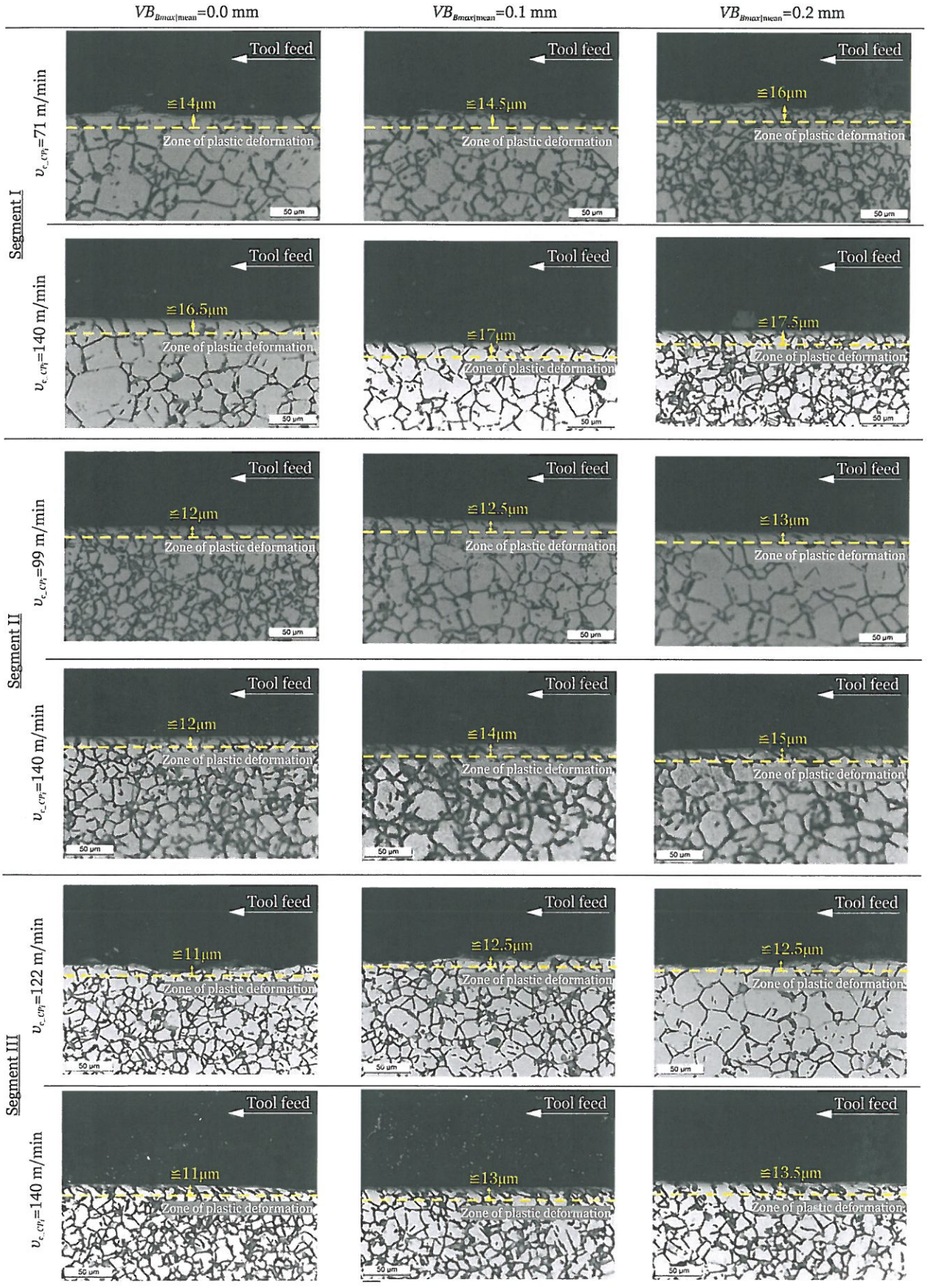

Fig. 12. Image under optical microscope showing the microstructure of the machined surfaces during CCs I and CCs II machining.

changing segment I to II and segment II to III), there is a greater shear deformation of the machined surface. Plastic deformation decreases with increasing depth. Locally, there are rare occurrences of uneven surface defects and torn-out material particles. This is probably due to the variable grain size in the research samples. This is due to the condition under which the samples were delivered for testing, which was revealed only at the stage of this analysis. Moreover, it was observed that with increasing tool wear degree, the thickness of the plastically deformed layer increases independently of the CCs.

This can be explained by the occurrence of strong friction phenomena.

For multi-axis finish milling process: (1) the surface roughness should be less than 1.6 μm [13,50] (see Fig. 14), (2) compression residual surface stresses and slight surface hardening should be preferred, and (3) severe plastic deformation or a white layer is undesirable. These requirements regarding surface morphology, residual stresses, and microstructural changes must be considered comprehensively to decide to what extent and to what extent the cutting capabilities of the torus cutter should be utilized in the ACESC technique. Therefore, in order to consider the influence of tool wear on the surface integrity characteristics, it is necessary to select an appropriate stage of the tool wear and an active cutting segment based on the requirement of surface integrity characteristics. Basically, it is necessary to rely on the residual stresses in the technological surface layer, which (taking into account the above analysis) may vary depending on the inclination angle δ and tool wear.

5.4. Residual stress distribution

The residual stress distributions depending on the stage of tool wear and CCs after multi-axis milling of Inconel 718 with a torus milling cutter using own ACESC technique are shown in Fig. 13. All cases that were defined and subjected to machining tests according to CCs I and II were assigned to one of four baskets. These baskets were determined taking into account the residual compression (−) and tensile (+) stress obtained in the feed directions (X) and the step (Y) detected on the analysed machined surfaces, which are summarised in Table 6.

Tensile residual stress, both in the X and Y directions, was detected mainly on the as-milled surfaces under the cutting conditions where the

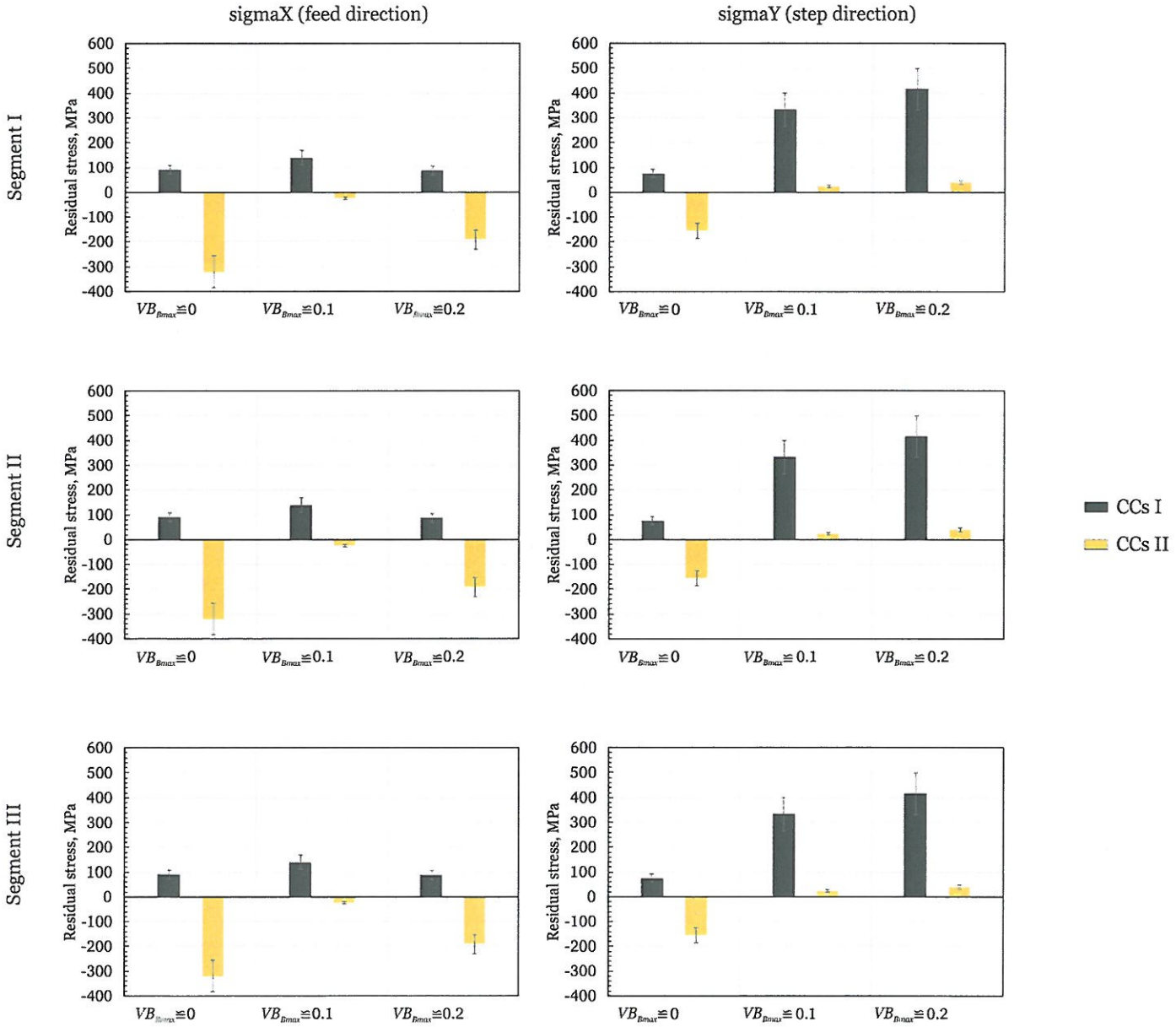

Fig. 13. Residual stress distribution for different tool flank wear widths and CCs along the feed and step directions.

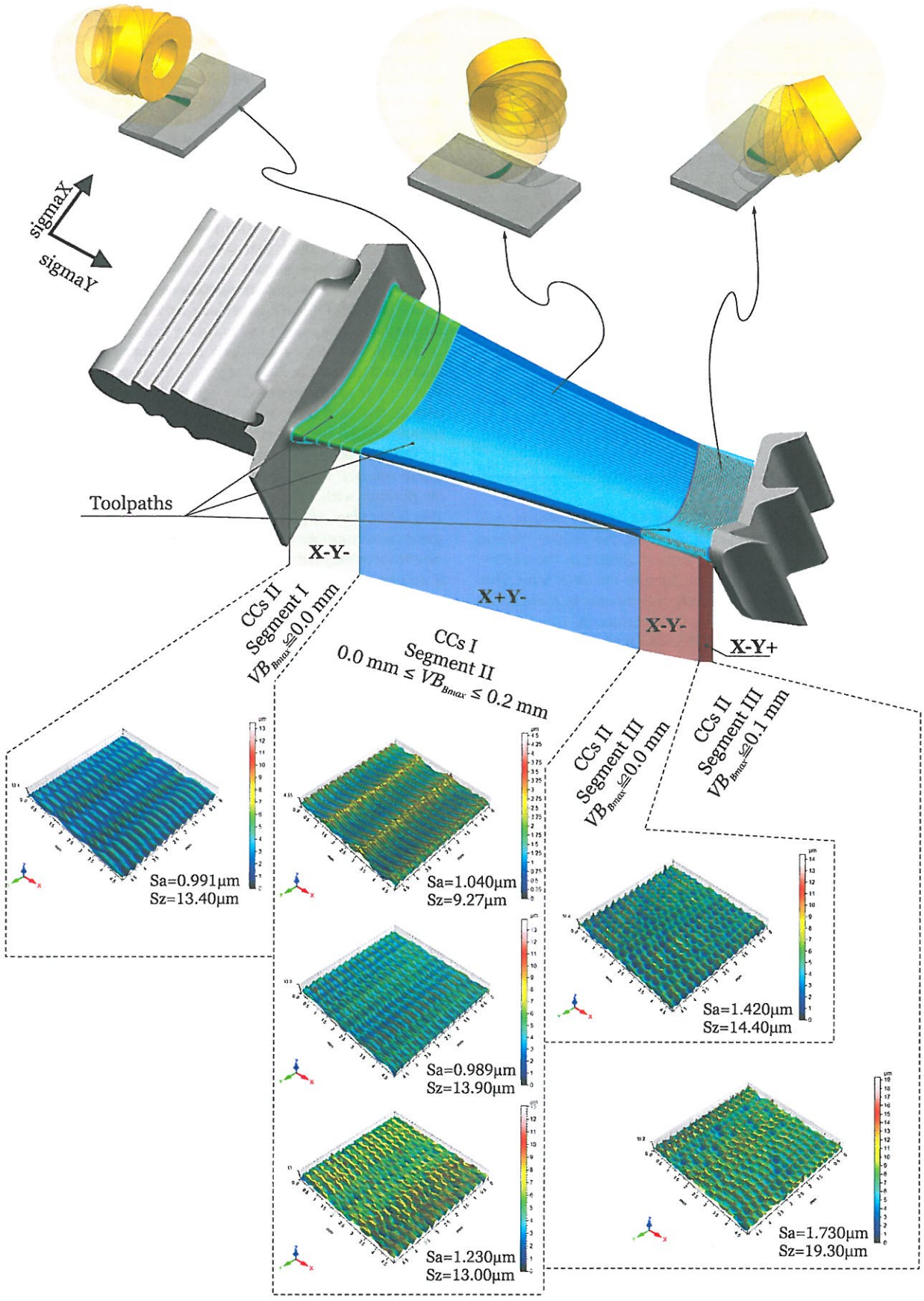

Fig. 14. Proposal for a new approach in multi-axis machining of an aircraft engine blade.

Table 6
Classification of CCs with regard to the tool wear and the residual stress distribution.

Tool wear	X + Y+	X-Y+	X + Y-	X-Y-
$VB_{Bmax} \leqq 0.0$	CCs I Seg. I	CCs I Seg. II		CCs II Seg. I
	CCs II Seg. II	CCs I Seg. III		
		CCs II Seg. III		
$VB_{Bmax} \leqq 0.1$	CCs I Seg. I	CCs I Seg. II	CCs II Seg. II	CCs II Seg. III
	CCs I Seg. III	CCs II Seg. I		
$VB_{Bmax} \leqq 0.2$	CCs I Seg. I	CCs I Seg. II		CCs II Seg. II
	CCs II Seg. III	CCs I Seg. III		
		CCs II Seg. I		

cutting speed at the contact point was the lowest and the distance between the toolpaths was the largest. In this case, the residual tensile stress can be explained by high temperature gradients in the cutting zone [11] due to strong friction and ploughing in the CWE zone. This indicates that the increased thermal effect is dominant in these cases regardless of the width of the tool wear, and this causes the formation of residual tensile stress. Residual tensile stress in both directions is undesirable in components such as aircraft engine blades; hence they are marked in red and will not be considered further.

The residual stress of compression in the X and Y directions was detected mainly on the as-milled surfaces under the cutting condition, where the cutting speed at the contact point was the highest. In this case, the residual compression stresses can be explained by the higher cyclic frequency of each cutting edge and the pulsating characteristics of the cutting forces [5]. A possible reason for this phenomenon is that the tangential component of the cutting force increases more markedly compared to the radial component of the cutting force. This is confirmed by the values of the edge coefficients of the cutting force. The stage of tool wear is also the cause of this phenomenon. Due to tool wear and compression residual stresses, the classification of active cutting edge segments is nonmonotonic, which constitutes an additional difficulty of this classification. Compression residual stress in both directions is preferred; hence, they are marked in green and will also be taken into account in the following.

All other surfaces machined with the remaining classified CCs and segments are characterised by a mixed residual stress distribution. In these cases, it is difficult at this stage to clearly indicate the cause and explain the distribution of residual stress. This aspect requires further detailed research to be carried out in the future. Mixed residual stress (tensile and compression) is optionally preferred; hence, they are marked in blue and will also be further considered in this work.

6. Outline of a new approach for machining aircraft engine blades

Based on all the research and analyses conducted so far by the author of this paper in the field of multi-axis milling of the Inconel 718 superalloy using own ACESC technique [5,13,50–53], an outline of a new approach for the mechanical machining of aircraft engine blades was developed. This new approach aims to: (1) optimise the distribution of residual stress (compression and tensile) in the aircraft engine blade in order to minimise the risk of material fatigue and, consequently, crack initiation and their propagation during exploitation, and (2) minimise the number of surface machining operations, including primarily the shot peening process. Nevertheless, conventional methods of managing residual stresses—such as shot peening or laser peening—are widely used in the aerospace industry and will remain a point of reference for comparing the effectiveness of the new approach. Shot peening, for instance, typically induces beneficial compressive stresses in the near-surface layers but requires an extra production step, adds processing time, and can increase overall manufacturing costs. Laser peening, on the other hand, allows more targeted treatment of critical zones but involves dedicated equipment, process parameters, and cost considerations. Demonstrating that the newly proposed multi-axis milling strategy can achieve similar or improved residual stress distributions without extensive secondary operations would therefore be of considerable industrial interest, especially from the standpoint of simplifying the manufacturing chain and ensuring consistent surface integrity.

The proposed new approach in the machining of aircraft engine blades is based on the divide of the blade geometry into zones, as shown in Fig. 14. In total, three machining zones were distinguished with a subzone in the third zone, and the division results from the adopted optimisation of the residual stress distribution.

The first zone (green) is the transition zone where the root and the airfoil connect. In this case, it is important to generate a residual stress distribution with a compression preference in both directions (X-Y-). This is the place of greatest changes in the blade geometry, where local stress concentrations can occur. Compressive stresses in this area will be beneficial as they reduce the risk of initiation of microcracks. This makes it necessary to avoid tensile stresses, especially in.

places where significant changes in the blade profile cross-section occur.

The second zone of the blade (blue) is the main working part (airfoil). In this zone, tensile stresses dominate due to centrifugal forces. To compensate for them, it will be advantageous to generate compressive residual stresses (Y-) in the axial direction of the blade and tensile stresses (X+) in the direction of the blade profile. This distribution of residual stresses in the central zone increases resistance to fatigue stresses and consequently delays crack initiation. Importantly, too high a level of tensile stress can lead to unfavorable degradation processes - creep and material fatigue, hence the important use of Ni-based superalloy materials for these products - single crystal, which will be analysed in the next stage of the research by the authors of this paper. Such single-crystal materials exhibit high anisotropy, which directly affects how tensile and compressive stresses form and relax under operational temperatures and loads. Understanding these effects is crucial, because while single-crystal blades can better resist creep and fatigue in certain directions, they may be more vulnerable in others. This research will therefore focus on verifying if the multi-axis milling strategies and cutting conditions proposed in the ACESC technique can be adapted to single-crystal variants; quantifying the degree and depth of residual stresses in these materials and ccomparing the extent to which different crystallographic orientations affect the onset of unfavorable creep or fatigue processes under tensile stress, and whether compressive residual stresses induced by milling can further delay crack initiation. Additionally, it will be important to investigate whether these residual stress states might accelerate local recrystallization during operation—leading to the formation of new grains and thus compromising the single-crystal microstructure, which could degrade the alloy's creep resistance and negate the advantages of using a single crystal material in such high-temperature applications. By extending the present approach to single-crystal superalloys, the authors aim to refine the guidelines for zone-specific machining so that critical regions on single-crystal blades can be optimized for both surface integrity and long-term fatigue resistance without extensive post-processing.

The third zone (red) is the top of the airfoil of the aircraft engine blade. In this part, compression residual stress (X-Y-) is preferred, but at

a very low value. The airfoil tip is exposed to vibrations and possible contact with the sealing ring, which can lead to wear and fatigue damage due to the high residual.

compression stress. Tensile stress is acceptable, but not too high, as it can lead to fatigue cracks and airfoil tip degradation. Therefore, a subzone with the X-Y+ residual stress distribution was distinguished.

In each zone, the required surface roughness criterion was met. Moreover, it can be concluded that a uniform surface roughness distribution can be obtained taking into account the stage of tool wear [13, 42].

7. Conclusion

In this work, the integrity of state of the technological surface layer was investigated, taking into account the stage of wear of the torus cutter during the multi-axis milling process of the Inconel718 superalloy. An own technique was used to change the active segment of the cutting edge during machining. The torus milling cutter was defined by the geometry of the round cutting inserts with PVD TiAlN coating. For each active cutting edge segment, taking into account the criterion of the same roughness in the feed direction and in the step direction, a mathematical model of the distance between the toolpaths was developed. This model is dedicated to the geometry of torus cutters and the ACESC technique. This study establishes a theoretical prediction model of $VB_{Bmax|\mathrm{mean}}$, and investigates the machined surface morphology, microstructure, and tool wear its corresponding residual stress distribution under CCs I and CCs II. Cutting tests were carried out in two stages: under variable machining conditions and under constant machining conditions, where the cutting speed was defined relative to the contact point between the tool and the machined surface in the CWE zone.

Furthermore, a new approach for multi-axis machining of aircraft engine blades was outlined, taking into account residual stress distribution and tool wear stage in the ACESC technique. The following conclusions are drawn.

- $VB_{Bmax|\mathrm{mean}}$ is positively correlated with K_{re}. It was noted that in the developed ACESC technique the wear rate closely depends on the cutting speed at the point of contact of the shaped surface. As the cutting speed increases, the $VB_{Bmax|\mathrm{mean}}$ index also increases, whereas when the cutting speed is kept constant at the CP_i point, regardless of the inclination angle δ, the $VB_{Bmax|\mathrm{mean}}$ index does not show any significant changes. The average prediction error of this theoretical model does not exceed 10 %, which indicates that the model developed is reliable.
- The machined surfaces in CCs I and CCs II are characterised by arc-shaped scratches, arranged according to the cutting speed vector as a function of tool rotation angle. It was noted that the mildest nature of the resulting scratches occurred in multi-axis machining with the use of the second active cutting edge segment. Regardless of the CCs, clearly visible marks of the feed per tooth f_z are observed. These distances are not identical, which is caused by the run-out of the cutting blades and the resulting slightly uneven wear of one blade relative to the other. In addition, the milled surfaces are characterized by chip fragments, and deep valleys and high peaks resulting from stochastic chip adhesion and tool wear respectively.
- The plastic deformation that occurs near the machined surface layer was more visible in milling at higher cutting speeds and with higher values of the edge force coefficients K_{te} and K_{re}. This caused a deformation of the grain structure near the machined surface. It was observed, that with an increase of the inclination angle δ of the torus cutter axis (that is, changing segment I to II and segment II to III), there is a greater shear deformation of the machined surface. Moreover, it was observed that with increasing tool wear degree, the thickness of the plastically deformed layer increases independently of the CCs.
- Tensile residual stresses was detected mainly on the as-milled surfaces under the cutting conditions where the cutting speed at the contact point was the lowest and the distance between the toolpaths was the largest. The residual compression stress was detected mainly on the as-milled surfaces under the cutting condition, where the cutting speed at the contact point was the highest.
- An outline of a new approach in multi-axis machining of aircraft engine blades using the own ACESC technique has been proposed, aiming to optimise the distribution of residual stress in the aircraft engine blade in order to minimise the risk of material fatigue and, consequently, crack initiation and their propagation during exploitation, and minimise the number of surface treatment operations, including primarily the shot peening process.

CRediT authorship contribution statement

Michał Gdula: Writing – review & editing, Writing – original draft, Visualization, Validation, Supervision, Resources, Methodology, Investigation, Formal analysis, Conceptualization. **Andrzej Nowotnik:** Writing – review & editing, Supervision, Investigation. **Grażyna Mrówka-Nowotnik:** Writing – review & editing, Investigation.

Funding

This research received no external funding.

Declaration of competing interest

The authors declare that they have no known competing financial interests or personal relationships that could have appeared to influence the work reported in this paper.

Data availability

Data will be made available on request.

References

[1] D. Zhu, X. Zhang, H. Ding, Tool wear characteristics in machining of nickel-based superalloys, Int. J. Mach. Tool Manufact. 64 (2013) 60–77, https://doi.org/10.1016/j.ijmachtools.2012.08.001.
[2] X. Yin, Y. Liu, S. Zhao, X. Li, D. Geng, D. Zhang, Tool wear and its effect on the surface integrity and fatigue behavior in high-speed ultrasonic peening milling of Inconel 718, Tribol. Int. 178 (2023) 108070, https://doi.org/10.1016/j.triboint.2022.108070.
[3] M.S. Kasim, M.S.A. Hafiz, J.A. Ghani, C.H.C. Haron, R. Izamshah, S.A. Sundi, et al., Investigation of surface topology in ball nose end milling process of Inconel 718, Wear 426–427 (2019) 1318–1326, https://doi.org/10.1016/j.wear.2018.12.076.
[4] A.H. Musfirah, J.A. Ghani, C.H.C. Haron, Tool wear and surface integrity of inconel 718 in dry and cryogenic coolant at high cutting speed, Wear 376–377 (2017) 125–133, https://doi.org/10.1016/j.wear.2017.01.031.
[5] M. Gdula, G. Mrówka-Nowotnik, Analysis of tool wear, chip and machined surface morphology in multi-axis milling process of Ni-based superalloy using the torus milling cutter, Wear 520–521 (2023) 204652, https://doi.org/10.1016/j.wear.2023.204652.
[6] M. Sarıkaya, M.K. Gupta, I. Tomaz, D.Y. Pimenov, M. Kuntoğlu, N. Khanna, et al., A state-of-the-art review on tool wear and surface integrity characteristics in machining of superalloys, CIRP Journal of Manufacturing Science and Technology 35 (2021) 624–658, https://doi.org/10.1016/j.cirpj.2021.08.005.
[7] E. Şirin, Ç.V. Yıldırım, Ş. Şirin, T. Kıvak, M. Sarıkaya, Comprehensive analysis of cutting temperature, tool wear, surface integrity and tribological properties in sustainable milling of Ti6Al4V alloy: LN2, nanofluid and hybrid machining, J. Manuf. Process. 131 (2024) 1360–1371, https://doi.org/10.1016/j.jmapro.2024.09.120.
[8] L. Tan, C. Yao, D. Zhang, M. Cui, X. Shen, Effects of tool wear on machined surface integrity during milling of Inconel 718, Int. J. Adv. Manuf. Technol. 116 (2021) 2497–2509, https://doi.org/10.1007/s00170-021-07626-x.
[9] A.H. Musfirah, J.A. Ghani, C.H.C. Haron, Tool wear and surface integrity of inconel 718 in dry and cryogenic coolant at high cutting speed, Wear 376–377 (2017) 125–133, https://doi.org/10.1016/j.wear.2017.01.031.
[10] S.M. Sajadmanesh, A. Mohseni, M. Mojaddam, Vortex dynamics mechanisms of separated boundary layer in a highly loaded low pressure turbine cascade, Int. J. Heat Fluid Flow 82 (2020) 108540, https://doi.org/10.1016/j.ijheatfluidflow.2020.108540.

[11] D. Yanjie, S. Yuwen, Mechanism analysis and prediction of bull-nose cutter wear in multi-axis milling of Ti6Al4V with TiAlN coated inserts, Wear (2024) 558–559, https://doi.org/10.1016/j.wear.2024.205580.
[12] M. Luo, H. Luo, D. Zhang, K. Tang, Improving tool life in multi-axis milling of Ni-based superalloy with ball-end cutter based on the active cutting edge shift strategy, J. Mater. Process. Technol. 252 (2018) 105–115, https://doi.org/10.1016/j.jmatprotec.2017.09.010.
[13] M. Gdula, J. Józwik, A. Skoczylas, Tool wear and surface topography shaping after TPl multi-axis milling of Ni-based superalloy of the torus milling cutter using the strategy of adaptive change of the active cutting edge segment, Wear 562–563 (2025) 205637, https://doi.org/10.1016/j.wear.2024.205637.
[14] K. Zhu, Y. Zhang, A generic tool wear model and its application to force modeling and wear monitoring in high speed milling, Mech. Syst. Signal Process. 115 (2019) 147–161, https://doi.org/10.1016/j.ymssp.2018.05.045.
[15] A. Zhang, J. Ni, X. Wei, Y. Su, X. Liu, A tool wear prediction method for free-form surface machining of ball-end mill, J. Manuf. Process. 130 (2024) 87–101, https://doi.org/10.1016/j.jmapro.2024.08.068.
[16] Z. Mao, M. Luo, D. Zhang, Tool wear prediction at different cutting edge locations for ball-end cutter in milling of Ni-based superalloy freeform surface part, Int. J. Adv. Manuf. Technol. 120 (2022) 2961–2977, https://doi.org/10.1007/s00170-022-08790-4.
[17] Y. Zhang, K. Zhu, X. Duan, S. Li, Tool wear estimation and life prognostics in milling: model extension and generalization, Mech. Syst. Signal Process. 155 (2021) 107617, https://doi.org/10.1016/j.ymssp.2021.107617.
[18] S. Yan, D. Zhu, K. Zhuang, X. Zhang, H. Ding, Modeling and analysis of coated tool temperature variation in dry milling of Inconel 718 turbine blade considering flank wear effect, J. Mater. Process. Technol. 214 (2014) 2985–3001, https://doi.org/10.1016/j.jmatprotec.2014.07.006.
[19] A. Bjerke, A. Hrechuk, F. Lenrick, A. Markström, H. Larsson, S. Norgren, et al., Thermodynamic modeling framework for prediction of tool wear and tool protection phenomena in machining, Wear 484–485 (2021) 203991, https://doi.org/10.1016/j.wear.2021.203991.
[20] M.S. Kasim, C.H. Che Haron, J.A. Ghani, M.A. Sulaiman, M.Z.A. Yazid, Wear mechanism and notch wear location prediction model in ball nose end milling of Inconel 718, Wear 302 (2013) 1171–1179, https://doi.org/10.1016/j.wear.2012.12.040.
[21] H. Zeng, R. Yan, P. Du, M. Zhang, F. Peng, Notch wear prediction model in high speed milling of AerMet100 steel with bull-nose tool considering the influence of stress concentration, Wear 408–409 (2018) 228–237, https://doi.org/10.1016/j.wear.2018.05.024.
[22] N.H.A. Halim, C.H.C. Haron, J.A. Ghani, M.F. Azhar, Tool wear and chip morphology in high-speed milling of hardened Inconel 718 under dry and cryogenic CO2 conditions, Wear 426–427 (2019) 1683–1690, https://doi.org/10.1016/j.wear.2019.01.095.
[23] Q. An, C. Cai, F. Zou, X. Liang, M. Chen, Tool wear and machined surface characteristics in side milling Ti6Al4V under dry and supercritical CO2 with MQL conditions, Tribol. Int. 151 (2020) 106511, https://doi.org/10.1016/j.triboint.2020.106511.
[24] Y. Chi, Z. Dong, M. Cui, C. Shan, Y. Xiong, D. Zhang, et al., Comparative study on machinability and surface integrity of γ-TiAl alloy in laser assisted milling, J. Mater. Res. Technol. 33 (2024) 3743–3755, https://doi.org/10.1016/j.jmrt.2024.10.028.
[25] W. Polini, S. Turchetta, Cutting force, tool life and surface integrity in milling of titanium alloy Ti-6Al-4V with coated carbide tools, Proc. IME B J. Eng. Manufact. 230 (2016) 694–700, https://doi.org/10.1177/0954405414558732.
[26] R.K. Bhushan, Effect of tool wear on surface roughness in machining of AA7075/10 wt.% SiC composite, Composites Part C: Open Access 8 (2022) 100254, https://doi.org/10.1016/j.jcomc.2022.100254.
[27] B. Wang, M. Tang, J. Zhao, C. Song, S. He, Q. Zhang, Effects of cutting edge radius on the surface integrity of milled Ti6Al4V alloy, J of Materi Eng and Perform (2023), https://doi.org/10.1007/s11665-023-08954-7.
[28] J. Xiang, S. Pang, L. Xie, X. Hu, S. Peng, T. Wang, Investigation of cutting forces, surface integrity, and tool wear when high-speed milling of high-volume fraction SiCp/Al6063 composites in PCD tooling, Int. J. Adv. Manuf. Technol. 98 (2018) 1237–1251, https://doi.org/10.1007/s00170-018-2294-1.
[29] P.C. Priarone, S. Rizzuti, G. Rotella, L. Settineri, Tool wear and surface quality in milling of a gamma-TiAl intermetallic, Int. J. Adv. Manuf. Technol. 61 (2012) 25–33, https://doi.org/10.1007/s00170-011-3691-x.
[30] C. Zhang, H. Zhang, Y. Li, L. Zhou, Modeling and on-line simulation of surface topography considering tool wear in multi-axis milling process, Int. J. Adv. Manuf. Technol. 77 (2015) 735–749, https://doi.org/10.1007/s00170-014-6485-0.
[31] C. Zhang, S. Guo, H. Zhang, L. Zhou, Modeling and predicting for surface topography considering tool wear in milling process, Int. J. Adv. Manuf. Technol. 68 (2013) 2849–2860, https://doi.org/10.1007/s00170-013-4989-7.
[32] F.J.G. Silva, N.P.V. Sebbe, R.D.F.S. Costa, A.F.V. Pedroso, R.C.M. Sales-Contini, M. L.S. Barbosa, et al., Investigations on the surface integrity and wear mechanisms of TiAlYN-coated tools in inconel 718 milling operations, Materials 17 (2024) 443, https://doi.org/10.3390/ma17020443.
[33] V. Sivalingam, Y. Zhao, R. Thulasiram, J. Sun, G. Kai, T. Nagamalai, Machining Behaviour, surface integrity and tool wear analysis in environment friendly turning of Inconel 718 alloy, Measurement 174 (2021) 109028, https://doi.org/10.1016/j.measurement.2021.109028.
[34] A. Iturbe, E. Giraud, E. Hormaetxe, A. Garay, G. Germain, K. Ostolaza, et al., Mechanical characterization and modelling of Inconel 718 material behavior for machining process assessment, Materials Science and Engineering: A 682 (2017) 441–453, https://doi.org/10.1016/j.msea.2016.11.054.
[35] X. Chen, J. Zhao, Y. Dong, A. Li, D. Wang, Research on the machined surface integrity under combination of various inclination angles in multi-axis ball end milling, Proc. IME B J. Eng. Manufact. 228 (2014) 31–50, https://doi.org/10.1177/0954405413496095.
[36] B. Bloul, H. Chanal, M. Meziane, Study of the influence of cutting parameters on tool wear and the state of the machined surface, Adv. Mech. Eng. 16 (2024) 16878132241273550, https://doi.org/10.1177/16878132241273550.
[37] W.J. Zong, Y.H. Huang, Y.L. Zhang, T. Sun, Conservation law of surface roughness in single point diamond turning, Int. J. Mach. Tool Manufact. 84 (2014) 58–63, https://doi.org/10.1016/j.ijmachtools.2014.04.006.
[38] A. Bougharriou, W. Bouzid, K. Saï, Analytical modeling of surface profile in turning and burnishing, Int. J. Adv. Manuf. Technol. 75 (2014) 547–558, https://doi.org/10.1007/s00170-014-6168-x.
[39] F. Marin, A. Fagali De Souza, H. Da Silva Gaspar, A. Calleja-Ochoa, L.N. López De Lacalle, Topography simulation of free-form surface ball-end milling through partial discretization of linearised toolpaths, Engineering Science and Technology, an International Journal 55 (2024) 101757, https://doi.org/10.1016/j.jestch.2024.101757.
[40] L. Nowakowski, M. Bronis, S. Blasiak, M. Skrzyniarz, A method for determining the minimum thickness of the cut layer in precision milling, Materials 18 (2025) 189, https://doi.org/10.3390/ma18010189.
[41] M. Gdula, Determination and analysis of working diameters and working angle of the torus cutter blade in multi-axis machining in the aspect of tool wear, IJMERR 13 (2024) 535–547, https://doi.org/10.18178/ijmerr.13.5.535-547.
[42] M. Gdula, G. Mrówka-Nowotnik, A. Nowotnik, Modeling and comprehensive mechanism analysis of torus milling cutter wear in multi-axis milling of Ni-based superalloy using the active cutting edge segment change technique, Tribol. Int. 204 (2025) 110509, https://doi.org/10.1016/j.triboint.2025.110509.
[43] M. Gdula, L. Knapčíková, J. Huśar, R. Vandžura, Modeling and measurement of tool wear during angular positioning of a round cutting insert of a toroidal milling tool for multi-axis milling. https://doi.org/10.20944/preprints202409.2088.v1, 2024.
[44] M. Gdula, J. Burek, Cutting layer and cutting forces in a 5-axis milling of sculptured surfaces using the toroidal cutter, Journal of Machine Engineering 4 (2017) 98–122, https://doi.org/10.5604/01.3001.0010.7009.
[45] E. Budak, Analytical models for high performance milling. Part I: cutting forces, structural deformations and tolerance integrity, Int. J. Mach. Tool Manufact. 46 (2006) 1478–1488, https://doi.org/10.1016/j.ijmachtools.2005.09.009.
[46] C. Arcona, ThA. Dow, An empirical tool force model for precision machining, J. Manuf. Sci. Eng. 120 (1998) 700–707, https://doi.org/10.1115/1.2830209.
[47] K.L. Johnson, Contact Mechanics, Cambridge University Press, Cabmridge, 1985.
[48] A.M. Shahl, A. Agarwal, L. Mears, Tool wear area estimation through in-process edge force coefficient in trochoidal milling of Inconel 718, Manufacturing Letters 35 (2023) 391–398, https://doi.org/10.1016/j.mfglet.2023.08.072.
[49] X. Chen, Q. Wang, W. Chen, J. Sun, Y. He, H. Guo, Mining method for cutting force coefficient with the impact of tool vibration and machine tool system, Adv. Mech. Eng. 16 (2024) 16878132241308932, https://doi.org/10.1177/16878132241308932.
[50] M. Gdula, Adaptive method of 5-axis milling of sculptured surfaces elements with a curved line contour, J. Mech. Sci. Technol. 33 (2019) 2863–2872, https://doi.org/10.1007/s12206-019-0534-4.

ARTYKUŁ
A2

dr inż. Michał Gdula
Politechnika Rzeszowska im. I. Łukasiewicza
Wydział Budowy Maszyn i Lotnictwa
Katedra Technik Wytwarzania i Automatyzacji

Rzeszów, dn. 07.07.2025 r.

OŚWIADCZENIE AUTORA

Oświadczam, że w pracy:

lp.: ....A2.....

Gdula M,: *Modeling and analysis of the instantaneous undeformed chip and its thickness distribution on the cutting blade in multi-axis torus milling in the aspect of tool wear.* Journal of Manufacturing Processes, vol. 150, (2025), 949-967 . IF 6.8, MNiSW 140 pkt.;

mój wkład w powstanie tej pracy polegał na: kompletnym opracowaniu manuskryptu obejmującym analizę aktualnego stanu wiedzy w zakresie tematu pracy, opracowaniu zależności matematycznych kinematyczno-geometrycznego sprzężenia torus-przedmiot obrabiany dla wieloosiowego frezowania, opracowanie modeli matematycznych nieodkształconego wióra z uwzględnieniem chwilowej lokalizacji punktu styku względem zarysów brzegowych nieodkształconego wióra co umożliwiło jego opis przestrzeni 3D, opracowaniu metodyki badań, przeprowadzeniu: badań symulacyjnych i eksperymentalnych, analizy trwałości narzędzia, analizy kąta pracy narzędzia, analizy rozkładu głębokości skrawania w funkcji kąta obrotu narzędzia, analizy rozkładu maksymalnej grubości warstwy skrawanej w płaszczyźnie podstawowej w funkcji kąta styku, interpretacji wyników i opracowaniu wniosków, wykonaniu wykresów, rysunków oraz tabel, koordynowaniu procesu wydawniczego.

.....

Podpis
dr inż. Michał Gdula

Journal of Manufacturing Processes 150 (2025) 949–967

Contents lists available at ScienceDirect

Journal of Manufacturing Processes

journal homepage: www.elsevier.com/locate/manpro

Modeling and analysis of the instantaneous undeformed chip thickness in multi-axis torus milling in the aspect of tool wear

Michał Gdula [a]

[a] Department of Manufacturing Techniques and Automation, Rzeszow University of Technology, al. Powstańców Warszawy 12, 35-959 Rzeszow, Poland

ARTICLE INFO

Keywords:
Multi-axis milling
Ni-based superalloy
Tool wear
Tool axis orientation
Torus milling cutter
Undeformed chip thickness

ABSTRACT

Tool wear is one of the main challenges for prediction and optimisation in machining. This becomes even more important in the multi-axis milling of Ni-based difficult-to-cut materials, once because of kinematics of the process, two because of properties of the material, and three because of unknown physical couplings. Tool wear is constituted in the area of the instantaneous undeformed chip. From the point of view of tool wear, in multi-axis machining with an inclined tool axis, it becomes important to know how the thickness of the undeformed chip is distributed over the cutting edge as a function of tool rotation angle. As this distribution has not yet been investigated, a three-dimensional model of the undeformed chip was developed in a function of the instantaneous contact angle between the torus cutter and the machined surface. Simulation studies based on this model were carried out together with the distribution of the maximum chip thickness in the basic plane of the cutter blade. In the following, experimental studies were carried out to verify this distribution and its comparability with the formation of the torus milling cutter wear forms for the declared threshold wear values given. From the results obtained, it was found that as the value of the tool axis inclination angle increases, the life of the torus milling cutter lengthens over the range of this inclination studied. This is due, among other things, to the demonstrated in this work to a reduction in the value of the tool's working angle while dispersing the value of the maximum chip thickness in the base plane of the cutting edge. The developed 3D model of the instantaneous undeformed chip can form the basis of tool wear prediction techniques and systems, and further investigations, particularly for the notching wear type of the multi-axis torus milling process. The precision of the developed model in terms of predicting tool wear area based on the maximum chip thickness distribution is 97 %. The error in predicting the maximum chip thickness does not exceed 15 %.

1. Introduction

Multi-axis milling is currently one of the main subtract shaping techniques of geometrically complex parts, and is widely used in precision milling of sculptured surfaces [1–6]. Torus milling cutters are increasingly being used to machine these surfaces. Tools with this type of geometry allow for better machined surface quality and dimensional accuracy of parts. When machining with a torus milling cutter (1) there is no zero cutting speed, (2) it is possible to significantly increase the values of the technological parameters of cutting up to the HSM range, (3) the cutting process is significantly more efficient compared to ball-end milling [2,7–11]. The multi-axis torus milling process is commonly used for machining sculptured surfaces in parts such as die/molds, propellers, and turbine blades. The quality of these machined parts depends greatly on the proper combination of work material, cutting tools, and the machining conditions in the multi-axis torus milling process. As one of the major outputs in the milling process, condition in the cutter-workpiece engagement (CWE) zone not only accelerates tool wear and degrades dimensional accuracy and surface finish, but also reflects the work material properties, tool geometry, and any changes taking place in the machining conditions, as shown in Fig. 1.

In multi-axis milling, the state of the geometric-kinematic coupling between the cutter and the workpiece directly determines the instantaneous interactions between the cutter and the workpiece in the contact zone. These interactions are specifically related to the variation in cutter/workpiece engagement conditions and the instantaneous undeformed chip thickness (IUCT). This has implications for the mechanics and dynamic properties of multi-axis milling and is of critical importance for the optimisation of the machining process [12–15]. It also follows that the real parameters of multi-axis milling are dependent on the toolpaths, the orientation of the tool axis and the associated change

E-mail address: gdulam@prz.edu.pl.

https://doi.org/10.1016/j.jmapro.2025.07.011
Received 23 February 2025; Received in revised form 14 June 2025; Accepted 4 July 2025
Available online 7 July 2025
1526-6125/© 2025 The Author. Published by Elsevier Ltd on behalf of The Society of Manufacturing Engineers. This is an open access article under the CC BY license (http://creativecommons.org/licenses/by/4.0/).

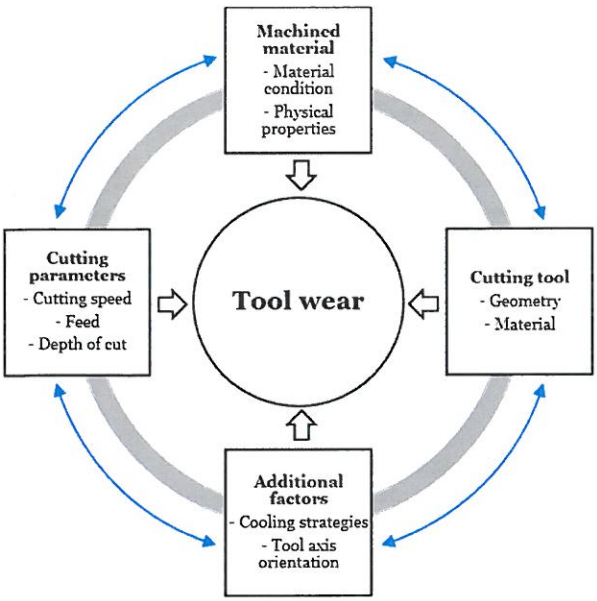

Fig. 1. Machining conditions affecting tool wear.

of cutting conditions in the CWE, the instantaneous depth of cut, etc. Consequently, it is currently one of the most significant areas of research in the field of machining, particularly multi-axis machining.

In the context of industrial implementation and academic research on cutter-workpiece engagement and chip thickness, researchers have proposed a range of analytical [14], solid [16], and discrete [17] modeling methods for determining CWE and IUCT. Approaches that combine these methods are also proposed in the literature [12,13]. Analytical methods primarily establish a spatial model of the cutting surface based on the cutting edge of the tool and uniquely characterise the surface machined in the machining process under investigation. The intersection points between the tool cut surface and the boundary surfaces of the workpiece are determined through numerical calculations. As posited in work [18], an analytical formula is proposed for the purpose of determining the IUCT. The axial depth of cut, the radial depth of cut and the position angle of the cutting edge in the CWE zone are all taken into account in the proposed formulas. While analytical and numerical methods can offer a high degree of accuracy, they are all time-consuming when it comes to calculating intersection points. This can limit their use in sculptured surfaces of the parts and in the analysis of machining processes with variable tool axis orientation.

Solid modeling methods employ parametric representations of primitive solids, surfaces and curves, in addition to associated information regarding their topology, to ascertain the interrelationships between them. This includes the machined surface and the tool. In this particular instance, the machining simulation is predicated on the logical operations between the workpiece model and the tool model. Boz et al. [16] proposed a methodology grounded in the utilisation of solid models of the workpiece and tool, employing the Parasolid solid modeller kernel. They obtained a uniform sequence from the individual tool positions in the form of a dragged volume. This volume was then subtracted from the workpiece model by logical subtraction. Li et al. [19] conducted a logical subtraction operation between the machined surface and the cutting edge of the cutter at the current position to calculate the IUCT.

In the field of research into the state of geometric-kinematic cutter-workpiece engagement and the instantaneous thickness of the undeformed chip, there is a significant preponderance of work in which information pertaining to CWE and IUCT is extracted for the development

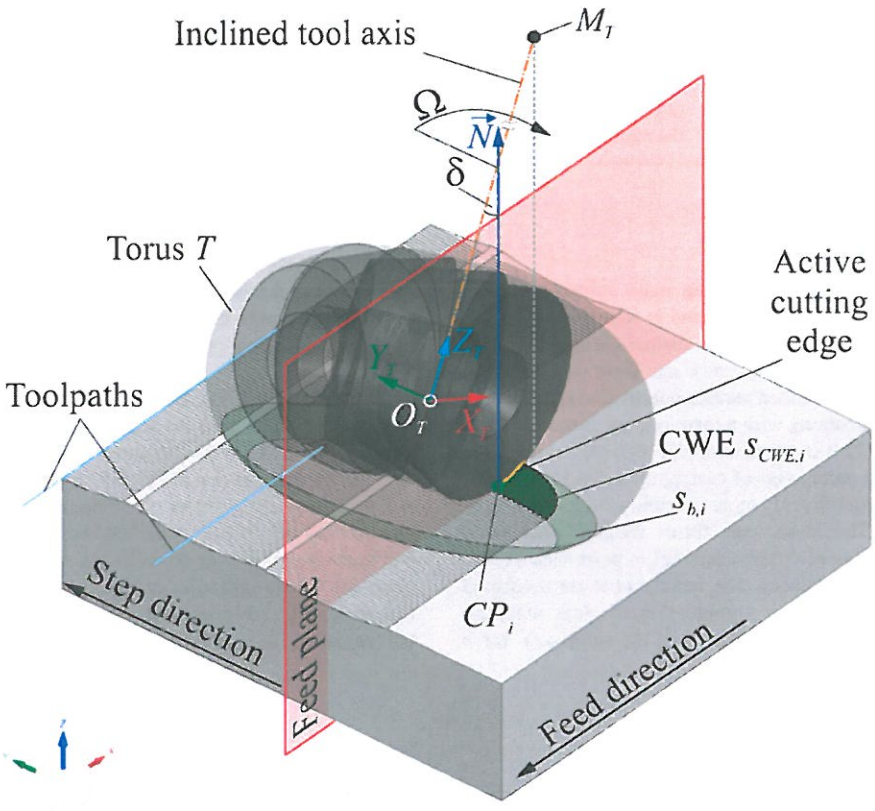

Fig. 2. Cutter-workpiece engagement in adopted multi-axis torus milling process.

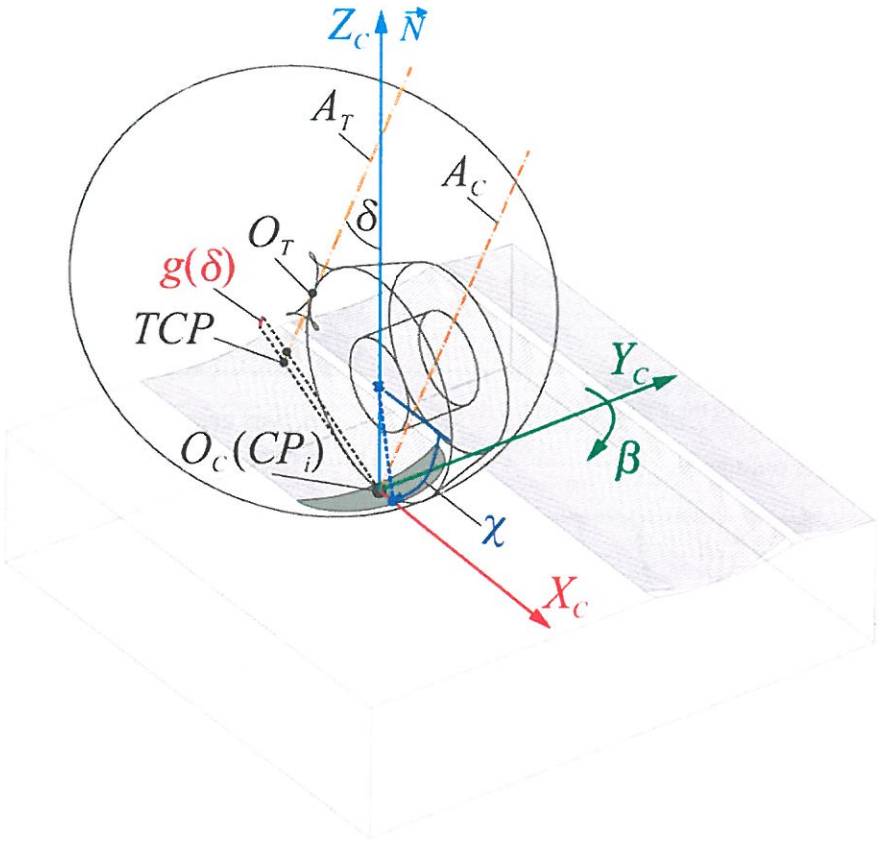

Fig. 3. Torus milling cutter – workpiece interface.

of increasingly improved cutting force models. Huang et al. [4] presented a method for calculating the thickness for a ball-end mill. They investigated the effect of lead and tilt angles on chip thickness. They showed that the real chip thickness is the sum of the thicknesses obtained under two separate cutting conditions, i.e. with a leading angle and a tilting angle. They analyzed the optimised leading and tilting angles in terms of cutting forces. Zhang et al. [12] proposed a method for determining CWE and IUCT based on a set of neighbouring cutter location points and local Boolean operations. The integration of analytical formulas resulted in the development of a precise model for the calculation of cutting force in relation to the position of the tool. Guo et al. [7] conducted a comprehensive CWE analysis for a ball-end milling cutter and then developed a model to predict the cutting force in multi-axis machining. They also took into account the radial run-out of the cutter blade. Wojciechowski et al. [20] focused on the analysis of edge forces that arise during ball-end milling of hardened steel. The forces under investigation take into account the influence of friction and furrowing mechanisms between the workpiece and the flank face of the cutter blade. The primary focus of the investigation pertained to the determination of edge forces, with these being contingent on the varying angles of inclination of the machined surface and the progressive wear of the tool. Lazoglu and Liang [21] developed an analytical model of the cutting force in multi-axis machining, based on the kinematic relationship between the geometry of the ball-end mill and the machined surface. They carried out an experimental verification of the model. Zhuang et al. [1] proposed an improved cutting force model for multi-axis ball-end milling based on the IUCT model. The model incorporates a consideration of the effects of lead and tilt angles. The model was subjected to verification through a combination of finite element analysis (FEM) and experimental methods. In contrast, Zhang et al. [13] proposed a method for quasi-real-time monitoring of variable multi-axis milling parameters. They developed for the purpose of collecting data from the CNC system. This data was then used for Boolean operations in CWE and for the determination of IUCT. They verified the method by, among other things, monitoring the cutting force. Wojciechowski [18] developed a method for calibrating the coefficients of the cutting force components. He carried out an analysis of forces as a function of feed per tooth, cutting speed, and surface angle. He considered the instantaneous cross-sectional area of the cut layer, the length of the active cutting edge, and radial run-out as a function of tool rotation angle. Gilles et al. [8] developed a strategy for positioning a torus milling cutter during five-axis machining of sculpture surfaces, based on balancing the transverse component of the cutting force, perpendicular to the plane containing the tool axis and the feed rate vector.

Furthermore, the scope of CWE and IUCT research encompasses works addressing the minimum chip thickness, quality, and accuracy of the machined surface. This includes laser beam-assisted machining processes and the machining of parts that have been premanufactured by 3D printing. Karakılınç et al. [22] conducted an experimental study of micro-milling of parts made of Ti-6Al-4 V alloy produced by SLM and forging methods. They considered a wide range of feed rates to determine the minimum thickness of the chip. They noted that micro-milled parts of SLM-made parts have lower surface roughness than forged parts. Kim et al. [23] developed a multi-axis laser-assisted milling machine and investigated the effect of the parameters of this machining on cutting force and surface roughness. Mikó and Zentay [24] presented a geometric background for solving the problem of variations in effective diameter values in a 3-axis ball-end milling process. They formulated the assumptions of a strategy that minimises the change in instantaneous effective diameter, providing more constant cutting conditions. Aslantas et al. [25] compared the micromachining of Ti6Al4V alloy, with Ti5553 alloy. They used different cutting parameters and studied the variation

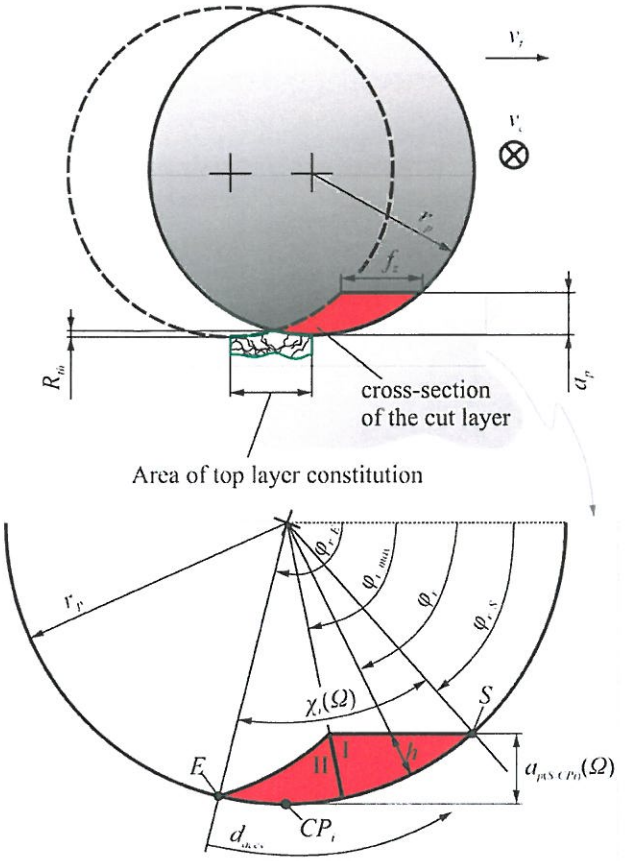

Fig. 4. Geometry of the undeformed chip for the torus milling cutter in the feed plane.

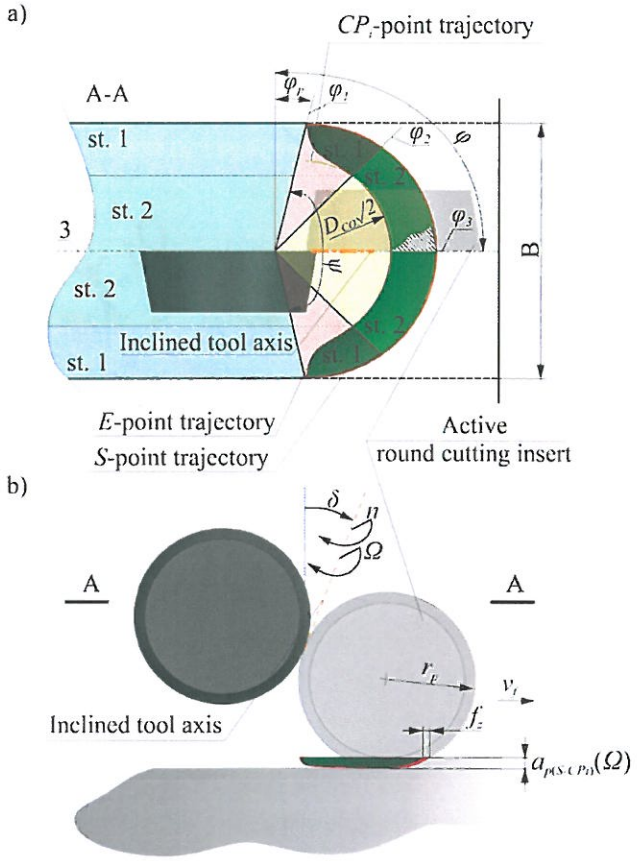

Fig. 5. The stages of CWE formation for $\delta > 0$: a) view of the machined surface, b) view of the feed plane.

in surface roughness, cutting forces, and burr width. They carried out an analysis and comparison of the minimum chip thickness. Ozkirimli et al. [26] proposed a numerical method to solve the milling stability problem in the frequency domain based on CWE and its limits. Nowakowski et al. [27] focused on the surface roughness of X37CrMoV51 steel machined by face milling. They developed a mathematical model to predict the surface roughness parameter taking into account the feed rate per tooth, the corner radius, the actual number of cutting teeth involved in the material removal process and the minimum thickness of the cut layer. They found that higher cutting speeds resulted in smaller minimum undeformed chip thicknesses.

It is worth mentioning the works that concern the phenomenon of ploughing and the accumulation of chip thickness. These phenomena are studied in a comprehensive manner by Wojciechowski et al. [28,29]. Ploughing phenomena occurring during precise machining processes affect the formation of surface finish and progress of tool wear. Therefore, in their study presents an evaluation of ploughing phenomenon by studying the ploughing forces in tool flank face – workpiece interface during precise ball-end milling of AISI L6 alloy steel. They developed model of ploughing forces involved the effect of minimum uncut chip thickness and ploughing volume during ball-end milling. They demonstrated that, estimated ploughing forces are sensitive to variations of surface inclinations and progressing tool wear. They stated that, intense growth of ploughing force during milling with worn tool is affected by irregular and non-circular profile of worn cutting edge below the stagnant point, and by the appearance of attrition and micro-grooves on tool flank face. They proposed a force model considers the micro end milling kinematics, geometric errors of the machine tool–toolholder–mill system, elastic and plastic deformations of workpiece correlated with the minimum uncut chip thickness, and flexibility of the slender micro end mill. They described the chip thickness accumulation phenomenon, which can be manifested as a chip thickness variation in the current tool rotation, resulting from material burnishing and elastic recovery in all previous tool rotations. They demonstrated that, the instantaneous and average micromilling forces determined using the proposed model have considerably better conformity with the experimental forces than those predicted using the commonly used rigid micro end milling model. Moreover, they found that, the non-linearity of the cutting forces as a function of feed per tooth is strongly affected by multiple cutting mechanism transitions observed during micromilling with uncut chip thicknesses close to the minimum uncut chip thickness value.

In the domain of research concerning the geometric-kinematic state of the engagement of the cutter-workpiece and the instantaneous thickness of the undeformed chip, there are extant works in which CWE and IUCT information is extracted for the purpose of studying tool wear [2] and residual stresses [30]. Uchikata et al. [31] developed a strategy to continuously change the axis orientation of a ball-end cutter so that the cutting edge is used uniformly. This extends the life of the tool and reduces wear. Similarly, Luo et al. [32] developed a multi-axis milling strategy based on the idea of moving the active cutting edge and a model for predicting tool wear as a function of path length. Zeng et al. [33] presented the mechanisms of notch wear formation and effects during face milling with a torus milling cutter. Based on a comparison of changes in the thickness of unmachined chips with two different types of cutting, they attempted to explain the appearance of notch wear from the point of view of stress concentration. They then developed a predictive model of notch wear depth taking into account the effect of stress concentration, which they then experimentally verified. Zhang et al. [34] by determining the area and angle of the wear position in the IUCT

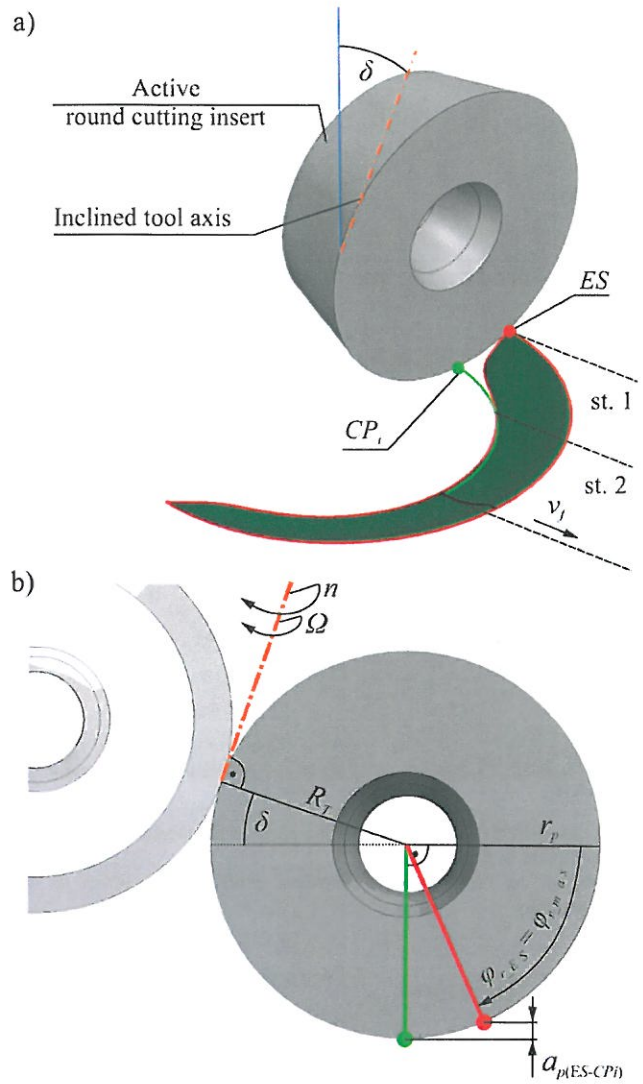

Fig. 6. The stages 1 of CWE formation – motion of the contact point CP_i outside of the undeformed chip (contact at point *ES*): a) 3D view, b) view in basic plane.

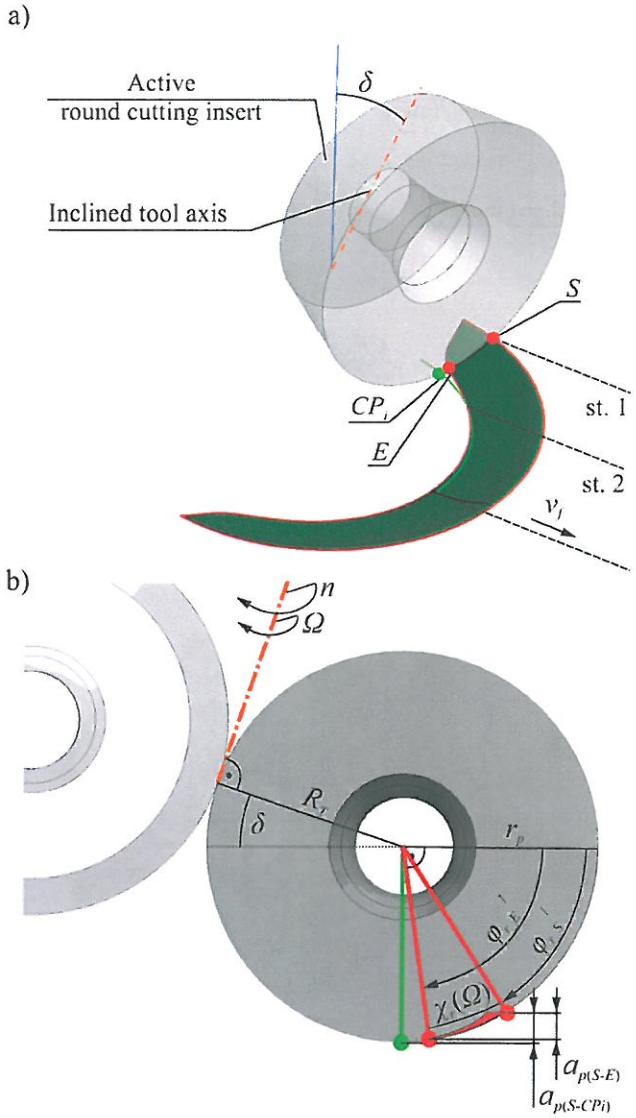

Fig. 7. The stages 1 of CWE formation – motion of the contact point CP_i outside of the undeformed chip (*ES* split point): a) 3D view, b) view in basic plane.

zone, they determined a model of the cutting edge line of the tool. Based on the principle of calculating tool movement trajectories and roughness, they obtained a roughness model that simulates the milling topography taking into account tool wear. They calibrated the tool wear parameters using image detection methods and compared the predicted values obtained by the model with the experimental values.

Following a thorough examination of the prevailing state of the art, the following conclusion was reached:

- It is evident that contemporary models of the instantaneous undeformed chip do not consider the position of the contact point relative to the outline of the undeformed chip, as a consequence of the rotational motion of the cutter around its axis.
- The distribution of maximum thickness of the instantaneous undeformed chip during surface machining with an inclined axis torus milling cutter was found not to be related to the tool wear notching type.

The objective of the present study was to develop a model that would demonstrate dependency on the instantaneous undeformed chip geometry. The model was subsequently utilised for three-dimensional analysis by employing a numerical direct CAD method, taking into account the position of the contact point. The acquisition of a 3D model of the undeformed chip in relation to the contact angle between the torus milling cutter blade and the machined surface was thus rendered feasible.

The model proposed in this paper, in relation to other existing ones, is distinguished by consideration of the contact point movement trajectory and the distribution of the maximum undeformed chip thickness. Considering the trajectory of movement of the contact point in the modeling of the undeformed chip allows the machining parameters to be related to the contact curve directly shaping the parameters of the technological surface layer of the workpiece. In turn, taking into account the distribution of the maximum chip thickness allows the prediction of the entire wear area with the location of the highest concentration of this distribution in the aspect of notching wear.

A study was conducted to ascertain the distribution of maximum thickness of the instantaneous undeformed chip within the fundamental plane of the cutter blade. Subsequent experimental studies were conducted to verify this distribution and its comparability with the formation of tool wear forms for the declared threshold values, based on the

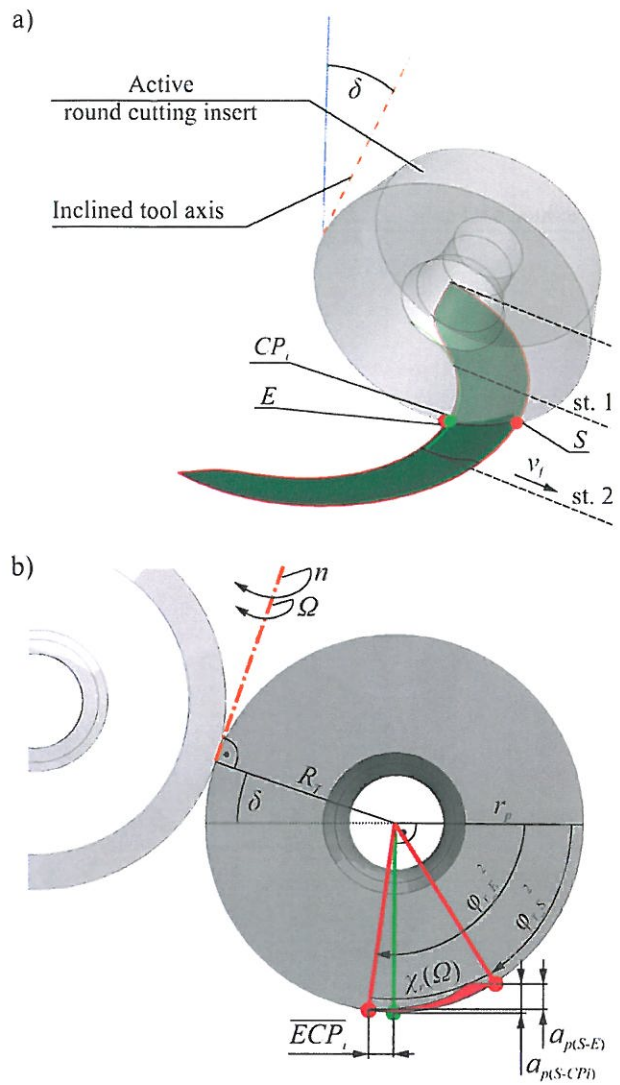

Fig. 8. The stages 2 of CWE formation – motion of the contact point CP_i inside of the undeformed chip: a) 3D view, b) view in basic plane.

wear curves obtained. On this basis, an assessment was conducted of the life of the torus cutter under varying multi-axis milling conditions, and further research directions were identified.

2. Modeling input assumptions

2.1. Cutter-workpiece engagement

In the multi-axis milling process, the tool axis – and by implication, the tool itself – is able to assume any position within 3D space, whether in three-plus-two machining or simultaneous machining, provided there is no collision. In multi-axis milling, the tool axis is oriented with respect to the normal vector of the workpiece surface, N. The orientation is defined in the feed plane by a parameter of the inclination angle, δ.

The point of the cutter attachment, M_T, precedes the contact point, CP_i, as illustrated in Fig. 2.

During movement along the programmed toolpath, the torus surface T of the cutter makes contact with the workpiece at a momentary lobe of the surface, which is known as the cutter-workpiece engagement (CWE). Within the limits of the CWE, an undeformed chip, or in other words, a cut layer, is constituted.

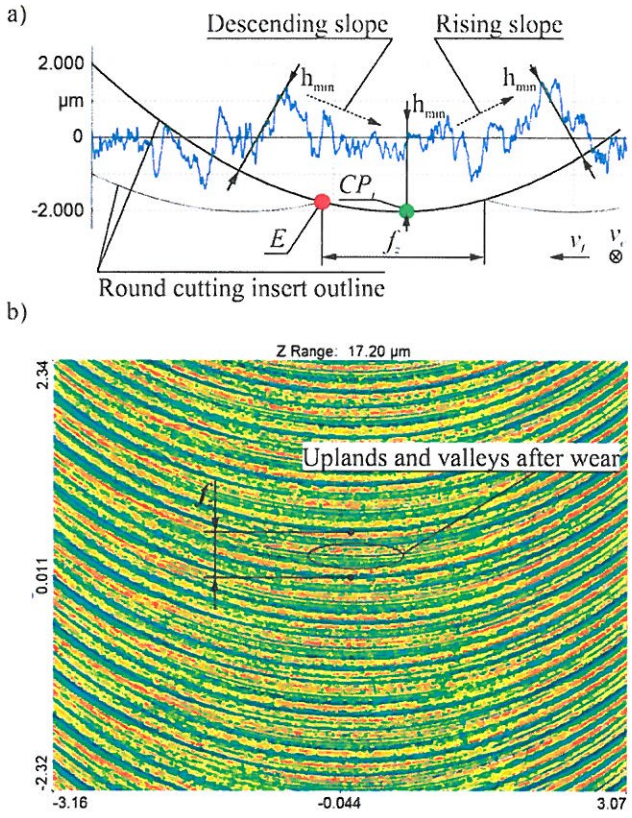

Fig. 9. Mapping the shape of the cutting edge on the machined surface for a fixed minimum chip thickness.
a) Mapping on the measured roughness profile, b) mapping on surface topography.

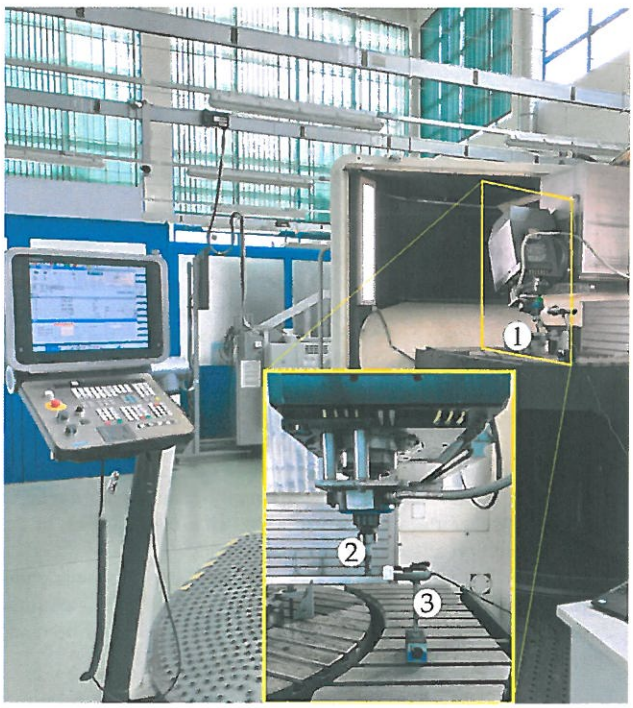

Fig. 10. Experimental test stand (1. Workpiece, 2. Torus milling cutter, 3. Dino-Lite 7000 CE series digital workshop microscope).

Table 1
Multi-axis milling parameters.

Experiment no.	Inclination angle δ [°]	Cutting speed v_c [m/min]	Feed per tooth f_z [mm/z]	Depth of cut a_p [mm]
1	1.37	100	0.25	0.5
2	10.00			
3	18.62			

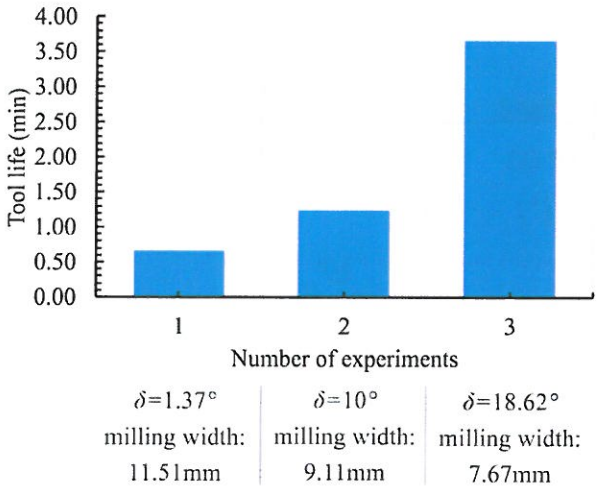

Fig. 11. Torus milling cutter life for different inclination angles values.

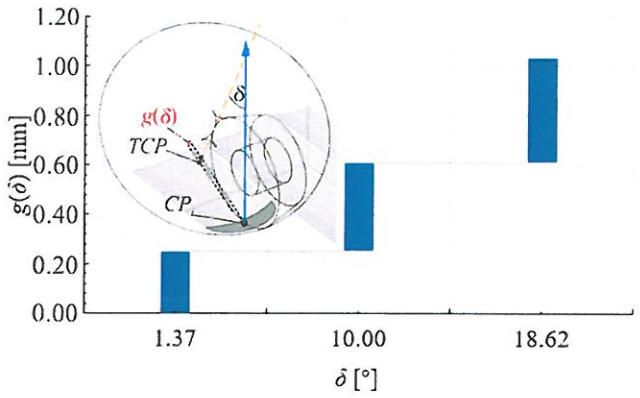

Fig. 12. Changes of the distance between the point of contact and the point of the cutter tip, measured along the tool axis, as a function of the inclination angle.

2.2. Kinematic-geometric relationship in the CWE zone

As illustrated in Fig. 3, a local coordinate system, denoted O_C, X_C, Y_C, Z_C can be established for the CP_i contact point, with the O_C origin located at the CP_i contact point. In this local coordinate system, it is assumed that the X_C axis represents the feed direction, that the Y_C axis denotes the step direction and that the Z_C, axis is congruent with the normal of the machined surface of the part, at the point designated as CP_i.

In the process of multi-axis milling, the axis of the torus milling cutter is inclined in a forward direction with respect to the unmachined surface by means of rotation about Y_C by an angle designated as β (lead angle). The rotation matrix can be expressed as:

$$R_{Y_C} = \begin{bmatrix} \cos\beta & 0 & \sin\beta \\ 0 & 1 & 0 \\ -\sin\beta & 0 & \cos\beta \end{bmatrix} \quad (1)$$

$$A_C = [0\ 0\ 1]R_{Y_C} = [-\sin\beta \quad 0 \quad \cos\beta] \quad (2)$$

The inclination angle δ between the tool axis A_T and the surface normal vector N can then be expressed as:

$$\delta = \beta \quad (3)$$

and the distance $g(\delta)$ between the contact point CP_i and the tip point of the cutter TCP measured along the tool axis as a function of the inclination angle is:

$$g(\delta) = r_p(1 - \cos\delta) \quad (4)$$

Taking into account, in the basic plane P_r, the angle χ of the positions of the characteristic points in the cross-sectional area of the undeformed chip, the relation (5) takes the form:

$$g(\delta) = r_p\left(1 - \cos\left(\frac{\pi}{2} - \chi + \delta\right)\right) \quad (5)$$

Based on Eq. (5), knowing the angles δ and χ, it is possible to determine the cutting strip on the surface of the torus and then determine the CWE within it, together with the length of the active cutting edge. In order to facilitate the calculation, the local curvature of the machined surface was estimated at the CP_i contact point with the tangent plane. Thus, taking into account in the basic plane P_r and at the point of contact CP_i the tool working angle χ_r and the radius of the round cutting insert r_p, the length of the active cutting edge segment d_{aces} can be calculated using the equation:

$$d_{ACES} = \frac{\chi_r}{360} \bullet 2\pi \bullet r_p \quad (6)$$

For a given nominal depth of cut a_p, the cutting belt in which the CWE is contained can be determined, and the boundaries of the undeformed chip and, within this, the variation in cutting speed in terms of tool wear, can be determined in 3D.

3. Modeling of the undeformed chip in the CWE zone taking into account the instantaneous position of the contact point

In the process of multi-axis torus milling, the undeformed chip in the CWE zone depends on the depth of cut a_p and the inclination angle δ the tool axis.

Due to the shape of the cutting edge of the torus milling cutter, the values of the geometric parameters of the undeformed chip (and cutting speed too) in the CWE zone change continuously along its active length.

It should be emphasised that the 3D modeling and analysis methodology used for the undeformed chip represents an original approach developed within this work.

3.1. Geometry of the undeformed chip in the feed plane

By first considering the undeformed chip in the special case (i.e. in the feed plane), where the cutting edge is in direct contact with the machined surface at CP_i contact point, it was found that its geometry is essentially influenced by the radius of the round cutting insert r_p, the feed per tooth f_z and the nominal depth of cut a_p, as shown schematically in Fig. 4.

The mathematical description of the discontinuous cross-sectional geometry of the undeformed chip is divided into two areas (I and II in Fig. 4). Such a division results from the adopted parameter of maximum chip thickness h_{max} in the cross-section, which separates the two areas. The boundaries of the two areas and the characteristic points of the cross-section were defined by determining the boundary angles φ_{r_S}, φ_{r_max}, φ_{r}, φ_{r_E}.

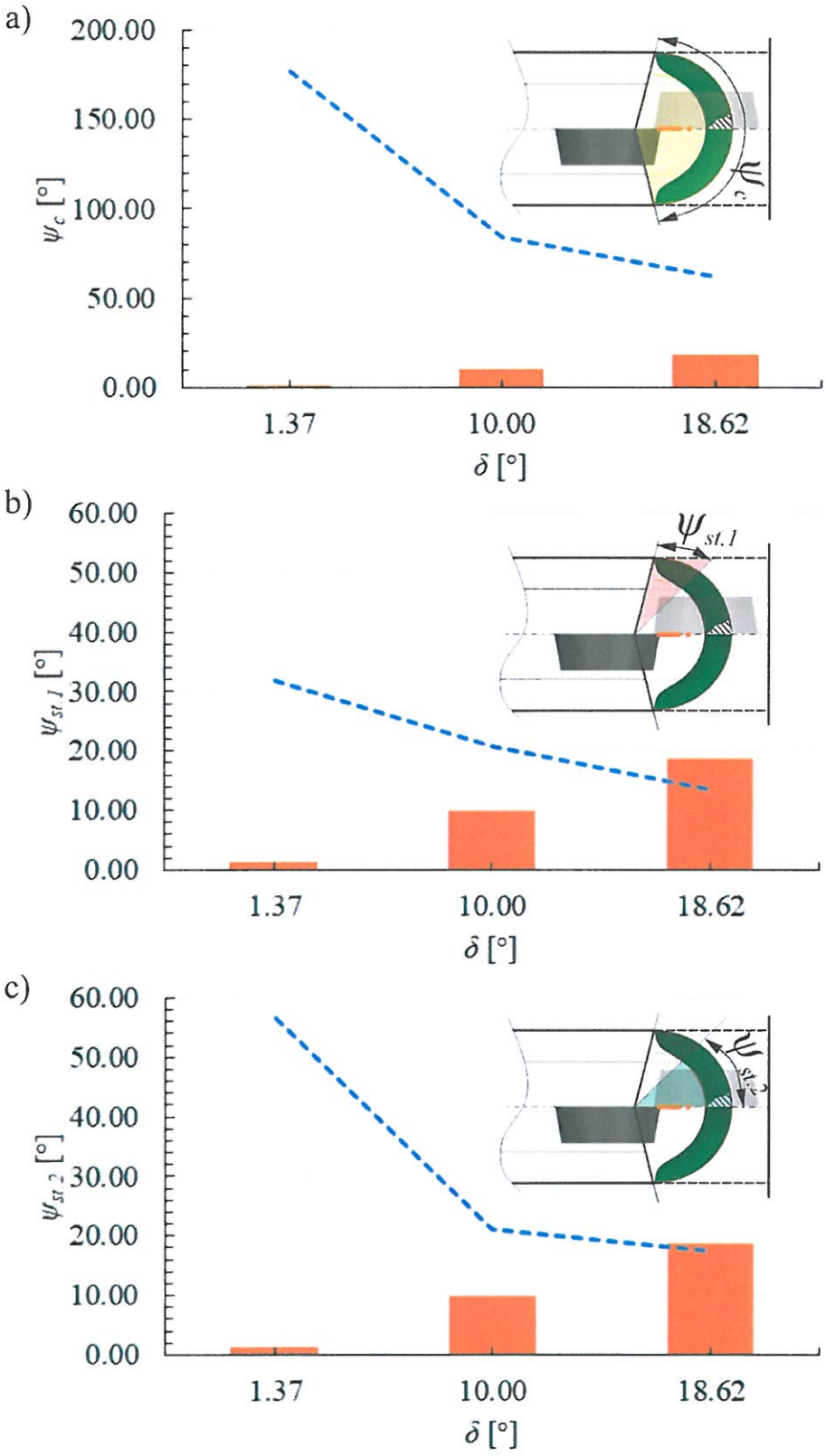

Fig. 13. Changes of the tool working angle as a function of inclination angle: a) total, b) in the zone where the contact point is outside the boundaries of the undeformed chip, c) in the zone where the contact point is within the boundaries of the undeformed chip.

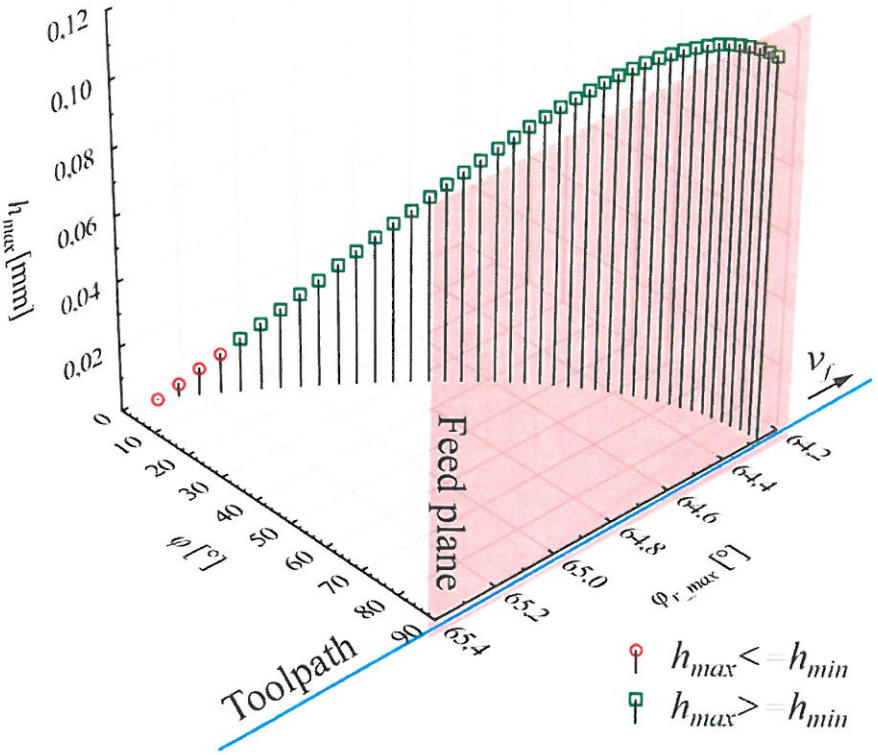

Fig. 14. Changes in the values of the maximum undeformed chip thickness h_{max} and the boundary angle φ_{r_max} as a function of the contact angle φ for multiaxis milling with angle $\delta = 1.37°$.

The angle φ_{r_S} – defines the start of area I and is expressed by the Eq. (7):

$$\varphi_{r_S} = \sin^{-1}\left(1 - \frac{a_{p(S-CP_i)}(\Omega)}{r_p}\right) \tag{7}$$

The angle φ_{r_max} – defines the boundary between areas I and II in which the maximum chip thickness hmax is contained, and is expressed by the Eq. (8):

$$\varphi_{r_max} = \tan^{-1}\left(\frac{r_p - a_{p(S-CP_i)}(\Omega)}{\sqrt{2r_p a_{p(S-CP_i)}(\Omega) - \left(a_{p(S-CP_i)}(\Omega)\right)^2} - f_z}\right) \tag{8}$$

The angle φ_{r_E} – defines the end of area II, and is expressed by the Eq. (9):

$$\varphi_{r_E} = \frac{\pi}{2} + \sin^{-1}\left(1 - \frac{f_z}{2r_p}\right) \tag{9}$$

Using the above angles, the thickness of the undeformed chip h in areas I and II can be calculated as a function of the angle φ_r, according to Eqs. (10) and (11).

Undeformed chip thickness h_I in area I (range from φ_{r_S} to φ_{r_max}):

$$h_I(\varphi_r) = r_p - \left(\frac{r_p - a_{p(S-CP_i)}(\Omega)}{\sin\varphi_r}\right) \tag{10}$$

Undeformed chip thickness h_{II} in area II (range from φ_{r_max} to φ_{r_E}):

$$h_{II}(\varphi_r) = r_p + f_z \bullet \cos(\varphi_r) - \sqrt{r_p^2 - f_z^2 \sin(\varphi_r)^2} \tag{11}$$

Furthermore, using the angles φ_{r_S} and φ_{r_E} it is possible to calculate the tool working angle in the basic plane, denoted by $\chi_r(\Omega)$ and dependent on the tool rotation angle Ω, expressed by the Eq. (12):

$$\chi_r(\Omega) = \frac{\pi}{2} + \sin^{-1}\left(1 - \frac{f_z}{2r_p}\right) - \sin^{-1}\left(1 - \frac{a_{p(S-CP_i}(\Omega)}{r_p}\right) \tag{12}$$

In the case under consideration, to solve Eq. (12), it is necessary to determine the value of the instantaneous depth of cut $a_{p(S\text{-}CPi)}(\Omega)$, which depends on the tool rotation angle Ω and is measured between the characteristic points S and CP_i. The determination of $a_{p(S\text{-}CPi)}(\Omega)$ was carried out using the direct numerical CAD method.

As previously stated, the φ_{r_max} angle delineates the boundary between areas I and II of the uncut chip cross-section. The maximum chip thickness, designated h_{max}, is delineated within this specified line of boundary. Considering that the tool axis is inclined and that the tool rotates around its on axis having its instantaneous angle of rotation Ω, the h_{max} value will be different in each instantaneous position. In the case considered, it takes the value 0 mm at the beginning of cutting (see Fig. 4a – angle φ_1) and the maximum value in the feed plane (see Fig. 4a – angle φ_3). Therefore, in the initial momentary positions of the cutting tooth, the value h_{max} may be smaller than the minimum chip thickness h_{min}. For the purpose of the present work and in view of the above findings, the minimum thickness of an undeformed chip h_{min} was expressed by the Eq. (13)

$$h_{min} = r_{ce} c_r \tag{13}$$

where: r_{ce} is the radius of the cutting edge formed in the first wear phase

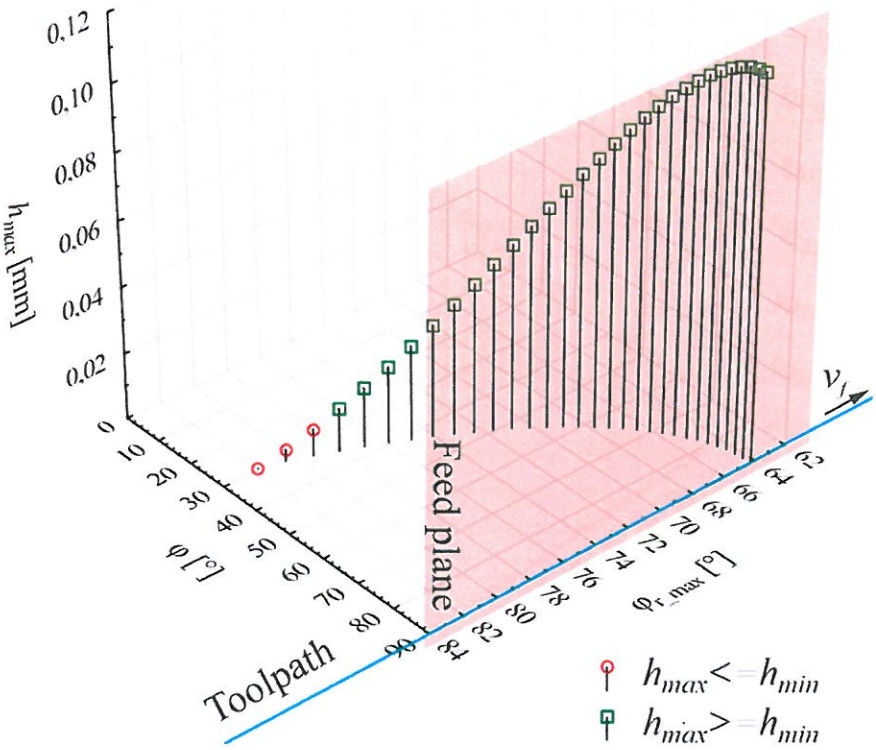

Fig. 15. Changes in the values of the maximum undeformed chip thickness h_{max} and the boundary angle φ_{r_max} as a function of the contact angle φ for multiaxis milling with angle $\delta = 10°$.

($r_{ce} = 0.04$ mm), the value of which is maintained in the remaining wear phases, and $c_r \in \langle 0.3, 0.4\rangle$. In this work $c_r = 0.325$. Hence, the minimum thickness of the undeformed chip is 0.013 mm and this was adopted for the purposes of this work.

3.2. Geometry of the undeformed chip in 3D terms

When considering the geometry of the undeformed chip in 3D terms, it is important to take into account the number of active teeth z_c and the tool working angle ψ. As the work [21] shows, the consequence of an increase in the inclination angle δ of the tool axis is a reduction in the number of active teeth and the tool working angle. This phenomenon occurs even at zero helix angle of the main cutting edge and constant cutting parameters. It acquires particular importance, especially under the conditions of precise finishing, which takes place at very small values of depth of cut a_p and feed per tooth f_z. Then, in the case of a torus milling cutter with a small number of cutting teeth, the number of active teeth can be zero or less than unity. This has the effect of generating a course of pulsating cutting forces, which has a significant impact on the tool life and the parameters of the machined surface being shaped. Therefore, for further research and analysis, it was assumed that the number of active teeth was about unity ($z_c \cong 1$), and the tool working angle ψ was derived from the setting of the inclination angle δ.

The stages of CWE formation when the inclination angle $\delta > 0^c$ are shown in Fig. 5.

It can be seen from Fig. 5 that, in the case of symmetric torus milling with an inclined tool rotation axis ($\delta > 0°$), it is possible to distinguish 3 stages of CWE formation as a function of the tool rotation angle Ω and thus the instantaneous position of the contact point CP_i (on the D_{CON} contact curve) relative to the boundary outline of the undeformed chip.

Stage 1 - motion of the contact point CP_i outside of the undeformed chip

In stage 1, as illustrated in Fig. 6, the formation of the CWE starts at point *ES*, which splits into points *S* and *E* as a result of the tool rotation about its axis by angle Ω (see also Figs. 4 and 5).

Hence, at the *ES* point of contact of the cutting edge of the tool with the workpiece, the tool working angle $\chi_r(\Omega)$ is 0. For this point, the limit angle $\varphi_{r_ES} = \varphi_{r_max}$ of cutting initiation, expressed by Eq. (14), can be determined:

$$\varphi_{r_ES} = \varphi_{r_{max}} = \sin^{-1}\left(1 - \frac{a_{p(ES-CP_i)}}{r_p}\right) \tag{14}$$

where $a_{p(ES\text{-}CPi)}$ is the value of the axial depth of cut between the *ES* and CP_i points when the cutter blade starts cutting in position φ_p. Both $a_{p(ES\text{-}CPi)}$ and φ_p are determined by a direct numerical CAD method.

As mentioned above, point *ES* is split into point *S* and point *E* as a result of the rotation of the tool about its axis by angle Ω. Importantly for these considerations, the CP_i point in the angle interval $(\varphi_1, \varphi_2]$ is located outside the modeled undeformed chip geometry, as shown in Fig. 7.

Hence, at this stage:the angle $\varphi^1_{r_S}$ is expressed by the Eq. (15):

$$\varphi_{r_S^1} = \sin^{-1}\left(1 - \frac{a_{p(S-CP_i)}(\Omega) - a_{p(S-E)}(\Omega)}{r_p}\right) \tag{15}$$

and the angle $\varphi^1_{r_E}$ is expressed by the Eq. (16)

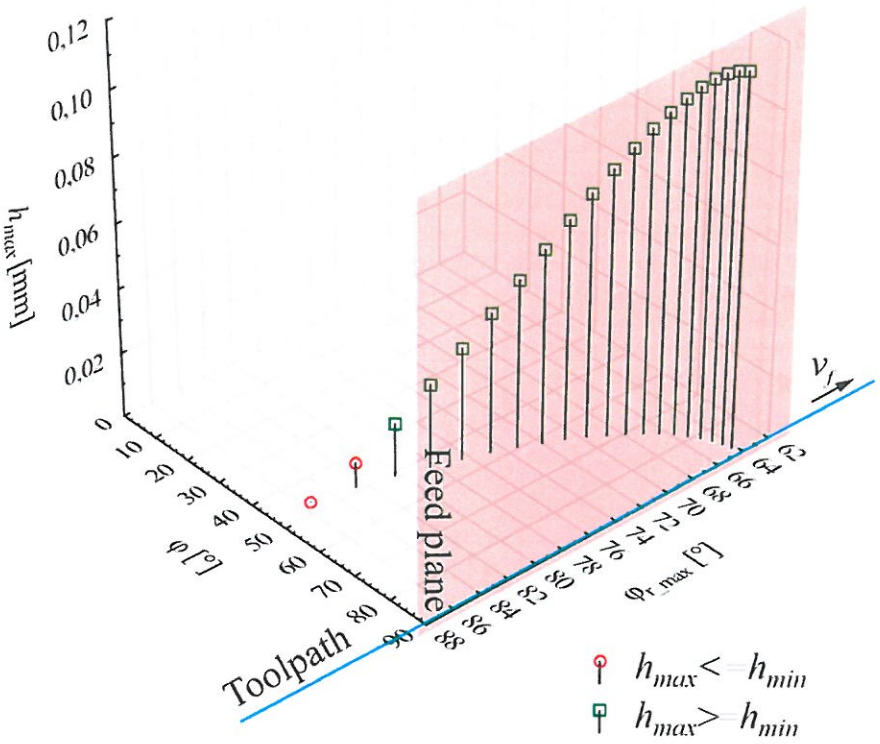

Fig. 16. Changes in the values of the maximum undeformed chip thickness h_{max} and the boundary angle φ_{r_max} as a function of the contact angle φ for multiaxis milling with angle $\delta = 18.62°$.

$$\varphi_{r_E^1} = \sin^{-1}\left(1 - \frac{a_{p(S-CP_i)}(\Omega)}{r_p}\right) \tag{16}$$

For this case, the tool working angle $\chi_r(\Omega)$, which depends on the tool rotation angle Ω, is expressed by the Eq. (17):

$$\chi_r(\Omega) = \varphi_{r_E^1} - \varphi_{r_S^1} \tag{17}$$

In Eqs. (15) and (16), the symbols $a_{p(S\text{-}CPi)}(\Omega)$ and $a_{p(S\text{-}E)}(\Omega)$ are, respectively, the value of the depth of cut between point S and CP_i and the value of the depth of cut between point S and E, both dependent on the tool rotation angle Ω. Both $a_{p(S\text{-}CPi)}$ and $a_{p(S\text{-}E)}(\Omega)$ are determined by a direct numerical CAD method.

Stage 2 – motion of the contact point CP_i inside of the undeformed chip

In stage 2, as illustrated in Fig. 8, the formation of the CWE starts, at point ECP_i (points E and CP_i are coincident), This point, as a result of the rotation of the tool around its axis by an angle Ω, splits into point E and CP_i (see also Figs. 4 and 5).

For consideration in this stage, the point CP_i in the interval of angles $[\varphi_2,\varphi_3]$ is located inside the undeformed chip modeled. Hence:the angle $\varphi^2_{r_S}$ is expressed by the Eq. (18):

$$\varphi_{r_S^2} = \sin^{-1}\left(1 - \frac{a_{p(S-CP_i)}(\Omega)}{r_p}\right) \tag{18}$$

and the angle $\varphi^2_{r_E}$ is expressed by the Eq. (19):

$$\varphi_{r_E^2} = \frac{\pi}{2} + \sin^{-1}\left(1 - \frac{\overline{ECP_i}}{r_p}\right) \tag{19}$$

For this case, the tool working angle $\chi_r(\Omega)$, which depends on the tool rotation angle Ω, is expressed by the Eq. (20):

$$\chi_r(\Omega) = \varphi_{r_E^2} - \varphi_{r_S^2} \tag{20}$$

In Eqs. (18) and (19), the symbol $a_{p(S\text{-}CPi)}(\Omega)$ represents the value of the depth of cut between the points S and CP_i, depending on the tool rotation angle Ω. The symbol $\overline{ECP_i}$, on the other hand, defined the segment contained between point E and CP_i. Both $a_{p(S\text{-}CPi)}$ and $\overline{ECP_i}$ are determined by a direct numerical CAD method.

It is worth mentioning that the line segment $\overline{ECP_i}$, (and thus the arc between points E and CP_i) is contained within the descending slope formation zone of the surface roughness profile. And the arc between the CP_i and S points is contained within the rising slope shaping zone of the roughness profile, as illustrated in Fig. 8a for an example.

Assuming that there is, in fact, an uncollected minimum chip thickness in the vicinity of the CP_i contact point, its constant value along the cutting edge must be assumed. The cutting edge of the tool displaces material of thickness h_{min} throughout the chip separation area from the base material, which springs back after passing through the cutting edge. Due to the constant thickness of this material, the geometry of the cutting edge including its defects as a result of wear, i.e. grooves and micro-fractures (2), is reproduced on the machined surface, as illustrated in Fig. 9b as an example.

Stage 3 - contact between the cutting edge of the blade and the machined surface in the feed plane (target position achieved for CP_i)

This stage is a special case where the cutting edge is in direct contact with the machined surface at point CP_i and, as a starting point for

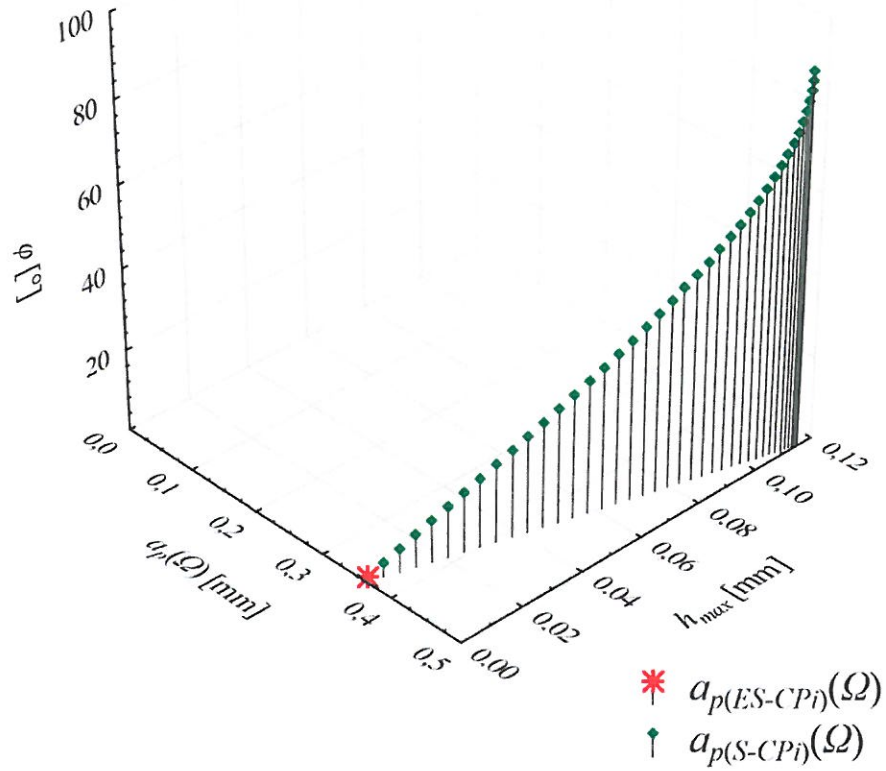

Fig. 17. Changes of the depth of cut $a_p(\Omega)$ as a function of contact angle φ for multi-axis milling with inclination angle $\delta = 1.37°$.

modeling and analysis, is described in detail in Section 3.1.

4. Methodology and research conditions

The research was carried out in two stages. The first stage was a simulation study based on the model relationships developed of the instantaneous undeformed chip using the numerical direct CAD method. The second stage was an experimental study, which was carried out in the aspect of the torus milling cutter notch wear in multi-axis milling. The study conditions were assumed to be constant for both stages. This allowed the correlation of the variables studied and a comprehensive comparative analysis to be carried out. It should be mentioned that the starting point for the research in the present study was the results obtained by the author from his earlier own research, presented in the paper [2].

Multi-axis milling tests were carried out using a torus cutter body with radius $R_T = 8$ mm and interchangeable round cutting inserts with radius $r_p = 4$ mm. The torus cutter was characterised by a neutral geometry. The round cutting inserts were made of wolfram carbide and coated with an anti-wear TiAlN coating. The round cutting inserts used in the tests had the following parameters: the rake angle is 15°, the clearance angle is 15°.

The experimental test stand is shown in Fig. 10. A 5-axis vertical CNC machining centre was used for the multi-axis milling tests, while the workpiece material was the Ni-based superalloy Inconel 718.

Experimental testing involved a series of passes in a symmetrical milling process. The torus milling cutter was inclined relative to the normal vector of the machined surface (see Fig. 2). In order to eliminate the impact of the toolpath distance on the nature of the recorded quantities and thereby facilitate analysis of quantities exclusively related to the kinematics of the process, the milling width values were reduced to be smaller than the toolpath distance.

The variable quantities and the cutting parameters for multi-axis milling are shown in Table 1. The wear of the tool was determining by the maximum flank wear (VB_{Bmax}), until a limit value of 0.3 mm was reached. The milling process was intermittently suspended at predetermined intervals in order to facilitate the identification of wear patterns and the measurement of wear rates. In addition, images of the worn areas were captured using a Dino-Lite 7000 CE series microscope in conjunction with DinoCapture 2.0 software.

5. Results and discussion

5.1. Torus milling cutter life in different inclination angles values

Since 3D modeling including the distribution and projection of the thickness of the undeformed chip h_{max} onto the P_r basic plane of the torus milling cutter in function of the instantaneous contact angle was carried out in aspect of tool wear, the tool life was first assessed for the selected cutter axis inclination angles, as shown in Fig. 11.

Analysing the results, it was noted that tool life increases with increasing values of the cutter axis inclination angle in the range of values tested. The tool life values were used to correlate the tool life with the distribution of the maximum undeformed chip thickness h_{max} along the active cutting edge segment. This will allow to observe and determine whether the concentrated or dispersed arrangement of the h_{max}

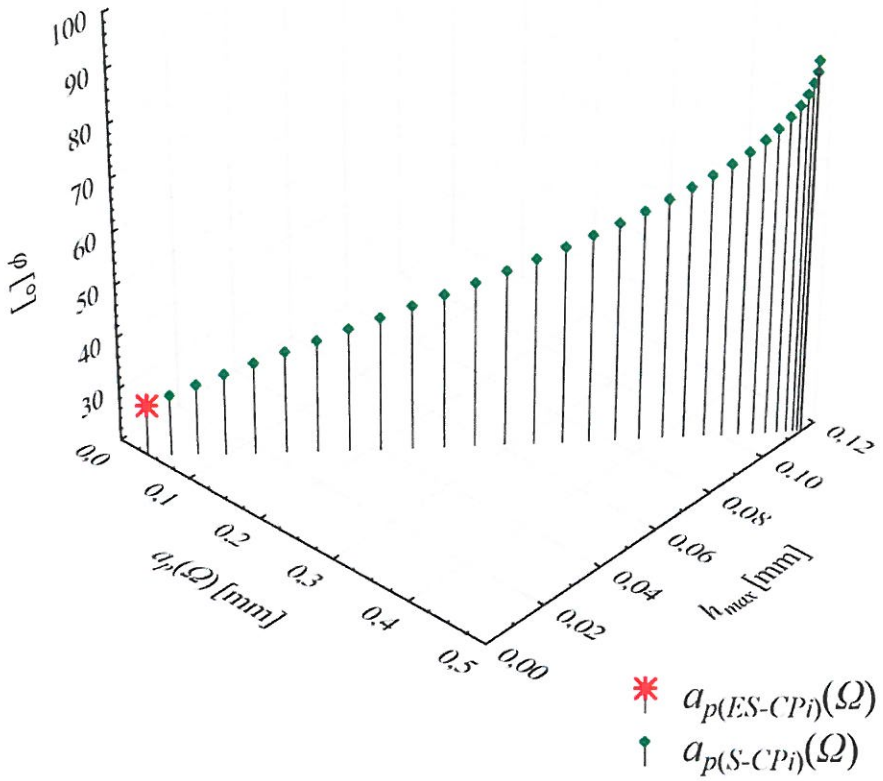

Fig. 18. Changes of the depth of cut $a_p(\Omega)$ as a function of contact angle φ for multi-axis milling with inclination angle $\delta = 10°$.

distribution affects the extension of tool life (see Section 5.5). The tool life values involve the average tool wear value between the two cutting teeth. Therefore, changes in the value of the distance $g(\delta)$ between the contact point CP_i and the cutter tip point TCP measured along the tool axis were first assessed as a function of the angle of inclination (range of variations in effective diameters and cutting speeds). Then, the change in the maximum length of the active cutting edge segment of the torus d_{ACES} in the CWE zone (change in the geometry of the zone of interaction of the physical cutting mechanisms on the cutting tooth) was assessed.

As shown in Fig. 12, as the value of the inclination angle increases, there is an increase in the distance between the point of contact and the point of the cutter tip, measured along the tool axis.

In addition, the active segment of the cutting edge is shifting along the circle of the edge. This means that increasing the value of the angle of inclination increases the zone defined by the effective diameters of the cutter [35] (as the value of these diameters increases). These diameters pass through the boundary points of the undeformed chip geometry in the feed plane. Subsequently, this increases the value of the cutting speed.

However, despite increasing the value of the inclination angle of the cutter axis, the maximum length of the active cutting edge segment of the torus d_{aces} in the CWE zone is constant at 2.14 mm. This is due to the constant machining parameters adopted (a_p and f_z) and therefore the constant value of the angle of work of the cutting tooth $\chi_r(\Omega)$ in the feed plane. This means that despite a gradual increase in the angle of inclination, the machining conditions in the feed plane remain constant.

5.2. Changes in the tool working angle depending on the angle of inclination and the position of the contact point

Based on the above, further investigations and analyses were carried out in 3D terms, that is, taking into account the tool working angle ψ as a function of the tool axis inclination angle δ and the position of the contact point CP_i relative to the boundary outline of the undeformed chip in function of the rotation angle Ω.

A graphical illustration of the tool work angle change is shown in Fig. 13. By analysing the results obtained, it can be seen that increasing the value of the tool axis inclination angle δ results in a significant reduction in the total tool working angle ψ_c (Fig. 13a). Hence, an increase in tool life can result (see Fig. 11), which is directly related to a reduction in milling width. As a result of the reduction in the value of the tool working angle, the cutting edge operates under shorter exposure to high temperatures, friction, stresses, etc. In the range of inclination angle $0° < \delta < 10°$, the reduction in ψ_c is steep, while in the range $10° < \delta < 18.62°$ it is soft. This is due, among other things, to smaller increases in the value of the parameter $g(\delta)$ and therefore smaller differences in the values of the effective diameters that determine the CWE boundary [35]. It was found that the soft characteristics of the changes in the tool working angle value ψ_c additionally can have a positive effect on the extension of tool life, which can also be observed in Fig. 11.

To find the reason for such characteristics of the changes in the parameter ψ_c, it was subdivided due to the position of the contact point CP_i relative to the boundary outline of the undeformed chip: $\psi_{st.1}$ – when the contact point is outside the boundaries of the undeformed chip

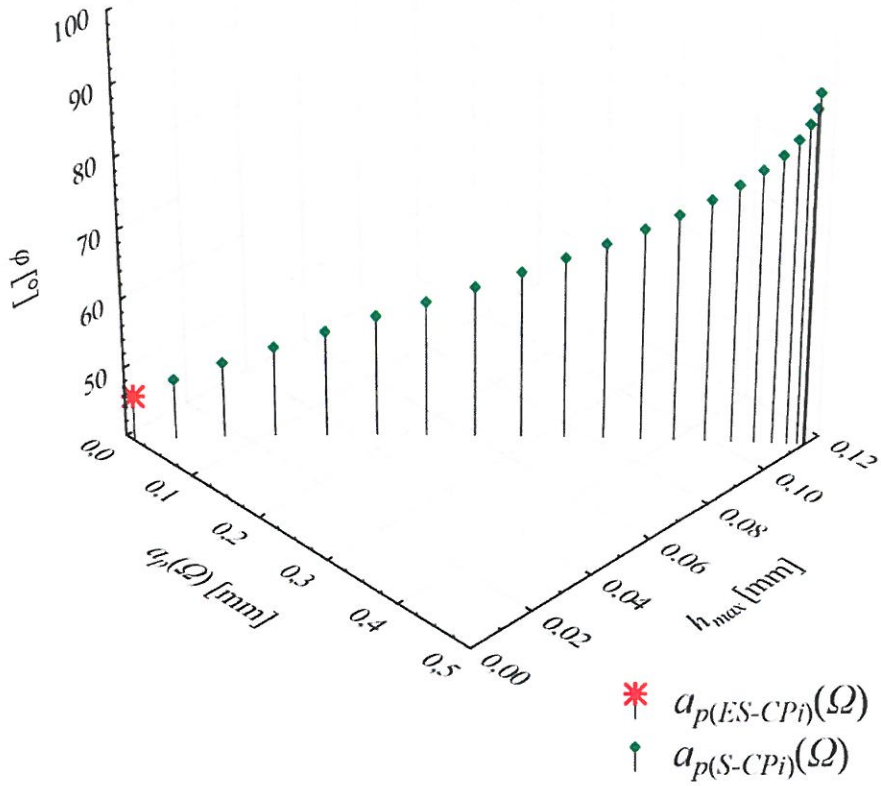

Fig. 19. Changes of the depth of cut $a_p(\Omega)$ as a function of contact angle φ for multi-axis milling with inclination angle $\delta = 18.62°$.

(Fig. 13b) and $\psi_{st.2}$ – when the contact point is within the boundaries of the undeformed chip (Fig. 13c). It is evident that the greatest fluctuations occur in the zone where the contact point is within the boundaries of the undeformed chip, and thus in the zone of formation of the technological surface layer parameters. In this zone, the tool working angle $\chi_r(\Omega)$ reaches its maximum values much faster and for a longer time as a function of the rotation angle Ω.

This happens especially in the range of small angles of inclination δ. Therefore, there is such a steep decrease in the value of the parameter $\psi_{st.2}$ as the value of the angle δ increases. On this basis, it can be assumed that the loading condition resulting from the local positions of the maximum thickness of the undeformed chip as a function of the angle of tool rotation will be most significant in terms of the wear and life of the torus milling cutter.

5.3. *Changes in the value of the maximum thickness of the undeformed chip and the boundary angle between areas I and II of the non-continuous cross-sectional geometry of the undeformed chip as a function of the contact angle*

Taking the above into account, in the next part of the paper determines the variations in the values of the maximum thickness of the undeformed chip h_{max} and the boundary angle φ_{r_max} between the two areas of non-continuous cross-sectional geometry of the undeformed chip as a function of the contact angle φ, as illustrated in Figs. 14–16 respectively.

Analysing the results obtained, it was found that as the value of the contact angle φ increases, the maximum thickness of the undeformed chip also increases, from a minimum value for the angle φ_p (point *ES*) that initiates the cutting process, up to a maximum value in the feed plane.

It was observed that, simultaneously with an increase in the tool axis inclination angle δ, the zone with values $h_{max} \leq h_{min}$ decreases. It can therefore be assumed that this compensates to some extent for the formation of the furrowing effect of the geometric structure of the surface.

Significantly, it was also furthermore observed that as the inclination angle δ of the tool axis increases, the value of the boundary angle φ_{r_max} in the feed plane also increases. This produces a certain slice of the local positions h_{max} on the rake face (in the basic plane P_r) as a function of the contact angle φ. These are, respectively: for an angle $\delta = 1.37°$ a slice with an angle of 1.0262°, for an angle $\delta = 10^{\circ}$ a slice with an angle of 17.6584° and for an angle $\delta = 18.62^{\circ}$ a slice with an angle of $21.1245°$.

This shows the dispersion of h_{max} along the active arc of the cutting edge segment of the round cutting insert of the torus milling cutter. As a result of this dispersion, the stress state acting on the cutting edge is probably distributed as a function of the rotation angle Ω around the tool axis to a larger area of the rake face and the flank face. Thus, it can be assumed that it is not a concentrated state of stress, e.g. at a point or its immediate surroundings.

It can be concluded that the above observations may explain why such a life of the tool was obtained and not a different one for a given inclination angle δ. It also follows that the 3D model developed for the undeformed chip can be used to predict wear forms, including notching forms, as will be verified in the next section of this work.

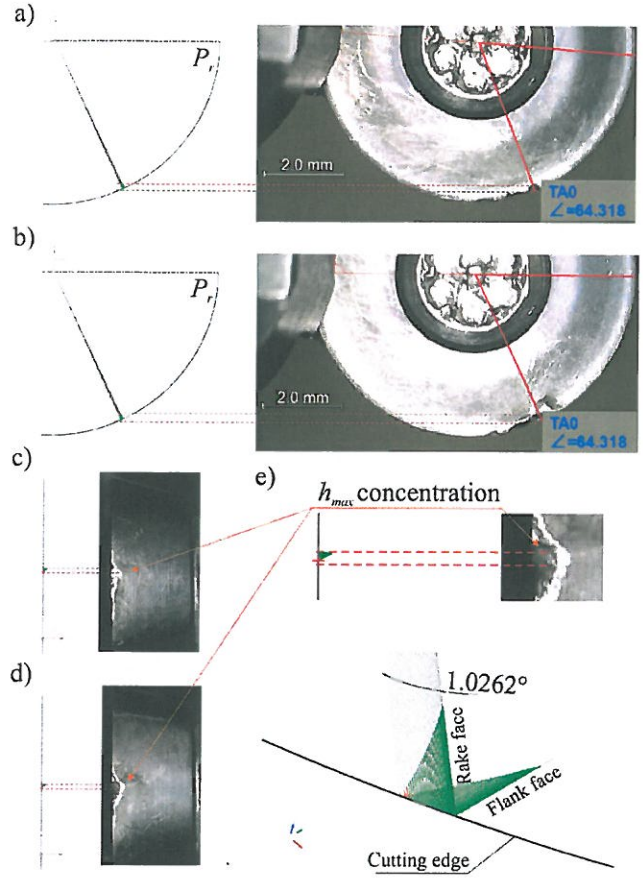

Fig. 20. Distribution of the maximum thickness of the undeformed chip h_{max} and wear images for $\delta = 1.37°$: a) on the rake face for dla VB_{Bmax}≦0.1 mm, b) on the rake face for VB_{Bmax}≦0.3 mm, c) on the flank face for VB_{Bmax}≦0.1 mm, d) on the flank face dla VB_{Bmax}≦0.3 mm, e) 3D view of the distribution of h_{max} obtained from the developed models.

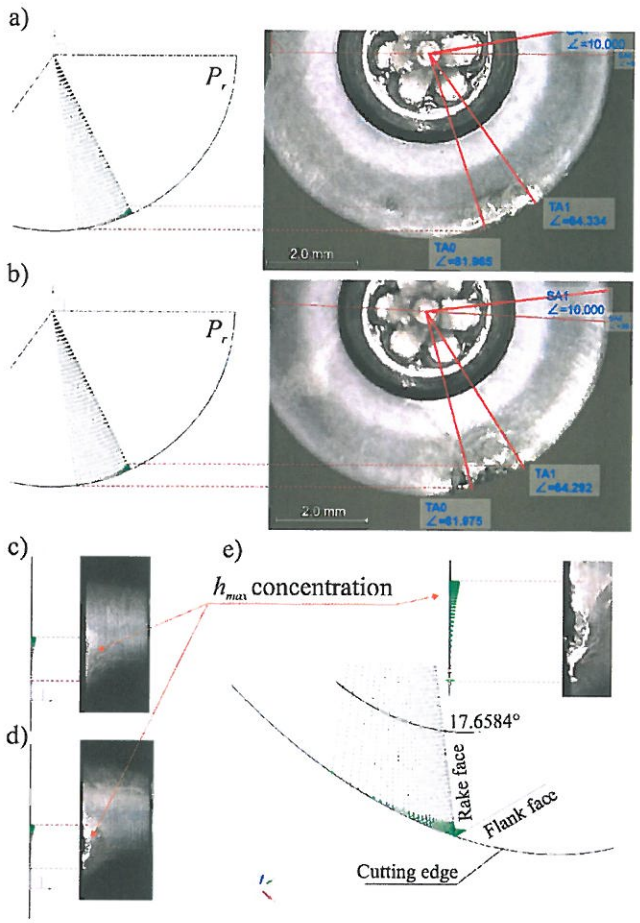

Fig. 21. Distribution of the maximum thickness of the undeformed chip h_{max} and wear images for $\delta = 10°$: a) on the rake face for dla VB_{Bmax}≦0.1 mm, b) on the rake face for VB_{Bmax}≦0.3 mm, c) on the flank face for VB_{Bmax}≦0.1 mm, d) on the flank face dla VB_{Bmax}≦0.3 mm, e) 3D view of the distribution of h_{max} obtained from the developed models.

5.4. Changes in the depth of cut values as a function of the contact angle

During the performance of simulation studies using the numerical direct CAD method and the model relationships developed of the undeformed chip in 3D terms, it was observed that there is a non-zero value of the depth of cut $a_{p(ES\text{-}CPi)}(\Omega)$ at the *ES* points (i.e. the initiation and end of the cut points), as illustrated in Figs. 17–19. The assumed value for the depth of cut (see Table 1) is only achieved if the base plane of the cutter blade coincides with the feed plane and is exactly 0.5 mm. It was observed that within the range of variables studied, as the angle of inclination δ increases, the angle of contact φ also increases. However, the value of the cut depth at the *ES* point decreases with an increase in the above parameters. It follows that the angle of inclination of the tool axis significantly affects the cutting conditions and the CWE, and thus the distribution of h_{max} in the basic plane P_r of the cutting edge and tool wear.

It is worth noting that there is a special case in multi-axis torus milling where the depth of cut will be zero at *ES* point. This situation occurs when the contact point CP_i lies on the contact diameter of the torus cutter [35], and the milling is then typically flank.

5.5. Correlation of the distribution of maximum thickness of an undeformed chip with tool wear images

As the final stage of the work, a comparative analysis of the distribution of the maximum thickness of an undeformed chip h_{max} was performed on the basic plane P_r of the tool cutting edge as a function of the contact angle φ (resulting from simulations of the mathematical models developed) with actual images of the cutting tooth flank and rake wear (taken during the experiments of the machining process). It was assumed that the comparative analysis would be carried out by assembling images of the h_{max} distribution with wear images, both on the rake face and on the flank face of the tool cutting tooth, for the two wear thresholds obtained, that is, $VB_{Bmax} = 0.1$ mm oraz $VB_{Bmax} = 0.3$ mm, as shown in Figs. 21–23.

By first analysing the distribution of the maximum thickness of the undeformed chip thickness h_{max} in the basic plane P_r of the torus milling cutter as a function of the contact angle φ (Figs. 20e, 21e oraz 22e), it is clear that the greater the angle of inclination angle δ of the tool axis, the greater is the dispersion of the parameter h_{max} in the basic plane P_r of the cutting edge. This is fundamentally due to two reasons. The first reason is that the distance between the contact point CP_i and the cutter tip point TCP, measured along the tool axis (see Fig. 11), increases as the inclination angle δ increases. The second reason is that the value of the total work angle ψ_c of the tool (see Fig. 13) decreases as the inclination angle δ increases, thus completely changing the cutting conditions in the CWE zone.

It was found that for an angle of inclination $\delta = 1.37°$ (thus, it can be assumed that for small values of angle δ), the parameter h_{max} is concentrated in a very narrow range of boundary angle variation of $0° < \varphi_{r_max} < 1.0262°$. Generalising the above issue to better illustrate the

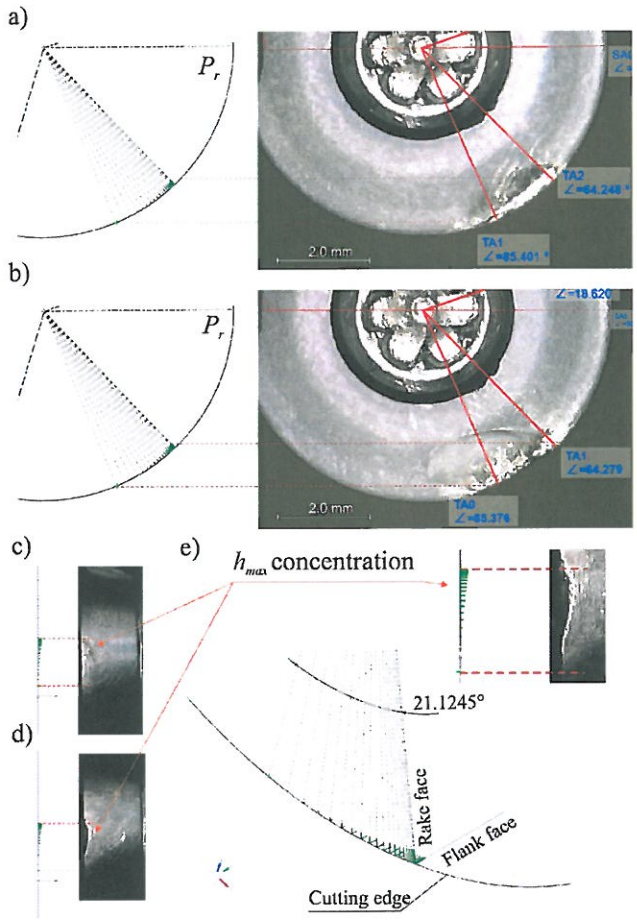

Fig. 22. Distribution of the maximum thickness of the undeformed chip h_{max} and wear images for $\delta = 18.62°$: a) on the rake face for dla $VB_{Bmax} \cong 0.1$ mm, b) on the rake face for $VB_{Bmax} \cong 0.3$ mm, c) on the flank face for $VB_{Bmax} \cong 0.1$ mm, d) on the flank face dla $VB_{Bmax} \cong 0.3$ mm, e) 3D view of the distribution of h_{max} obtained from the developed models.

problem, this is an almost point concentration (Fig. 20a–d). This also implies a concentrated state of maximum stress acting on the cutting edge in this part of the active cutting edge segment.

In the rest of the active cutting edge segment, an equally unfavourable tribological condition from friction and elastic-plastic deformation will prevail. Hence, the tool life for this case is the shortest.

However, for the inclination angles $\delta = 10°$ and $\delta = 18.62°$, due to the dispersion of the parameter h_{max} in the basic plane P_r of the cutting edge, the boundary between the concentrated state of the maximum stresses acting on the blade in the range of the active cutting edge segment and the tribological state resulting from friction and elastic-plastic deformation becomes blurred. The primary confirmation of this is provided by the wear and tear images obtained (Figs. 21a–d and 22a–d). These states occur simultaneously, but, due to the dispersion of h_{max} in the active cutting edge segment, they have a significantly smaller effect on tool wear, resulting in a longer tool life for these cases (see Fig. 11).

Another very important aspect should be noted in the context of the results obtained and their analysis. In the range of the distribution angles of the maximum thickness of the undeformed chip h_{max} in the basic plane P_r of the cutting edge as a function of the contact angle φ, regardless of the value of the inclination angle δ, the formation of a notching-type wear form was observed. This can be seen in all the comparative images of the model and wear (Figs. 20, 21 and 22). In this way, the model relationships developed, their adaptation to the numerical direct CAD method and the addition of stress models can provide a comprehensive model for predicting notch wear (Figs. 21d and 22d).

5.6. Chip morphology and its correlation with the undeformed chip thickness

In the multi-axis milling process studied, using the torus milling cutter with round cutting inserts, in each case analyzed, obtained a chip which is concave in shape with trailing effect at its end, as shown in Figs. 23 and 24.

Fig. 24 show the free surfaces of the chip respectively obtained in the individual experiments analyzed. The basic features of the back surface can be identified by its smooth and shiny appearance due to high contact pressure, frictional forces, and contact temperature developed when the chip slides over the tool rake face during cutting. The free surface of the chip showed a serrated and rough appearance, attributed to the shearing actions, causing a large plastic deformation on the surface.

The lamella structure on the free surface can be separated into a main area and a corner area. At the main area (see Fig. 24 area A), the structure is uniform, with relatively consistent shape and thickness, and varying according to the kinematic variant of multi-axis cutting. This area was sheared by the tool side edge. At the corner area (see Fig. 24 area B), it can be seen that the lamella is sheared by the tool nose edge, thus its inclination to have a trailing effect at the end of the chip, which can be attributed to the geometry of the round cutting insert. The end of the chip also touches and slides on the uncut workpiece surface. Thus, its shape can also be affected by the rubbing action, thermal effects and cutting condition of multi-axis milling induced at the interface cutting edge-machined surface.

Using the developed model relationships, an undeformed chip was generated for each case analyzed (see Table 1 and Fig. 23). The chip thickness correlation was performed in the feed plane taking into account the calculated and measured values. Due to the constant maintenance of the machining parameters, the calculated values were identical in each case and were: $h_{max} = 0.12$ mm. The measured values were in the range: $0.128 < h_{max} < 0.137$ mm. The measured values were observed to be higher than the calculated values by approximately 14 %, which is due to the phenomenon of swelling of the chips. The percentage prediction error of the model is 14.16 %. This means that the developed model positively correlates with the chip morphology. However, it should be noted that this error will increase with increasing tool wear. This problem constitutes a future stage of research.

6. Conclusion

In this study, the kinematic-geometric engagement of cutter-workpiece (CWE) and the active cutting edge was determined, and the relationship between tool axis orientation and CWE in the process of multi-axis torus milling was developed. On this basis, in the next step, a 3D modeling of the instantaneous undeformed chip in the CWE zone was carried out, taking into account the instantaneous position of the contact point, using a numerical direct CAD method. Then, comparative studies, both simulation and experimental, were carried out in terms of tool wear. Based on the results obtained and their analysis, the following conclusions were drawn.

- When developing 3D models of the undeformed chip using the numerical direct CAD method as a function of contact angle, the position of the contact point relative to the boundary outline of the undeformed chip and the instantaneous depth of cut parameter as a function of tool rotation angle must be taken into account. This is an original approach developed under of this work.
- Within the framework of the 3D model of the developed instantaneous undeformed chip, the distribution of the maximum thickness of the undeformed chip along the active segment of the cutting tooth

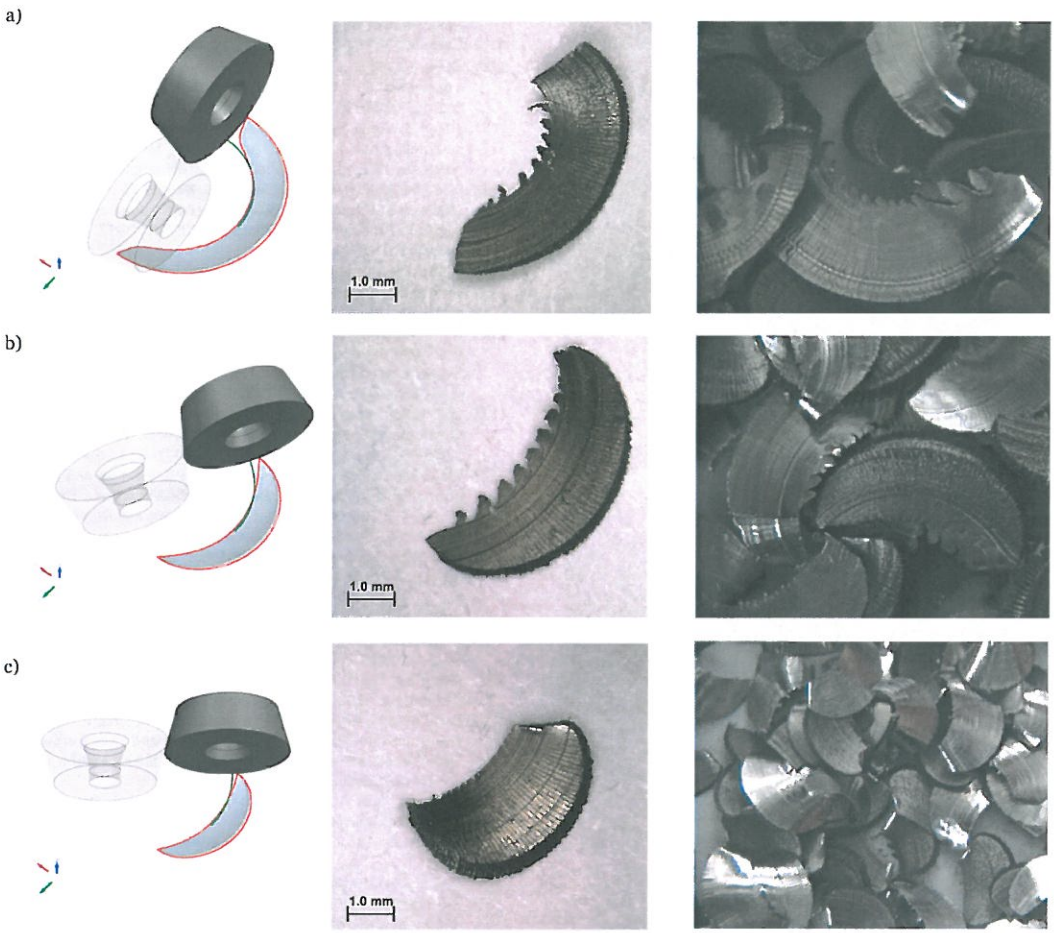

Fig. 23. Correlation the chip morphology with the undeformed chip for: a) $\delta = 1.37°$,b) $\delta = 10°$ and c) $\delta = 18.62°$.

in the basic plane of the cutting edge was carried out, which is also an original approach developed within the framework of this work.

- Within the range of tested variables, the life of the torus milling cutter increases with increasing values of the inclination angle. This is essentially due to a decrease in the value of the work angle of the tool with a simultaneous dispersion of the value of the maximum thickness of the undeformed chip in the basic plane of the cutting edge.
- For small inclination angles, the values of the maximum thickness of the undeformed chip in the basic plane of the cutting edge (as a function of the contact angle) are more concentrated, resulting in a significant reduction in tool life and a faster formation of a notching-type wear form.
- For larger inclination angles, the values of the maximum thickness of the undeformed chip in the basic plane of the cutting edge (as a function of contact angle) are more widely dispersed along the length of the active arc of the cutting tooth segment, which generally results in milder loading conditions for the cutting edge, thus extending tool life.
- The precision of the developed model in terms of predicting tool wear area based on the maximum chip thickness distribution is 97 %. The error in predicting the maximum chip thickness does not exceed 15 %.

The developed 3D model of the instantaneous undeformed chip, together with the distribution of the maximum thickness of the undeformed chip along the active segment of the cutting edge in the basic plane of the cutting tooth, can form the basis of techniques and systems for predicting notching-type wear, in the process of multi-axis torus milling.

The developed model and the findings made in this work allow, among others, to approximate the wear area on the tool flank, model the wear along the active segment of the cutting edge and can be the basis for a method for predicting the location of stress concentration causing notching wear, which was demonstrated in the work [36].

The following recommendations for future studies are suggested in relation to the subject of this paper: firstly, consideration of the machining system's errors, and secondly, an extension of the torus milling cutter axis orientation in the step direction and tool deflection.

CRediT authorship contribution statement

Michał Gdula: Writing – review & editing, Writing – original draft, Visualization, Validation, Supervision, Resources, Methodology, Investigation, Formal analysis, Conceptualization.

Funding

This research received no external funding.

Declaration of competing interest

The authors declare that they have no known competing financial interests or personal relationships that could have appeared to influence the work reported in this paper.

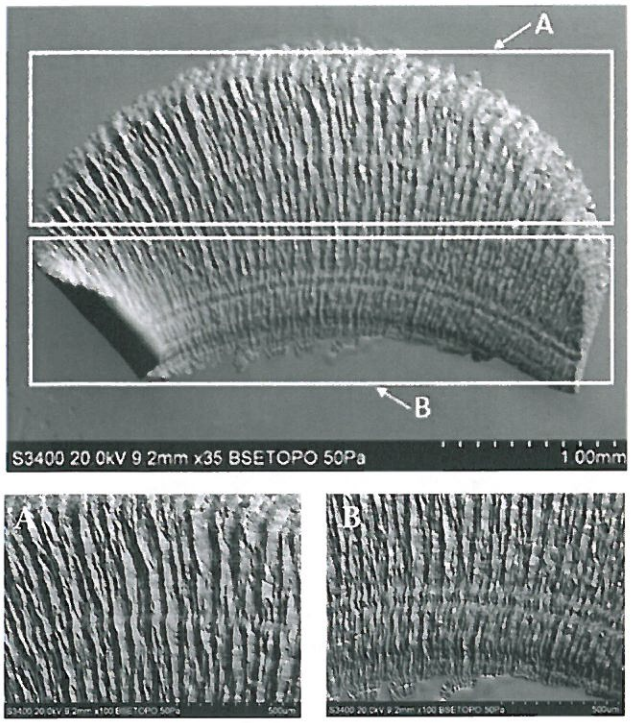

Fig. 24. Free surface chip characteristics: A-lamella structure at main area: and B-lamella structure at contact point motion area.

Data availability

Data will be made available on request.

References

[1] Zhuang K, Yang Y, Dai X, Weng J, Tian C, Gao Z. Multi-axis ball-end milling force prediction model considering the influence of cutting edge. Int J Adv Manuf Technol 2023;128:357–71. https://doi.org/10.1007/s00170-023-11890-4.

[2] Gdula M, Mrówka-Nowotnik G. Analysis of tool wear, chip and machined surface morphology in multi-axis milling process of Ni-based superalloy using the torus milling cutter. Wear 2023;520–521:204652. https://doi.org/10.1016/j.wear.2023.204652.

[3] Shi D-M, Huang T, Zhang X-M, Zhao S. Real-time monitoring of depth of cut in the multi-axis milling process with ball-end cutter. Procedia CIRP 2021;102:287–92. https://doi.org/10.1016/j.procir.2021.09.049.

[4] Huang T, Zhang X, Ding H. Decoupled chip thickness calculation model for cutting force prediction in five-axis ball-end milling. Int J Adv Manuf Technol 2013;69:1203–17. https://doi.org/10.1007/s00170-013-5099-2.

[5] Yang P, Yao C, Xie S, Zhang D, Tang DX. Effect of tool orientation on surface integrity during ball end milling of titanium alloy TC17. Procedia CIRP 2016;56:143–8. https://doi.org/10.1016/j.procir.2016.10.044.

[6] Silva LBD, Yoshioka H, Shinno H, Zhu J, Body Production Engineering Division, Honda Engineering Co., Ltd. 6–1 Hagadai, Haga-machi, Haga-gun, Tochigi 321–3395, Japan, Laboratory for Future Interdisciplinary Research of Science and Technology (FIRST), Institute of Innovative Research (IIR), Tokyo Institute of Technology, Yokohama, Japan. Tool orientation angle optimization for a multi-axis robotic milling system. IJAT 2019;13:574–82. https://doi.org/10.20965/ijat.2019.p0574.

[7] Guo M, Wei Z, Li S, Wang M, Gao H, Zhao Z, et al. Force model of freeform surface multi-axis machining with fillet end mill based on analytical contact analysis. Int J Adv Manuf Technol 2022;118:1283–94. https://doi.org/10.1007/s00170-021-07962-y.

[8] Gilles P, Cohen G, Monies F, Rubio W. Torus cutter positioning in five-axis milling using balance of the transversal cutting force. Int J Adv Manuf Technol 2013;66:965–73. https://doi.org/10.1007/s00170-012-4381-z.

[9] Chang Z, Qian J, Chen ZC, Wan N, Zhang D. Geometrical theory of cutting stock with torus end mills in five-axis CNC machining and its applications in machining simulation. Int J Adv Manuf Technol 2019;105:27–46. https://doi.org/10.1007/s00170-019-04064-8.

[10] Zhang Y, Xu R, Li X, Cheng X, Zheng G, Meng J. A tool path generation method based on smooth machine rotary angle and tilt angle in five-axis surface machining with torus cutters. Int J Adv Manuf Technol 2020;107:4261–71. https://doi.org/10.1007/s00170-020-05271-4.

[11] Sun S, Sun Y, Xu J, Lee Y-S. Iso-planar feed vector-fields-based streamline tool path generation for five-Axis compound surface machining with torus-end cutters. J Manuf Sci Eng 2018;140:071013. https://doi.org/10.1115/1.4039653.

[12] Zhang X, Wang X, Zhang P, Chen K, Cao F. Fast extraction of cutter-workpiece engagement for milling force prediction in multi-axis machining. Measurement 2024;231:114490. https://doi.org/10.1016/j.measurement.2024.114490.

[13] Zhang X, Wang X, Cao F, Zhang P. Quasi-real-time monitoring of variable milling parameters during multi-axis machining. Mechanical Systems and Signal Processing 2024;211:111196. https://doi.org/10.1016/j.ymssp.2024.111196.

[14] Sai L, Belguith R, Baili M, Dessein G, Bouzid W. An approach to modeling the chip thickness and cutter workpiece engagement region in 3 and 5 axis ball end milling. Journal of Manufacturing Processes 2018;34:7–17. https://doi.org/10.1016/j.jmapro.2018.05.018.

[15] Sadílek M, Poruba Z, Čepová L, Šajgalík M. Increasing the accuracy of free-form surface multiaxis milling. Materials 2020;14:25. https://doi.org/10.3390/ma14010025.

[16] Boz Y, Erdim H, Lazoglu I. A comparison of solid model and three-orthogonal dexelfield methods for cutter-workpiece engagement calculations in three- and five-axis virtual milling. Int J Adv Manuf Technol 2015;81:811–23. https://doi.org/10.1007/s00170-015-7251-7.

[17] Li Z, Xiao J, Han X, Zhang W. Z-map based cutting force prediction for elliptical ultrasonic vibration-assisted milling process. Int J Adv Manuf Technol 2022;120:3237–49. https://doi.org/10.1007/s00170-022-08976-w.

[18] Wojciechowski S. The estimation of cutting forces and specific force coefficients during finishing ball end milling of inclined surfaces. Int J Mach Tool Manuf 2015;89:110–23. https://doi.org/10.1016/j.ijmachtools.2014.10.006.

[19] Li G, Liu Y, Zhao D, Dai L, Zhou H, Jing X. A general method for instantaneous undeformed chip thickness calculation in five-axis milling based on Boolean operations. Int J Adv Manuf Technol 2021;116:2325–34. https://doi.org/10.1007/s00170-021-07576-4.

[20] Wojciechowski S, Maruda RW, Nieslony P, Krolczyk GM. Investigation on the edge forces in ball end milling of inclined surfaces. International Journal of Mechanical Sciences 2016;119:360–9. https://doi.org/10.1016/j.ijmecsci.2016.10.034.

[21] Lazoglu I, Liang SY. Modeling of ball-end milling forces with cutter Axis inclination. J Manuf Sci Eng 2000;122:3–11. https://doi.org/10.1115/1.538885.

[22] Karakılınç U, Ergene B, Yalçın B, Aslantaş K, Erçetin A. Comparative analysis of minimum Chip thickness, surface quality and Burr formation in Micro-milling of wrought and selective laser melted Ti64. Micromachines 2023;14:1160. https://doi.org/10.3390/mi14061160.

[23] Kim D-H, Woo W-S, Chu W-S, Ahn S-H, Lee C-M. Development of multi-axis laser-assisted milling device. 2017.

[24] Mikó B, Zentay P. A geometric approach of working tool diameter in 3-axis ball-end milling. Int J Adv Manuf Technol 2019;104:1497–507. https://doi.org/10.1007/s00170-019-03968-9.

[25] Aslantas K, Alatrushi LK, Bedir F, Kaynak Y, Yılmaz N. An experimental analysis of minimum chip thickness in micro-milling of two different titanium alloys. Proceedings of the Institution of Mechanical Engineers, Part B: Journal of Engineering Manufacture 2020;234:1486–98. https://doi.org/10.1177/0954405420933098.

[26] Ozkirimli O, Tunc LT, Budak E. Generalized model for dynamics and stability of multi-axis milling with complex tool geometries. J Mater Process Technol 2016;238:446–58. https://doi.org/10.1016/j.jmatprotec.2016.07.020.

[27] Nowakowski L, Blasiak S, Skrzyniarz M. Influence of the relative displacements and the minimum Chip thickness on the surface texture in shoulder milling. Materials 2023;16:7661. https://doi.org/10.3390/ma16247661.

[28] Wojciechowski S, Krajewska-Śpiewak J, Maruda RW, Krolczyk GM, Nieslony P, Wieczorowski M, et al. Study on ploughing phenomena in tool flank face – workpiece interface including tool wear effect during ball-end milling. Tribology International 2023;181:108313. https://doi.org/10.1016/j.triboint.2023.108313.

[29] Wojciechowski S, Matuszak M, Powałka B, Madajewski M, Maruda RW, Królczyk GM. Prediction of cutting forces during micro end milling considering chip thickness accumulation. Int J Mach Tool Manuf 2019;147:103466. https://doi.org/10.1016/j.ijmachtools.2019.103466.

[30] Wang Z, Zhou J, Ren J, Shu A. Predicting surface residual stress for multi-axis milling of Ti-6Al-4V titanium alloy in combined simulation and experiments. Materials 2022;15:6471. https://doi.org/10.3390/ma15186471.

[31] Uchikata S, Beaucamp A, Takeuchi Y. 5-Axis control finishing for decreased tool Wear. Procedia CIRP 2017;63:313–7. https://doi.org/10.1016/j.procir.2017.03.320.

[32] Luo M, Luo H, Zhang D, Tang K. Improving tool life in multi-axis milling of Ni-based superalloy with ball-end cutter based on the active cutting edge shift strategy. J Mater Process Technol 2018;252:105–15. https://doi.org/10.1016/j.jmatprotec.2017.09.010.

[33] Zeng H, Yan R, Du P, Zhang M, Peng F. Notch wear prediction model in high speed milling of AerMet100 steel with bull-nose tool considering the influence of stress concentration. Wear 2018;408:228–37. https://doi.org/10.1016/j.wear.2018.05.024.

[34] Zhang L, Zheng M, Zhang W, Li K. Influence and prediction of tool wear on workpiece surface roughness based on milling topography analysis. Int J Adv Manuf Technol 2022;122:1883–96. https://doi.org/10.1007/s00170-022-09939-x.

[35] Gdula M. Determination and analysis of working diameters and working angle of the torus cutter blade in multi-axis machining in the aspect of tool Wear. IJMERR 2024;13:535–47. https://doi.org/10.18178/ijmerr.13.5.535-547.

[36] Gdula M, Nowotnik A, Mrówka-Nowotnik G. Analysis the surface integrity taking into account the tool wear stage in the multi-axis torus milling of a Ni-based

superalloy using the active cutting edge segment change technique and new approach for machining aircraft engine blades. Wear 2025;574:206095. https://doi.org/10.1016/j.wear.2025.206095.

ARTYKUŁ

A3

dr inż. Michał Gdula
Politechnika Rzeszowska im. I. Łukasiewicza
Wydział Budowy Maszyn i Lotnictwa
Katedra Technik Wytwarzania i Automatyzacji

Rzeszów, dn. 23.04.2025 r.

OŚWIADCZENIE WSPÓŁAUTORA

Oświadczam, że w pracy:

lp.: ....A3.....

Gdula M., Mrówka-Nowotnik G., Nowotnik A.: *Modeling and comprehensive mechanism analysis of torus milling cutter wear in multi-axis milling of Ni-based superalloy using the active cutting edge segment change technique.* Tribology International, Vol. 204 (2025) 110509. IF 6.1, MNiSW 200 pkt.;

mój wkład w powstanie tej pracy polegał na: analizie aktualnego stanu wiedzy w zakresie tematu pracy, opracowaniu metodyki badań, przeprowadzeniu badań eksperymentalnych oraz modelowych, opracowaniu modeli trwałości oraz modeli zużycia narzędzia w oparciu o procedurę estymacji nieliniowej modelem regresji o charakterze quasi-liniowym, tj. funkcji wykładniczej, opracowaniu statystycznym modeli metodą analizy wariancji ANOVA, przeprowadzeniu analizy zużycia narzędzia wraz z walidacją opracowanych modeli, przeprowadzeniu analizy mechanizmów zużycia, interpretacji wyników i opracowaniu wniosków, wykonaniu wykresów, rysunków oraz tabel, współudziale w opracowaniu manuskryptu, koordynowaniu procesu wydawniczego.

Gdula Michał
.....
Podpis
dr inż. Michał Gdula

dr hab. inż. Grażyna Mrówka-Nowotnik, prof. PRz
Politechnika Rzeszowska im. I. Łukasiewicza
Wydział Budowy Maszyn i Lotnictwa
Katedra Nauki o Materiałach

Rzeszów, dn. 23.04.2025 r.

OŚWIADCZENIE WSPÓŁAUTORA

Oświadczam, że w pracy:

lp.: A3

Gdula M., Mrówka-Nowotnik G., Nowotnik A.: *Modeling and comprehensive mechanism analysis of torus milling cutter wear in multi-axis milling of Ni-based superalloy using the active cutting edge segment change technique.* Tribology International, Vol. 204 (2025) 110509. IF 6.1, MNiSW 200 pkt.;

mój wkład w powstanie tej pracy polegał na: przeprowadzeniu obserwacji i wykonaniu mikrofotografii powierzchni przyłożenia zużytych ostrzy skrawających, z zastosowaniem mikroskopu skaningowego (SEM) wyposażonego w układy EDS i WDS do analizy składu chemicznego oraz układ EBSD umożliwiającego wyznaczenie tekstury materiałów oraz identyfikację składników fazowych, współudziale w opracowaniu korekty wersji roboczej manuskryptu.

.....
Podpis
dr hab. inż. Grażyna Mrówka-Nowotnik, prof. PRz

dr hab. inż. Andrzej Nowotnik, prof. PRz
Politechnika Rzeszowska im. I. Łukasiewicza
Wydział Budowy Maszyn i Lotnictwa
Katedra Nauki o Materiałach

Rzeszów, dn. 23.04.2025 r.

OŚWIADCZENIE WSPÓŁAUTORA

Oświadczam, że w pracy:

lp.: A3

Gdula M., Mrówka-Nowotnik G., Nowotnik A.: *Modeling and comprehensive mechanism analysis of torus milling cutter wear in multi-axis milling of Ni-based superalloy using the active cutting edge segment change technique.* Tribology International, Vol. 204 (2025) 110509. IF 6.1, MNiSW 200 pkt.;

mój wkład w powstanie tej pracy polegał na: przeprowadzeniu obserwacji i wykonaniu mikrofotografii powierzchni natarcia zużytych ostrzy skrawających, z zastosowaniem mikroskopu skaningowego (SEM) wyposażonego w układy EDS i WDS do analizy składu chemicznego oraz układ EBSD umożliwiającego wyznaczenie tekstury materiałów oraz identyfikację składników fazowych, współudziale w opracowaniu korekty wersji roboczej manuskryptu.

.....
Podpis
dr hab. inż. Andrzej Nowotnik, prof. PRz

Tribology International 204 (2025) 110509

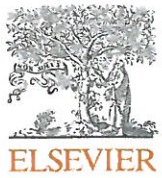

Contents lists available at ScienceDirect

Tribology International

journal homepage: www.elsevier.com/locate/triboint

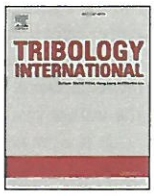

Modeling and comprehensive mechanism analysis of torus milling cutter wear in multi-axis milling of Ni-based superalloy using the active cutting edge segment change technique

Michał Gdula [a,*], Grażyna Mrówka-Nowotnik [b], Andrzej Nowotnik [b]

[a] Department of Manufacturing Techniques and Automation, Rzeszow University of Technology, al. Powstańców Warszawy 12, Rzeszow 35-959, Poland
[b] Department of Materials Science, Rzeszow University of Technology, al. Powstańców Warszawy 12, Rzeszow 35-959, Poland

ARTICLE INFO

Keywords:
Multi-axis milling
Ni-based superalloy
Active cutting edge segment
Wear modeling
Wear mechanism

ABSTRACT

Tool wear is a significant challenge in the milling of difficult-to-cut materials such as Ni-based superalloys, as it directly impacts the machining process and surface integrity. In multi-axis torus milling, the complex and varying cutting conditions of cutter-workpiece engagement make predicting wear particularly difficult. This paper proposes models for predicting the life and flank wear of a torus milling cutter equipped with round cutting inserts in a multi-axis milling process. A novel technique for changing the active segment of the cutting edge, specifically designed for torus milling cutters, was used. The cutter-workpiece engagement (CWE) zone was determined and equal width cutting belts were determined on the torus surface. Analysis of wear mechanisms revealed the uneven distribution of flank wear. Based on cutting tests under defined CWE and high-speed machining conditions, predictive models for tool life and flank wear were developed for each active cutting edge segment. These models were calibrated using multi-axis milling experiments on the Inconel718 superalloy. Results demonstrate that the predictive models achieve high accuracy, with average percentage errors below 15 % for tool life and 13 % for flank wear. The models enable precise predictions of torus milling cutter life and flank wear in multi-axis milling of Inconel718 while utilizing the active cutting edge segment change technique. Analysis of wear mechanisms indicated that abrasive and adhesive wear dominates, and flaking and notching wear was also observed.

1. Introduction

Continuous advances in the field of aviation, particularly in aircraft engine technology, are resulting in the increasing use of difficult-to-cut materials. This necessitates a greater need for advanced methods and new techniques for machining these materials. One of the main representatives of this group of materials are Ni-based superalloys, which are a class of metallic materials that combine high strength at high temperature, high strength and resistance to degradation in corrosive or oxidising environments [1]. In addition, Ni-based superalloys even exhibit excellent properties in terms of thermal fatigue and thermal stability, which is why they are widely used in aerospace engine parts such as compressor disks, turbine disks, bearing rings, housings, blades, and other parts operating at high temperatures [2]. However, these materials are characterised by low thermal conductivity and high precipitation hardening, making machining at high cutting speeds significantly more difficult. These are the main reasons for the rapid wear of the tool, which affects both the cutting process and the technological surface layer [3–5]. Hence, tool wear is one of the main challenges in precision machining of Ni-based superalloys commonly used in the aerospace industry [6,7].

One of the main and still being developed methods of machining aerospace parts is multi-axis machining [8,9], including precision face multi-axis milling in the tool-attraction type variant [10,11]. The capabilities of this technological variant of multi-axis machining have, in turn, recently been significantly supplemented by special strategies: adaptive control strategy of the tool axis depending on the radius of curvature of the workpiece profile in terms of geometric accuracy and surface quality [12] and continuous variation of the tool axis vector along the curvature of the workpiece profile [13] and shift of the active cutting edge [7] in terms of tool wear. In the last two works, a ball end-mill tool was used for machining. Gdula at work [14], used a torus

* Corresponding author.
E-mail address: gdulam@prz.edu.pl (M. Gdula).

https://doi.org/10.1016/j.triboint.2025.110509
Received 2 December 2024; Received in revised form 23 December 2024; Accepted 2 January 2025
Available online 9 January 2025
0301-679X/© 2025 Elsevier Ltd. All rights are reserved, including those for text and data mining, AI training, and similar technologies.

milling cutter for machining, and developed a model of the torus milling cutter axis orientation technique by varying the active segment of the cutting edge based on the working angle of the cutting blade, also in terms of wear. This article continues the series [6,12,15] of research by the author in this area.

It is now worth noting that, in industrial practice, the torus milling cutter is increasingly being used to machine the surfaces of complex aerospace parts made from Ni-based superalloys. This cutter, both in its monolithic form and essentially in the form of indexable round cutting inserts, is used especially in the finishing stage, mainly because of its unique geometry [16]. However, changing the torus milling cutter axis orientation leads, among other things, to a change in the active cutting edge, a displacement of the contact point and thus a change in the cutting conditions [17]. Chang et al. [18] developed mathematical models for the three-dimensional simulation of undeformed chips in multi-axis machining with a torus milling cutter. They formulated the geometrical basis for the determination of cutting edges and their critical points. Zhu et al. [19] conducted a study of the mechanism of the effect of the axis orientation of the torus milling cutter on the machining errors induced by the cutting force. They based their research on a model of the instantaneous cutting force at the contact point. On this basis, they determined the optimal subset of tool axis orientation angle values. Musfirah et al. [20] conducted an experimental study and evaluation of the effectiveness of cryogenic cooling during Inconel 718 milling compared to the dry milling process. This comparison included the wear rate of a single-edge torus milling cutter, cutting force, surface roughness, and microstructure changes in a three-axis high speed machining (HSM) milling process. They showed that the use of the cryogenic technique reduces cutting force by up to 23 % and improves roughness by up to 88 %. Zeng et al. [4] conducted an analysis of the mechanisms of notch formation and the impact of wear in the three-axis milling process using the torus milling cutter. They quantitatively characterised the degree of stress concentration at the cutting edge. Halim et al. [2] conducted a performance study of a single-edge torus milling cutter. They conducted experiments at different machining parameters and the analysis included tool life, wear patterns and mechanisms, and their relationship to chip morphology.

It can be seen from the above that tool wear has a huge direct impact on both the cutting process and the surface integrity and dimensional accuracy of the finished part. Hence, researchers are attempting to model wear but are generally limited to turning and three-axis milling processes using the ball end-mills. Attanasio et al. [21] conducted a comparative study of response surface methodology (RSM) and artificial neural network (ANN) fitting techniques for tool wear prediction. They experimentally verified the models, showing that the ANN model provides a better approximation than RSM in predicting the magnitude of tool wear parameters. Kasim et al. [22] developed a model to predict the location of notch wear and used it to calculate the maximum load exerted on the cutting blade during the cutting process. Yan et al. [23] developed a thermal model to describe the variation in temperature at the cutting edge of the tool, taking into account its wear. They proposed a way to optimise the feed rate in terms of temperature distribution and validated the developed model. Luo et al. [7] developed a ball end-mill wear model using a linear approximation. In turn, Zeng et al. [4] developed a predictive model of notch wear depth that takes into account the effect of stress concentration. Manso et al. [24] performed micro-milling tests and the magnitude of the parameters that affected wear was determined using ANOVA analysis of variance. Zhu and Zhnag [25] proposed and verified a wear model with adjustable coefficients to predict the cutting force, taking into account different stages of wear. An et al. [5] developed an analytical model of the width of the flank wear band in the side milling process, for which the average prediction error is 15.87 %. Wiciak-Pikuła et al. [26] proposed multilayer perceptron models (MLP) to predict tool wear, and used mean square error (MSE) as the main criterion for model selection and quality assessment. Baig et al. [27] proposed using the vibration signature during turning to predict tool life using an ANN. Bjerke et al. [28] attempted to develop a thermodynamic framework for a method to predict the interaction between tool, coating, workpiece material, coolant and atmospheric oxygen. This method can predict the phase composition and the driving force of degradation and the formation of protective interaction products in the cutting zone. Zhang et al. [29] proposed and verified a general wear model with adjustable coefficients. They experimentally verified the model developed by comparing it with other wear models. They used analysis of variance methods for modelling, for which the coefficient of determination was 98 % for the experimental data. Huang i Lee [30] used sensor fusion in conjunction with deep machine learning to estimate tool wear and surface roughness. They obtained their input from the experimental tests carried out. As a result, they developed a system to monitor tool wear in online consumption with an alarm. Wang et al. [31] proposed a tool wear prediction model based on power signals. They conducted drilling process experiments to calibrate and validate the model. Cheng et al. [32] developed a method to predict the tool wear curve during machining based on the relationship between tool wear rate and cutting parameters. They derived the wear influence factor, as a modulating parameter, from the model developed. They experimentally verified the model, obtaining an accurate prediction of tool wear. Kamble et al. [33], on the other hand, developed a hybrid Taguchi-ANN tool wear prediction method. In order to develop the hybrid model, they carried out numerous turning tests and parameters were selected by Taguchi analysis and a response table. In contrast, they used ANNs to predict and analyse tool wear. They showed that using the Lvenberg-Marquard algorithm to train the neural network, they obtained the lowest MSE value. Du and Sun [34] proposed a model for predicting torus cutter wear in Ti6Al4V multi-axis milling with TiAlN coated inserts. They analysed the cutting zone with the determination of the contact length of the cutting edge wear. By analysing the properties of the wear profile of the cutter in multi-axis milling, i.e. abrasive and adhesive wear, they established a model for the prediction of lateral surface wear, which takes into account the hardness of the coating and the cutting temperature model. They calibrated and validated the proposed model experimentally. They obtained the accuracy of the model with an average percentage error of 12.76 %. It is also worth noting the thorough position of physics-based tool wear models. They can contribute significantly to the development of the models proposed in this work. Feng et al. in the paper [35] They proposed an analytical predictive model of tool blade wear during laser-assisted milling, based on the principles of abrasive, adhesive and diffusive wear. They accounted for the laser effect by treating the laser beam as a heat source on the top surface. They also took into account the convection of heat between the top surface and the surroundings. In turn, in the paper [36], they performed an inverse analysis of tool life based on five process parameters, predicting tool life from guessed process parameters, which is defined as a progressive problem, and using an iterative gradient search to find the process parameters for the next iteration, which is defined as an inverse problem. And in the paper [37], they proposed a predictive model for the flank wear rate of the end-mill tool during ultrasonic vibration-assisted milling.

In summary, in the field of multi-axis milling, the strategy of changing the orientation of the cutter axis in order to extend the life of the cutter is currently an important focus of research. This is due to the complex machining conditions in the cutter-workpiece engagement (CWE) zone, which makes the prediction of wear significantly more difficult. This paper presents models for the prediction of flank wear dedicated to an independently developed technique that changes the active cutting edge segment of the torus milling cutter (ACESCT) [14]. Tests were carried out for multi-axis milling of a selected Ni-based superalloy using the torus milling cutter with indexable TiAlN coated carbide round cutting inserts. In doing so, the CWE for each active segment was analysed by adopting machining parameters relative to the nominal diameter of the cutter (conventional approach) and relative to the contact point (proposed unconventional approach). An uneven

distribution of flank wear characteristics for individual segments was revealed, indicating the influence of a geometric-kinematic factor in the process studied. Therefore, the models were developed using a non-linear estimation method and deriving the free word as a constant in the given model, while taking into account the multi-axis milling conditions. The coefficients of the developed models are calibrated using the Levenberg-Marquardt algorithm, and the accuracy of the models is based on treatment tests. Finally, cutting tests were performed to validate the torus cutter life and wear models developed in this work. The wear mechanisms of the active cutting edge segments are analysed by SEM and EDS, taking into account selected tool wear criterion thresholds.

2. Material and methods

2.1. Experimental stand

Inconel 718, a Ni-based superalloy commonly used in the aerospace industry, was selected as the workpiece material. As shown in Fig. 1, the precision milling experiments were carried out on a multi-axis CNC machining centre. This machine tool is equipped with a SINUMREIK 840Di numerical control system. The producer of this control recommends programming the rotary axes to five decimal places to increase the accuracy and tolerance of the multi-axis toolpath. The TPL multi-axis milling process was conducted by applying steel torus milling cutter body R300–016A20L-08L for indexable round cutting inserts R300–0828E-PL. The cutter body has a neutral geometry. Round cutting inserts are made of S30T cemented carbide grade. Grade S30T has fine-grain cemented carbide and a TiAlN PVD coating. TiAlN PVD coated WC inserts are used for milling Ni-based superalloys, which has good mechanical properties, including high hardness and Young's modulus and high wear resistance [38]. The round cutting inserts used in the tests have the following parameters: the rake angle is 20°, the clearance angle is 15° and the insert radius is 4 mm. Thus, a special case of a torus cutter (*Horn Torus*) was used for the machining tests, where the geometric-kinematic theories of the machining process can be extended to the other two geometric types of this tool [14].

The digital microscope Dino-Lite (AM7515MZT) is used to capture the wear image. The microscope uses a 5MP sensor (with a magnification range of 10x to 220x and Automatic Magnification Reading) and a maximum resolution of 2592 × 1944 pixels. It is equipped with Dino-Capture 2.0 software for image acquisition and analysis. The measurement was carried out directly on the CNC machine tool without the need to remove the cutting tool from the spindle socket, according to a own developed procedure for measuring wear on a multi-axis CNC machine tool [14].

2.2. Experiments of multi-axis milling with torus cutter

A general schematic of the projected toolpaths together with the CWE zone is shown in Fig. 2. On the basis of his own research, the kinematic case of multi-axis milling of the pulling-tool type (TPL) was adopted [6]. In each experiment, flood cooling was used and, starting each new experiment, the round cutting inserts were replaced with a new set. The multi-axis milling process using the active cutting edge segment change technique [14] generally involves four axes of the machine tool. The fifth axis is activated in the case of free surface machining.

As shown in Fig. 1, the X-axis and the Z-axis determine the plane and direction of the feed, while the Y-axis determines the direction perpendicular to the feed direction. The inclination angle δ is determined by the B axis around the Y axis. The life of the torus milling cutter was determined by the local flank wear (VB_{Bmax}), until it reached the threshold value of 0.2 mm [39]. The multi-axis milling process was interrupted at specified intervals to identify wear patterns and measure wear rates. The research was carried out in two stages, for which two groups of treatment conditions were adopted, respectively. For the first stage, conditions were determined conventionally relative to the principal diameter of D_{PRIN}, while for the second stage, conditions were determined unconventionally, i.e. relative to the contact diameter of

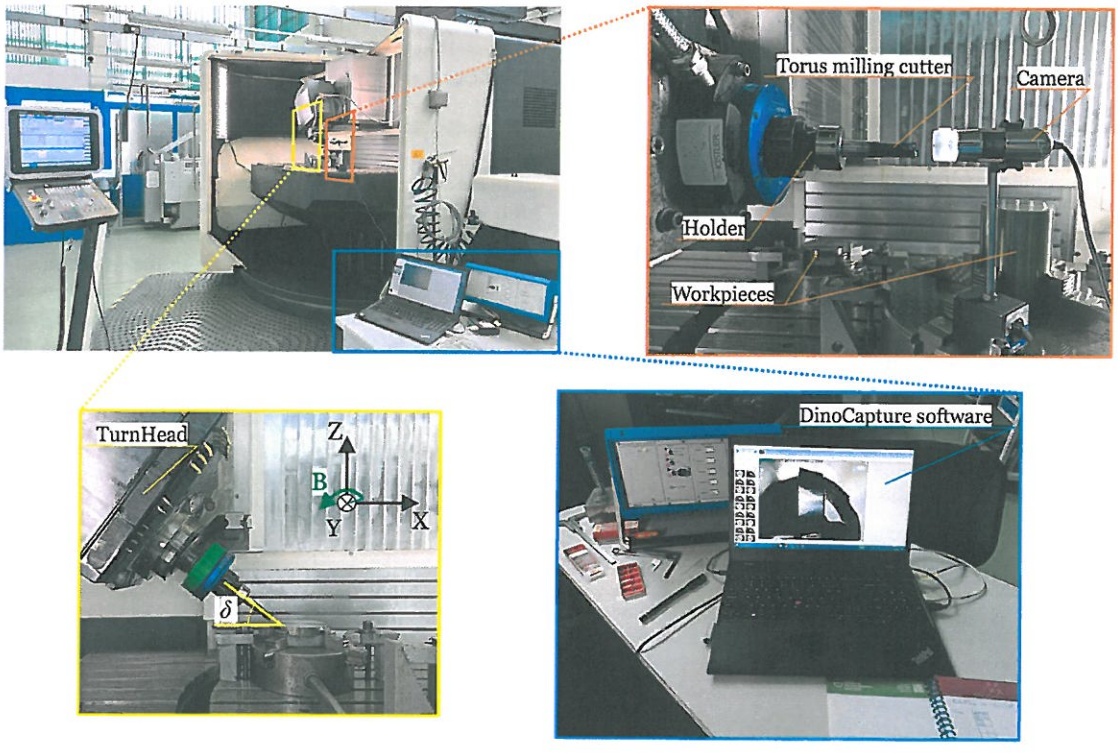

Fig. 1. Experimental stand.

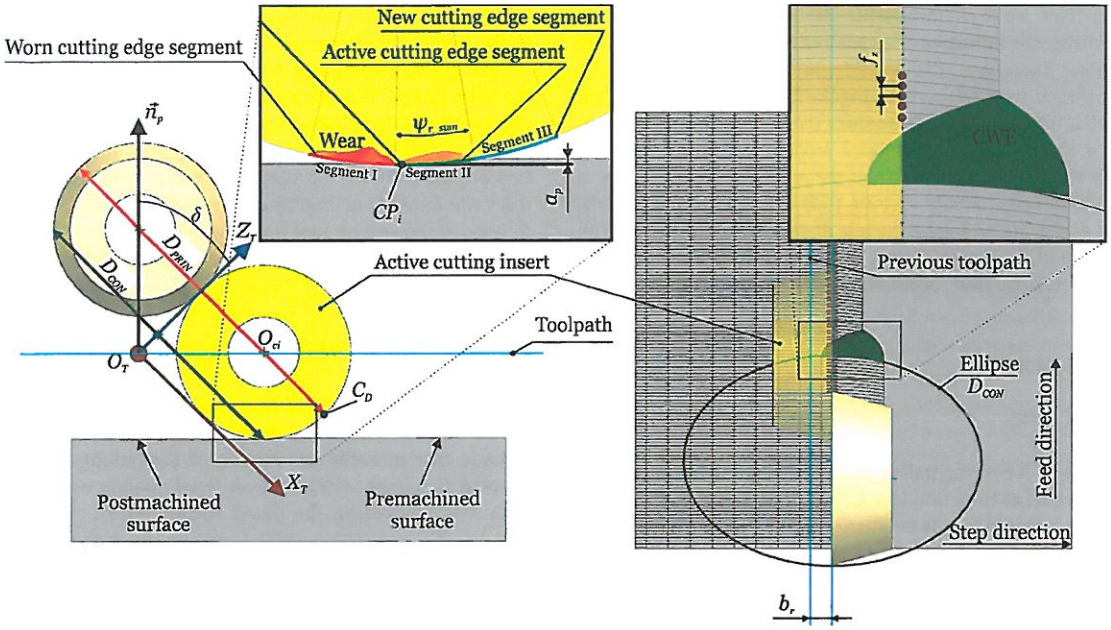

Fig. 2. Torus cutter trajectory.

D_{CON} (i.e. at the contact point CP_i) [14]. The cutting conditions (CCs) for stages I and II are given in Table 1 and Table 2, respectively. The b_r step value was calculated according to a model of own development, which was based on the criterion of uniform roughness. During the machining process, vibration, clamping errors, and blade run-out inevitably occur, resulting in uneven wear on each tooth. Therefore, VB_{Bmax} is the average maximum flank wear of each tooth. In order to determine the wear mechanisms of the torus milling cutter, the worn round cutting inserts were then thoroughly investigated using a Scanning Electron Microscope (SEM) (model HITACHI S–3400 N). This microscope is equipped with EDS and WDS systems for chemical composition analysis and an EBSD system for determining the texture of the materials and identifying phase components.

2.3. Torus cutter wear progression analysis

As shown in Fig. 3(a), the resulting reference wear curves present a classic three-phase pattern. Then, as shown in Fig. 3(b), in the initial wear phase of the cutter, mainly adhesion of the chip substrate to the cutting edge (built-up-edge BUE) was observed. This is because the cutting edge is sharp and undergoes lapping at a relatively high wear rate in the first wear phase. During the cutting process in the second phase, a protective layer is formed both on the flank and in a certain section in the zone near the cutting edge on the rake surface, the rate of wear gradually decreases taking on a steady exploitation wear of a quasilinear nature. The cutter blade and workpiece are subjected to constant friction, with scratches and chips forming on the flank surface, leading to wear of the coating exposing the base material of the cutting blade. The cutting edge gradually dulls. As shown in Fig. 3(c), there are scratches on the workpiece surface and adhesion of residual chip fragments, indicating that the main wear mechanisms are abrasive wear and adhesive wear. Tool wear in HSM cutting is most influenced by the cutting speed, as well as the cutting heat. This heat is generated by the intense friction between the tool cutting blade and the chip and the tool cutting blade (cutting edge) and the surface being shaped. In the precision milling process, due to the short contact time between the cutting blade of the tool and the chip and the cutting blade of the tool and the surface of the shaped workpiece, the temperature in the cutting zone does not exceed 500°C [23,34]. On this basis, it can be assumed that there is no obvious elemental diffusion phenomenon [40].

3. Modelling of the torus milling cutter life and wear for ACESC technique

3.1. Outline of the ACESCT

In the active cutting edge segment change technique (ACESCT) of the torus milling cutter, the basis of which is described in work [14], it is assumed that the kinematic roughness height R_{th} is uniformly distributed over the machined surface both in the feed direction and in the direction perpendicular to it. Therefore, for torus geometry, changing the orientation of the tool axis forces a change in the toolpath distance b_r. Therefore, in this proposed machining technique, two things are determined, the inclination angle δ of the tool axis based on the cutting blade working angle ψ_r and the distance of the toolpaths br based on the criterion R_{th}. The wear of the torus milling cutter at any point on the cutting edge can be viewed as a monotonic increasing function of the cutting time t_c. The wear of the torus milling cutter is assumed to be

Table 1
Cutting Conditions (CCs) for I-st stage of the research.

	Inclination angle δ [°]	Total work angle of cutting blade ψ_{r_sum} [°]	Distance between toolpaths b_r [mm]	Axial depth of cut a_p [mm]	Feed per tooth f_t [mm/t]	Cutting speed (at p. C_D) v_c [m/min]	Cutting speed (at p. CP_i) v_c [m/min]	Criterion R_{th}=R_{thvf} [mm]	Criterion VB_{Blim} [mm]
Segment I	1.10946	24.55056	1.6				71		
Segment II	24.55056	47.99167	0.411	0.3	0.1549	140	99	0.0015	0.2
Segment III	47.99167	71.43277	0.335				122		

Table 2
Cutting Conditions (CCs) for II-nd stage of the research.

	Inclination angle δ [°]	Total work angle of cutting blade ψ_{r_sum} [°]	Distance between toolpaths b_r [mm]	Axial depth of cut a_p [mm]	Feed per tooth f_t [mm/t]	Cutting speed (at p. C_D) v_c [m/min]	Cutting speed (at p. CP_i) v_c [m/min]	Criterion $R_{th}=R_{thvf}$ [mm]	Criterion VB_{Blim} [mm]
Segment I	1.10946	24.55056	1.6			274			
Segment II	24.55056	47.99167	0.411	0.3	0.1549	197	140	0.0015	0.2
Segment III	47.99167	71.43277	0.335			160			

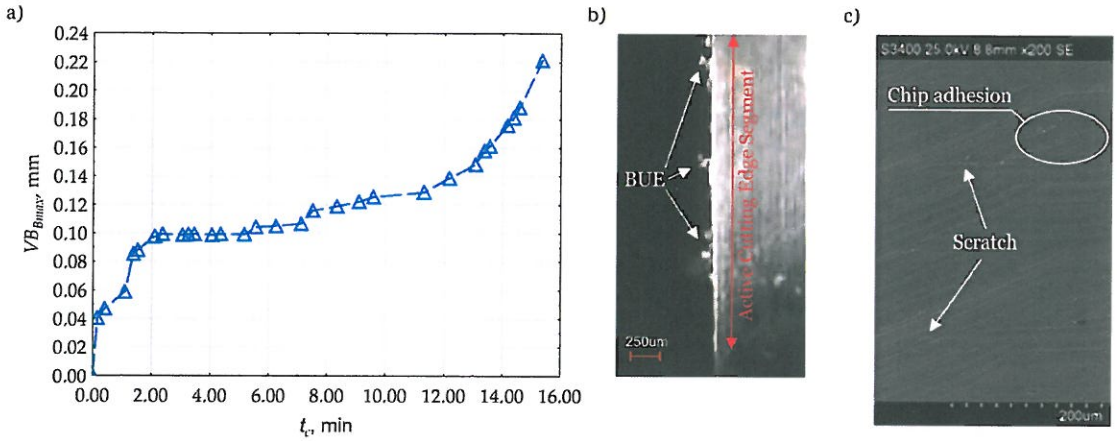

Fig. 3. (a) Wear curve [39], (b) Wear behavior of round cutting insert and BUE, (c) Machined surface morphology picture of workpiece.

essentially determined by the cutting speed v_c. Thus, it is also assumed that within the CP_i contact point and within the range of a given active cutting edge segment, the differences in cutting speed are negligibly small and insignificant in terms of wear. Thus, let $VB_B(g_{CPi},t_c)$ denote the wear of the torus milling cutter, which is a function of both the conventional latitude of the contact point CP_i and the cutting time t_c.

Let VB_{Blim} be the given wear threshold of the torus cutter (assumed to be 0.2 mm). The inverse of $VB_B(g_{CPi},t_{c_max})$ then gives the maximum allowable cutting time (MACT$\equiv t_{c_max}$) for a cutting belt $s_{b,i}$ based on the CP_i contact point of a given active cutting edge segment, as described by relation (1):

$$\left(g_{CP_i}, t_{c_\max}\left(g_{CP_i}\right)\right) = VB_B^{-1}(VB_{Blim}) \tag{1}$$

The idea behind the ACACES strategy can be described as follows. During the movement of the cutter, the cutter is in contact with the workpiece on a temporary patch of the machined surface, which is called cutter - workpiece engagement, and the material removed is the cut layer in the form of a chip. The CWE is located on the torus action surface of the cutter within the adopted depth of cut a_p, as shown in Fig. 4.

Because the tool continues to rotate about its axis, the CWE $s_{CWE,i}$ at the contact point CP_i forms a belt $s_{b,i}$, which was named the cutting belt. At any moment of cutting, the segment on the cutting edge that is inside the CWE is called the active cutting edge segment, i.e. the cutting edge of the active segment is cutting at that moment. n addition, segments that are outside the CWE have been extracted that are passive cutting edge segments where, in the first boundary condition, the edge of the passive segment is not cutting and is sharp and, in the second boundary condition, the edge of the passive segment is not cutting and is worn according to a defined criterion. During multi-axis milling of collision-free surfaces, the active cutting belt can be arranged segment by segment, as well as according to any combination. Each segment has a unique inclination angle δ, and the t_{c_max} of the corresponding active cutting belt is calculated using the relationship (1). When this time is reached, the inclination angle δ is adjusted so that the new segment becomes active. This process is iterated until all usable segments are involved in the cutting process. In the case of multi-axis milling of flat surfaces and sculptured surfaces with a convex, biconvex, or saddle form, a limiting criterion was applied due to collisions. This criterion rejects from use segments for which, at a given angle orientation δ, the total cutting blade working angle $\psi_{r_sum} \geq 90°$, (i.e. the sum of the cutting blade working angles from the individual cutting edge segments is equal to or greater than 90°).

Taking into account the results obtained by Zhang et al. [41], relationship (1) should be supplemented with wear prediction models dedicated to each segment separately, in order to obtain the appropriate surface layer parameters taking into account tool wear.

3.2. Tool life models relative to the contact point for ACES

First, the torus milling cutter life was determined with reference to the contact point in the CWE for each active cutting edge segment (ACES). In this way, the maximum cutting times t_{c_max} were obtained for the assumed VB_{Blim} criterion under the specified machining conditions (see Table 1 and Table 2). Thus, threshold information was obtained as to when a given active cutting edge segment had to be changed to a new one.

The tool life can be expressed as a function of the machining conditions, as described by relationship (2) [42].

$$t_{c_\max} = C_t v_c^p f_t^q \tag{2}$$

Given that in this work, all further testing and analysis is done by reference to the point of formation of the machined surface, i.e. the CP_i, contact point, the cutting speed vc must also be done by reference to the CP_i point. Hence, after taking this into account, relationship (2) takes the form (3).

$$t_{c_\max} = C_t\left(\frac{2\pi\left(R_T + r_p\sin(\delta)\right)n}{1000}\right)f_t^q \tag{3}$$

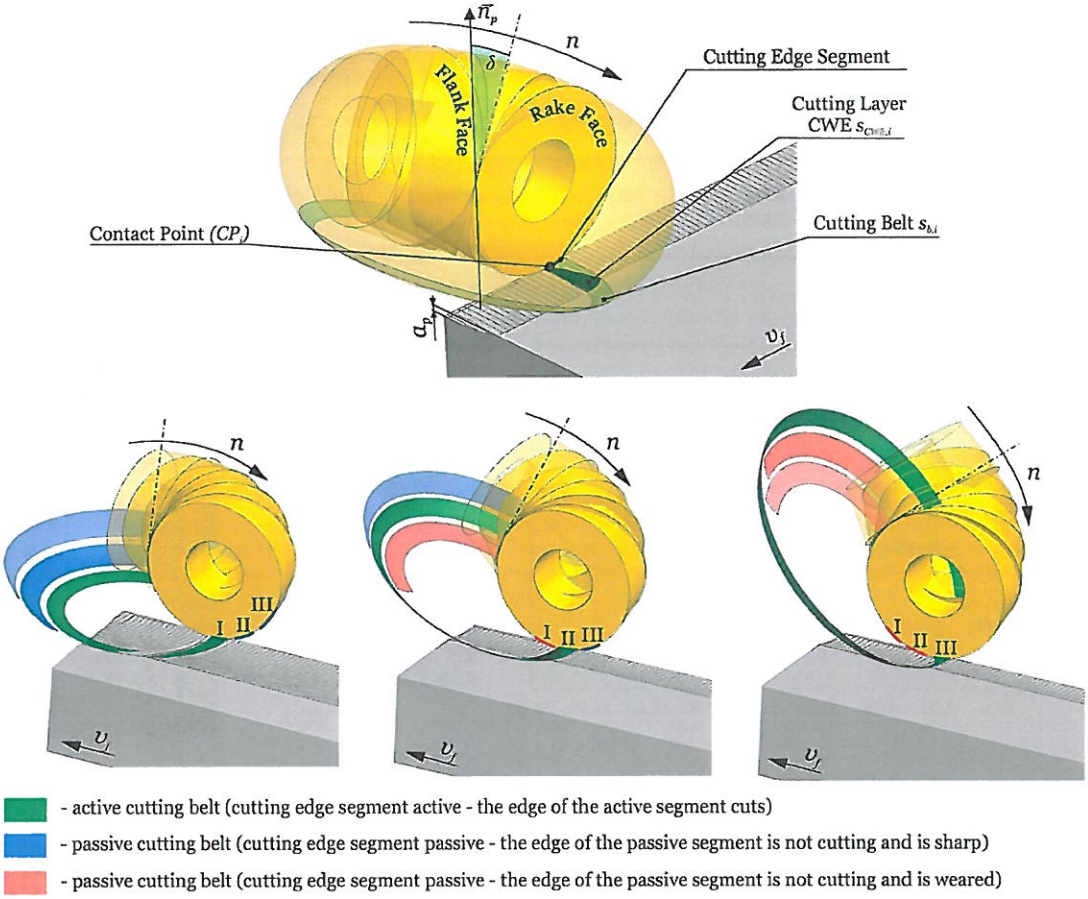

Fig. 4. The idea of the ACESC technique and sequences of active cutting belts.

where t_c is tool life, R_T and r_p are geometrical parameters of the torus, n is spindle speed, and δ is inclination angle of the tool axis, C_t, p and q are constants for a given cutter-workpiece material pair and are identified from machinability tests.

Inconel718 superalloy machinability tests were performed for three groups at different cutting speeds and feed rates with three repetitions of these tests. The arithmetic mean was then calculated for each group, respectively. The first and second groups had the same feed per blade but different cutting speeds, while the second and third groups had the same cutting speed but different feed per blade values. In each test group, the cutter is used to cut with constant cutting conditions until the tool wear reaches the set VB_{Blim} threshold. The durability of the tool was then recorded. So for each active segment of the cutting edge of the torus milling cutter. Based on the above, the machinability test results are shown in Table 3.

From tests No. 1 and No. 2 the first constant parameter p was calculated by Eq. (4), and from tests No. 2 and No. 3 the second constant parameter q was calculated by Eq. (5).

Table 3
Machinability tests for each stage of the research.

No.	Cutting speed v_c [m/min]	Feed per tooth f_t [mm/t]	I segment T_c [min]	II segment T_c [min]	III segment T_c [min]
1	40	0.2	22	61	90
2	140	0.2	1	6	6
3	140	0.1	2	10	8

$$p = \frac{\ln(T_{c1}/T_{c2})}{\ln(v_{c2}/v_{c1})} \tag{4}$$

$$q = \frac{\ln(T_{c3}/T_{c2})}{\ln(f_{c2}/f_{c3})} \tag{5}$$

Substituting p and q into Eq. (6) gives the third constant parameter C_t as

$$C_t = \frac{t_{c_max(no.of\ segment)}}{\left(\frac{2\pi(R_T + r_p\sin(\delta))n}{1000}\right)^p f_t^q} \tag{6}$$

Then the resulting torus milling cutter life Equations for tested tool-Inconel718 pair becomes:

$$t_{c_maxI} = 5.237{\cdot}10^4 \left(\frac{2\pi(R_T + r_p\sin(\delta))n}{1000}\right)^{2.384} f_t^{1.112} \tag{7}$$

for segment I

$$t_{c_maxII} = 2.523{\cdot}10^4 \left(\frac{2\pi(R_T + r_p\sin(\delta))n}{1000}\right)^{1.851} f_t^{0.877} \tag{8}$$

for segment II

$$t_{c_maxIII} = 1.787{\cdot}10^5 \left(\frac{2\pi(R_T + r_p\sin(\delta))n}{1000}\right)^{2.161} f_t^{0.415} \tag{9}$$

for segment III

It can be seen that the cutting speed has a greater influence than the

feed rate per tooth on the torus milling cutter life in the parameter range studied under HSM cutting conditions. As the cutter axis inclination increases, the effect of feed per tooth on the tool life decreases. This indicates that the toolpaths distance b_r is positively correlated with the parameter q in the developed models. In contrast, the effect of cutting speed on tool life with increasing values of the milling axis inclination for segment I is greatest, while it is smallest for segment II. For segment III, it is increasing again. This may be due to changes in the CWE zone, which requires a separate study in this scope.

3.3. Tool wear models relative to the contact point for ACES

The modelling of torus milling cutter wear for individual active cutting edge segments (ACES) was carried out through data analysis engineering. These data were acquired as a result of multi-axis milling tests performed in accordance with the adopted cutting conditions (see Table 1 and Table 2). The cutting parameters in these tests, as well as the results obtained from these tests, are related relatively to the forming point of the machined surface, i.e. the CP_i contact point (see Fig. 2 and Fig. 4). This represents an original approach by the lead author in the context of wear modelling for the case of multi-axis milling.

For each segment, the machining tests were repeated three times, always for a new set of round cutting inserts. These inserts were appropriately angularly positioned in the cutter body according to a method of own development [39]. The wear of VB_{Bmax} was measured at defined intervals. These intervals were defined on the basis of previous own studies [6]. This definition was supplemented by the maximum cutting times t_{c_max} determined in Subsection 3.2. for the assumed VB_{Blim} criterion and taking into account the uniform distribution of the kinematic roughness parameters on the machined surface []. In this way, a complete data set of VB_{Bmax} wear was obtained over the full range of cutting time $0 \leq t_c \leq t_{c_max}$.

To modelling of the tool wear an advanced nonlinear estimation procedure was used with a regression model according to a own quasi-linear function. This function is described by the equation in exponential form (10), in the set of real numbers $\boldsymbol{R}$:

$$y = b0 + b1 \cdot (b2^{x}); \quad f : \mathbb{R} \rightarrow \mathbb{R} \tag{10}$$

where: y is the dependent variable, i.e. wear VB_{Bmax} , $b0$ is the free word, $b1$ and $b2$ are parameters (for the x independent variable), x is the independent variable, i.e. cutting time t_c.

The modelling procedure adopted is based on nonlinear regression. Each of the models presented in the overview Table 4 is estimated using ANOVA/MANOVA analysis of variance techniques, i.e. using the least-squares estimation procedure of the nonlinear model. The objective of least-squares estimation is to minimise the sum of squares of deviations from predicted values, i.e. to find the parameter set of the best fit. The Levenberg-Marquardt (L-M) algorithm, which is an extension of the Gauss-Newton algorithm, was used as the estimation method. For finding estimates of the least squares parameters, second-order derivatives are not calculated. Instead, the L-M algorithm solves a system of linear equations in each iteration to calculate the gradient of the fit. In each of the six modelling cases considered, the maximum number of iterations was set at 8000, the convergence criterion at 0.000001 and the initial values of the parameters $b0$, $b1$ and $b2$ at 0.00001.

Tibco Statistica 13 software was used to model consumption, which, in the case of this work, allows the introduction of a own regression function (10). The results of torus milling cutter wear modelling are shown below. Overview Table 4 shows the modelling relationships obtained from the modelling of the VB_{Bmax} wear of the torus milling cutter for the active cutting edge segments (I, II, and III) of the round cutting insert, respectively, in the range for stage one and stage two of the adopted cutting conditions (see Table 1 and Table 2). Table 5 presents the estimation statistics and ANOVA variation analysis results for models (11), (12) and (13), while Table 6 presents the estimation statistics and ANOVA variation analysis results for models (14), (15) and (16).

As mentioned above, estimation statistics and ANOVA analysis of variance were used to assess the quality of the fit. They are measures of the quality of forecasting with the developed model. The significance level was established at $p = 0.05$, and the confidence intervals of the parameter scores at 95 %.

For all the models obtained, the values of the parameters $b0$, $b1$, and $b2$ are significant. The standard errors for these parameters fall within the two-sided closed set $SE \in < 0.001, 0.008 >$.

Based on the estimation statistics and the results of the ANOVA analysis of variance for the models obtained, it can be concluded that there are statistically significant differences between the mean values of the dependent variable y, i.e. VB_{Bmax} wear during cutting time t_c. This is essentially evidenced by the test in the last line for each model (Regression of the adjusted total). This test assesses the level of statistical significance of an improvement in the prediction of the value of the dependent variable compared to a simple prediction based only on the mean (for the dependent variable). This is the F Snedecor test. As can be seen, an F-statistic greater than the critical value of F_{kr} was obtained for each model. This value was determined by the number of degrees of freedom (DF) and the adopted significance level p and was selected from publicly available statistical tables of the F distribution.

The quality of the fit of the model to the data is indicated by the coefficient of determination R^2. The closer the value is to unity, the better the fit. For all the models received, the fit can be described as very good. In each case, R^2 is above 0.9 meaning that the regression explains more than 90 % of the variation in the dependent variable. Complementing the coefficient of determination R^2 is the coefficient of convergence φ^2. This coefficient determines what proportion of the observed variation in the dependent variable in the sample does not fit the model, i.e. falls within its error. The fit of the model is better the closer the value of φ^2 is to zero. In the modelling procedure, the convergence factor was set at $\varphi^2 = 0.000001$ for all cases.

Figs. 5 and 6 show the curves of the developed models and the normalcy graphs of the rests.

The normality graphs of the rests (i.e. the errors) follow a normal distribution. This graph is produced as a scatterplot of expected normal values relative to the rests. In each case, the rests were observed to align along a straight line. The rests appear to closely match the normal distribution, so it can be concluded that the proposed own exponential model in the form of Eq. (10) is an accurate fit to the data.

Based on the observation of the model plots of the wear curves and the values of the parameters $b0$, $b1$, and $b2$ of the models themselves, it was noted that the way in which the cutting speed is determined, i.e., relating it relatively to the C_D or CP_i point (see Fig. 2), is important in terms of tool wear.

When the cutting speed is determined relative to the CD point, the tool wear in the first phase differs significantly between the active segments I, II, and III of the cutting edge. This is due to the varying cutting

Table 4
Overview of derived torus milling cutter wear models for active cutting edge segments.

	Tool wear models for CCs of the I-st stage range	Tool wear models for CCs of the II-nd stage range
Segment I	VB_{Bmax} =0.092 +0.001•1.306^{tc} (11)	VB_{Bmax} =0.066 +0.0001•9.805^{tc} (14)
Segment II	VB_{Bmax} =0.068 +0.008•1.105^{tc} (12)	VB_{Bmax} =0.063 +0.0134•1.272^{tc} (15)
Segment III	VB_{Bmax} =0.006 +0.040•1.146^{tc} (13)	VB_{Bmax} =0.012 +0.0383•1.465^{tc} (16)

Table 5
Estimation statistics and ANOVA variance analysis results for the derived models by CCs I-stage range.

$VB_{Bmax} = 0.092 + 0.001 \bullet 1.306^{tc}$	Sum of squares	Degrees of freedom	Mean square	*F*-value	*p*-value	R^2
Regression	1.409	3.0	0.4696	3643.746	0.0000	0.95
Residual	0.010	85.0	0.0001			
Total	1.419	88.0				
Adjusted grand total	0.114	87.0				
Regression of the adjusted total	1.409	3.0	0.4696	358.173	0.0000	
$VB_{Bmax} = 0.068 + 0.008 \bullet 1.105^{tc}$	Sum of squares	Degrees of freedom	Mean square	*F*-value	*p*-value	R^2
Regression	1.3160	3.0	0.4386	6518.912	0.0000	0.98
Residual	0.0055	82	0.0001			
Total	1.3215	85				
Adjusted grand total	0.1610	84				
Regression of the adjusted total	1.3160	3.0	0.4386	228.792	0.0000	
$VB_{Bmax} = 0.006 + 0.040 \bullet 1.146^{tc}$	Sum of squares	Degrees of freedom	Mean square	*F*-value	*p*-value	R^2
Regression	0.9250	3.0	0.3083	2065.925	0.0000	0.97
Residual	0.0064	43	0.0001			
Total	0.9314	46				
Adjusted grand total	0.1524	45				
Regression of the adjusted total	0.9250	3.0	0.3083	91.005	0.0000	

Table 6
Estimation statistics and ANOVA variance analysis results for the derived models by wg CCs II-stage range.

$VB_{Bmax} = 0.066 + 0.0001 \bullet 9.805^{tc}$	Sum of squares	Degrees of freedom	Mean square	*F*-value	*p*-value	R^2
Regression	0.8512	3.0	0.2837	406.097	0.0000	0.94
Residual	0.0300	43	0.0006			
Total	0.8812	46				
Adjusted grand total	0.2473	45				
Regression of the adjusted total	0.8512	3.0	0.2837	51.621	0.0000	
$VB_{Bmax} = 0.063 + 0.0134 \bullet 1.272^{tc}$	Sum of squares	Degrees of freedom	Mean square	*F*-value	*p*-value	R^2
Regression	1.2305	3.0	0.4101	2590.087	0.0000	0.97
Residual	0.0115	73	0.0001			
Total	1.2420	76				
Adjusted grand total	0.1906	75				
Regression of the adjusted total	1.2305	3.0	0.4101	161.324	0.0000	
$VB_{Bmax} = 0.012 + 0.0383 \bullet 1.465^{tc}$	Sum of squares	Degrees of freedom	Mean square	*F*-value	*p*-value	R^2
Regression	0.6925	3.0	0.2308	1127.859	0.0000	0.96
Residual	0.0075	37	0.0002			
Total	0.7000	40				
Adjusted grand total	0.1134	39				
Regression of the adjusted total	0.6925	3.0	0.2308	79.336	0.0000	

conditions at the CP_i, contact point, as can be seen in Table 1. This has a negative impact on the run-in phase of the tool in these segments, which can result in the tool losing its cutting properties more quickly. Differences in the first wear phase between segments can also be observed in the values of the parameter *b0* of the developed models for the CCs I-st stage. On average, in the first wear phase, the increase in flank wear as a function of cutting speed for the torus milling cutter was: $VB_{Bmax} = 0.01$ mm at $v_{c_CPi} = 25.5$ m/min.

In contrast, when the cutting speed is determined relative to the CP_i, point, the tool wear in the first phase does not show significant differences between the active segments I, II, and III of the cutting edge. This is due to the constant cutting conditions at the CP_i contact point, as can be seen in Table 2 (the parameter that changes is the distance between the toolpaths b_r). This has a positive impact on the lapping phase of the tool in these segments. This can result in a uniform progression of tool wear and also in a uniform distribution of the technological surface layer parameters, regardless of the currently active cutting edge segment. The lack of significant differences in the first wear phase between the segments can also be seen in the values of the parameter *b0* of the models developed for the CCs II-nd stage. However, on the other hand, some anomalous value of the parameter *b0* was observed for model (16). An attempt to explain this is made in subsection 4.1.

4. Experimental verification and mechanism analysis

4.1. Torus milling cutter life models verification

In Fig. 7 are shown the experimental and predicted t_{c_max} values for each of the three segments of the ACESC technique, according to the adopted CCs I-st stage. In contrast, Fig. 8 shows the experimental and predicted t_{c_max} values for the specified three segments of the ACESC startegy, according to the adopted CCs II-st stage. The error bar represents the standard deviation.

The average prediction error of the models under CCs I-stage conditions does not exceed 5 %, indicating a high accuracy of these models. The torus milling cutter life for this case study followed a decreasing distribution in order: Segment II > Segment I > Segment III. This is consistent with the distribution of the *p* parameter values in the models developed for the individual active cutting edge segments. This indicates that the tool life is positively correlated with the *p* parameter, and that this parameter has a significant influence on the tool life of the machining technique analysed.

In contrast, the average prediction error of the models under CCs II-nd stage conditions is significantly different between the segments. It generally does not exceed 25 %, except in the case of segment III, for which it is 102 %. Rapid progressive flank wear of the notching type was observed for this segment (see Fig. 11 and Fig. 12). This is mainly due to the high cutting speed (friction) and the pulse forces generated during the cutting process with this segment [], so the carbide was subjected to progressive fatigue damage. The torus milling cutter life for stage II-nd

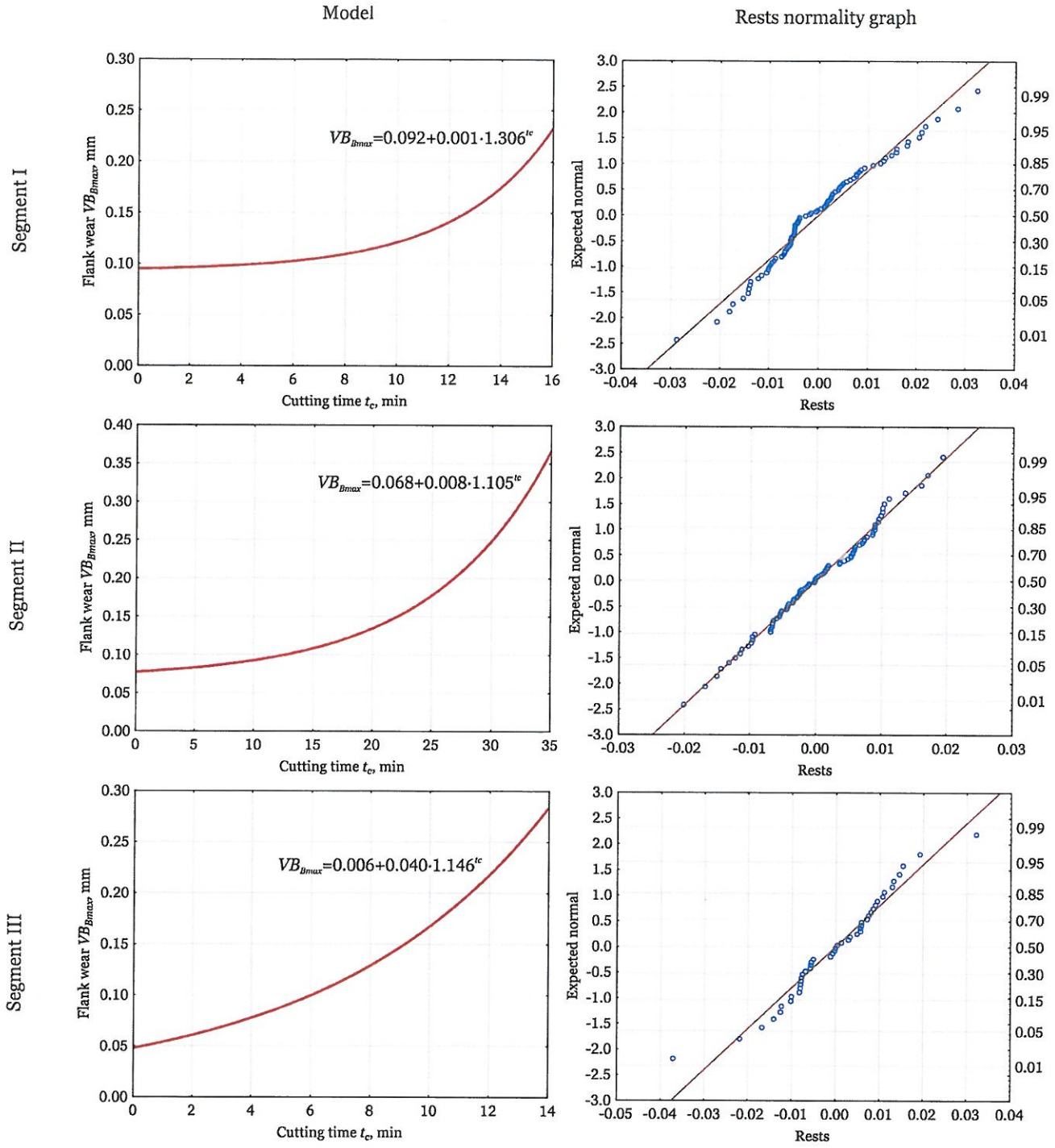

Fig. 5. The model wear curves graphs and the normality of the rests graphs for segments I, II, and III for CCs I-st stage.

CCs also adopts a decreasing distribution, but in the order: Segment II > Segment III > Segment I. This may be due to changes in the CWE zone contributed to, among other things, by the cutting speed in the contact zone, i.e. a completely different impact coefficient may have in this case the distance between toolpaths b_r. It should be taken into account that the largest b_r line distances, and thus cutting widths, occur for the first segment. There will also be longer contact between the blade and the workpiece. The tool life distribution obtained for the CCs II-nd stage corresponds to that of the p parameter from the developed models, which also adopts a decreasing distribution in the order Segment II > Segment III > Segment I. This indicates the validity of defining the cutting speed relative to the CP_i contact point.

Surprisingly, the longest torus milling cutter life was obtained for segment II under both adopted cutting conditions, regardless of whether the cutting speed was defined relative to the C_D or CP_i point. This is also independent of the decreasing row distance b_r. These and the issues described above clearly indicate the complexity of the changes occurring in the CWE zone as a result of changing the value of the inclination angle δ of the tool axis and thus the active segment of the cutting edge.

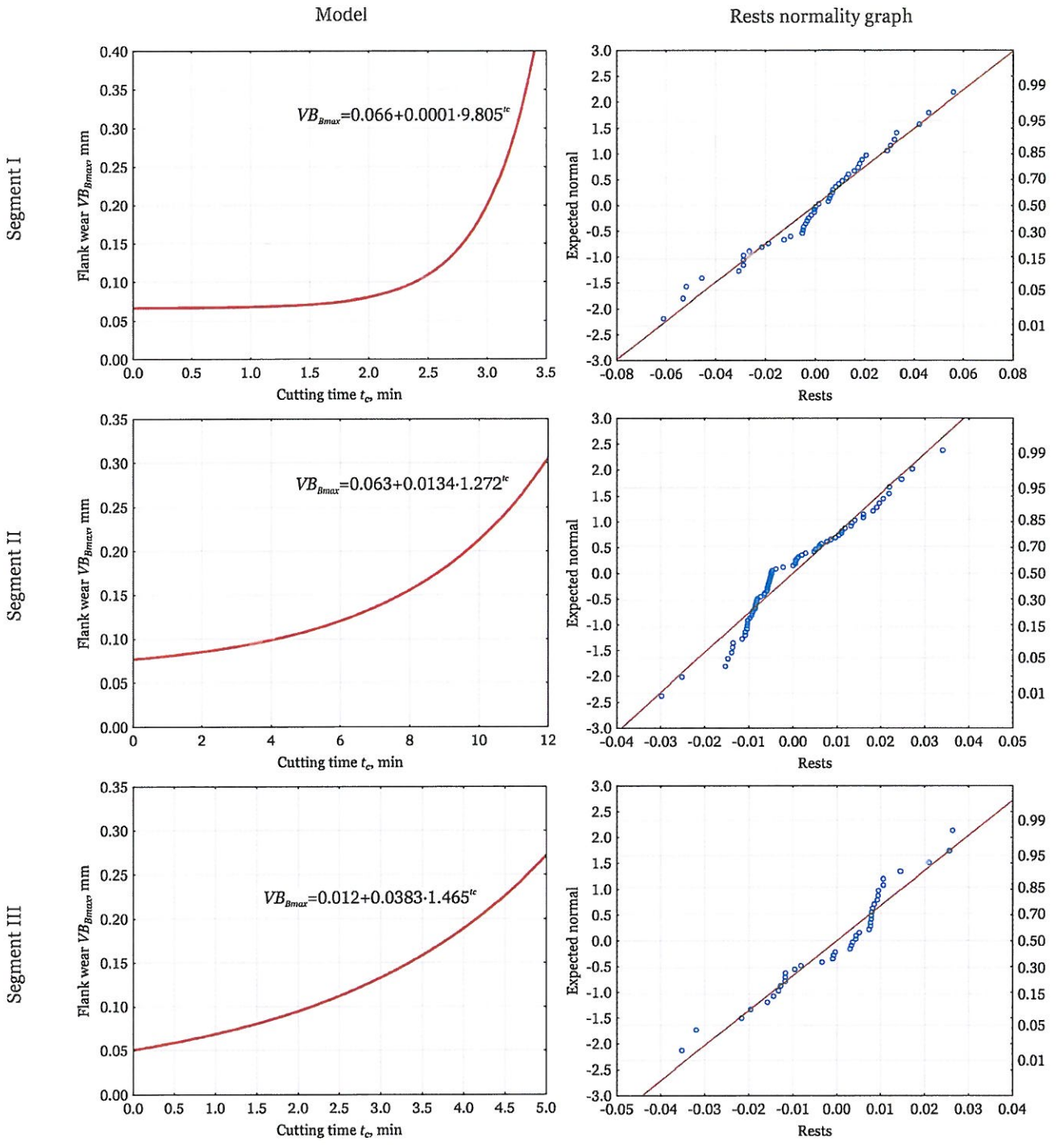

Fig. 6. The model wear curves graphs and the normality of the rests graphs for segments I, II, and III for CCs II-nd stage.

4.2. Torus milling cutter flank wear models verification

The flank wear models developed for each segment are validated under the conditions defined in Table 2 and Table 3. The results show that the measured values agree well with the predicted values. The average percentage errors for the segments do not exceed 16 %, as shown in Fig. 9. On this basis, it can be concluded that, using the developed models, it is possible to predict the wear trend for a given active cutting edge segment in multi-axis milling of Inconel 718 superalloy under HSM cutting conditions with a high degree of accuracy. The results clearly show that the inclination angle δ of the torus milling cutter axis has a significant effect on the cutting conditions in the CWE zone and therefore on the wear of the tool. This is mainly due to the following fact. Assuming that the spindle rotates at a constant speed n, along the curved outline of the cutting edge, the cutting speed varies, as demonstrated in the work [14,15]. In order to comprehensively show the impact of this phenomenon on tool wear, modelling and wear analyses were carried out according to the CCs I-st stage. As the inclination angle increases, the cutting speed at the cutting edge in these CCs also increases. On this basis, it can be assumed that this accelerates tool wear.

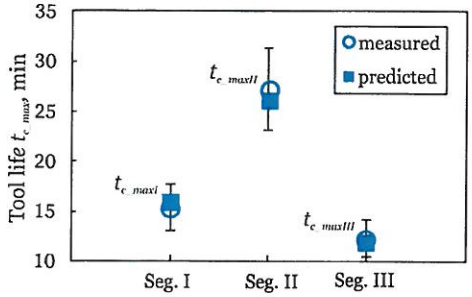

Fig. 7. Predicted and experimental values of T_c for segments from first stage of CCs.

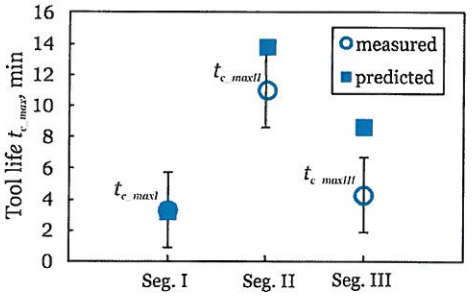

Fig. 8. Predicted and experimental values of T_c for segments from second stage of CCs.

However, as we find in the present study, the trend in tool wear and tool life is slightly different for each angle of inclination. A similar conclusion can be reached by analysing the flank wear of the bull-nose cutter results presented in the paper [34]. Therefore, it was decided to perform modelling and analysis according to CCs II-nd stage, i.e. the cutting speed was constant at the CP_i contact point regardless of the inclination angle δ. It was found, that the tool wear trend in these CCs is almost identical to that for CCs I-st stage. However, a fundamental difference occurs in the initial run-in phase and in the uniform wear phase between the models for the active cutting edge segments, for CCs I and CCs II respectively. When the cutting speed is defined as constant at the contact point CP_i, the flank wear values in the aforementioned phases are very close to each other, regardless of the angle of inclination of the tool axis. This was found on the basis of the free word values in the developed models (11) - (16) and on the basis of model wear curves (see Fig. 5 and Fig. 6). This can have an effect on the technological surface layer and surface integrity.

Furthermore, on the basis of relations (11), (12), (13) (free word) and the model wear curves shown in Fig. 5, it was found that an increase in the cutting speed at the CP_i contact point (CCs I-st stage) as a result of an increase in the inclination angle, influences the resulting tool wear values in the lapping stage. Wear in this phase decreases as the cutting speed increases. This means that, as a result of the predominantly adhesive wear while the blade is still sharp, the wear of the tool is already moving into the second phase at lower wear values. However, the progression of tool wear is clearly accelerated during cutting time t_c. On the other hand, on the basis of relations (14), (15), (16) (free word) and the model wear curves shown in Fig. 6, it was found that a constant cutting speed at the CP_i contact point (CCs II-nd stage), irrespective of the inclination angle of the tool axis, equally influences the obtained wear values in the lapping stage. Wear values do not vary. This is a major advantage because, regardless of the changes in CWE due to changes in inclination angle, the cutting process due to wear proceeds under similar conditions after the lapping phase for all active segments. It is important to note the relationship (16). In this case, the difference in the free word value can be attributed to the occurrence of cutting edge chipping and notching phenomena, mainly derived from friction and progressive fatigue damage, over a fairly short period of time.

As shown in Fig. 9, the error is reflected mainly in the lapping phase and at the beginning of the second wear phase of the torus milling cutter. This is because, as can be assumed, the temperature in the contact zone reaches an abruptly higher value than the ambient temperature. In addition, the cutter is sharp. Therefore, mainly adhesive wear occurs at this stage. The error is then reflected in the third phase of accelerated flank wear. This is due to the numerous microchipping and notching as well as flaking wear. In addition, there are many other causes of error throughout the cutting process, mainly including unavoidable machining vibrations, pulsating cutting forces, assembly errors and tool run-out, all of which affect the accuracy of the prediction.

4.3. Torus milling cutter wear mechanism analysis

After cutting tests, the round cutting inserts, and more specifically the worn segments of the cutting edge obtained as a result of machining, were subjected to observation of the morphological characteristics of wear using scanning electron microscopy (SEM) and energy dispersive spectrometry (EDS). It was found that there was mainly abrasive wear, adhesive wear, and friction of the coating. In addition, there is also notching and flaking wear. The wear in individual segments of the cutting edge is the result of the simultaneous interaction of various forms of wear, therefore a single form of wear does not fully reveal the wear mechanism as a whole [6].

Fig. 10. shows the wear morphology and elemental distribution of the initial wear phase of the side surface of segment I of the cutting edge, where v_c= 71 m/min and δ= 1.10946°. The coating directly within the cutting edge is damaged and exposes the substrate material. Arched scratches on the lateral surface were seen from tool rotation. The elemental content of Ni, Cr and Fe indicates that the bonding and deposition of Inconel718 elements on the coating surface occurs within the limits of wear. At this stage, the coating has not yet been completely peeled off and the deposited layer of elements takes on some protective function. Beyond the wear boundary, the chemical composition of the coating remains stable. This indicates that no rupture or oxidation reaction has occurred. Identical conclusions were also reached for the other cutting edge segments, so we are limited to discussing one representative example.

Fig. 11 and Fig. 12 shows the wear morphology and elemental distribution at the final wear stage of the torus milling cutter flank wear. It was observed that the wear characteristics are relatively obvious and that the wear limit has a distribution shaped like a triangle. Along the marked wear direction, the formation of notch type wear occurs, which is particularly evident for segment III. This may indicate that, due to changes in the CWE as a result of the inclination of the tool axis, there may be significant differences in the thickness distribution of the cut layer. At the wear boundary, the content of W and Al elements indicates that the coating has completely peeled off, exposing the cutter substrate. As can be observed in the EDS images and from the elemental percentages, there are numerous areas of binding and deposition of the workpiece material on the surface of the cutter substrate. It was found that within the wear boundary, due to continuous cutting, there is a propagation of the protective coating friction phenomenon along the wear direction and thus the cutting speed vector. It has been observed that the protective coating becomes lighter. It can only be assumed that the initiation of oxidation of the coating may be occur. No peeling or delamination of the coating was observed at the wear boundary. In turn, there are singular cracks. This shows the good adhesion of the coating to the substrate of the round cutting insert. The coating is removed from the tile substrate mainly by abrasion. The exposed substrate is gradually degraded, revealing numerous micro-chipping and micro-cracking of the cutting edge. Progressive notch type wear was found with increasing cutting speed. From the wear SEM images obtained, it can be concluded

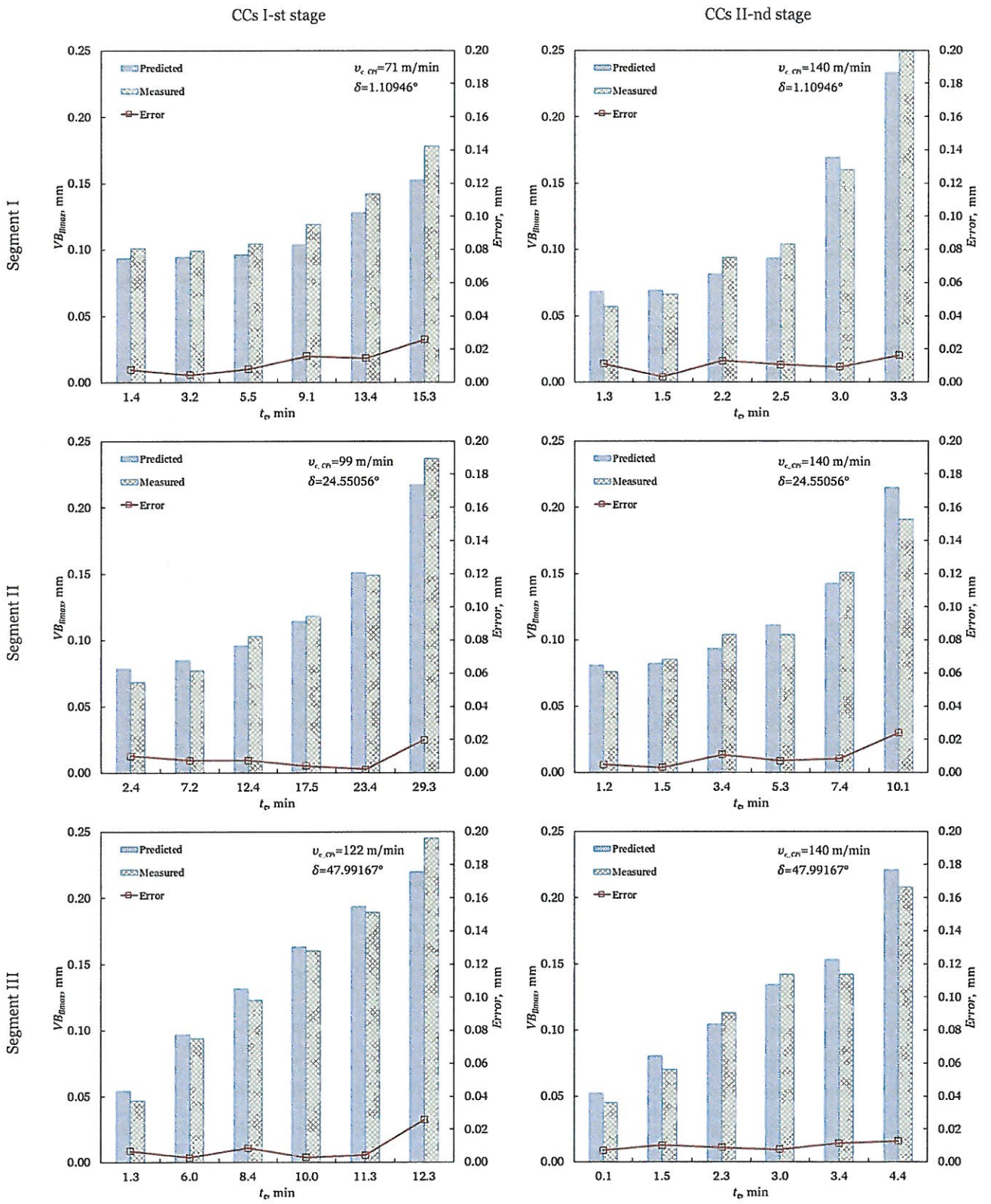

Fig. 9. Comparison of torus milling cutter flank wear results.

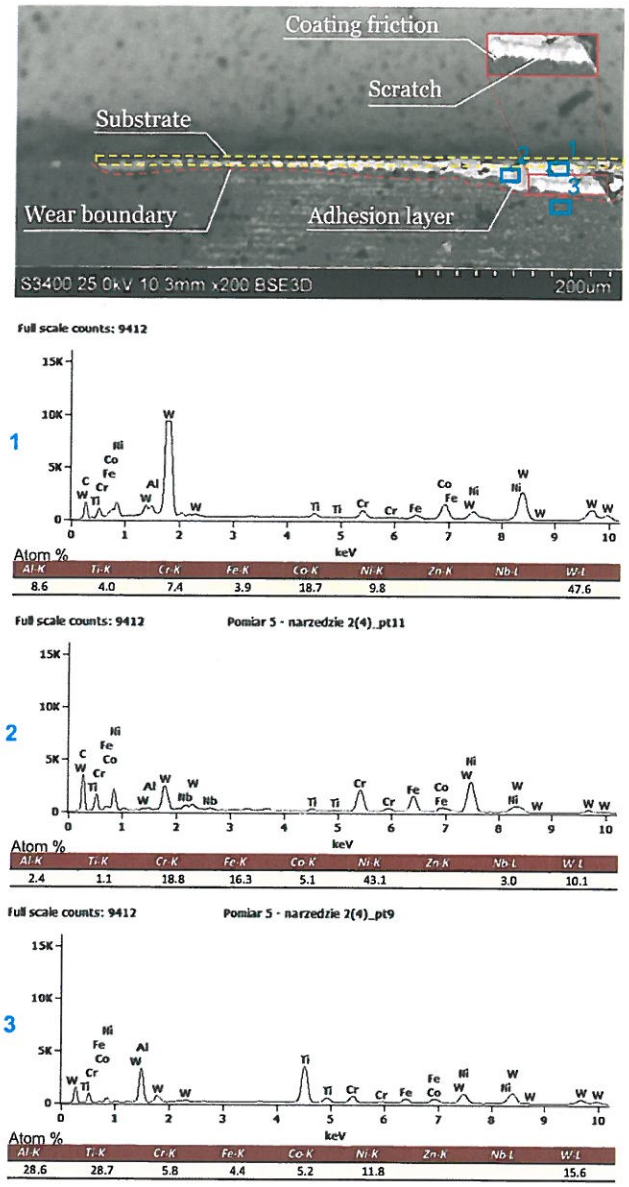

Fig. 10. Wear morphology and element distribution in the initial stage of flank wear.

that the wear of the notch is related to the thickness of the cut layer and the cutting conditions in the CWE. The main forms of wear are abrasive wear, adhesive wear and coating friction.

Fig. 13 and Fig. 14 shows the wear morphology and element distribution of the torus milling cutter rake face in the final wear stage. SEM images revealed severe crater wear on the rake surface, mainly due to abrasive and adhesive wear during the cutting process. Crater wear is caused by the continuous rubbing of the chip against the cutting surface, resulting in numerous scratches and the accumulation of workpiece material in the form of microchips. This significantly alters the geometry of the round cutting insert and the shape of the chip [6]. At the wear boundary, the element W content increases, indicating that the coating has been damaged and flaked (flaking), exposing the substrate and causing progressive wear. Flaking wear occurs mainly in the second segment. This indicates that there are some changes in the CWE due to the inclination of the tool axis that affect this type of wear. Outside the wear limit, the element *O* appears, indicating that the cutter coating has oxidised, forming an Al2O3 barrier. To some extent, this barrier plays a protective role, which may explain the significantly longer life of the cutter when machining with segment II. This is because the cutter-chip interface is not fully engaged, resulting in oxidation of the coating.

On both the flank and rake faces, the substrate of the round cutting insert within the wear ridge in all segments is exposed. This shows that the protective coating is peeling off completely. Elemental contents of Ni, Cr, Fe, Co, Nb, C and W were found in the range of the exposed area of the cutting insert substrate. This means that a certain amount of Inconel718 workpiece material is bound and deposited on the surface of the substrate.

No unambiguous build-up was observed on the cutting edge. This indicates effective chip removal during multi-axis milling. It is worth mentioning that a low content of element V was observed on the contact surface. This suggests minimal deposition and diffusion of workpiece material. This was not found on the lateral surface of the tool. This shows good cooling of the cutting zone at the CP_i contact point of the cutter-workpiece and, at the same time, poorer cooling conditions in the contact zone of the chip rake face. In this area, there is direct frictional contact and therefore the interaction of high temperatures and the formation of diffusion can be expected. This explains the occurrence of crater wear of round cutting inserts, which is mainly caused by abrasive, adhesive, and oxidative discolouration of the coating.

5. Conclusion

In the present work, a study of the wear of the torus milling cutter during the multi-axis milling process of the Ni-based superalloy Inconel718 has been carried out. An own technique was used to change the active segment of the cutting edge during machining. The torus milling cutter was defined by the geometry of the round cutting inserts with PVD TiAlN coating. For each active cutting edge segment, a life model and a flank wear prediction model were developed for high-speed machining. Cutting tests were carried out in two stages: under variable machining conditions and under constant machining conditions, where the cutting speed was defined relative to the contact point between the tool and the machined surface in the CWE zone. Validation tests of the models and a comprehensive analysis of the tool wear mechanisms were carried out, after which the following main conclusions were drawn:

1. The cutter-workpiece engagement zone was defined in multiaxis milling. On this basis, the active segments of the cutting edge and the cutting belts on the surface of the torus were determined. This forms the basis of the tool axis inclination angle distribution.
2. Based on machinability tests, torus milling cutter life models were determined for each segment, respectively. This is due to a change in the geometry of the cutter-workpiece engagement zone and thus the variable cutting conditions. These models take into account the geometrical parameters of the torus and the inclination angle of the tool axis. The results of the tests carried out showed that the durability models have good consistency, with an average percentage error of less than 15 %. The proposed tool life models can accurately predict the tool life of torus cutters for multi-axis high-speed machining.
3. Based on separate machinability tests, models were developed to predict the flank wear of the torus milling cutter, respectively, for each active cutting edge segment. To determine these models, an own nonlinear estimation function in exponential form was adopted. The models were developed for defined zones of cutter-workpiece engagement and therefore take into account abrasive wear and adhesive wear in multi-axis milling. The results showed that the models have good consistency, with an average percentage error of less than 13 %. The proposed models enable the accurate prediction of flank wear of the torus milling cutter in multi-axis high-speed machining.
4. Multi-axis milling of the Ni-based superalloy Inconel718 using a torus milling cutter with TiAlN coated round cutting inserts tests was carried out. The wear mechanisms in the individual active segments

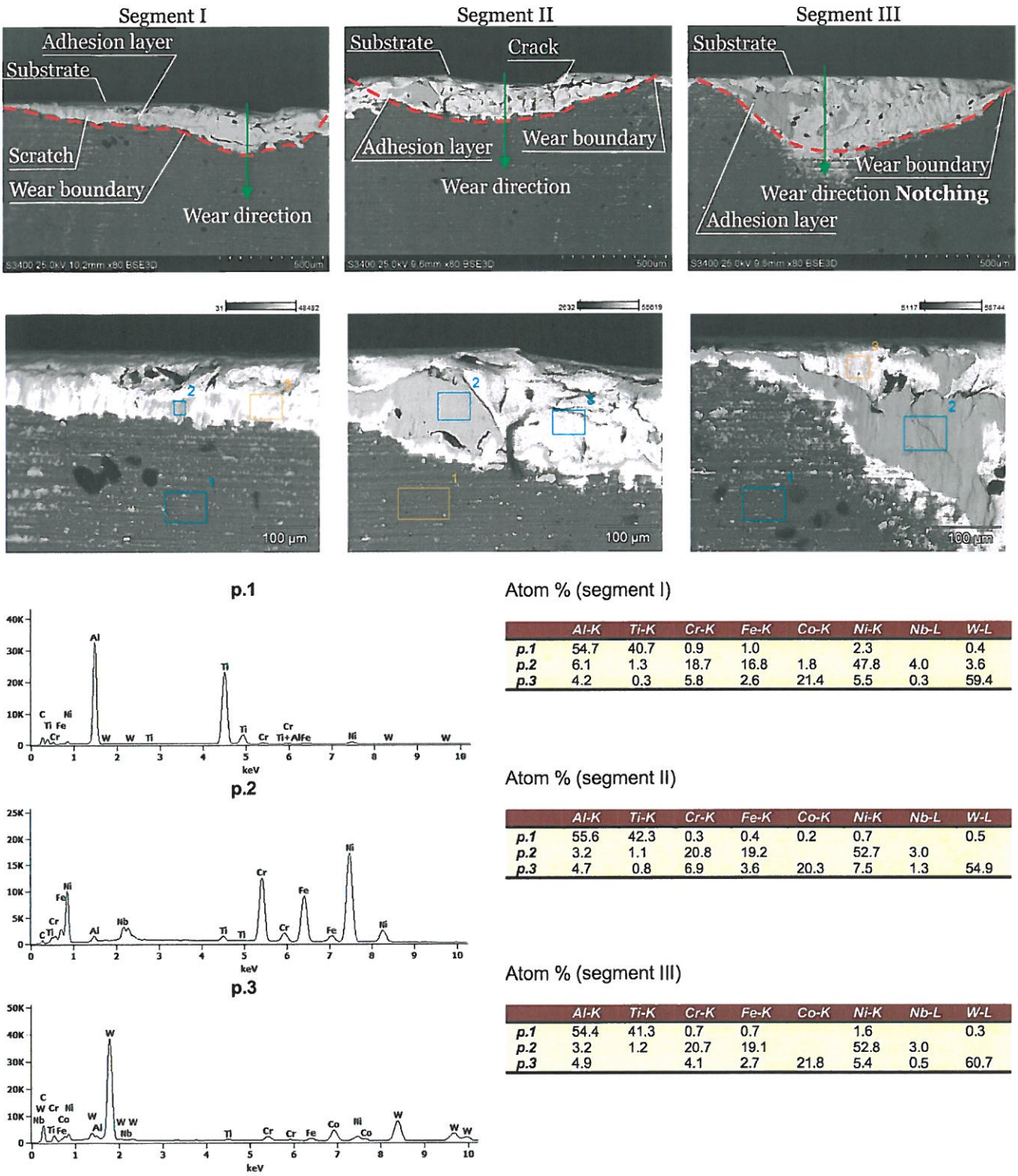

Atom % (segment I)

	Al-K	Ti-K	Cr-K	Fe-K	Co-K	Ni-K	Nb-L	W-L
p.1	54.7	40.7	0.9	1.0		2.3		0.4
p.2	6.1	1.3	18.7	16.8	1.8	47.8	4.0	3.6
p.3	4.2	0.3	5.8	2.6	21.4	5.5	0.3	59.4

Atom % (segment II)

	Al-K	Ti-K	Cr-K	Fe-K	Co-K	Ni-K	Nb-L	W-L
p.1	55.6	42.3	0.3	0.4	0.2	0.7		0.5
p.2	3.2	1.1	20.8	19.2		52.7	3.0	
p.3	4.7	0.8	6.9	3.6	20.3	7.5	1.3	54.9

Atom % (segment III)

	Al-K	Ti-K	Cr-K	Fe-K	Co-K	Ni-K	Nb-L	W-L
p.1	54.4	41.3	0.7	0.7		1.6		0.3
p.2	3.2	1.2	20.7	19.1		52.8	3.0	
p.3	4.9		4.1	2.7	21.8	5.4	0.5	60.7

Fig. 11. Wear morphology and element distribution in the final stage of flank wear for CCs I-st stage.

of the cutting edge were then analysed. It was found that, flank wear increases the contact area between the flank face of the tool and the workpiece, resulting in numerous scratches, cracks, and adhesion of workpiece material layers on the flank face of the tool, as well as on the contact surface. SEM and EDS images reveal that there is no major exfoliation or delamination of the coating. A comprehensive analysis shows that the wear mechanism mainly involves abrasive and adhesive wear, with oxidative wear also occurring at the wear boundary on the tool rake face.

The proposed models will take into account factors such as CWE, the geometry of the torus milling cutter, and the properties of the workpiece and the tool. These models make it possible to accurately predict the tool life and flank wear of the torus milling cutter during multi-axis milling of

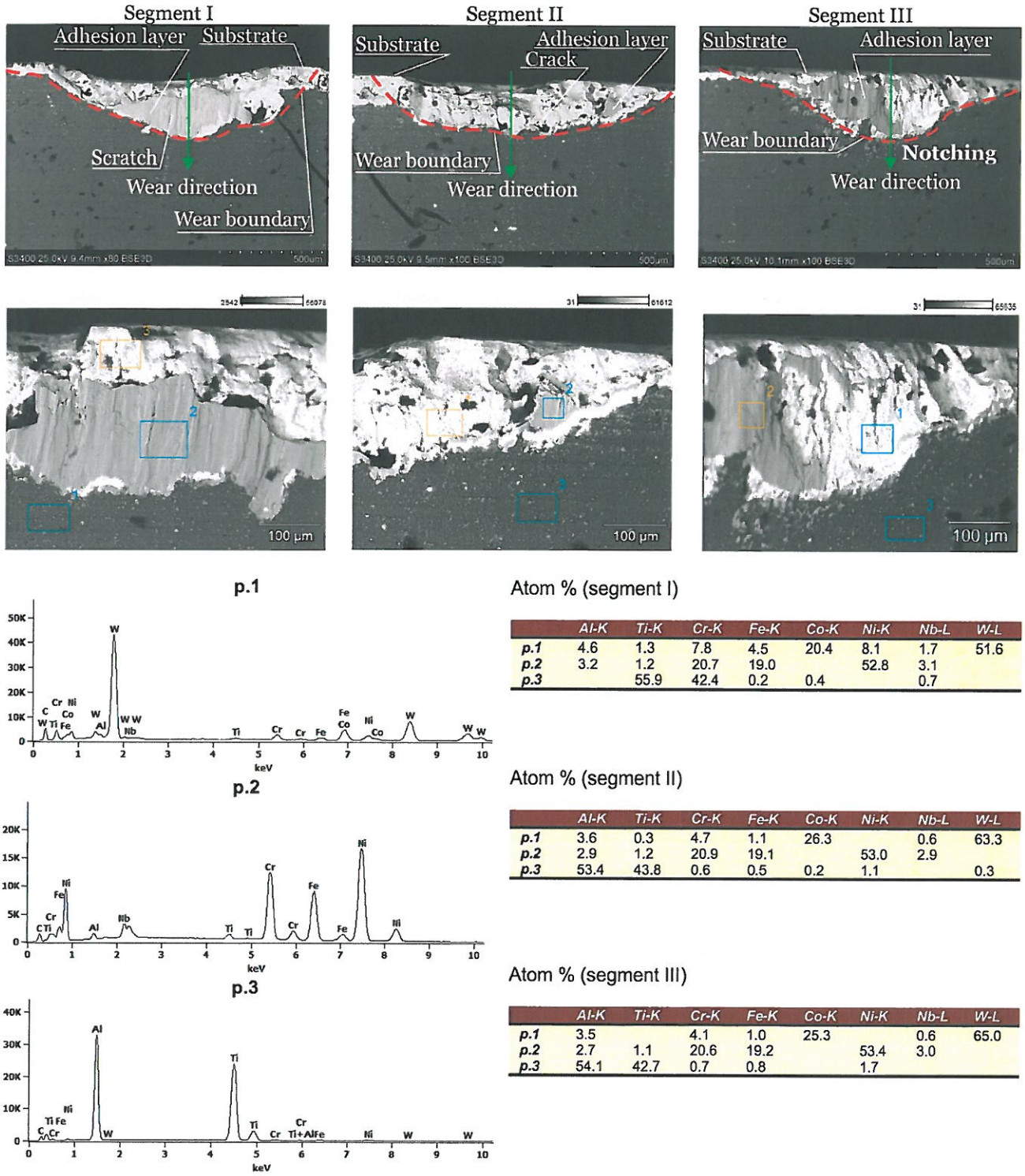

Atom % (segment I)

	Al-K	Ti-K	Cr-K	Fe-K	Co-K	Ni-K	Nb-L	W-L
p.1	4.6	1.3	7.8	4.5	20.4	8.1	1.7	51.6
p.2	3.2	1.2	20.7	19.0		52.8	3.1	
p.3		55.9	42.4	0.2	0.4		0.7	

Atom % (segment II)

	Al-K	Ti-K	Cr-K	Fe-K	Co-K	Ni-K	Nb-L	W-L
p.1	3.6	0.3	4.7	1.1	26.3		0.6	63.3
p.2	2.9	1.2	20.9	19.1		53.0	2.9	
p.3	53.4	43.8	0.6	0.5	0.2	1.1		0.3

Atom % (segment III)

	Al-K	Ti-K	Cr-K	Fe-K	Co-K	Ni-K	Nb-L	W-L
p.1	3.5		4.1	1.0	25.3		0.6	65.0
p.2	2.7	1.1	20.6	19.2		53.4	3.0	
p.3	54.1	42.7	0.7	0.8		1.7		

Fig. 12. Wear morphology and element distribution in the final stage of flank wear for CCs II-nd stage.

the Ni-based superalloy Inconel718 using the ACESC technique. The undoubted advantages of the new multi-axis technique, which changes the active segments of the cutting edge and establishes life and wear prediction models for each active segment of the cutting edge, are primarily: extending tool life by utilising the cutting capabilities of the entire cutting edge, and while exploiting the potential of the multi-axis machine tool. This is particularly relevant for monolithic tools. In addition, the change in the active segment of the cutting edge is fully controlled while maintaining the same cutting speed at the point of contact, which is important in terms of the technological aspect of the surface layer.

The experimental results confirm that, when compared with the traditional method of fixed active cutting edges [14], the proposed technique is able to effectively improve the tool service life in milling,

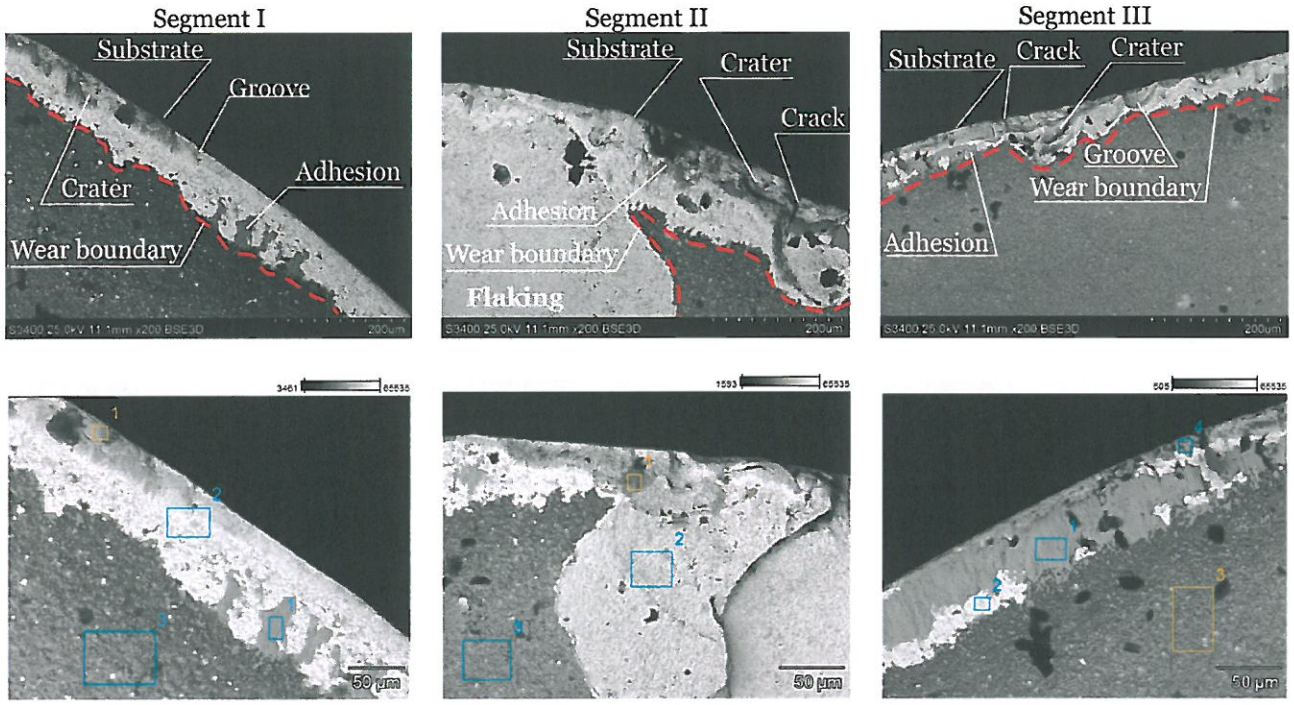

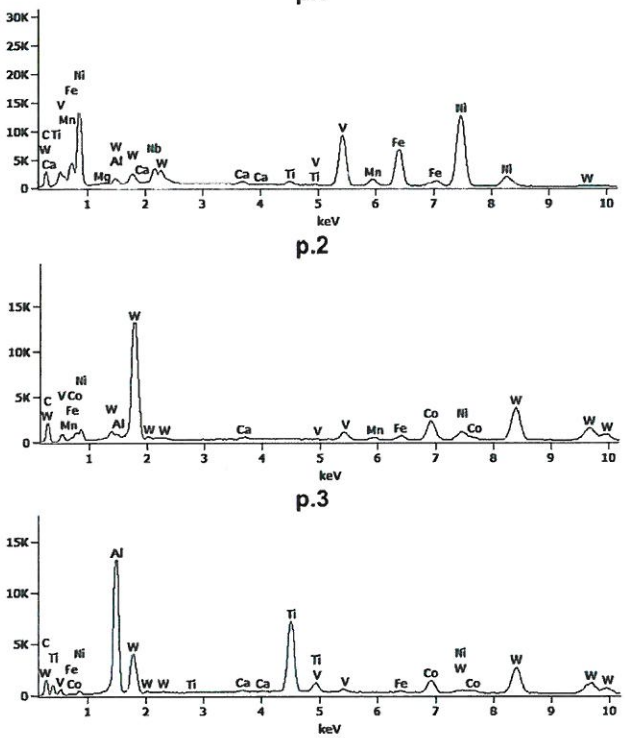

Atom % (segment I)

	O-K	Al-K	Si-K	Ca-K	Ti-K	V-K	Mn-K	Fe-K
p.1	29.0	2.1		0.2	0.8	1.3	3.8	14.7
p.2	36.9	3.7		0.7	0.8	1.0	1.2	3.7
p.3	2.7	45.3		1.3	24.3	0.5		0.8
	Co-K	Ni-K	Nb-L	W-L				
p.1		42.7	3.3	2.0				
p.2	10.6	9.5	1.9	30.0				
p.3	6.0	1.6		17.4				

Atom % (segment II)

	Mg-K	Al-K	Ca-K	Ti-K	V-K	Mn-K	Fe-K	Co-K
p.1	0.7	4.2	1.0	1.0	1.7	5.1	20.0	
p.2		3.4	1.8		1.0	1.7	3.7	24.0
p.3		46.9	0.6	26.0	0.5		0.5	6.3
	Ni-K	Nb-K	W-L					
p.1	58.5	4.8	2.9					
p.2	9.8		54.6					
p.3	1.1		18.2					

Atom % (segment III)

	Mg-K	Al-K	Ca-K	Ti-K	V-K	Mn-K	Fe-K	Co-K
p.1		3.0		1.3	1.8	5.6	21.1	
p.2		6.4		1.9	1.4	1.5	5.1	17.6
p.3		47.7		26.5	0.5		0.9	5.8
	Ni-K	Nb-K	W-L					
p.1	63.3	4.0						
p.2	13.8		52.3					
p.3	2.1		16.5					

Fig. 13. Wear morphology and element distribution in the final stage of rake face for CCs I-st stage.

often significantly. The predictive model proposed in this paper, in addition to accurately predicting tool wear when machining nickel-based superalloys, has general applicability when machining other hard-to-machine materials, such as titanium. The prerequisite is to calibrate the model using experiments on cutting another material. Furthermore, the proposed predictive models can be adapted for torus with other macro-geometry parameters, provided that the calibrated cutting speed at the point of contact is maintained.

Statement of originality

We the undersigned declare that this manuscript is original, has not been published before and is not currently being considered for publication elsewhere. We confirm that the manuscript has been read and

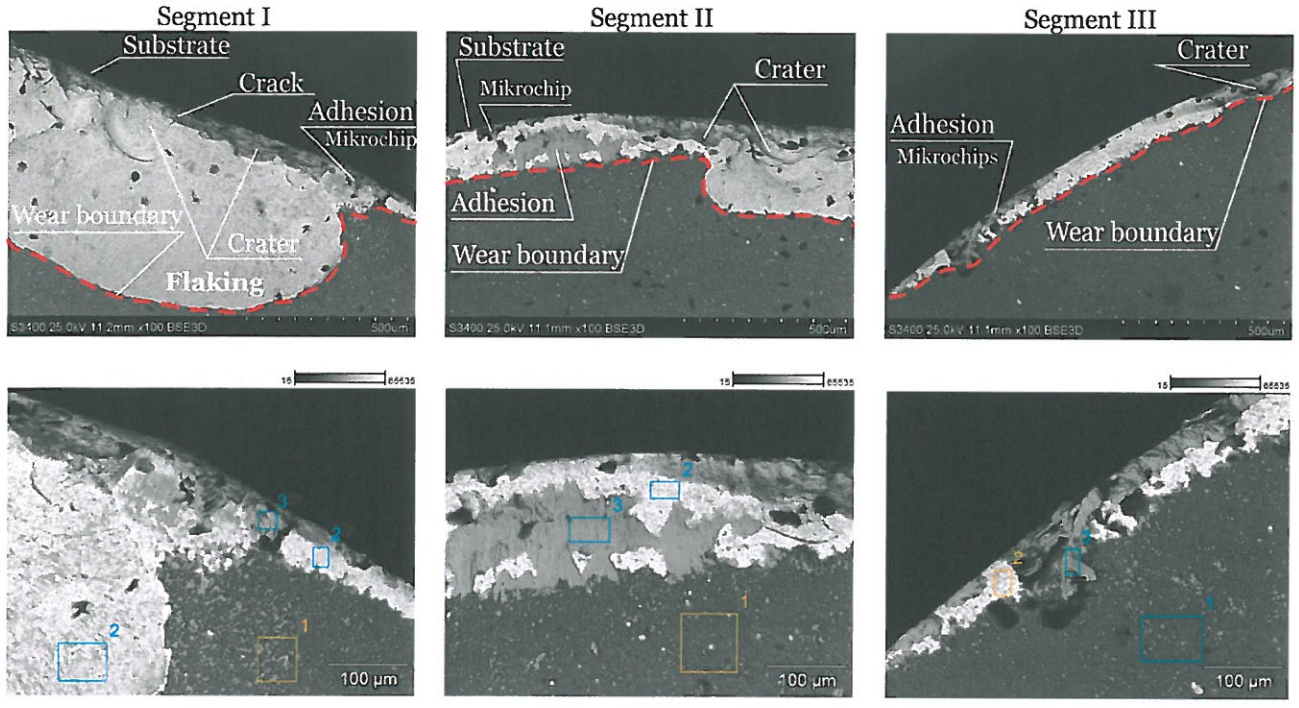

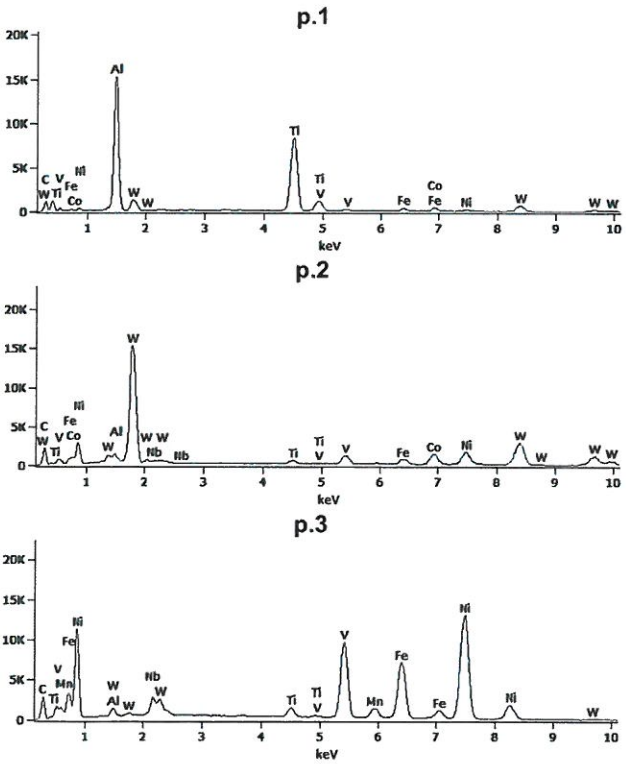

Atom % (segment I)

	Al-K	Ti-K	V-K	Mn-K	Fe-K	Co-K	Ni-K	Nb-L
p.1	51.0	32.2	1.2		2.4	1.8	6.4	0.5
p.2	11.7	4.8	0.7	1.5	2.7	18.9	7.1	
p.3	2.5	1.2	1.7	5.6	21.4		63.5	4.1

	W-L
p.1	4.5
p.2	52.7
p.3	

Atom % (segment II)

	Al-K	Ti-K	V-K	Mn-K	Fe-K	Co-K	Ni-K	Nb-L
p.1	52.2	34.1	0.5		0.8	2.9	1.6	
p.2	4.3	0.8	1.3	2.0	5.3	18.9	14.3	2.8
p.3	3.3	1.9	1.8	5.9	21.0		61.4	4.7

	W-L
p.1	7.8
p.2	50.4
p.3	

Atom % (segment III)

	Al-K	Ti-K	V-K	Mn-K	Fe-K	Co-K	Ni-K	Nb-L
p.1	54.8	34.1	0.6		1.7	2.1	1.4	
p.2	8.5	3.2	1.6		7.4	14.7	17.9	2.4
p.3	4.6	2.2	1.7	5.5	20.5		60.5	4.1

	W-L
p.1	5.4
p.2	44.4
p.3	0.9

Fig. 14. Wear morphology and element distribution in the final stage of rake face for CCs II-nd stage.

approved by all named authors and that there are no other persons who satisfied the criteria for authorship but are not listed. We further confirm that the order of authors listed in the manuscript has been approved by all of us. We understand that the Corresponding Author is the sole contact for the Editorial process. He is responsible for communicating with the other authors about progress, submissions of revisions and final approval of proofs.

Funding

This research received no external funding.

CRediT authorship contribution statement

Andrzej Nowotnik: Writing – review & editing, Supervision.

Grażyna Mrówka-Nowotnik: Writing – review & editing, Methodology, Investigation. **Michał Gdula:** Writing – review & editing, Writing – original draft, Visualization, Validation, Resources, Methodology, Investigation, Formal analysis, Conceptualization.

Declaration of Competing Interest

The authors declare that they have no known competing financial interests or personal relationships that could have appeared to influence the work reported in this paper.

Data Availability

The authors do not have permission to share data.

References

[1] Zhu D, Zhang X, Ding H. Tool wear characteristics in machining of nickel-based superalloys. Int J Mach Tools Manuf 2013;64:60–77. https://doi.org/10.1016/j.ijmachtools.2012.08.001.

[2] Halim NHA, Haron CHC, Ghani JA, Azhar MF. Tool wear and chip morphology in high-speed milling of hardened Inconel 718 under dry and cryogenic CO2 conditions. Wear 2019;426–427:1683–90. https://doi.org/10.1016/j.wear.2019.01.095.

[3] Wang J, Luo M, Xu K, Tang K. Generation of tool-life-prolonging and chatter-free efficient toolpath for five-axis milling of freeform surfaces. J Manuf Sci Eng 2019;141:031001. https://doi.org/10.1115/1.4041949.

[4] Zeng H, Yan R, Du P, Zhang M, Peng F. Notch wear prediction model in high speed milling of AerMet100 steel with bull-nose tool considering the influence of stress concentration. Wear 2018;408–409:228–37. https://doi.org/10.1016/j.wear.2018.05.024.

[5] An Q, Cai C, Zou F, Liang X, Chen M. Tool wear and machined surface characteristics in side milling Ti6Al4V under dry and supercritical CO2 with MQL conditions. Tribology Int 2020;151:106511. https://doi.org/10.1016/j.triboint.2020.106511.

[6] Gdula M, Mrówka-Nowotnik G. Analysis of tool wear, chip and machined surface morphology in multi-axis milling process of Ni-based superalloy using the torus milling cutter. 204652 Wear 2023:520–1. https://doi.org/10.1016/j.wear.2023.204652.

[7] Luo M, Luo H, Zhang D, Tang K. Improving tool life in multi-axis milling of Ni-based superalloy with ball-end cutter based on the active cutting edge shift strategy. J Mater Process Technol 2018;252:105–15. https://doi.org/10.1016/j.jmatprotec.2017.09.010.

[8] González H, Pereira O, Fernández-Valdivielso A, López De Lacalle L, Calleja A. Comparison of flank super abrasive machining vs. flank milling on inconel® 718 surfaces. Materials 2018;11:1638. https://doi.org/10.3390/ma11091638.

[9] González H, Calleja A, Pereira O, Ortega N, Norberto López de Lacalle L, Barton M. Super Abrasive machining of integral rotary components using grinding flank tools. Metals 2018;8:1–11. https://doi.org/10.3390/met8010024.

[10] Li Z, Peng F, Yan R, Tang X, Xin S, Wu J. A virtual repulsive potential field algorithm of posture trajectory planning for precision improvement in robotic multi-axis milling. Robot Comput-Integr Manuf 2022;74:102288. https://doi.org/10.1016/j.rcim.2021.102288.

[11] Yang B, Zhang G, Ran Y, Yu H. Kinematic modeling and machining precision analysis of multi-axis CNC machine tools based on screw theory. Mech Mach Theory 2019;140:538–52. https://doi.org/10.1016/j.mechmachtheory.2019.06.021.

[12] Gdula M. Adaptive method of 5-axis milling of sculptured surfaces elements with a curved line contour. J Mech Sci Technol 2019;33:2863–72. https://doi.org/10.1007/s12206-019-0534-4.

[13] Uchikata S, Beaucamp A, Takeuchi Y. 5-Axis control finishing for decreased tool wear. Procedia CIRP 2017;63:313–7. https://doi.org/10.1016/j.procir.2017.03.320.

[14] Gdula M, Józwik J, Skoczylas A. Tool wear and surface topography shaping after TPl multi-axis milling of Ni-based superalloy of the torus milling cutter using the strategy of adaptive change of the active cutting edge segment. 205637 Wear 2025:562–3. https://doi.org/10.1016/j.wear.2024.205637.

[15] Gdula M. Determination and analysis of working diameters and working angle of the torus cutter blade in multi-axis machining in the aspect of tool wear. IJMERR 2024;13:535–47. https://doi.org/10.18178/ijmerr.13.5.535-547.

[16] Cao L-X, Gong H, Liu J. The offset approach of machining free form surface. J Mater Process Technol 2007;184:6–11. https://doi.org/10.1016/j.jmatprotec.2006.10.048.

[17] Gdula M, Burek J. Cutting layer and cutting forces in a 5-axis milling of sculptured surfaces using the toroidal cutter. J Mach Eng 2017;4:98–122. https://doi.org/10.5604/01.3001.0010.7009.

[18] Chang Z, Qian J, Chen ZC, Wan N, Zhang D. Geometrical theory of cutting stock with torus end mills in five-axis CNC machining and its applications in machining simulation. Int J Adv Manuf Technol 2019;105:27–46. https://doi.org/10.1007/s00170-019-04064-8.

[19] Zhu Z, Peng F, Yan R, Li Z, Wu J, Tang X, et al. Influence mechanism of machining angles on force induced error and their selection in five axis bullnose end milling. Chin J Aeronaut 2020;33:3447–59. https://doi.org/10.1016/j.cja.2019.12.019.

[20] Musfirah AH, Ghani JA, Haron CHC. Tool wear and surface integrity of inconel 718 in dry and cryogenic coolant at high cutting speed. Wear 2017;376–377:125–33. https://doi.org/10.1016/j.wear.2017.01.031.

[21] Attanasio A, Ceretti E, Giardini C. Analytical models for tool wear prediction during AISI 1045 turning operations. Procedia CIRP 2013;8:218–23. https://doi.org/10.1016/j.procir.2013.06.092.

[22] Kasim MS, Che Haron CH, Ghani JA, Sulaiman MA, Yazid MZA. Wear mechanism and notch wear location prediction model in ball nose end milling of Inconel 718. Wear 2013;302:1171–9. https://doi.org/10.1016/j.wear.2012.12.040.

[23] Yan S, Zhu D, Zhuang K, Zhang X, Ding H. Modeling and analysis of coated tool temperature variation in dry milling of Inconel 718 turbine blade considering flank wear effect. J Mater Process Technol 2014;214:2985–3001. https://doi.org/10.1016/j.jmatprotec.2014.07.006.

[24] Manso CS, Thom S, Uhlmann E, De Assis CLF, Del Conte EG. Tool wear modelling using micro tool diameter reduction for micro-end-milling of tool steel H13. Int J Adv Manuf Technol 2019;105:2531–42. https://doi.org/10.1007/s00170-019-04575-4.

[25] Zhu K, Zhang Y. A generic tool wear model and its application to force modeling and wear monitoring in high speed milling. Mech Syst Signal Process 2019;115:147–61. https://doi.org/10.1016/j.ymssp.2018.05.045.

[26] Wiciak-Pikuła M, Felusiak-Czyryca A, Twardowski P. Tool wear prediction based on artificial neural network during aluminum matrix composite milling. Sensors 2020;20:5798. https://doi.org/10.3390/s20205798.

[27] Baig RU, Javed S, Khaisar M, Shakoor M, Raja P. Development of an ANN model for prediction of tool wear in turning EN9 and EN24 steel alloy. 168781402110267 Adv Mech Eng 2021;13. https://doi.org/10.1177/16878140211026720.

[28] Bjerke A, Hrechuk A, Lenrick F, Markström A, Larsson H, Norgren S, et al. Thermodynamic modeling framework for prediction of tool wear and tool protection phenomena in machining. 203991 Wear 2021:484–5. https://doi.org/10.1016/j.wear.2021.203991.

[29] Zhang Y, Zhu K, Duan X, Li S. Tool wear estimation and life prognostics in milling: model extension and generalization. Mech Syst Signal Process 2021;155:107617. https://doi.org/10.1016/j.ymssp.2021.107617.

[30] Huang P-M, Lee C-H. Estimation of tool wear and surface roughness development using deep learning and sensors fusion. Sensors 2021;21:5338. https://doi.org/10.3390/s21165338.

[31] Wang Q, Chen X, An Q, Chen M, Guo H, He Y. A tool wear prediction and monitoring method based on machining power signals. Int J Adv Manuf Technol 2023;11:5387–401. https://doi.org/10.1007/s00170-023-12656-8.

[32] Cheng Y, Yaoyao S, Hongmin X, Zhao T, Zhang N, Xian C. Tool wear prediction model based on wear influence factor. Int J Adv Manuf Technol 2023;3:1829–44. https://doi.org/10.1007/s00170-023-12323-y.

[33] Kamble PD, Giri J, Makki E, Sunheriya N, Sahare SB, Chadge R, et al. An application of hybrid Taguchi-ANN to predict tool wear for turning EN24 material. AIP Adv 2024;14:015206. https://doi.org/10.1063/5.0186432.

[34] Yanjie D, Yuwen S. Mechanism analysis and prediction of bull-nose cutter wear in multi-axis milling of Ti6Al4V with TiAlN coated inserts. Wear 2024:558–9. https://doi.org/10.1016/j.wear.2024.205580.

[35] 1-s2.0-S1526612518315354-main.pdf n.d..

[36] Feng Y, Hung T-P, Lu Y-T, Lin Y-F, Hsu F-C, Lin C-F, et al. Inverse analysis of the tool life in laser-assisted milling. Int J Adv Manuf Technol 2019;103:1947–58. https://doi.org/10.1007/s00170-019-03695-1.

[37] Feng Y, Hsu F-C, Lu Y-T, Lin Y-F, Lin C-T, Lin C-F, et al. Tool wear rate prediction in ultrasonic vibration-assisted milling. Mach Sci Technol 2020;24:758–80. https://doi.org/10.1080/10910344.2020.1752240.

[38] Sousa VFC, Da Silva FJG, Pinto GF, Baptista A, Alexandre R. Characteristics and wear mechanisms of TiAlN-based coatings for machining applications: a comprehensive review. Metals 2021;11:260. https://doi.org/10.3390/met11020260.

[39] Gdula M., Knapčíková L., Huśar J., Vandžura R. Modeling and Measurement of Tool Wear During Angular Positioning of a Round Cutting Insert of a Toroidal Milling Tool for Multi-axis Milling 2024. https://doi.org/10.20944/preprints202409.2088.v1.

[40] Wang B, Wang Z, Yin Z, Yuan J. Wear behavior of ultrafine WC-Co cemented carbide end mills during milling of Inconel 718. Wear 2024:546–7. https://doi.org/10.1016/j.wear.2024.205359.

[41] Zhang L, Zheng M, Zhang W, Li K. Influence and prediction of tool wear on workpiece surface roughness based on milling topography analysis. Int J Adv Manuf Technol 2022;122:1883–96. https://doi.org/10.1007/s00170-022-09939-x.

[42] Altintas Y. Manufacturing automation. Metal Cutting Mechanics, Machine Tool Vibrations, and CNC Design. Second ed. University of British Columbia: Cambridge University Press; 2012.

ARTYKUŁ

A4

dr inż. Michał Gdula
Politechnika Rzeszowska im. I. Łukasiewicza
Wydział Budowy Maszyn i Lotnictwa
Katedra Technik Wytwarzania i Automatyzacji

Rzeszów, dn. 23.04.2025 r.

OŚWIADCZENIE WSPÓŁAUTORA

Oświadczam, że w pracy:

lp.: A4

Gdula M,. Józwik J., Skoczylas A.: *Tool wear and surface topography shaping after TPl multi-axis milling of Ni-based superalloy of the torus milling cutter using the strategy of adaptive change of the active cutting edge segment.* WEAR, Vol. 562-563 (2025) 205637. IF 5.3, MNiSW 200 pkt.;

mój wkład w powstanie tej pracy polegał na: współudziale w analizie aktualnego stanu wiedzy w zakresie tematu pracy, opracowaniu podstaw matematycznych własnej techniki zmiany czynnego segmentu krawędzi skrawającej (ACESC) torusa, opracowaniu zależności modelowej parametru sterującego zmianą orientacji osi frezu torusowego i tym samym zmiany czynnego segmentu krawędzi skrawającej w technice ACESC, opracowaniu metodyki badań, przeprowadzeniu badań eksperymentalnych i modelowych, udziale w wykonaniu analizy zużycia narzędzia, opracowaniu metody pomiaru zużycia narzędzia bezpośrednio na maszynie CNC, pomiarze i analizie momentu skrawania, udziale w analizie struktury geometrycznej powierzchni, interpretacji wyników i opracowaniu wniosków, wykonaniu wykresów, rysunków oraz tabel, współudziale w opracowaniu manuskryptu, koordynowaniu procesu wydawniczego.

Gdula Michał

Podpis
dr inż. Michał Gdula

dr hab. inż. Jerzy Józwik, prof. PL
Politechnika Lubelska
Wydział Mechaniczny
Katedra Podstaw Inżynierii Produkcji

Lublin, dn. 05.12.2024 r.

OŚWIADCZENIE WSPÓŁAUTORA

Oświadczam, że w pracy:

lp.: ..A4..

GDULA M., JÓZWIK J., SKOCZYLAS A.: *Tool wear and surface topography shaping after TPI multi axis-milling of Ni-based superalloy of the torus milling cutter using the strategy of adaptive change of the active cutting edge segment*. WEAR (Elsevier), 562-563 (2025) 205637, https://doi.org/10.1016/j.wear.2024.205637;

mój wkład w publikację polegał na udziale w analizie stanu zagadnienia z zakresu pomiarów i monitorowania zużycia ostrza oraz udziale w opracowaniu manuskryptu.

Politechnika Lubelska
WYDZIAŁ MECHANICZNY
Katedra Podstaw Inżynierii Produkcji
dr hab. inż. Jerzy Józwik
profesor uczelni

.....
Podpis
dr hab. inż. Jerzy Józwik, prof. PL

dr inż. Agnieszka Skoczylas
Politechnika Lubelska
Wydział Mechaniczny
Katedra Podstaw Inżynierii Produkcji

Lublin, dn. 05.12.2024 r.

OŚWIADCZENIE WSPÓŁAUTORA

Oświadczam, że w pracy:

lp.: A4

GDULA M., JÓZWIK J., SKOCZYLAS A.: *Tool wear and surface topography shaping after TPI multi axis-milling of Ni-based superalloy of the torus milling cutter using the strategy of adaptive change of the active cutting edge segment.* WEAR (Elsevier), 562-563 (2025) 205637, https://doi.org/10.1016/j.wear.2024.205637;

mój wkład w publikację polegał na udziale w analizie stanu zagadnienia z zakresu pomiarów struktury geometrycznej powierzchni, doborze parametrów i przeprowadzeniu pomiarów struktury geometrycznej powierzchni oraz udziale w opracowaniu manuskryptu.

Agnieszka Skoczylas

Podpis
dr inż. Agnieszka Skoczylas

Wear 562–563 (2025) 205637



Contents lists available at ScienceDirect

Wear

journal homepage: www.elsevier.com/locate/wear

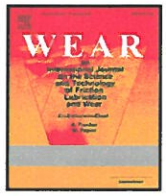

Tool wear and surface topography shaping after TPl multi-axis milling of Ni-based superalloy of the torus milling cutter using the strategy of adaptive change of the active cutting edge segment

Michał Gdula [a,*], Jerzy Józwik [b], Agnieszka Skoczylas [b]

[a] Department of Manufacturing Techniques and Automation, Rzeszow University of Technology, W. Pola Street 2, 35-959 Rzeszow, Poland
[b] Department of Production Engineering, Lublin University of Technology, Nadbystrzycka Street 36, 20-618 Lublin, Poland

ARTICLE INFO

Keywords:
Tool wear
Multiaxis milling process
Torus milling cutter
Ni-based superalloy 718
Cutting edge segmentation
Cutting speed at contact point
Surface roughness

ABSTRACT

This paper details an investigation of the process of multi-axis high-speed milling of the surface of Ni-based superalloy Inconel 718 parts used the torus milling cutter. Presents the issues and development of the own models of the multi-axis milling in a kinematic variant of the TPl (Tool Pulling) type in terms of tool wear. Because the cutting speed in finishing high-speed milling is the parameter with the greatest influence on tool life and surface roughness, the dependence of the variation of the cutting speed at the torus part of the cutter was first determined as a function of the distance from the tip point along the axial direction and the geometrical parameters of the torus. A model for multi-axis milling of the TPl type was developed and described in a simplified manner, which forms the basis of an own ACACES strategy for segmenting the cutting edge of a torus milling cutter. The adaptation of a given segment to the active cutting edge during machining was based on tool wear and kinematic roughness criteria. Simulations and experiments of multi-axis milling were carried out, and the necessary analyses were performed. In this paper, in addition to testing an in-house strategy for multi-axis milling used the torus milling cutter, the problem of defining the cutting speed in relation to the nominal diameter and effective diameter of the tool is investigated for the first time. In addition, wear measurement was carried out using an in-house methodology, taking full advantage of the capabilities of the multi-axis machining centre, which significantly reduced measurement time and positively influenced the effectiveness of tool life assessment. Using the own ACACES strategy of the multi-axis surface milling of parts made of Ni-based superalloys, an almost fourfold increase in torus cutter life was achieved compared to the conventional strategy, while maintaining the required machined surface roughness parameters.

1. Introduction

Ni-based superalloys have been the primary material in the group of structural materials of greatest importance in aerospace technology for several decades. They are used for structural components of aircraft engines operating in severe conditions of high alternation loads, high temperatures, and oxidizing gas environments. They are the basic material of the components of the hot part of the engine, including the blades of the 1st and 2nd stage of a high-pressure turbine [1]. The properties of this material, such as its good mechanical characteristics under stress, low thermal conductivity, high hardenability, and tendency to adhere to the tool material, make it significantly more difficult-to-cut at high cutting speeds in HSM cutting conditions (CCs), leading to the consequences of high temperature in the cutting zone, rapid tool wear, and poor surface integrity of the machined surface [2–4]. In the literature, it has been reported that the main source of rapid tool wear when cutting Inconel 718 at high speeds is the high cutting temperature, and yes, it is essential in roughing machining [3,5]. However, in finish machining, cutting speed and milling width become more important in terms of tool wear [6]. One of the methods used to increase the machinability of these materials is the use of a cutting fluid.

Multi-axis milling is one of the main methods for the subtractive shaping of surfaces of parts made mainly of difficult-to-cut materials, including Ni-based superalloys, among others, and is widely used in the finishing of sculptured surfaces with the continuous development of new strategies or technological variants of this method [7–10].

For surface machining of parts made from Ni-based superalloys, the torus milling cutter is increasingly being used, especially in the finishing process of multi-axis face milling. Tools with this type of geometry achieve better surface quality by eliminating zero-speed machining. In

* Corresponding author.
E-mail address: gdulam@prz.edu.pl (M. Gdula).

https://doi.org/10.1016/j.wear.2024.205637
Received 12 December 2023; Received in revised form 28 August 2024; Accepted 7 November 2024
Available online 26 November 2024
0043-1648/© 2024 Elsevier B.V. All rights are reserved, including those for text and data mining, AI training, and similar technologies.

addition, its geometry allows for an increase in cutting speed, cutting width, and feed rate, making the milling process much more efficient compared to milling with ball-end milling cutters [11–15].

One of the parameters that negatively affects the machining process is tool wear, or more precisely the VB length of wear [16]. Tool wear is the result of a series of mechanical (abrasion) and chemical (diffusion) interactions between the cutting blade and the surface being shaped. In the machining of Ni-based superalloys, mechanical wear, adhesive wear, diffusion wear and oxidation wear become much more severe, resulting in a significant reduction in tool life [17,18]. Therefore, the consequences of tool wear include dimension and shape errors, and, in general, a deterioration in the quality of the machined surface, i.e. an overall increase in the values of the 2D and 3D surface roughness parameters [8,9,19].

Researchers involved in calculating and monitoring tool wear have carried out many analyses in the aspect of conventional machining techniques [20,21], but there are only a few works in the field of multi-axis milling. Uchikata et al. [8] proposed a machining method with a continuous and at the same time variable inclination of the axis vector of the ball-end mill cutter, thus reducing its wear due to the uniform use of the cutting edge. Luo et al. [10] proposed a multi-axis milling strategy using different cutting edges on a spherical cutter to machine free-form surfaces. They estimated the wear rate with some approximation so as to predict the tool life. Gdula and Mrówka-Nowotnik [6] presented a study of the torus milling cutter life in the multi-axis milling process of Inconel 718 superalloy under high - speed cutting conditions in different kinematic variants of multiaxis machining. They evaluated the possibility of extending the life of a torus cutter by changing the orientation of its axis. They carried out an analysis of tool life, tool wear patterns and mechanisms, as well as its relationship to chip and machined surface morphology and kinematic variants of multi-axis cutting. They found that the kinematic variant of multi-axis cutting: tool pulling and obliquely positive tool pulling (i.e. axis orientation) using the torus milling cutter for machining Ni-based superalloys plays an important role in the possibility of extending tool life.

In turn, other researchers have carried out a number of studies on detecting and predicting tool wear. Wu et al. [22] used industrial cameras to collect images of worn blades and then processed and calculated the wear area of the collected images using a convolutional neural network algorithm. Malhotra and Jha [23], on the other hand, proposed a wear monitoring algorithm based on a fuzzy clustering technique directly implied in the acquired colour micrograph images. The results obtained and the image analysis made it possible to classify the various cutting conditions. Rizal et al. [24] used multiple sensors and the Mahalanobis Taguchi system to classify tool wear and proposed a new method to detect tool wear. In turn, Jurko et al. [25] conducted a comprehensive study to prove that the use of confocal chromatic sensor (CCHS) technology is effective and suitable for verifying the integrity parameters of machined surfaces for cutting tool wear. They evaluated the results using the grey relational analysis method (GRA) in combination with the Taguchi method, and the significance of the factors using the analysis of variance (ANOVA) method.

The aim of the following work, carried out in terms of a torus milling cutter wear, is:

1. Development of a model relationship that describes the distribution of cutting speeds on a two-dimensional rotating surface of the torus milling cutter, where in paper [10] such a relationship developed only for the ball-end mill cutters.

2. Development of model relationships that describe the relationship between the orientation of the torus milling cutter axis and the cutter-workpiece engagement (CWE) in the contact area for the case of multi-axis kinematic cutting type: tool pulling (TPl), where in papers [8,10] such a model developed only for the ball-end mill cutters, and in paper [6] kinematic roughness constant not taken into account.

3. On the basis of the above, the development of a own adaptive change active cutting edge segment (ACACES) strategy based on the cutting blade working angle parameter of a torus milling cutter, wchich will significantly extend the tool life of this tool in multiaxis milling of Ni-based superalloys under HSM conditions. The basic research and analysis carried out covers tool wear and tool life and their relationship to: the cutting conditions in the proposed own ACACES strategy, the cutting torque, the overall wear mechanism and the surface roughness after machining.

2. Multiaxis milling using the torus milling cutter in the kinematic cutting variant — tool pulling (TPl)

2.1. Cutting speed on a two-dimensional rotating surface of a torus milling cutter

When milling using the torus milling cutter, with the spindle speed set to an arbitrary and constant value, the cutting speed varies along the blade cutting edge from the level of the tool centre point (TCP) towards the tool attachment point in the spindle. Similar considerations, but for a ball-end milling cutter, are presented in his work [10]. The cutting speed $v_{c,g}$ (m/min) at a point with height g from the apex of the torus milling cutter can be expressed as Eq. (1):

$$v_{c,g} = \frac{2\pi n\left(R_T + \sqrt{2r_p g - g^2}\right)}{1000} \tag{1}$$

where n (rev/min, rpm) is the spindle speed, R_T (mm) is the radius from the axis of rotation of the cutter to the centre point of the round cutting insert, and r_p (mm) is the radius of the round cutting insert. As shown in Fig. 1, the cutting speed varies significantly given the parameter g along the torus milling cutter axis. Simulation of the cutting speed values in this case was carried out for a cutter work angle blade in the range $0° \leq \psi_r \leq 90°$ in the tool base plane P_r coinciding with the tool feed plane. Furthermore, for this type of tool, the cutting speed varies not only taking into account the g parameter but also the geometrical parameters of the torus, i.e. R_T and r_p. Therefore, three geometric cases of the torus are specified: *ring torus*, *horn torus* and *spindle torus*. The distribution of variations in cutting speed for these geometric cases is shown in Fig. 2.

It was found that for the cases of geometries: the ring torus and the spindle torus, an increase in the value of the R_T parameter causes a radial move of the cutting edge and thus an increase in the value of the cutting speed over the entire range of the cutter work angle blade ψ_r adopted for the simulation. The maximum distance g from the TCP apex of the cutter in the assumed range of the cutting blade working angle ψ_r does not change. However, the increase parameter r_p, also increases the value of the cutting speed throughout range of the cutting blade working angle ψ_r adopted for the simulation, while the maximum distance g from the TCP apex of the cutter also increase. This indicates an elongation of the cutting edge arc of the round cutting insert of the cutter. Furthermore, by changing the value of the r_p parameter, the cutting speed for $g = 0$ does not change, while by changing the parameter R_T value for $g = 0$ the cutting speed also changes. In terms of the sequences of change of v_c as a function of R_T and r_p described above, the case of horn torus cutter geometries is special, as these sequences occur simultaneously. In terms of the changes in cutting speed change as a function of R_T and r_p described above, the case of horn torus geometries is special, as these sequences of change occur simultaneously. In each of the three torus cutter geometries considered, regardless of changes in the values of the geometric parameters, along the distance g from the TCP point of the cutter the value of the cutting speed increases.

The cutting speed has a very strong influence on the tool wear and on the quality indicators of the machined surface, and, in addition, the tool wear rate is different at different locations on the cutting edge — torus surface of the cutter. At the same spindle speed, the tool life will vary in different zones on the torus surface of the cutter. This difference in cutting speed (and thus tool wear rate) is the basis for extending the

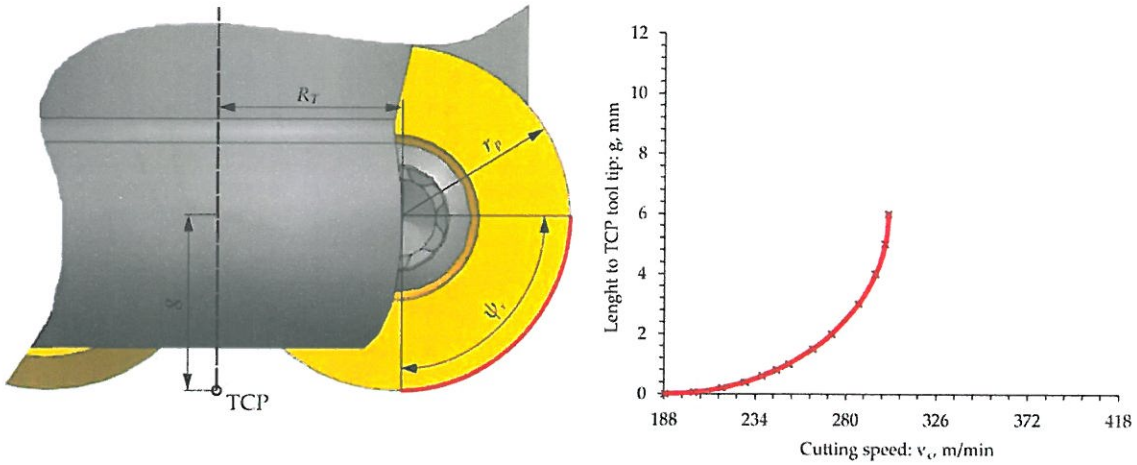

Fig. 1. Cutting speed variation along the torus milling cutter axis. (Cutter diameter: 32 mm, round cutting insert: 6 mm, spindle speed: 3000 rpm).

concept of an adaptive tool axis orientation control method, described in a paper [26], to include a technique for actively managing the contact area between the cutting surface of a torus milling cutter and the workpiece during a multiaxis milling process to maximize tool life while exploiting the maximum possible cutting edge length and the potential of multiaxis machines.

2.2. Torus milling cutter — workpiece engagement and active cutting edges

In a multiaxis milling process, the tool can, at least in theory, have any axis orientation as long as there is no collision. In the present study, the kinematic variant of multiaxis milling: tool pulling (TPl) will be considered, and the own results presented in the paper [6] were taken as the basis for further research. During the movement of the cutter, the cutter is in contact with the workpiece on a temporary patch of the machined surface, which is called cutter - workpiece engagement (CWE), and the material removed is the cut layer in the form of a chip. The CWE is located on the torus action surface of the cutter within the adopted depth of cut a_p, as shown in Fig. 3. Because the tool continues to rotate about its axis, the CWE $s_{CWE,i}$ at the cutter contact point (*CCP*) forms a belt $s_{b,i}$, which was named the cutting belt, located on the surface action of the torus milling cutter. At any moment of cutting, the segment on the cutting edge that is inside the CWE is called the active cutting edge segment, i.e. the cutting edge of the active segment is cutting at that moment. In addition, segments that are outside the CWE have been extracted that are passive cutting edge segments where, in the first boundary condition, the edge of the passive segment is not cutting and is sharp and, in the second boundary condition, the edge of the passive segment is not cutting and is worn according to a defined criterion.

2.3. Relationship between the torus milling cutter axis orientation and CWE

In order to determine the geometry of the torus milling cutter and its axis orientation relative to the machined surface, a reference coordinate system $(O_{ci}; X_{ci}, Y_{ci}, Z_{ci})$ was created with starting O_{ci} at the point $(0, 0, 0)$ of the centre of the cutting edge of a circular cutting edge insert with radius r_p, as shown in Fig. 4. The Z_{ci} axis is constant, in terms of both direction and axis return. The parametric equation of the torus T of the cutter is then expressed as column matrix (2):

$$T(\phi, \tau) = \begin{bmatrix} (R_T + r_p \cos\phi)\cos\tau - R_T \\ (R_T + r_p \cos\phi)\, sin\tau \\ r_p \sin\phi \end{bmatrix} \tag{2}$$

where: r_p - radius of the circle defining the torus (cutting edge of the round cutting insert), R_T - distance of the rotation axis of the torus from the centre of the circle defining it (radius of the torus), ϕ - angle of rotation of any point belonging to the circle defining the torus and lying in the $X_{ci}Z_{ci}$ plane, τ - angle of rotation of the circle defining the torus around the axis of rotation of the torus.

The contat point CP_i between the torus milling cutter blade and the machined surface was determined relative to the adopted coordinate system $(O_{ci}; X_{ci}, Y_{ci}, Z_{ci})$ using column matrix (2). The unambiguous and fixed position of this point in the CWE zone of $s_{CWE,i}$ was obtained by applying conditions (3) to the column matrix (2) and assuming that initially the axis of the torus milling cutter is in the reference position, i.e. parallel to the Z_{ci} axis:

$$\begin{cases} \phi = -90° \\ \tau = 0° \end{cases} \tag{3}$$

by which following the parametric equation of the CP_i contact point was obtained, which describes the matrix (4):

$$CP_i(\phi, \tau) = \begin{bmatrix} 0 \\ 0 \\ -r_p \end{bmatrix} \tag{4}$$

By creating a reference coordinate system $(O_{ci}; X_{ci}, Y_{ci}, Z_{ci})$ with the origin of O_{ci} at the point $(0, 0, 0)$ of the centre of the cutting edge of a round cutting insert of radius r_p, and adopting conditions (3) to column matrix (2), it was caused that the parametric equation of the torus T is also the equation of the contact point CP_i in the CWE zone $s_{CWE,i}$. By basing further proceedings on the reference coordinate system and the obtained matrices and performing additional mathematical operations, i.e. translation and/or rotation, it is possible to model and simulate any multiaxis cutting kinematics [6]. Assumed, that the workpiece is fixed and movable in a 3D space is the tool.

In the next step, the local coordinate system $(C_{Pi}; X_{PO}, Y_{PO}, Z_{PO})$ of the workpiece (PO) is defined with the origin at the CP_i contact point. This allows the geometry of the PO to be determined autonomously, together with the value of the depth of cut a_p, and the kinematic relationship between the PO and the torus of the cutter in the CWE zone $s_{CWE,i}$ is still preserved through the relationships described above at the CP_i contact point. The coordinate system $(C_{Pi}; X_{PO}, Y_{PO}, Z_{PO})$ was obtained by translating the unit matrix (assuming it to be identity to the reference coordinate system $(O_{ci}; X_{ci}, Y_{ci}, Z_{ci})$) by vector (4), what describes the relation (5):

$$PO = \begin{bmatrix} 1 & 0 & 0 \\ 0 & 1 & 0 \\ 0 & 0 & 1 \end{bmatrix} \cdot \begin{bmatrix} 0 \\ 0 \\ -r_p \end{bmatrix} = \begin{bmatrix} 0 \\ 0 \\ -r_p \end{bmatrix} \tag{5}$$

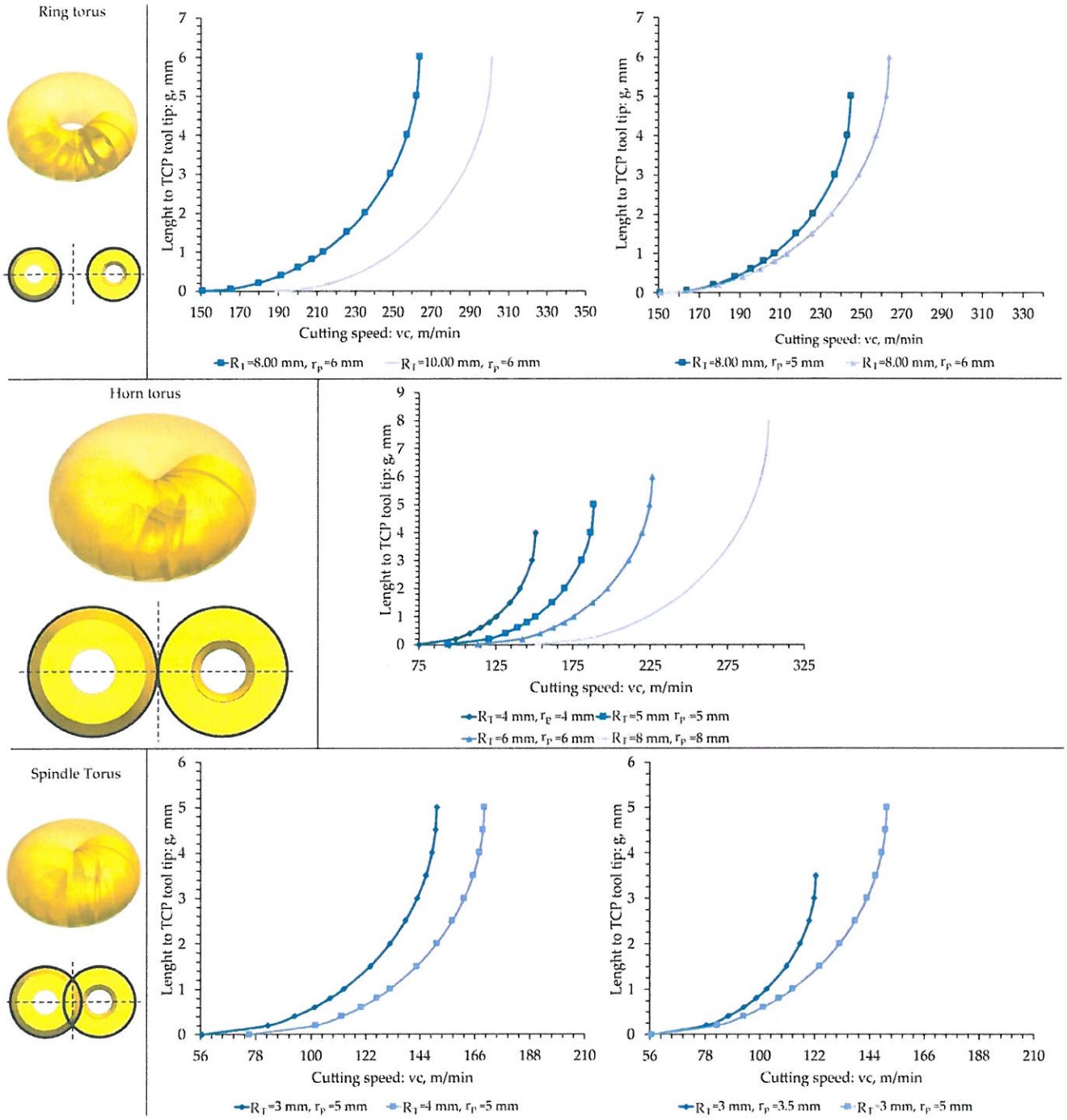

Fig. 2. Cutting speed variation along the torus milling cutter axis for its geometric types. (Spindle speed: 3000 rpm).

Finally, to obtain an inclination by an angle δ of the torus milling cutter axis in the feed direction f in the plane $X_{ci}Z_{ci}$ relative to the normal vector $(\vec{n_{Ci}})$ of the machined surface and hooked at the contact point CP_i in the multiaxis cutting kinematic variant — tool pulling (see Fig. 4), the central origin of the torus cutter OT was determined and the rotation matrix $R(Y_{Ci})(\delta)$ was defined with respect to the Y_{Ci} axis of the reference coordinate system $(O_{ci}; X_{ci}, Y_{ci}, Z_{ci})$, which was expressed respectively by relations (6) and (7).

$$O_T = \begin{bmatrix} -R_T \\ 0 \\ 0 \end{bmatrix} \tag{6}$$

$$R_{Yci} = \begin{bmatrix} \cos\delta & 0 & \sin\delta \\ 0 & 1 & 0 \\ -\sin\delta & 0 & \cos\delta \end{bmatrix} \tag{7}$$

Then a local coordinate system $(O_T; X_T, Y_T, Z_T)$ was defined with the origin of the O_T at the point $(-R_T, 0, 0)$. The Z_T axis of this coordinate system is also the axis of rotation of the circle defining the torus T and lying in the $X_{ci}Z_{ci}$ plane. The inclination of the tool axis by an angle δ is obtained by applying the relation (8) to rotate the O_T around Y_{Ci} and then rotating the system $(O_T; X_T, Y_T, Z_T)$ by an angle δ around the

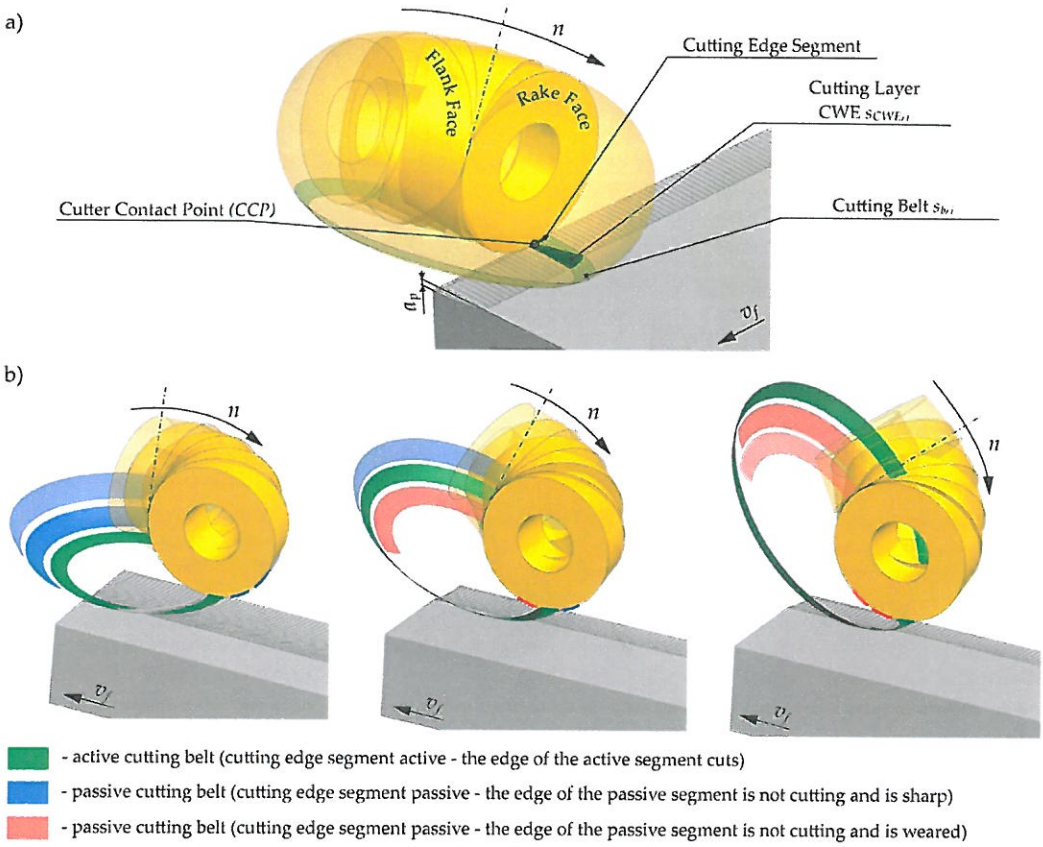

Fig. 3. Multiaxis milling using the torus milling cutter: (a) contact conditions, (b) cutting edge segments and cutting belts at different milling axis inclinations.

Y_T axis, according to expression (9).

$$O_{TYci} = \begin{bmatrix} -R_T \cos\delta \\ 0 \\ R_T \sin\delta \end{bmatrix} \tag{8}$$

$$Y_T(\delta) = \begin{bmatrix} \cos\delta & 0 & \sin\delta \\ 0 & 1 & 0 \\ -\sin\delta & 0 & \cos\delta \end{bmatrix} \tag{9}$$

Based on the multiaxis milling model described above in the kinematic variant of tool pulling using the torus milling cutter, when the angle δ is known, the cutting belt on the torus action surface of the cutter can be determined and the CWE can then be determined therein. To simplify further calculations, the tangent plane at CP_i is assumed to approximate the local machined surface of the PO, and considerations will be considered in the P_r basic plane of the tool. For the depth of cut a_p along the normal direction ($\vec{n_{Ci}}$) of the machined surface, the cutting strip $s_{b,i}$, in which the CWE and the segment of the active cutting edge are located, can be defined, and its limits can be determined using the parameter ψ_r of the cutter work angle blade in the basic plane P_r, as shown in Fig. 5. As noted, the boundaries of the cutting belt $s_{b,i}$ and thus the projection interval change with the change in the value of the inclination angle δ of the cutter axis, i.e. is a function of the inclination angle δ. Furthermore, it can also be seen that in the multiaxis cutting process with a torus milling cutter, the cutting speed v_c is also a function of the inclination angle δ and depends not only on the spindle speed n and the tool diameter D, but also on the depth of cut a_p ($v_c = f(D, n, a_p, \delta)$). In order, to calculate the cutting speed v_c, linking it to the cutter work angle blade ψ_r and the inclination angle δ, was used Eq. (10):

$$v_c = \frac{\pi D_{ef} n}{1000} \tag{10}$$

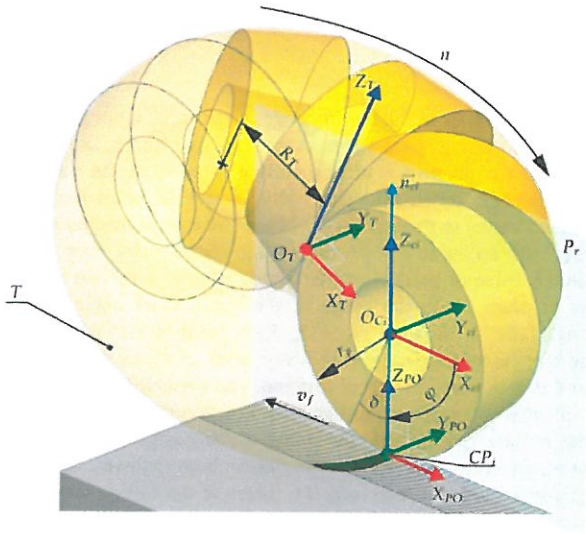

Fig. 4. Relationship between the torus milling cutter axis orientation and CWE.

In Eq. (10), generally, D_{ef} denotes the effective diameter of the tool, shown in Fig. 5. The value of the parameter D_{ef} at the contact point CP_i between the cutter blade and the machined surface can be determined using Eqs. (11) and (12):

$$D_{ef_{CP_i}} = 2R_T, \quad \text{when} \quad \delta = 0° \tag{11}$$

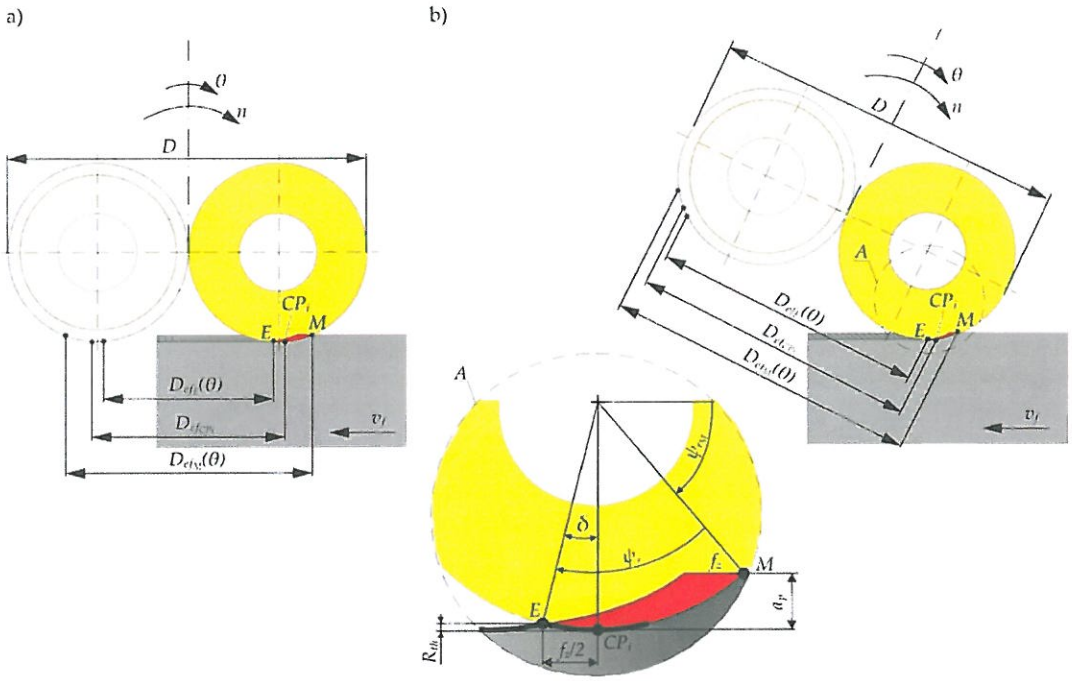

Fig. 5. Designation of the effective diameter Def of the torus milling cutter in the multiaxis milling process: (a) with a tool axis inclination angle $\delta = 0°$; (b) with a tool axis inclination angle $\delta \geq 0°$.

$$D_{ef_{CP_i}} = 2\left(R_T + r_p \sin\delta\right), \quad \text{when} \quad \delta > 0° \tag{12}$$

However, the value of the D_{ef} parameter when $\delta = 0°$, at point M and E, respectively, using Eqs. (13) and (14):

$$D_{ef_M} = 2\left[R_T + \left(r_p \cos\psi_{r_M} \cos(-\delta) - r_p \sin\psi_{r_M} \sin(-\delta)\right)\right] \tag{13}$$

$$D_{ef_E} = 2\left[R_T + \left(2r_p \cos\left(\psi_{r_M} + \psi_r\right) \cos(-\delta) - 2r_p \sin\left(\psi_{r_M} + \psi_r\right) \sin(-\delta)\right)\right] \tag{14}$$

Due to the shaping of the cutting edge of the torus milling cutter, the value of the cutting speed varies along its active length. In the case of cutting with an angle $\delta = 0°$, the cutting speed v_c at the CP_i contact point reaches a minimum value, while at the M point it reaches a maximum value. In the considered kinematic case of machining, when cutting with an angle $\delta > 0°$, the cutting speed varies from a certain minimum value at point E of the cutting edge to a certain maximum value at point M. In the range of the cutter work angle ψ_r of the cutting blade in the basic plane P_r, both point M and point E move along the cutting edge, moving away from or closer to the contact point CP_i as a function of tool rotation. The variability in the value of D_{ef} effective diameter in turn impinges on the variation in the value of the cutting speed along the active cutting edge from point E to point M, which can also significantly affect both tool wear and surface roughness indicators. Therefore, the course of the cutting speed v_c was determines in a function of the instantaneous contact angle θ and the inclination angle δ, and the variability of v_c are shown in Figs. 6 and 7, respectively.

Fig. 6 shows that an increase in the value of the inclination angle δ of the torus milling cutter axis results in an increase in the value of the cutting speed (while keeping the values of the parameters a_p, n, D constant). It was also observed that the effect of instantaneous contact angle θ on cutting speed values at each of the analysed points on the cutting edge was nonmonotonic. Fig. 7, on the other hand, shows that the differences between the maximum cutting speed v_{cmax} values at point M on the cutting edge and the values of the cutting speed v_c values at points CP_i and E on the cutting edge are even more than three times in the range of the higher inclination angle δ. An increase in the angle δ value of the results in an increase in the value of the v_{cmax} / v_c ratio. The aforementioned discrepancies can have a significant impact on the intensity of phenomena occurring in the contact zone between the CWE of the cutting edge and the workpiece material, particularly tool wear, and on the quality indicators of the machined surface.

In this connection, it should also be noted that, for milling, the spindle speeds n and thus the cutting speeds v_c are programmed by both researchers and practitioners of technology with reference to the diameter D (point C_D in Fig. 5) of the tool. In multiaxis machining, when the tool axis is inclined relative to the normal vector of the machined surface, the actual value of the cutting speed v_c at the contact point CP_i is different from the programmed one. What is more, it is less than the programmed value. This is important because the CP_i contact point is also the point of direct shaping of the machined surface. Thus, for further consideration, the cutting speeds were assumed to be constant over the entire active length of the cutting edge of the segment in question and equal to the value calculated for the CP_i point, whereby in the first stage of the cutting tests these will be the actual values relative to a reference on the tool diameter D, while in the second stage they will be values adapted to the contact point CP_i and constant regardless of the inclination of the torus milling cutter axis, i.e. different values of the rotational speed n will be adapted.

The assignment of a fixed inclination and/or rotation angle is a conventional strategy for controlling tool axis orientation. This strategy is widely used in multiaxis milling of complex surfaces, for example, to finish milling of turbine blades. However, since the tool axis is now set in the local coordinate system (see Fig. 4), that is, the inclination angle δ is a control variable, the active cutting edge segments remain the same in a given toolpath. Consequently, the CWE also remains the same over the entire programmed trajectory of the cutter in a given toolpath. This results in a long contact time between the active cutting edge segment in a given cutting belt and the workpiece. Since in this case the tool axis orientation varies in the local coordinate system, the CWE, as well as the cutting belt, moves from one preset position to

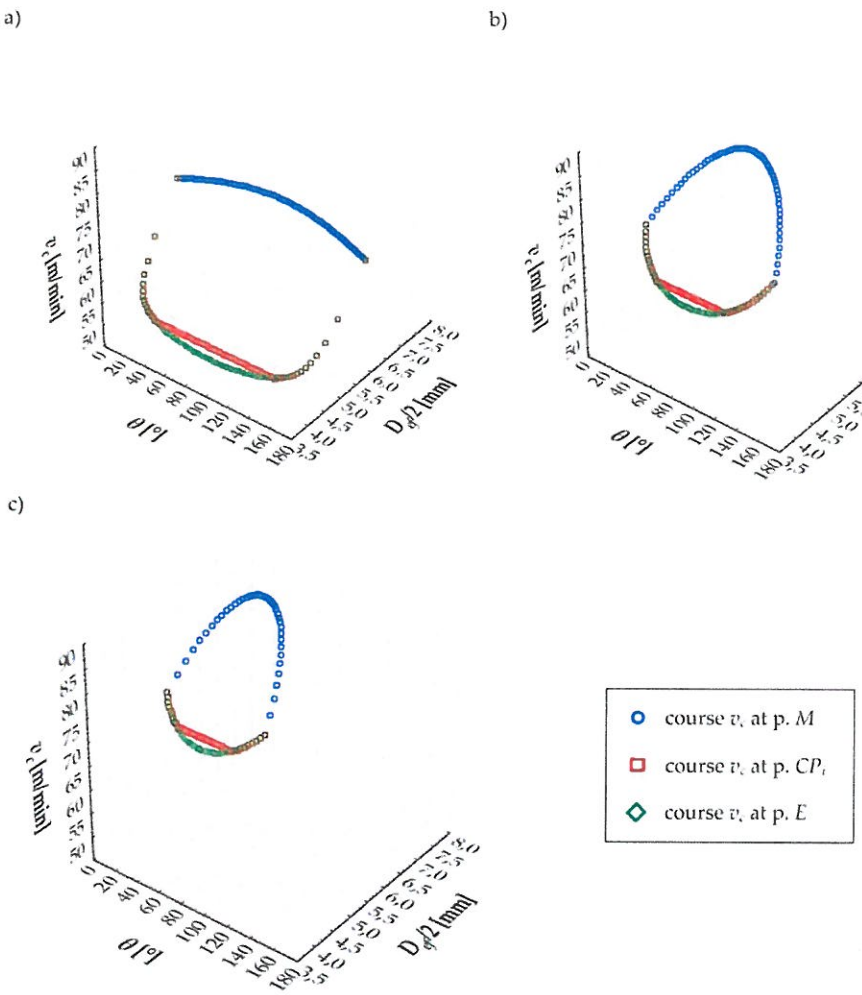

Fig. 6. Course of variability of cutting speed at point M, CP_i and E, as a function of instantaneous contact angle θ for: (a) $\delta = 1.37°$, (b) $\delta = 10°$, (c) $\delta = 18.62°$.

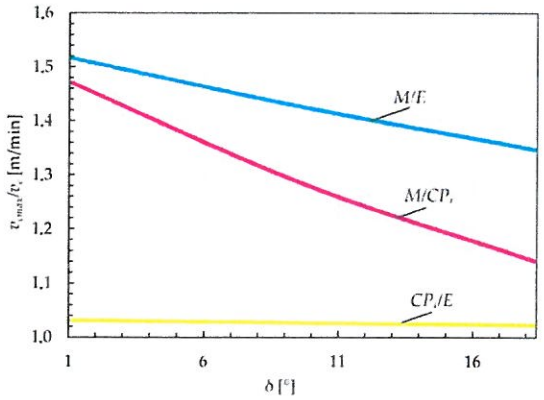

Fig. 7. Ratio of the maximum cutting speed at point M of the cutting edge to the cutting speed at point E and CP_i, and the ratio of the maximum cutting speed at point CP_i of the cutting edge to the cutting speed at point E, as a function of the angle of the torus milling cutter axis inclination δ.

another. This approach allows the contact area between the torus of the cutter and the workpiece to be increased, thereby making fuller use of the tool's cutting capabilities while exploiting the kinematic capabilities of multiaxis CNC machine tool.

3. ACACES strategy of adaptive change of the active cutting edge segment in the multiaxis kinematic cutting variant — tool pulling (TPl)

3.1. Torus milling cutter cutting edge segmentation

In Eqs. (13) and (14), the symbol ψ_r denotes the cutter work angle blade in the basic plane P_r, expressed by Eq. (15):

$$\psi_r = \frac{1}{2}\left(-2\sin^{-1}\left(1-\frac{a_p}{r_p}\right)+2\sin^{-1}\left(1-\frac{f_z}{2r_p}\right)+\pi\right) \tag{15}$$

Once the depth of cut a_p has been defined, for a given point CP_i and angle δ, the CWE and active cutting belt are defined completely and unambiguously. Since the entire cutting belt crosses the cutting layer and shapes the parameters of the technological surface layer from point M to p. E, rather than a single ellipse on the surface of the torus, the zone of this belt shaping the surface layer between point CP_i and point E is also taken into account (see Fig. 5). This aspect is overlooked and/or simplified in many works to an analysis ending at the point CP_i boundary. In addition, consideration of this zone prevents adjacent cutting belts from overlapping without leading to an undesirable surface finish. Once the depth of cut a_p has been determined, the height of the segment of the active cutting edge in a given active cutting belt disposed on the rotational axis of the cutter can be calculated using Eq. (15), with all the belts connecting without overlapping.

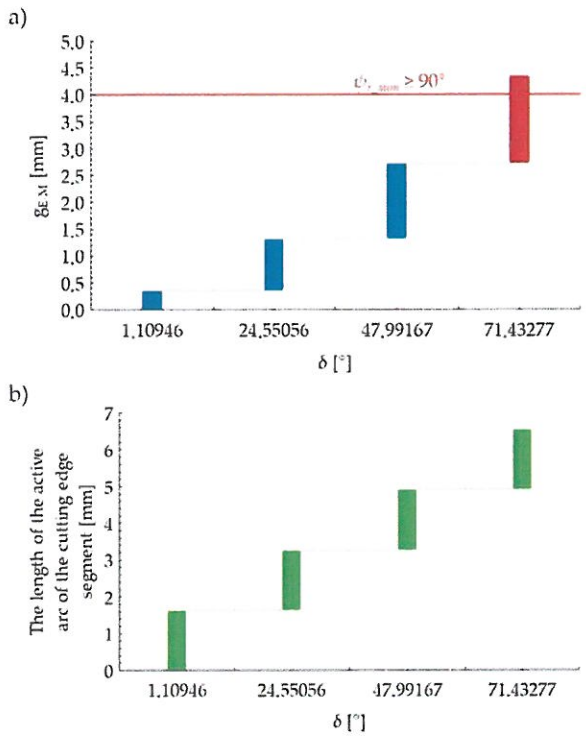

Fig. 8. Cutting edge segments on the torus part of the tool (D = 16 mm).

The reference initial setting of the inclination angle δ was defined with a value of 1.10946°, eliminating the so-called back blade from shaping the machined surface when it is not in contact with it at point CP_i. Therefore, the cutting edge starts from the zone defined by the defined reference angle δ, and the corresponding subsequent angle of orientation of the tool axis for each successive cutting belt can be calculated according to Eq. (15). For example, the first cutting segment closest to the cutter TCP results from an angle setting of $\delta = 1.10946°$, as shown in Fig. 8a, the subsequent angles for the corresponding segments are 24.55056°, 47.99167°, and 71.43277°. In the case of milling of planar surfaces and sculptured surfaces with a convex, biconvex, or saddle - convex form, a limiting criterion for Machine Tool-Check-Workpiece-Tool, collisions has been applied, which rejects from use segments for which, at a given angle orientation δ, the total work angle of the blade $\psi_{r_sum} \geq 90°$, (i.e. the sum of the work angles of the blade in the basic plane P_r of the individual cutting edge segments is equal to or greater than 90°). The length of the active arc of the cutting edge segment in each of the calculated tool axis orientations remains unchanged, as shown in Fig. 8b.

3.2. Torus milling cutter move trajectory and axis orientation planning

Based on the developed model (see Section 2.3) and using Eq. (15), specific adjustable values can be determined for the inclinaition angle δ, which is also closely related to the cutting edge segmentation procedure described above. In general, the process of planning the orientation of the cutter axis consists of the following steps. (1) Determination of the first reference orientation of the cutter axis, where the concept of collision analysis applies. (2) Relative to the first reference inclination angle δ and at a given depth of cut a_p value using formula (15), the work angle of the cutter blade is calculated in the first active cutting edge segment. The value of this angle is at the same time an taken value for the inclination angle δ for segments II and III. According to the limiting criterion (see Section 3.1), segment IV is rejected.

Table 1
Chemical composition of Ni-based superalloy Inconel718.

Material chemical composition (% wt.)				
Ni: 53.0	Cr: 18.30	Fe: 18.7	Nb: 5.05	Cu: 0.04
Al: 0.49	B: 0.004	C: 0.051	Co: 0.3	P: <0.005
Mo: 3.05	Ti: 1.05	Mn: 0.23	Si: 0.08	S: <0.002

Table 2
Chemical composition of round cutting insert S30T.

Base material chemical composition (% wt.)		
WC: 79.0	TiC+TaC+NbC: 13.0	Co: 8.0

The consequence of the inclination of the torus milling cutter axis in the feed plane (which is also the basic plane P_r) is a reduction in the width of the machined strip for a given tool trajectory. In this case, a significant deterioration in the quality of the machined surface will occur at the same b_r toolpaths distances. Therefore, in order to keep constant the values of the kinematic roughness criterion R_{th} in the feed direction and in the direction perpendicular to it independently of the changes in CWE due to the inclination of the cutter axis, a separate value of b_r was calculated for each segment according to the function $b_r = f(R_{th})$. The kinematic roughness criterion $R_{th} = 0.0015$ mm in both the feed direction and the direction perpendicular to it according to relation (16) was applied separately to each designated active cutting edge segment.

$$R_{th} = R_{thvf} = \frac{r_p}{2} - \sqrt{\frac{r_p^2 - f_z^2}{4}} \tag{16}$$

The kinematic roughness is the input variable to the model for determining the distance between toolpaths b_r (own elaboration), as schematically shown in Fig. 9.

In general, the course of planning a cutter trajectory also consists of several steps. (1) Determination of the ring of circle that passes through the point CP_i and lying on the torus surface of the cutter. (2) Making a projection of the circle on the $Y_{PO}Z_{PO}$ plane in each adjacent machined strip. (3) In the ellipses thus formed, the interference points (nodes), which are also the vertices of the kinematic roughness profile, were determined. (4) By introducing the R_{th} criterion and using nodes, the steering of the distance between toolpaths b_r takes place.

4. Multi-axis milling experiment

4.1. Materials and tools

Test material is NI-based superalloy Inconel 718. Its chemical composition is shown in Table 1. The TPI multi-axis milling process using a proprietary strategy to change the active cutting edge segment was conducted by applying steel torus milling cutter body R300-016A20L-08L for indexable round cutting inserts R300-0828E-PL. The body of the torus milling cutter has a neutral geometry and is the horn torus cutter. Round cutting inserts are made of S30T cemented carbide grade. Grade S30T has fine-grain cemented carbide and a TiAlN PVD coating. Cementet carbide grade S30T is fine-grade Tungsten-Titanium-Cobalt carbide, used for the machining of steel, cast steel and particularly difficult-to-cut materials. The chemical composition of the round cutting insert is shown in Table 2. The round cutting inserts have the following parameters: the rake angle is 20°, the flank angle is 15° and the insert radius is 4 mm. Furthermore, the cutting insert does not have a typical roundness radius r_ε of the cutting edge, but an asymmetrical chamfer with the following dimensions: length 0.1 mm measured along the line of intersection of the reference plane and orthogonal plane, and an angle of 15° measured in the orthogonal plane between the edge of the chamfer and the line of intersection of the reference plane and orthogonal plane in the Orthogonal Rake System (ORS) of the tool

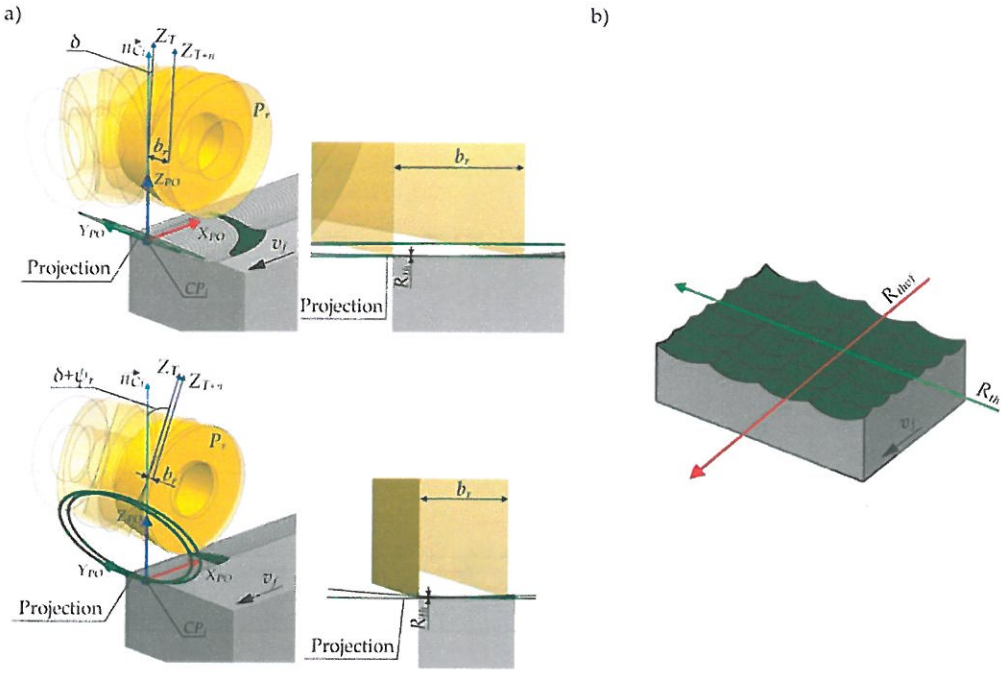

Fig. 9. Schematic illustration of: (a) the operating principle of the toolpaths planning model and the orientation of the torus cutter axis, (b) the adopted of the kinematic roughness parameters of the machined surface.

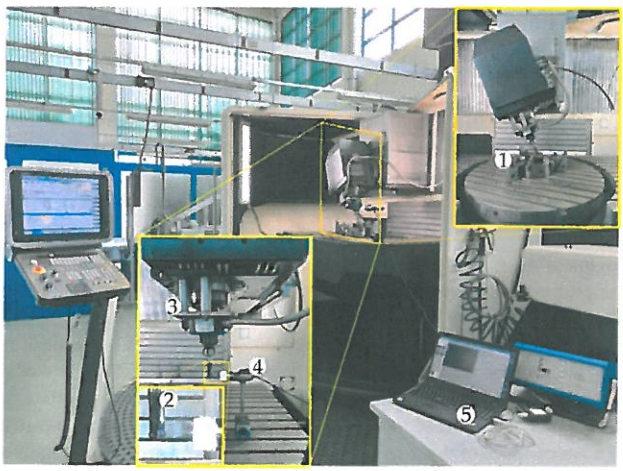

Fig. 10. Experimental test bench (1. Workpiece, 2. Torus milling cutter, 3. Adapter, 4. Dino-Lite 7000 CE series digital workshop microscope, 5. Computer with software for viewing, recording and analysis of measuring signals/pictures).

geometry. These 8 mm diameter round cutting inserts was attached in to a 16 mm diameter tool body at an overhang measuring 65 mm.

4.2. Test conditions and methodology

The experimental set-up is shown in Fig. 10. A 5-axis vertical CNC machining centre, model DMU 100 MonoBLOCK, was used to carry out multi-axis milling tests. The 4-component piezoelectric rotary dynamometer (Kistler 9123C), with 4-channel charge amplifier (Kistler 5223B) and data acquisition system (guickDAQ software and KUSB-3100 measuring card) is utilized for acquisition of cutting torque.

The experimental tests comprised a series of passes in a multi-axis milling process with a torus milling cutter, the axis of which was inclined relative to the normal vector of the machined surface in the feed direction (see Fig. 4) according to the model described in Section 3.1 and the ACACES strategy of our own elaboration. Thus, from a kinematic point of view, the technological variant of TPl (Tool Pulling) multi-axis milling was clearly defined, referring to the results of the reference study presented in the work [6]. In addition, to obtain the appropriate inclination of the cutter axis for a given cutting edge segment, the headstock of the machining centre was inclined by the value of the inclination angle δ, as shown in Tables 3 and 4, where the cutting conditions (CCs) are presented.

The experimental investigations were carried out in two main stages, as a result of the methodology adopted for selecting the cutting speed v_c (see Section 2.3). In stage one, a constant cutting speed v_c = 140 m/min was determined relative to the C_D point irrespective of the inclination angle δ, and the actual cutting speed v_c at the CP_i contact point of shaping the machined surface for the designated segments I, II and III was 71, 99 and 122 m/min, respectively, as shown in Table 3, together with other machining parameters.

However, in the second stage, a constant cutting speed v_c = 140 m/min was determined with respect to the CP_i contact point of the machined surface shaping also independ on the angle of the inclination angle δ, and the actual cutting speed v_c at the C_D point for designated segments I, II and III was 274, 197 and 160 m/min, respectively, as shown in Table 4, together with other machining parameters.

Experimental tests for each segment were performed in both main stages of the tests with three repetitions, making a total of 18 machining tests. In each of the 18 machining tests, flood cooling was used, and, starting each new experiment (repetition), the round cutting inserts were replaced with a new set.

The useful life of the tool, considering each designated active cutting edge segment separately and as the sum of the active cutting edge segments per tool, was determined by the wear (VB_{max}) located on the flank face of the cutting blade, until it reaches 0.2 mm, the maximum limit of the VB criterion in the proprietary ACACES strategy developed. The adoption of this limit value of the VB criterion was aimed at avoiding excessive wear of the torus milling cutter on the workpiece surface due to higher temperatures, and this approach was comparable to work done by researchers such as [27,28]. The multi-axis milling process was

Table 3
Cutting conditions (CCs) for I-st stage of the research.

	Inclination angle δ [°]	Total work angle of blade ψ_{r_sum} [°]	Distance between toolpaths b_r [mm]	Axial depth of cut a_p [mm]	Feed per tooth f_t [mm/t]	Cutting speed (at p. C_D) v_c [m/min]	Cutting speed (at p. CP_i) v_c [m/min]	Criterion $R_{th} = R_{thf}$ [mm]	Criterion VB_{max} [mm]
Segment I	1.10946	24.55056	1.6				71		
Segment II				0.3	0.1549	140		0.0015	0.2
Segment III	24.55056	47.99167	0.411				99		
Segment IV	47.99167	71.43277	0.335				122		
	71.43277	94.87387			$\psi_{r_sum} \geq 90°$ - test rejected				

Table 4
Cutting conditions (CCs) for II-nd stage of the research.

	Inclination angle δ [°]	Total work angle of blade ψ_{r_sum} [°]	Distance between toolpaths b_r [mm]	Axial depth of cut a_p [mm]	Feed per tooth f_t [mm/t]	Cutting speed (at p. C_D) v_c [m/min]	Cutting speed (at p. CP_i) v_c [m/min]	Criterion $R_{th} = R_{thf}$ [mm]	Criterion VB_{max} [mm]
Segment I	1.10946	24.55056	1.6			274			0.2
Segment II				0.3	0.1549		140	0.0015	
Segment III	24.55056	47.99167	0.411			197			
Segment IV	47.99167	71.43277	0.335			160			
	71.43277	94.87387			$\psi_{r_sum} \geq 90°$ - test rejected				

interrupted at specified intervals to identify wear patterns and measure wear rates using a Dino-Lite 7000 CE workshop microscope.

Since an adaptive change in the inclination angle δ of the torus cutter axis due to a change in the active cutting edge in the ACACES strategy also generates a change in the position of the contact point CP_i, measuring the wear rate with a workshop microscope of a given zone in the location of this point becomes a difficult issue affecting the accuracy of the measurement. Therefore, an in-house method has been developed to measure the wear rate in the zone of any cutting edge segment, based on the location of the CP_i point in the segment, using a workshop microscope without having to remove the tool from the spindle seat of a multi-axis CNC machining centre. At the same time, the kinematic-motion and CNC numerical control capabilities of the multi-axis machine tool were utilized. Thus, the measurement is carried out directly on the CNC machine without interfering with the Machine Tool-Check-Workpiece-Tool system, thus avoiding the position error resulting from the removal of the tool assembly from the spindle socket and its reinstallation in the socket after the measurement is completed, as is the case with traditional measurement. In general terms, the method involves programming the position of the tool relative to the workshop microscope on the CNC machine in such a way that the CP_i contact point is always on axis and at a constant distance from the microscope objective. This applies both to the measurement on the flank face and on the rake face of the tool, as illustrated in Fig. 11.

For surface topography measurements, the Hommel-Etamic T800 RC120-400 was used to measure surface roughness, surface topography, and contour. It is a contact device. A tip for standard surface roughness measurements, designated TKU300, was used, which has a diamond needle with a rounding radius of r_k = 5 μm. The area of the scanned surface was 4.8 x 4.8 mm. The rowing step (needle passage distances between successive measurement paths) was 20 μm, resulting in 241 paths for an area of 4.8 x 4.8 mm. The elementary stretch l_r was assumed to be numerically equal to the filter wavelength λ_c = 0.8 mm, and the measurement stretch l_n = 4.8 mm. After measurement, the surface topography was levelled and the shape error was removed using a 4th degree polynomial function.

5. Results and discussion

5.1. Torus milling cutter wear

Fig. 12 illustrates the comparison of the torus milling cutter life for the CCs of the first and second stages of the tests based on all experiments carried out for the individual active cutting edge segments. The experimental value of the torus milling cutter life is the average for all cutter inserts. For the purpose of the experiments, a limiting criterion of VB_{max} = 0.2 mm was adopted, as shown in Tables 2 and 3. In addition, the VB subcriteria, that is, VB = 0.04 mm and VB = 0.1 mm, were also adopted for a comprehensive analysis of the results obtained. Optical micrographs of the flank face for all cutting blades and cutting conditions for which $VB_{max} \cong 0.2$ mm are shown in Fig. 13.

By analysing the results obtained, it was found that the life of the torus cutter is different in the individual active segments of the cutting edge. Furthermore, irrespective of the CCs, whether in stage I or stage

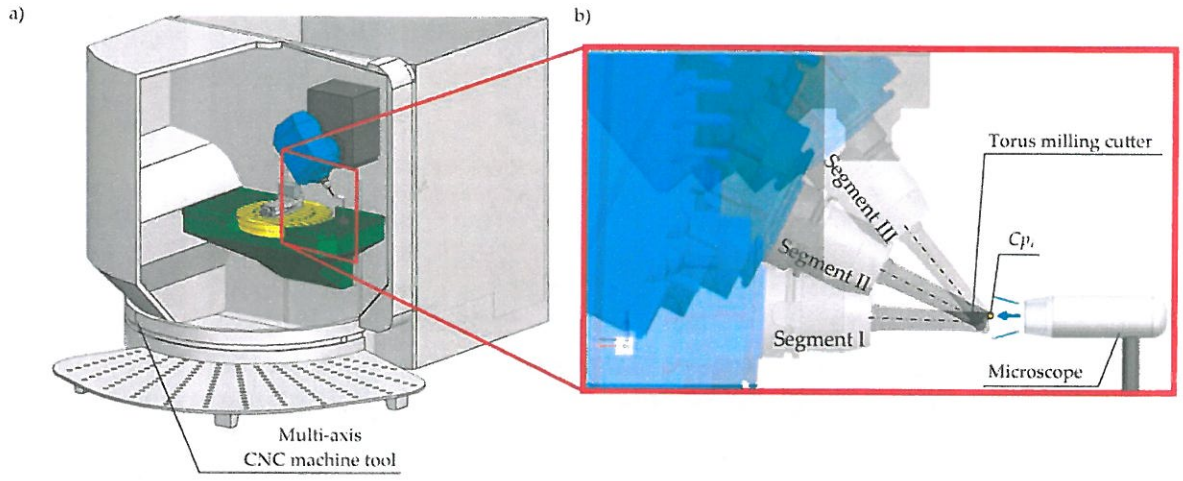

Fig. 11. Method of wear measurement (VBmax) located on the flank face of the cutting insert: (a) the multiaxis CNC machine tool, (b) the concept of measurement.

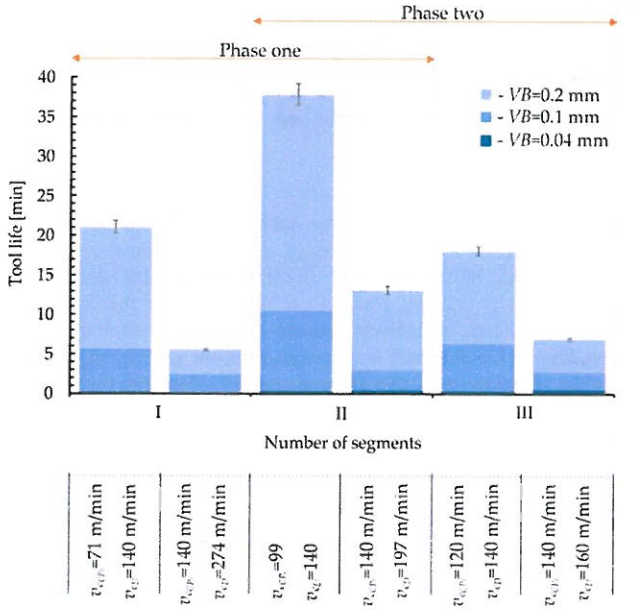

Fig. 12. Torus milling cutter life comparison between CCs in stage I and stage II.

II, the trend in the change in the life values of the torus milling cutter is almost identical. Considering the machining conditions for both stages, it can be concluded that in the proposed model (Section 2.3) of multi-axis TPl milling used the torus milling cutter and the ACACES strategy (Section 2) of changing the active cutting edge, tool life is strongly dependent on the kinematic machining conditions in the CWE. This is influenced by the following parameters and factors.

As a result of the inclination of the torus milling cutter axis according to the ACACES strategy together with the criteria, there is an indirect change in the values of essentially two parameters: the distance between the toolpaths b_r and the cutting speed v_c. Given these parameters, two phases of changes in the are detailed of the torus milling cutter durability in the ACACES strategy.

In phase one, the durability of the torus milling cutter in segment II is 80% greater than its durability in segment I for the first stage of the tests and 116% greater for the second stage of the tests. In contrast, the b_r distance between toolpaths moving from segment I to segment II decreased by 74.32%, by 1.189 mm to be precise. This shows that, in the first phase, the durability of the torus milling cutter is more strongly dependent on the b_r parameter than on the parameter v_c. This is also confirmed, among other things, by the results obtained in the second stage of the tests, where v_c = 140 m/min and was kept constant at the CP_i contact point for both segments of phase one. It should also be noted that as the value of the b_r parameter decreased, the geometrical parameters of the cutting layer in CWE, such as the cross-section, changed. The cross-section of the uncutting layer in the CWE for the II-nd segment is smaller than in the CWE for the I-nd segment, this in turn affects the thermomechanical loading of the cutting edge and results in the longest torus milling cutter life in the II-nd segment.

However, in the second phase, the durability of the torus milling cutter in the second segment is 53% higher compared to its durability in the third segment for the first stage of the tests and 47% higher for the second stage of the tests. However, the b_r distance between toolpaths moving from segment II to segment III decreased by 18.5%, or more precisely by 0.076 mm, which is only 6% in relation to the change in b_r values in phase one. This shows that, in the second phase, the durability of the torus milling cutter is more strongly dependent on the parameter v_c than on the parameter b_r and, in addition, other factors must also be taken into account in view of the test results obtained. Taking into account these for both tests stage, it can be concluded that by increasing the v_c value, the frequency of entry of each cutting edge segment into the workpiece and the friction velocity between the tool and the workpiece and the between chip and tool also increased. Due to the intermittent operation of the cutting inserts along with the increased frequency, the active segments of the cutting edges are more subject to varying thermal stresses. Because carbide cutting inserts are sensitive to sudden and rapid changes in heat over time, they are more susceptible to fatigue damage in the CCs under consideration. It should also be noted that in the second phase, a significant inclination of the torus milling cutter axis was achieved relative to the machined surface, which contributes to an increase in the cutting (circumferential or tangential) component of the cutting force. As a result, with the occurrence of radial run-out of the milling cutter blades and the intermittent operation of each blade, the phenomenon of vibration between the cutting edge segment and the workpiece is amplified, and this in turn can significantly cause rapid progressive "notching" wear, which is a fatigue failure.

In all machining cases resulting from the CCs (see Tables 3 and 4), the chips easily adhere to the cutting edges (see Fig. 13), exacerbating the inhomogeneity of the thermal stress distribution. Furthermore, the blade material can peel off with the adhering chips during the cutting process. As can also be seen in Fig. 13, in addition to abrasive wear,

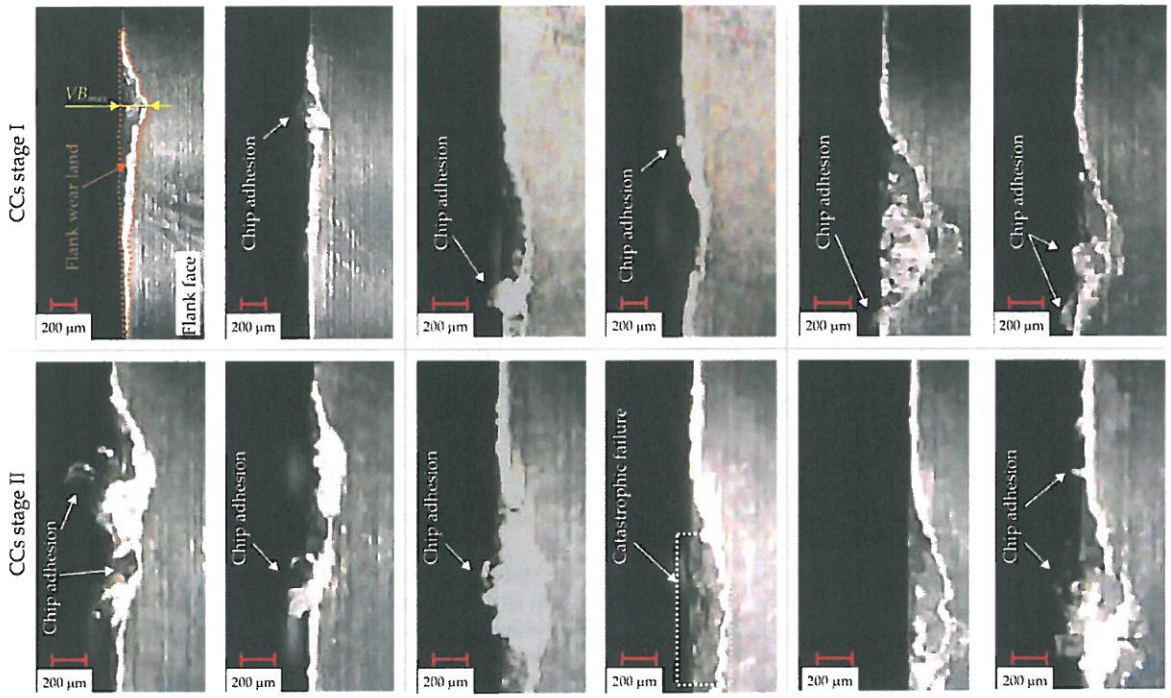

Fig. 13. Optical micrographs of flank wear land for all teeth and CCs.

catastrophic brittle exfoliation of the cutting blade material is observed, confirming the above assumptions.

In addition, it is also worth noting the tool life obtained for the criterion VB = 0.1 mm in both stages of the tests. It can be clearly seen that when the cutting speed v_c in the second stage of the tests is programmed as constant at the CP_i contact point, the parameter VB has a comparable value regardless of the currently active cutting edge segment. This means that maintaining a constant value of the cutting speed v_c at the CP_i contact point, and therefore in the zone of direct formation of the machined surface geometric structure, can result in a uniform change in tool geometry, especially during the lapping stage.

Fig. 14 shows SEM images and EDS analysis for a selected segment of the cutting blade and the wear area of this cutting blade on the flank face. This work is limited to a single example of SEM-EDS due to the similarities in wear mechanisms, whereas a comprehensive analysis of wear mechanisms in correlation with the active cutting edge segment in the given CCs is the subject of subsequent extensive research work by the lead Author research.

Analysing the resulting SEM-EDS images, it was found that along the active cutting edge segment of the round insert, essentially three wear areas can be distinguished due to the elemental components of the (part and tool) materials in the CWE. The first is the area within the notching wear (p. 6 of the EDS analysis). Within this area, components of Ni, Cr, Fe parts (including chip adhesion) as well as W, Nb, Ti, Al tools are present (see Tables 1 and 2). This indicates both adhesive and diffusion wear in this area. The second is the area within the extreme vicinity of the active cutting edge segment (p. 2, 7, 11, 1 of the EDS analysis). Within this area there are both components of Ni, Cr, Fe parts and, in a higher percentage of the tool, W, Nb, Ti, Al. This indicates mainly adhesive wear. The third is the area within the flaking wear and the blade coating layer intact in the machining process (p. 3, 8, 10 of the EDS analysis). Within this area, there are only exposed components of the W part as well as components of the Ti, Al coating. This indicates a lack of materials interaction.

Furthermore, in practically all cases resulting from the adopted CCs, chips and microchips are observed adhering to the cutting edge. Chip adhesion occurs mainly on the flank face, whereas microchip adhesion occurs on both the flank and the rake faces. The adhesion of the microchips to the flank face is more serious than on the rake face. The mechanism of adhesive wear is confirmed by EDS analysis. Tool wear is generally uniform. However, it has been noted that as the flank face is worn down, a notching phenomenon also occurs. Interestingly, depending on the currently active segment of the cutting edge, starting from the 1-st to the 3-rd, this phenomenon, together with the maximum width of the wear band VB_{max}, is displaced along the cutting edge from the M point towards the CP_i contact point. This is the case for both CCs in the first and second stages of research. This is confirmed by photographs of the flank faces (Fig. 13). This may have a significant impact on the roughness of machined surfaces, were shaped separately by the currently active segment of the cutting edge of the torus cutter, which resulting from the adopted CCs.

5.2. Cutting torque

The cutting torque Mz around the tool axis was determined by relation (17):

$$M_z = R_{eff}\sqrt{F_{cN}^2 + F_c^2} \tag{17}$$

where, F_{cN} and F_c are the instantaneous values of the normal (feed force) and cutting (circumferential or tangential) components of the resultant cutting force, respectively, and R_{eff} is the effective tool radius at the CP_i contact point.

Fig. 15 shows polar diagrams of the cutting torque M_z changing with the rotation angle of the torus milling cutter for each of the 12 cases (which results from the adopted CCs and the separated active cutting edge segments) in the first passes of the cutting blades when VB≅ 0 mm and when VB≅ 0.1 mm. For all graphs in CCs of stage I and for segment I in CCs of stage II of the tests, 70 full rotation cycles were taken into account, and due to the large disturbances generated during the cutting process resulting from high values of cutting speed, for segments II and III in CCs of stage II of the tests, 20 full rotation cycles were taken into account.

Each "petal" in the polar diagram represents the cutting torque of each cutting blade. The inconsistency of the cutting torque results

a)

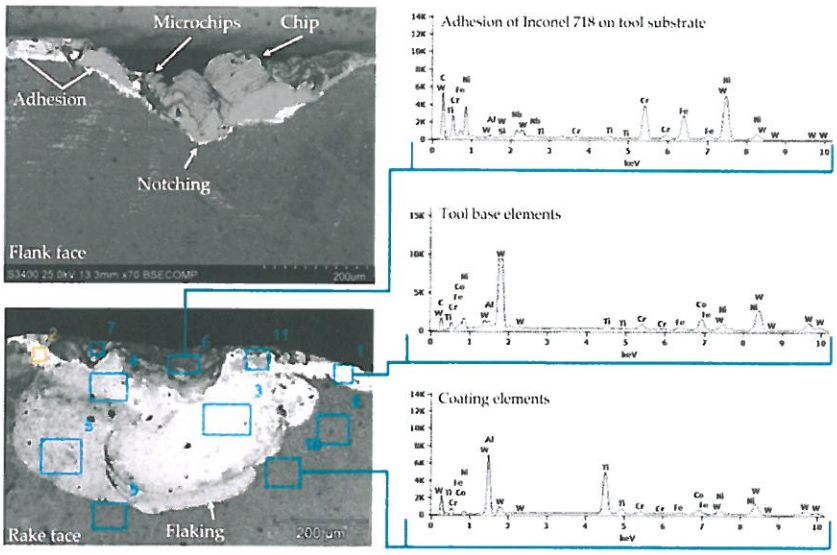

b)

Weight %

	Al	Ti	Cr	Fe	Co	Ni	Zn	Nb	W
pt1	2.0	1.7	3.4	1.9	9.6	5.0			76.4
pt2	1.5	0.6	4.2	4.3	9.2	6.5		2.1	71.6
pt3		0.1	1.7	0.6	12.0	1.3			84.3
pt4			1.7	0.4	12.7	0.8			84.4
pt5			1.6	0.5	12.2	0.6			85.1
pt6	0.8	1.1	19.7	19.5		53.2		4.8	0.8
pt7	0.9	1.0	17.2	16.7		41.6	9.2	5.4	8.1
pt8	21.2	27.3	2.4	1.9	3.9	4.7			38.7
pt9	11.8	20.9	4.6	3.7	4.7	10.6			43.7
pt10	17.6	24.9	2.1	1.4	4.6	3.6			45.8
pt11	0.9	0.7	14.0	13.0	4.3	36.3		4.1	26.6

Fig. 14. SEM images of wear on the flank and rake faces of the round cutting insert (a) together with EDS plots with detailed element components description (b) of selected areas for v_{cCP_i} = 71 m/min.

from the run-out of the cutter cutting blades, i.e., cutting blade No. 1 takes on a larger volume of the cutting layer than cutting blade No. 2. Moreover, can be seen on the graphs clearly show a displacement of course of the cutting torque between different rotation periods. This should be interpreted in such a way that the torque course in cycle n-1 is overtaken by the torque course in the tool rotation cycle n-2. As time passes, each "petal" becomes thicker. Similarly, state the authors in the work [29]. This happens for two main reasons. First, the data acquisition card has a certain clipping error, which causes the rotation angle recorded by the computer to be constantly delayed compared to the actual rotation angle. Secondly, the wear and chipping reduce the actual tool radius. The tool must then rotate at a larger angle (engagement angle) to contact the cutting layer in the CWS. Since the data acquisition card in each of the CCs adopted in the research is the same, comparison of the cutting torque wave offset angle (defined as the angle of each "petal" between its boundary contours on polar diagrams) allows for a qualitative analysis of the tool wear. As shown in Fig. 15, the wave offset angles for each case reflect the wear VB, according as shown in Fig. 12. This indicates that the cutting torque is a sensitive parameter for monitoring tool wear. Furthermore, due to tool wear, the amplitude of the cutting torque in each engagement period changes drastically in all CCs for VB ≅ 0 mm, while it is relatively stable in all CCs for VB ≅ 0.1 mm. The exceptions are the amplitudes for segments II and III in CCs of stage II of the tests, where gradually progressive wear recorded in each run of a singular cycle can be clearly observed. This is another confirmation that cutting torque is a sensitive parameter that allows monitoring of tool wear in the milling process, especially finishing high-speed milling.

5.3. Surface roughness

Fig. 16 shows the graphs of the *Sa* and *Sz* parameters of the machined surface roughness, obtained as a result of multi-axis milling according to the adopted CCs. Analysing individual graphs separately, it can be seen that, due to the wear of the torus milling cutter blades, the roughness of the machined surface changes. Moreover, each of the charts, representing a specific case resulting from the adopted CCs, illustrates the completely different nature of these changes, although some similarities between them can be noticed.

The roughness parameters *Sa* and *Sz* in Fig. 16(a) are: for VB ≅ 0 mm, 0.59 μm and 4.09 μm, respectively; for VB ≅ 0.1 mm, 0.54 μm and 4.56 μm respectively; and for VB ≅ 0.2 mm, 0.76 μm and 4.77 μm, respectively. In this case, despite the progressive wear of the tool, the roughness of the machined surface initially decreases (to VB ≅ 0.1 mm) and then increases. A similar course was obtained for cases (c) and (d) in Fig. 16. In turn, the parameters *Sa* and *Sz* in Fig. 16 (b) are: for VB ≅ 0 mm, 0.99 μm and 13.40 μm, respectively; for VB ≅ 0.1 mm, 1.65 μm and 8.01 μm, respectively; and for VB ≅ 0.2 mm, 1.01 μm and 6.16 μm, respectively. In this case, even though the wear limit VB = 0.2 mm is reached, the roughness parameters of the machined surface are not the highest. The reason for this is that the parameters of multi-axis milling (inclination angle δ, distance between tool paths h_r, cutting speed v_c) and the material properties of the cutting blades and the workpiece influence the size and number of valleys and peaks of the machined surface, which is confirmed by the summary of *Sa*, *Sz* and topography images for cases in the II-nd stage of the CCs, as shown in Fig. 17. Additionally, the change in tool geometry during the lapping

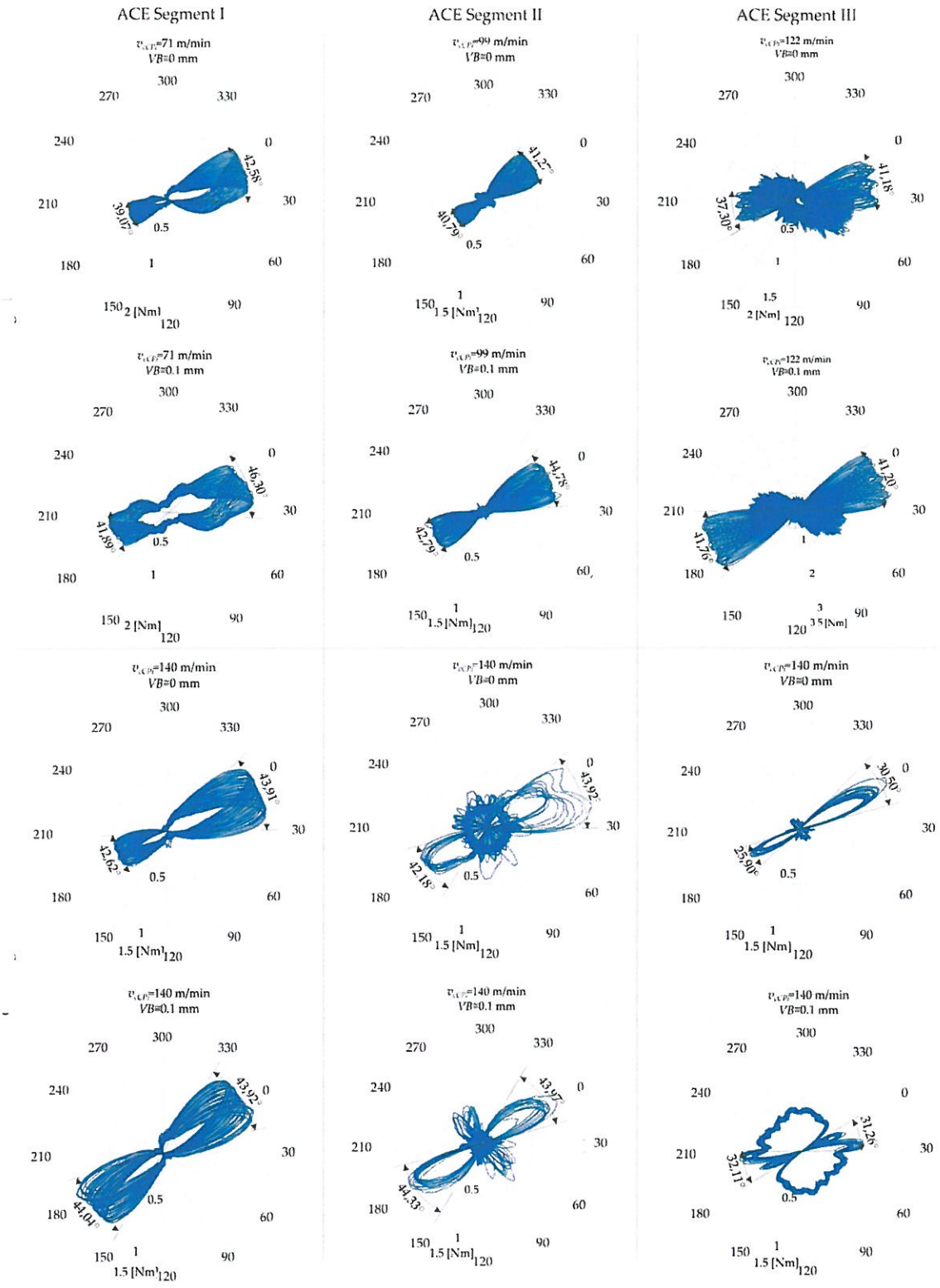

Fig. 15. Polar diagrams of the cutting torque Mz varying with the rotation angle.

stage and the formation of flashes or chips stuck on the machined surface should be taken into account. Therefore, on this basis, it can be concluded that the influence of the torus milling cutter wear on the roughness of the machined surface is not a simple linear relationship, but relationship between: the parameters of multi-axis milling, tool wear, and the roughness of the machined surface, and is a coupled relationship. Based on the above, it can also be concluded that the graphs presented in Fig. 16(a) and (b) represent two extremely different cases of the distribution of roughness parameters, taking into account the criterion degrees of torus milling cutter wear adopted in the work.

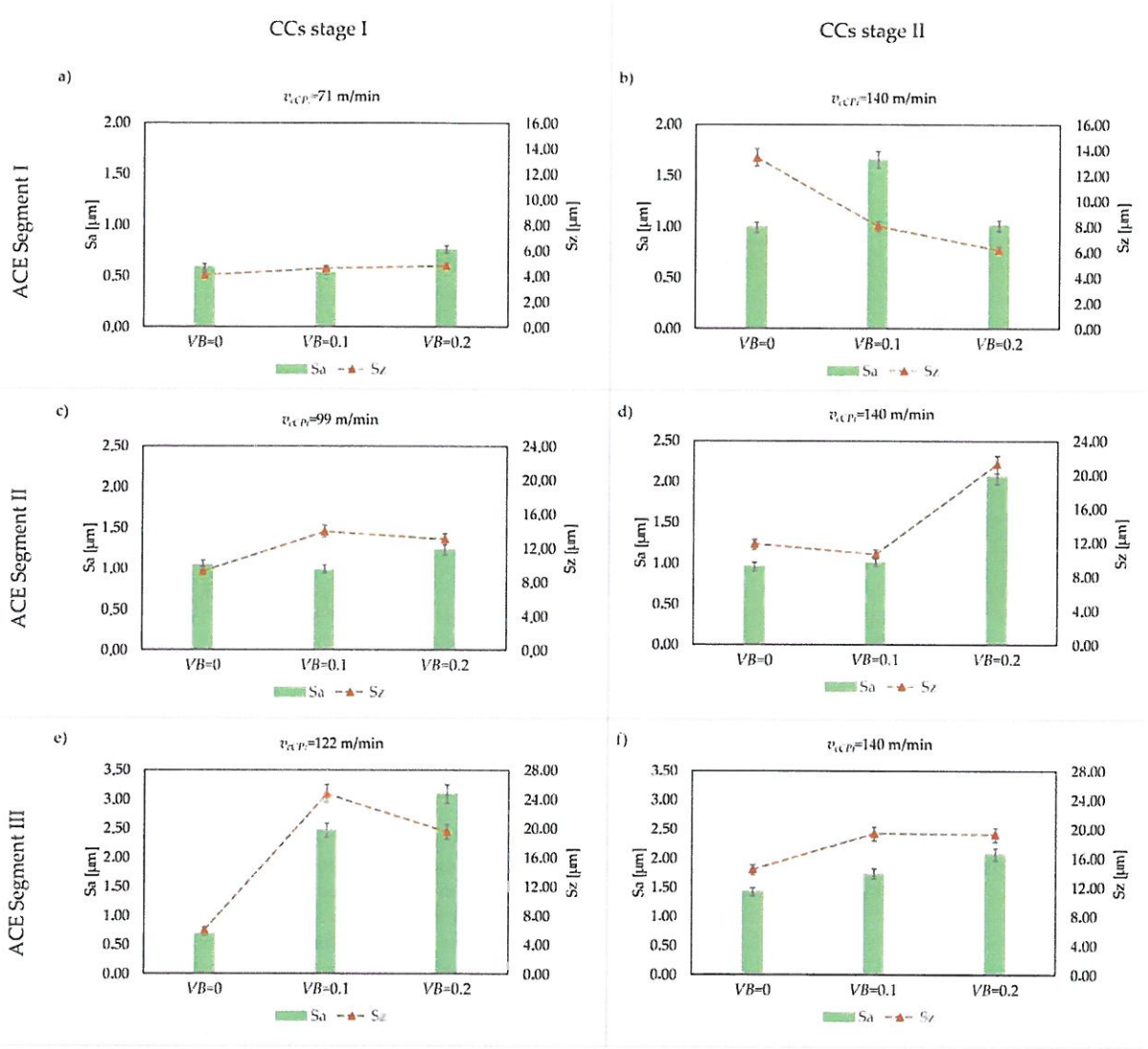

Fig. 16. Surface roughness obtained as a result of machining according to the adopted CCs.

Therefore, Fig. 18 shows a comparison chart of the measured topography of machined surfaces obtained after the multi-axis milling process using the first active segment of the cutting edge of a torus milling cutter for CCs I and CCs II, taking into account the criteria of tool wear stages adopted in the work. Based on these topography images, it can be seen that with the change of conditions in the CWE and the progressive wear of the cutter cutting blades, the topography of the machined surfaces also changes. Analysing the topographies obtained for the ACE Segment I in CCs stage I (images on the left), it can be seen that when the wear indicator VB ≅ 0 mm the parameter Sz = 4.09 µm, when the wear indicator VB ≅ 0.1 mm the parameter Sz = 4.56 µm, and when the wear indicator VB ≅ 0.2 mm, the parameter Sz = 4.77 µm. Therefore, in this case, as the tool wear degree increases, the height of the topography peaks also gradually increases. Based on this, it can be concluded that as the degree of tool wear increases, the profile of the topography valleys will gradually, but to a small extent, increase due to the abrasion of the flank face within the CP_i point, with a simultaneous minimal increase in the topography peaks along with their widening due to the notching and the resulting narrowing of the topographic width of the machined strip e (for VB ≅ 0 mm, the parameter e = 1 mm, and for VB ≅ 0.2 mm, the parameter e = 0.75 mm). This is confirmed by topography images and optical micrographs of the flank face of the cutting blade for VB ≅ 0.2 mm. In turn, the Sa parameter first decreases and then increases with the increase in the wear stage.

However, when analysing the topography obtained for the ACE Segment I in CCs stage II (images on the right), it can be seen that when the wear indicator VB ≅ 0 mm the parameter Sz = 13.40 µm, when the wear indicator VB ≅ 0.1 mm the parameter Sz = 8.01 µm, and when the wear indicator VB ≅ 0.2 mm, the parameter Sz = 6.16 µm. Therefore, in this case, as the tool wear stage increases, the height of the topography peaks gradually decreases. Based on this, it can be concluded that as the degree of tool wear increases, the profile of the topography valleys will gradually increase due to the abrasion of the cutting blade flank face and the notching occurring within the CP_i contact point due to the cutting speed. The increase in topography peaks with their widening is negligible in this case, and the boundary between topography peaks and valleys is blurred. This is confirmed by topography images and optical micrographs of the cutting blade flank face for VB ≅ 0.2 mm. In turn, the Sa parameter first increases and then decreases with the increase in the wear stage.

Until now, it was believed that tool wear always had a negative impact on the roughness of the machined surface. However, this work

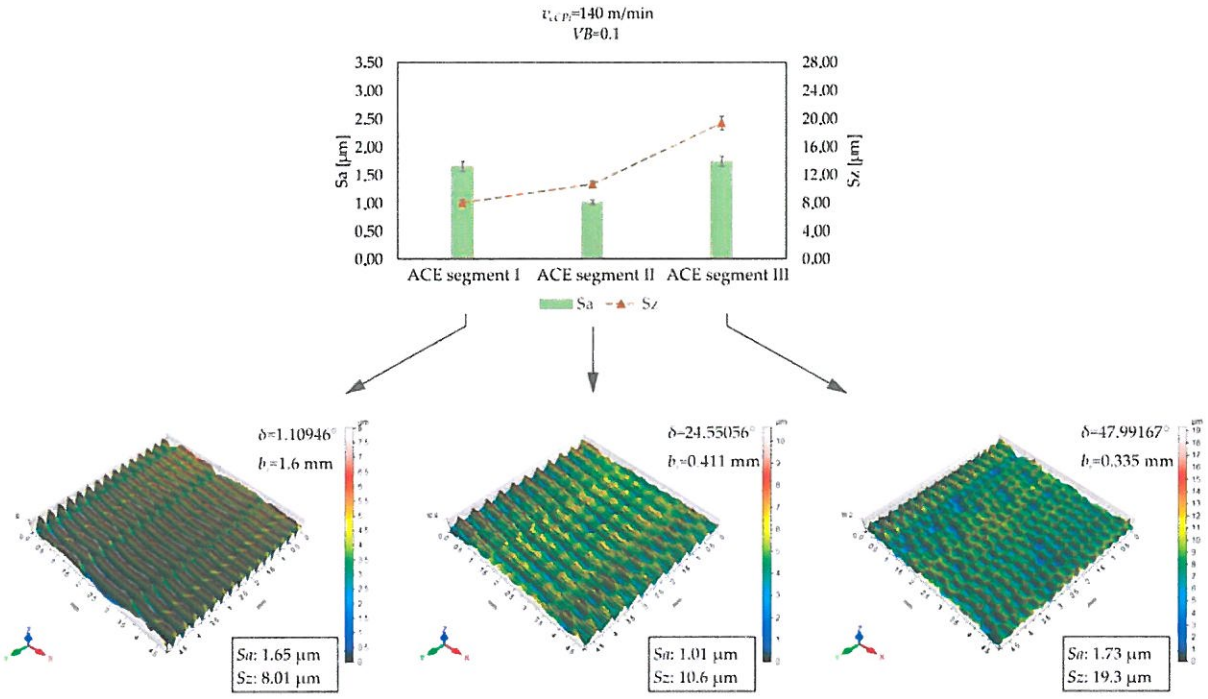

Fig. 17. Overview of *Sa*, *Sz* and topography images for CCs stage II cases, illustrating the influence of multi-axis milling parameters on the size and number of valleys and peaks of the machined surface.

proves that when tool wear is controlled within a specific range, it can significantly improve the surface quality of the workpiece, as also on the total tool life with the proposed own strategy of adaptive segmentation of the active cutting edge of the torus milling cutter in the process of multi-axis milling of Ni-based superalloys.

6. Conclusion

This work presents the issues and development of the own models of the process of multi-axis high-speed milling of the surface of Ni-based superalloy Inconel 718 parts used the torus milling cutter in a kinematic variant of the TPl (Tool Pulling) type in terms of tool wear. As the cutting speed in finishing high-speed milling is the parameter with the greatest influence on tool life and surface roughness, the dependence of the variation of the cutting speed at the torus part of the cutter was first determined as a function of the distance from the tip point along the axial direction and the geometrical parameters of the torus. A model for multi-axis milling of the TPl type was then developed and described in a simplified manner, which forms the basis of an in-house strategy for segmenting the cutting edge of a torus milling cutter. The adaptation of a given segment to the active cutting edge during machining is based on tool wear and kinematic roughness criteria. Simulations and experiments of multi-axis milling were carried out, and the necessary analyses were performed. In this paper, in addition to testing an in-house strategy for multi-axis milling used the torus milling cutter, the problem of defining the cutting speed in relation to the nominal diameter and effective diameter of the tool is investigated for the first time. In addition, wear measurement was carried out using an in-house methodology, taking full advantage of the capabilities of the multi-axis machining centre, which significantly reduced measurement time and positively influenced the effectiveness of tool life assessment. The following conclusions were drawn from the results obtained:

- Based on the developed model dependence of the cutting speed $v_{c,g}$ at a point of height g from the apex of the TCP torus milling cutter and the simulations carried out in the range of the cutting blade work angle $0° \leq \psi_r \leq 90°$, it was found that the cutting speed changes not only taking into account the parameter g, but also the geometric parameters of the torus, i.e. R_T and r_p. Therefore, three geometrical cases of the torus were specified: ring torus, horn torus, and spindle torus.
- It was found that for the cases of: ring torus and spindle torus geometries, the R_T parameter causes a radial displacement of the cutting edge and thus an increase in the value of the cutting speed $_v$c over the entire range of the cutting blade work angle ψ_r adopted for the simulation. The maximum distance g from the TCP apex of the torus milling cutter in the assumed range of the cutting blade work angle ψ_r does not change. The parameter r_p also increases the cutting speed v_c throughout the range of the cutting blade work angle ψ_r adopted for the simulation, while also increasing the maximum distance g from the TCP apex of the cutter. In terms of the sequences of change of v_c and g as a function of R_T and r_p described above, the case of horn torus geometries is special, as these sequences occur simultaneously.
- An increase in the value of the inclination angle δ of the torus milling cutter axis results in an increase in the value of the cutting speed (while keeping the values of the parameters a_p, n, D constant) and a decrease in the work angle of the cutter. The effect of the instantaneous contact angle θ on the cutting speed values at each of the points on the cutting edge was observed to be nonmonotonic. The differences between the maximum cutting speed v_{cmax} values at point M on the cutting edge and the values of the cutting speed v_c values at points CP_i and E on the cutting edge are even more than three times in the range of the higher inclination angle δ. An increase in the angle δ value of the results in an increase in the value of the v_{cmax} / v_c ratio. The aforementioned discrepancies can have a significant impact on the intensity of phenomena occurring in the contact zone between the CWE of the cutting edge and the workpiece material, particularly tool wear, and on the quality indicators of the machined surface.

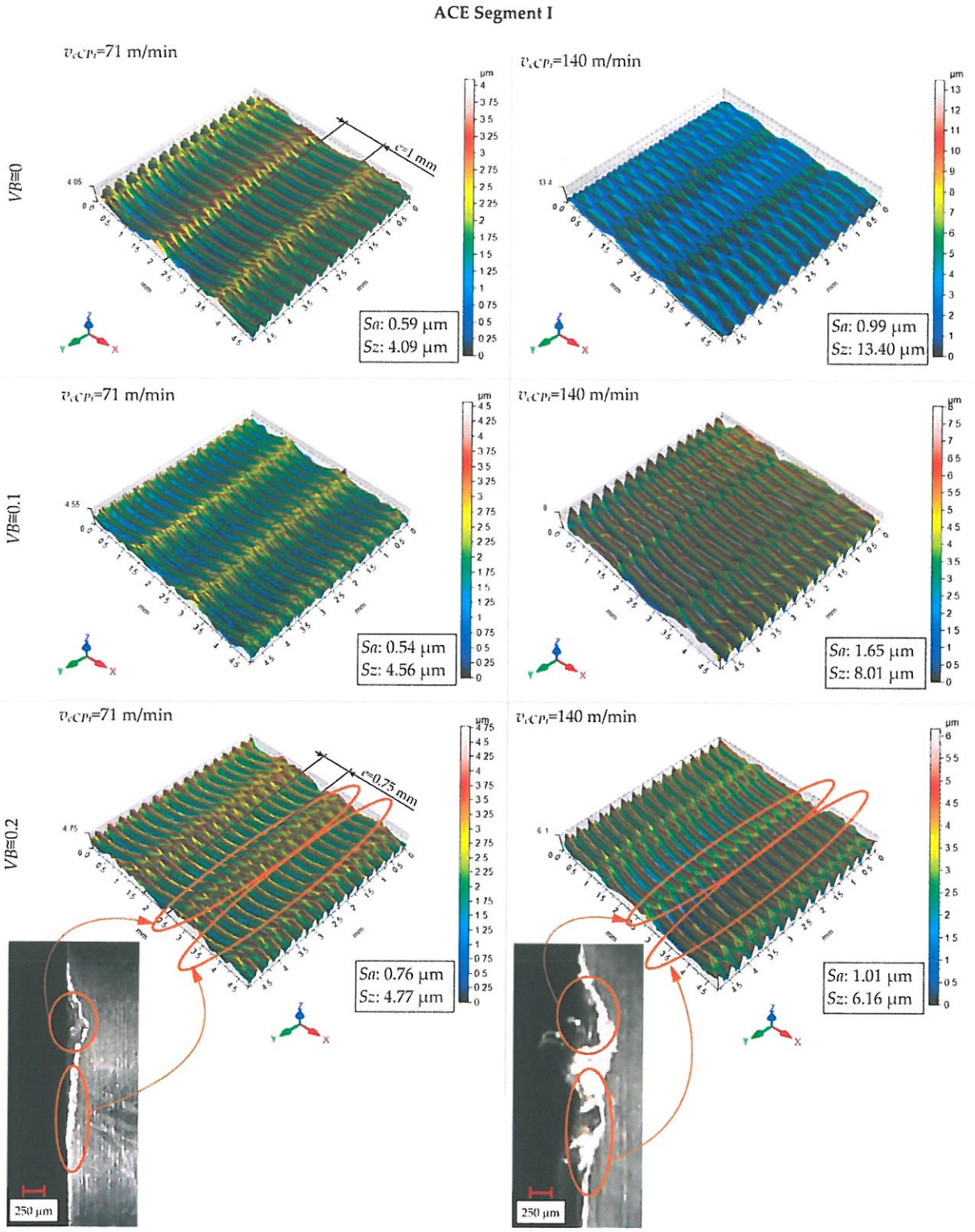

Fig. 18. Overview of the machined surfaces topography obtained after the multi-axis milling process using the first active segment of the cutting edge of a torus milling cutter for CCs stage I and CCs stage II, taking into account the criteria of tool wear stages adopted in the work.

- The torus milling cutter life to vary in machining with the individual active segments of the cutting edge. Furthermore, irrespective of the machining conditions, i.e. the definition of the cutting speed relative to the nominal diameter (C_D point) or effective diameter (CP_i contact point) of the cutter, the trend in the change in the tool life values of the torus milling cutter is comparable.
- As a result of the inclination of the torus milling cutter axis according to the ACACES own strategy together with the criteria,

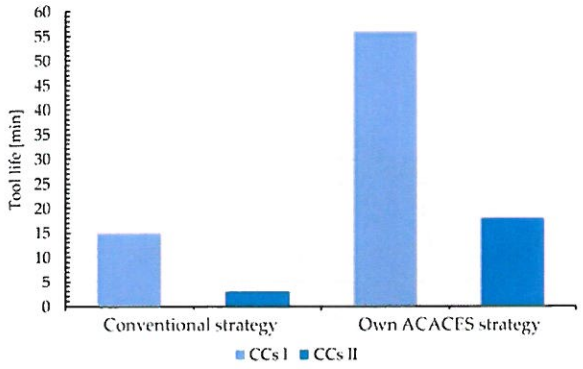

Fig. 19. Comparative comparison of torus milling cutter life for a conventional strategy and an own ACACES strategy for multi-axis milling of Ni-based superalloys.

there is a change in the values of two parameters, the distance between toolpaths b_r and the cutting speed v_c. Given these parameters, two phases of changes in the are detailed of the torus milling cutter durability in the ACACES strategy.

- The mechanism of tool wear consists of abrasion, strong chip adhesion, and chipping, caused by increased friction at the tool-workpiece interface and varying thermal stresses. As the flank face wears away, a notching phenomenon also appears. Depending on the currently active segment of the cutting edge, starting from the 1-st to the 3-rd, this phenomenon, together with the maximum width of the wear band VB_{max}, is displaced along the cutting edge from the M point towards the CP_i contact point.
- Tool wear causes the cutting torque to be constantly lag behind the rotation angle and causes variations in the amplitude of the cutting torque. The cutting torque is a sensitive parameter for monitoring tool wear.
- The influence of the torus milling cutter wear on the roughness of the machined surface is not a simple linear relationship, but relationship between: the parameters of multi-axis milling, tool wear, and the roughness of the machined surface, and is a coupled relationship. In general, the effect of tool wear on the roughness of the machined surface is positively correlated, but the present study showed that as tool wear increased, the surface roughness first decreased and then increased.
- When the wear of the torus milling cutter is controlled within a certain range, it is possible to significantly improve the surface quality of the workpiece as well as the total tool life with the proposed own ACACES strategy, relative to the conventional strategy, in the multiaxis milling of Ni-based superalloys with a torus milling cutter, as shown in Fig. 19.

CRediT authorship contribution statement

Michał Gdula: Writing – original draft, Visualization, Resources, Methodology, Investigation, Conceptualization. **Jerzy Józwik:** Writing – review & editing, Supervision. **Agnieszka Skoczylas:** Writing – review & editing, Investigation.

Declaration of competing interest

The authors declare that they have no known competing financial interests or personal relationships that could have appeared to influence the work reported in this paper.

Acknowledgements

The research leading to these results has received funding from the commissioned task entitled "VIA CARPATIA Universities of Technology Network named after the President of the Republic of Poland Lech Kaczyński" *contract no.* MEiN/2022/DPI/2578 *action entitled "In the neighbourhood - inter-university research internships and study visits".*

The authors would like to thank the editors and anonymous reviewers for providing insightful suggestions and comments to improve the quality of research paper.

Data availability

No data was used for the research described in the article.

References

[1] A. Nowotnik, Nickel-based superalloys, in: Reference Module in Materials Science and Materials Engineering, Elsevier, 2016, B9780128035818025741, http://dx.doi.org/10.1016/B978-0-12-803581-8.02574-1, URL https://linkinghub.elsevier.com/retrieve/pii/B9780128035818025741.

[2] M. Lotfi, M. Jahanbakhsh, A. Akhavan Farid, Wear estimation of ceramic and coated carbide tools in turning of Inconel 625: 3D FE analysis, Tribol. Int. 99 (2016) 107–116, http://dx.doi.org/10.1016/j.triboint.2016.03.008, URL https://linkinghub.elsevier.com/retrieve/pii/S0301679X16300020.

[3] A. Musfirah, J. Ghani, C.C. Haron, Tool wear and surface integrity of inconel 718 in dry and cryogenic coolant at high cutting speed, Wear 376–377 (2017) 125–133, http://dx.doi.org/10.1016/j.wear.2017.01.031, URL https://linkinghub.elsevier.com/retrieve/pii/S0043164817301060.

[4] A. Magri, A.E. Diniz, D.I. Suyama, Evaluating the use of high-pressure coolant in turning process of Inconel 625 nickel-based alloy, Proc. Inst. Mech. Eng. B 232 (7) (2018) 1182–1192, http://dx.doi.org/10.1177/0954405416664373, URL http://journals.sagepub.com/doi/10.1177/0954405416664373.

[5] N. Patil, A. Asem, R. Pawade, D. Thakur, P. Brahmankar, Comparative study of high speed machining of inconel 718 in dry condition and by using compressed cold carbon dioxide gas as coolant, Procedia CIRP 24 (2014) 86–91, http://dx.doi.org/10.1016/j.procir.2014.08.009, URL https://linkinghub.elsevier.com/retrieve/pii/S2212827114009858.

[6] M. Gdula, G. Mrówka-Nowotnik, Analysis of tool wear, chip and machined surface morphology in multi-axis milling process of Ni-based superalloy using the torus milling cutter, Wear 520–521 (2023) 204652, http://dx.doi.org/10.1016/j.wear.2023.204652, URL https://linkinghub.elsevier.com/retrieve/pii/S0043164823000352.

[7] Y. Wan, Z.Q. Liu, X. Ai, Cutting forces and tool wear patterns in five-axis milling Fe-based super alloy with bull-nose end mill, Adv. Mater. Res. 97–101 (2010) 2049–2052, http://dx.doi.org/10.4028/www.scientific.net/AMR.97-101.2049, URL https://www.scientific.net/AMR.97-101.2049.

[8] S. Uchikata, A. Beaucamp, Y. Takeuchi, 5-axis control finishing for decreased tool wear, Procedia CIRP 63 (2017) 313–317, http://dx.doi.org/10.1016/j.procir.2017.03.320, URL https://linkinghub.elsevier.com/retrieve/pii/S2212827117305085.

[9] P. Yang, C. Yao, S. Xie, D. Zhang, D.X. Tang, Effect of tool orientation on surface integrity during ball end milling of Titanium Alloy TC17, Procedia CIRP 56 (2016) 143–148, http://dx.doi.org/10.1016/j.procir.2016.10.044, URL https://linkinghub.elsevier.com/retrieve/pii/S2212827116310368.

[10] M. Luo, H. Luo, D. Zhang, K. Tang, Improving tool life in multi-axis milling of Ni-based superalloy with ball-end cutter based on the active cutting edge shift strategy, J. Mater. Process. Technol. 252 (2018) 105–115, http://dx.doi.org/10.1016/j.jmatprotec.2017.09.010, URL https://linkinghub.elsevier.com/retrieve/pii/S0924013617304090.

[11] A. Warkentin, F. Ismail, S. Bedi, Multi-point tool positioning strategy for 5-axis mashining of sculptured surfaces, Comput. Aided Geom. Design 17 (1) (2000) 83–100, http://dx.doi.org/10.1016/S0167-8396(99)00040-0, URL https://linkinghub.elsevier.com/retrieve/pii/S0167839699000400.

[12] L.-X. Cao, H. Gong, J. Liu, The offset approach of machining free form surface, J. Mater. Process. Technol. 184 (1–3) (2007) 6–11, http://dx.doi.org/10.1016/j.jmatprotec.2006.10.048, URL https://linkinghub.elsevier.com/retrieve/pii/S0924013606009034.

[13] M. Gdula, Empirical models for surface roughness and topography in 5-axis milling based on analysis of lead angle and curvature radius of sculptured surfaces, Metals 10 (7) (2020) 932, http://dx.doi.org/10.3390/met10070932, URL https://www.mdpi.com/2075-4701/10/7/932.

[14] Z. Chang, J. Qian, Z.C. Chen, N. Wan, D. Zhang, Geometrical theory of cutting stock with torus end mills in five-axis CNC machining and its applications in machining simulation, Int. J. Adv. Manuf. Technol. 105 (1–4) (2019) 27–46, http://dx.doi.org/10.1007/s00170-019-04064-8, URL http://link.springer.com/10.1007/s00170-019-04064-8.

[15] Z. Zhu, F. Peng, R. Yan, Z. Li, J. Wu, X. Tang, C. Chen, Influence mechanism of machining angles on force induced error and their selection in five axis bullnose end milling, Chin. J. Aeronaut. 33 (12) (2020) 3447–3459, http://dx.doi.org/10.1016/j.cja.2019.12.019, URL https://linkinghub.elsevier.com/retrieve/pii/S1000936120300765.

[16] D. Zhu, X. Zhang, H. Ding, Tool wear characteristics in machining of nickel-based superalloys, Int. J. Mach. Tools Manuf. 64 (2013) 60–77, http://dx.doi.org/10.1016/j.ijmachtools.2012.08.001, URL https://linkinghub.elsevier.com/retrieve/pii/S0890695512001575.

[17] E. Ezugwu, Key improvements in the machining of difficult-to-cut aerospace superalloys, Int. J. Mach. Tools Manuf. 45 (12–13) (2005) 1353–1367, http://dx.doi.org/10.1016/j.ijmachtools.2005.02.003, URL https://linkinghub.elsevier.com/retrieve/pii/S0890695505000544.

[18] N. Halim, C. Haron, J. Ghani, M. Azhar, Tool wear and chip morphology in high-speed milling of hardened Inconel 718 under dry and cryogenic CO2 conditions, Wear 426–427 (2019) 1683–1690, http://dx.doi.org/10.1016/j.wear.2019.01.095, URL https://linkinghub.elsevier.com/retrieve/pii/S0043164819302698.

[19] L. Zhang, M. Zheng, W. Zhang, K. Li, Influence and prediction of tool wear on workpiece surface roughness based on milling topography analysis, Int. J. Adv. Manuf. Technol. 122 (3–4) (2022) 1883–1896, http://dx.doi.org/10.1007/s00170-022-09939-x, URL https://link.springer.com/10.1007/s00170-022-09939-x.

[20] V.F.C. Sousa, F. Fernandes, F.J.G. Silva, R.D.F.S. Costa, N. Sebbe, R.C.M. Sales-Contini, Wear behavior phenomena of TiN/TiAlN HiPIMS PVD-Coated tools on milling Inconel 718, Metals 13 (4) (2023) 684, http://dx.doi.org/10.3390/met13040684, URL https://www.mdpi.com/2075-4701/13/4/684.

[21] M. Zawada-Michałowska, P. Pieśko, J. Józwik, Tribological aspects of cutting tool wear during the turning of stainless steels, Materials 13 (1) (2019) 123, http://dx.doi.org/10.3390/ma13010123, URL https://www.mdpi.com/1996-1944/13/1/123.

[22] X. Wu, Y. Liu, X. Zhou, A. Mou, Automatic identification of tool wear based on convolutional neural network in face milling process, Sensors 19 (18) (2019) 3817, http://dx.doi.org/10.3390/s19183817, URL https://www.mdpi.com/1424-8220/19/18/3817.

[23] J. Malhotra, S. Jha, Fuzzy c-means clustering based colour image segmentation for tool wear monitoring in micro-milling, Precis. Eng. 72 (2021) 690–705, http://dx.doi.org/10.1016/j.precisioneng.2021.07.013, URL https://linkinghub.elsevier.com/retrieve/pii/S0141635921001823.

[24] M. Rizal, J. Ghani, M. Nuawi, C. Haron, Cutting tool wear classification and detection using multi-sensor signals and Mahalanobis-Taguchi system, Wear 376–377 (2017) 1759–1765, http://dx.doi.org/10.1016/j.wear.2017.02.017, URL https://linkinghub.elsevier.com/retrieve/pii/S0043164817303095.

[25] J. Jurko, M. Miškiv-Pavlík, J. Husár, P. Michalik, Turned surface monitoring using a confocal sensor and the tool wear process optimization, Processes 10 (12) (2022) 2599, http://dx.doi.org/10.3390/pr10122599, URL https://www.mdpi.com/2227-9717/10/12/2599.

[26] M. Gdula, Adaptive method of 5-axis milling of sculptured surfaces elements with a curved line contour, J. Mech. Sci. Technol. 33 (6) (2019) 2863–2872, http://dx.doi.org/10.1007/s12206-019-0534-4, URL http://link.springer.com/10.1007/s12206-019-0534-4.

[27] W. Li, Y. Guo, M. Barkey, J. Jordon, Effect tool wear during end milling on the surface integrity and fatigue life of Inconel 718, Procedia CIRP 14 (2014) 546–551, http://dx.doi.org/10.1016/j.procir.2014.03.056, URL https://linkinghub.elsevier.com/retrieve/pii/S2212827114001991.

[28] O. Pereira, A. Rodríguez, J. Barreiro, A.I. Fernández-Abia, L.N.L. De Lacalle, Nozzle design for combined use of MQL and cryogenic gas in machining, Int. J. Precis. Eng. Manuf.-Green Technol. 4 (1) (2017) 87–95, http://dx.doi.org/10.1007/s40684-017-0012-3, URL http://link.springer.com/10.1007/s40684-017-0012-3.

[29] Q. An, C. Cai, F. Zou, X. Liang, M. Chen, Tool wear and machined surface characteristics in side milling Ti6Al4V under dry and supercritical CO2 with MQL conditions, Tribol. Int. 151 (2020) 106511, http://dx.doi.org/10.1016/j.triboint.2020.106511, URL https://linkinghub.elsevier.com/retrieve/pii/S0301679X20303431.

ARTYKUŁ
A5

dr inż. Michał Gdula
Politechnika Rzeszowska im. I. Łukasiewicza
Wydział Budowy Maszyn i Lotnictwa
Katedra Technik Wytwarzania i Automatyzacji

Rzeszów, dn. 23.04.2025 r.

OŚWIADCZENIE WSPÓŁAUTORA

Oświadczam, że w pracy:

lp.: ..A5..

Gdula M., Knapčíková L., Husár J., Vandžura R.: *Modeling and Measurement of Tool Wear During Angular Positioning of a Round Cutting Insert of a Toroidal Milling Tool for Multi-Axis Milling*. Applied Sciences-Basel (2024) 14, 10405. IF 2.5, MNiSW 100 pkt.;

mój wkład w powstanie tej pracy polegał na: współudziale w analizie aktualnego stanu wiedzy w zakresie tematu pracy, opracowaniu podstaw geometrycznych i matematycznych metody pozycjonowania kątowego okrągłej płytki skrawającej w korpusie frezu w aspekcie frezowania wieloosiowego oraz zużycia narzędzia, współudziale w opracowaniu metodyki pozycjonowania kątowego, opracowaniu metodyki badań, przeprowadzeniu badań eksperymentalnych, opracowaniu modelu zużycia frezu w oparciu o metodę najmniejszych kwadratów i algorytm Levenberga-Marquardta, przeprowadzeniu analizy zużycia narzędzia dla pozycjonowania kątowego, interpretacji wyników i opracowaniu wniosków, wykonaniu wykresów, rysunków oraz tabel, współudziale w opracowaniu manuskryptu, koordynowaniu procesu wydawniczego.

Gdula Michał

.....

Podpis
dr inż. Michał Gdula

Assoc. Prof. Dr. Lucia Knapčíková
Technical University of Košice
Faculty of Manufacturing Technologies
with a seat in Prešov

Prešov, dn. 05.12.2024 r.

OŚWIADCZENIE WSPÓŁAUTORA

Oświadczam, że w pracy:

lp.: A5

GDULA M., KNAPČÍKOVÁ L., HUSÁR J, VANDŽURA R.: *Modeling and Measurement of Tool Wear During Angular Positioning of a Round Cutting Insert of a Toroidal Milling Tool for Multi-Axis Milling*. Applied Science (MDPI), 2024, 14, 10405 https://doi.org/10.3390/app142210405;

mój wkład w publikację polegał na udziale w analizie stanu zagadnienia z zakresu pozycjonowania kątowego współpracujących części składanych narzędzi skrawających oraz udziale w opracowaniu manuskryptu.

.....
Podpis
Assoc. Prof. Dr. Lucia Knapčíková

Assoc. Prof. Dr. Jozef Hušar
Technical University of Košice
Faculty of Manufacturing Technologies
with a seat in Prešov

Prešov, dn. 05.12.2024 r.

OŚWIADCZENIE WSPÓŁAUTORA

Oświadczam, że w pracy:

lp.: ..... A 5 .....

GDULA M., KNAPČÍKOVÁ L., HUSÁR J, VANDŽURA R.: *Modeling and Measurement of Tool Wear During Angular Positioning of a Round Cutting Insert of a Toroidal Milling Tool for Multi-Axis Milling.* Applied Science (MDPI), 2024, 14, 10405 https://doi.org/10.3390/app142210405;

mój wkład w publikację polegał na udziale w zakresie opracowania metodyki pozycjonowania kątowego współpracujących części składanych narzędzi skrawających oraz udziale w opracowaniu manuskryptu.

.....
Podpis
Assoc. Prof. Dr. Jozef Hušar

Dr. Radoslav Vandžura
Technical University of Košice
Faculty of Manufacturing Technologies
with a seat in Prešov

Prešov, dn. 05.12.2024 r.

OŚWIADCZENIE WSPÓŁAUTORA

Oświadczam, że w pracy:

lp.: ..A5..

GDULA M., KNAPČÍKOVÁ L., HUSÁR J, VANDŽURA R.: *Modeling and Measurement of Tool Wear During Angular Positioning of a Round Cutting Insert of a Toroidal Milling Tool for Multi-Axis Milling*. Applied Science (MDPI), 2024, 14, 10405 https://doi.org/10.3390/app142210405;

mój wkład w publikację polegał na udziale w zakresie opracowania metodyki i przeprowadzeniu pomiarów zużycia ostrza, uwzględniając jego pozycje kątowe.

.....

Podpis
Dr. Radoslav Vandžura

applied sciences

MDPI

Article

Modeling and Measurement of Tool Wear During Angular Positioning of a Round Cutting Insert of a Toroidal Milling Tool for Multi-Axis Milling

Michał Gdula [1,*], Lucia Knapčíková [2], Jozef Husár [2] and Radoslav Vandžura [3]

[1] Department of Manufacturing Techniques and Automation, Faculty of Mechanical Engineering and Aeronautics, Rzeszow University of Technology, al. Powstańców Warszawy 12, 35-959 Rzeszów, Poland
[2] Department of Industrial Engineering and Informatics, Faculty of Manufacturing Technologies, Technical University of Košice, Bayerova 1, 080 01 Prešov, Slovakia; lucia.knapcikova@tuke.sk (L.K.); jozef.husar@tuke.sk (J.H.)
[3] Department of Automobile and Manufacturing Technologies, Faculty of Manufacturing Technologies, Technical University of Košice, Šturova 31, 080 01 Prešov, Slovakia; radoslav.vandzura@tuke.sk
* Correspondence: gdulam@prz.edu.pl; Tel.: +48-17-865-1372

Abstract: The aim of this study was to develop a concept for an angular positioning method for a round cutting insert in a torus cutter body dedicated to the multi-axis milling process under high-speed machining cutting conditions. The method concept is based on a developed wear model using a non-linear estimation method adopting a quasi-linear function. In addition, a tool life model was developed, taking into account the cutting blade work angle parameter, the laser marking method for the round cutting insert, and a wear measurement methodology. The developed tool wear model provides an accuracy of 90% in predicting the flank wear of the cutting blade. The developed procedure for angular positioning of the round cutting insert enables the entire cutting edge to be fully utilized, extending the total tool life. In addition, the measured largest defect values between the worn cutting edge and the nominal outline of the round cutting insert indicate the location of notching-type wear.

Keywords: multi-axis machining; torus milling cutter; angular positioning; round cutting insert; tool wear modeling; optical and digital measurements

check for updates

Citation: Gdula, M.; Knapčíková, L.; Husár, J.; Vandžura, R. Modeling and Measurement of Tool Wear During Angular Positioning of a Round Cutting Insert of a Toroidal Milling Tool for Multi-Axis Milling. *Appl. Sci.* **2024**, *14*, 10405. https://doi.org/10.3390/app142210405

Academic Editor: Mark J. Jackson

Received: 24 September 2024
Revised: 31 October 2024
Accepted: 6 November 2024
Published: 12 November 2024

Copyright: © 2024 by the authors. Licensee MDPI, Basel, Switzerland. This article is an open access article distributed under the terms and conditions of the Creative Commons Attribution (CC BY) license (https://creativecommons.org/licenses/by/4.0/).

1. Introduction

Continuous technological advances in the aerospace and energy industries, as well as molds and dies, are resulting in the increasing use of difficult-to-cut materials for responsible machine parts [1–5]. This necessitates the need for methods and strategies to extend the life of cutting tools. Difficult-to-cut materials, i.e., Ti alloys, Ni-based superalloys, and hardened steels, are generally characterized by low thermal conductivity and high hardening, which makes machining at high cutting speeds significantly more difficult. These are the main reasons for the rapid wear of tools, which has a negative impact on both the cutting process and the technological surface layer [6–9]. Therefore, tool wear is one of the main challenges in the precision machining of difficult-to-cut materials, especially nowadays in multi-axis machining [10,11].

In industrial practice, the torus milling cutter is increasingly being used to machine the surfaces of geometrically complex parts. This cutter, both in its monolithic form and essentially in the form of indexable round cutting inserts, is used especially in the finishing stage, mainly because of its unique geometry [12]. The vast majority of the work concerns the torus milling cutter in terms of the mechanics of the cutting process [12–15]. From the analysis of the issue to date, it appears that there is a lack of work that addresses the angular positioning of the round cutting inserts in the torus cutter body. This positioning

would aim to utilize all possible active cutting edge segments on the circle of the cutting insert in a given fixed tool axis orientation.

Positioning is defined as the exact location of a given object relative to an assumed reference point or line, which is usually the origin of a given Cartesian Coordinate System. Positioning, or more precisely, precise positioning, is also widely used in many areas of mechanical engineering, especially in the era of the Industry 4.0 industrial revolution [16]. In this case, the most tangible examples of precision positioning tasks are as follows: locating the probe of a measuring instrument relative to the measurement target, determining the position of the cutter relative to the workpiece, montaging a screw in the target hole using a robot arm, etc. All examples of engineering tasks related to precise positioning described above are supported by advanced systems and technologies, including measurement systems [16–26].

The measurement basis for precise positioning are the latest sensor technologies for single-axis, linear, or rotational measurements. The vast majority of practical applications require positioning in a plane or in a 3D space, and one of the most frequently used ones is angular positioning. These are realized by multi-axis coordinate measurement methods, such as triangulation and multilateration, as well as measurements in Cartesian and polar systems. The work in [27] presents the results of measuring the deviation of the shaft diameter after the turning process using the LTS laser triangulation sensor. A program was developed and verified whose task is to communicate between the PLC controller in the measurement system and the software for recording data obtained from the LTS laser triangulation sensor. In this case, inspection of the manufactured product is one of the most important operations in the technological production process [28]. Based on the test results, the authors concluded that this type of sensor is suitable for measuring the deviation parameter of the diameter of the machined surface. Another important issue is to reduce the positioning error of the rotary table of a multi-axis machine tool. The angular positioning error in this case causes poor quality milling of the workpiece surface. Therefore, in [29], the authors developed a system to improve this issue, using the Laser R-Test to calibrate angular positioning and compensate for positioning errors of the numerically controlled axes of the machine tool. Uncertainty analysis and calibration were implemented to predict the system. As evaluated by the authors of this work, the proposed measurement method can also solve the problems of coaxiality between the measuring devices and the rotary table. The system developed in this work achieves an angular error of 0.00121° for real workpieces, which is smaller than the error achieved by the commercial system, which is approximately 0.0022°. In turn, in [30], the angular positioning error of the rotary axis caused by the tilt movement error and the spindle radial movement error was analyzed and experimentally verified. In addition, the offset value introduced to the encoder was analyzed and experimentally verified. Angular positioning is also an important parameter that determines the proper operation of force systems. Hence, in [31], a non-contact optical sensing method was developed to simultaneously detect the linear and angular position of the rotor of a prototype 2DOF-SRM reluctance motor. In [32], the authors proposed a method for calibrating the angular positioning deviation of a precision rotary table of a coordinate measuring machine based on a measurement system with a laser marker. The Levenberg–Marquardt algorithm and the singular value distribution transformation were used to calculate the coordinates of the laser marker station. The fixed-interval angular deviation was calibrated using a geometric relationship model between the coordinates of the laser marker station and the rotation angle of the turntable. The work in [33] presents an angular position measurement system based on a sensor consisting of a single transmitter and two receiving coils. The mutual inductance between the transmitter coils was spatially modulated using conductive lenses. The measurement results form the basis for estimating the absolute angle. The advantage of this solution is resistance to many harmful factors, such as moisture, poor lighting, or oil contamination. Therefore, this system could be successfully used for angular positioning, e.g., indexable cutter blades. Angular positioning is also important from a military point of view. In [34], a system

was developed based on an algorithm to calculate the angular position of the rocket in real time when it is ready to launch from the rocket launcher. For this purpose, video streams recorded from three different cameras were used. Finally, the algorithm was implemented on a programmable SoPC chip using FPGA programmable array gates. In addition to systems based on sensors or optics, flexible mechanical systems are also used for precise angular positioning [35]. These are usually flexible micro-angular position measurement systems.

However, in order to measure along with determining the positioning of the circular cutting edge insert, it is necessary to know after what time this insert needs to be turned in the cutter body due to wear. For this, there is a need to develop tool wear and life models. In terms of multi-axis milling, Luo et al. [11] proposed such a model, but it is a linear model. The linear model does not predict the variable nature of wear progression during the operational wear progression phase. Hence, in this thesis, a non-linear estimation is proposed that predicts this variable nature.

The purpose of this study is to develop the basis for an angular positioning method for the circular cutting insert of a torus cutter that takes into account its wear and life. To achieve this, the parameters for the orientation of the tool axis with respect to the normal vector of the machined surface and the technique for avoiding undercutting the machined surface in multi-axis milling were first defined. A relationship was then determined for the working angle of the cutting blade, which is also a parameter controlling the orientation of the tool axis, and in its range, the wear progress of the active cutting edge segment is observed. A study of the machinability of the selected material was carried out, and a life and wear model for the torus milling cutter was developed from the resulting database. Integral to the above steps and the proposed method are measurements of tool wear and angle for angular positioning of the round cutting insert. The paper concludes with conclusions and the identification of directions for further research.

2. Fundamentals of the APofRCI Method, Taking into Account Torus Milling Cutter Cutting Blade Wear

In multi-axis face milling, the milling cutter can have any orientation in the Cartesian space when machining a sculptured surface, assuming, of course, that there is no collision—in the sense of undercutting. Consequently, different tool orientations can also be defined for a given toolpath. The geometrical characteristics of the milling cutter used for machining, the geometrical characteristics of the machined surface, and the resulting contact conditions (CWE: cutter-workpiece engagement) between the tool and the machined surface must also be taken into account.

2.1. Definition of the Torus Milling Cutter Axis Orientation

In the present work, in order to obtain the orientation of the tool axis for the kinematic variant of TPL (tool pulling) multi-axis cutting, the inclination angle was used as the process adjustment variable. In the present work, in order to obtain the tool axis orientation for the kinematic variant of TPL (tool pulling) multi-axis cutting, the inclination angle was used as the process adjustment variable. It is the same as the advance angle in this variant. The lead angle β, along with the tilt angle α, is an essential adjustable variable in CAM systems at the pre-processing stage. On the other hand, in the NC code, based on the conversion relationship between angles β and α, the inclination angle setpoint adjustable variable δ obtained in the post-processing stage of the CAM system is derived and, in this version, interpreted by the CNC control of the machine tool. Figure 1 illustrates the set variables of the tool axis, and the conversion relationship is described by Equation (1). Equation (2) defines the condition when the inclination angle is the same as the lead angle.

$$\delta = \cos^{-1}[\cos(\alpha)\cdot\cos(\beta)], \tag{1}$$

$$\beta = \delta, \quad \text{when}: \ \alpha = 0^{\circ}, \tag{2}$$

where β is the lead angle; α is the tilt angle; and δ is the inclination angle.

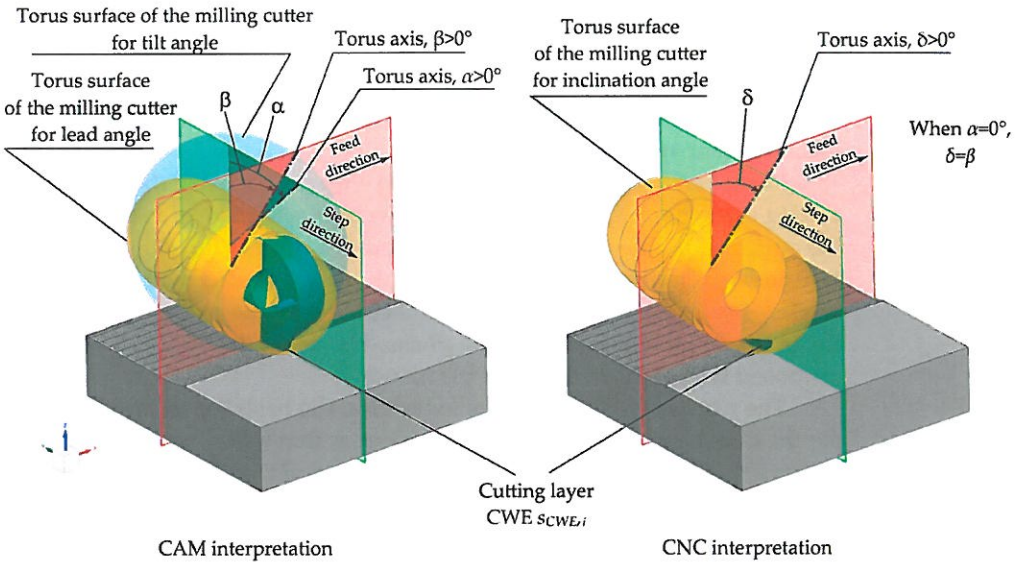

Figure 1. Tool axis orientation and its interpretation at pre-processor and post-processor stages.

2.2. *Characteristics of the Torus Milling Cutter*

In industrial practice, torus cutters are increasingly used in the multi-axis face milling process of TPL. These cutters enable larger cutting widths to be achieved, allowing efficiency to increase and machining time to be reduced. The design of torus cutters also allows higher cutting speeds and feed rates to be used. These are usually folding cutters with indexable Round Cutting Inserts (RCIs) for nominal diameters of these cutters from 12 mm.

The design advantage of this type of cutter is that the indexable round cutting insert can be rotated around the axis of its mounting hole to use a new, unused cutting edge segment for machining. This allows the tool life to be significantly extended. Currently, this rotation is carried out without any control of the angular position of the round cutting insert, leading to an unreasonable use of the real segments of the cutting edge around its circumference. The tool life decreases. The possible cases are schematically illustrated in Figure 2.

The first illustrated case (Figure 2a) shows the overlap of part of a new cutting edge segment with a worn segment. This erroneous angular position can result in significant deterioration of the technological surface layer and progressive catastrophic tool wear. The second case (Figure 2b) illustrates the occurrence of an excessive gap between adjacent segments after uncontrolled rotation of the RCI. In turn, this erroneous angular position reduces the cutting capacity of the tool due to incomplete use of the entire cutting edge. In contrast, the third case (Figure 2c) illustrates a worn and new segment, directly adjacent to each other. This will only happen if the rotation of the round cutting insert around the axis of the mounting hole is controlled.

The main objective of this article is to develop an angular positioning method for the round cutting insert of the torus milling cutter that allows the full cutting potential of the entire edge of the insert to be exploited by adhering segments with uniform angular dividing.

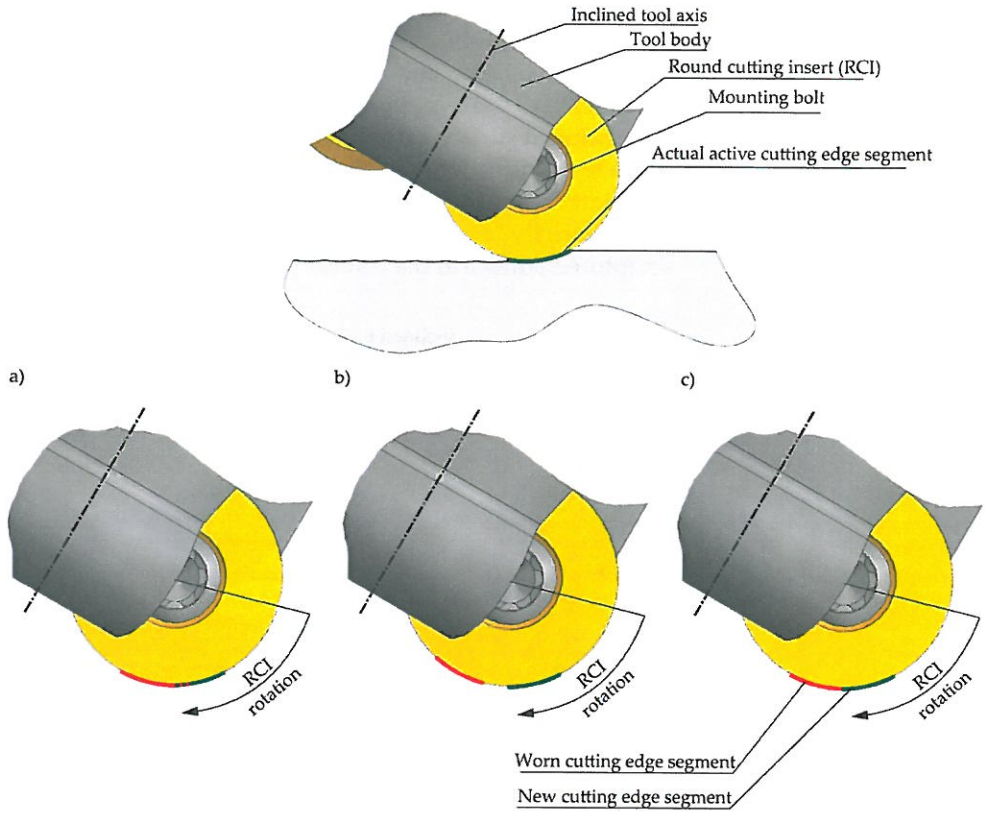

Figure 2. Possible cases of the round cutting insert rotation: (**a**) overlapping of a new segment with a worn segment—wrong; (**b**) too large a gap between segments—wrong; (**c**) segments adjacent to each other—correct.

2.3. Method to Avoid Undercutting the Machined Surface

In order to develop an angular positioning method for round cutting inserts of the torus milling cutter, dedicated to the multi-axis milling process, it is first necessary to determine the minimum required inclination angle δ. The minimum inclination angle required is to ensure that the torus milling cutter axis is positioned in such a way that no undercutting of the workpiece surface occurs. Three surface types were selected in terms of shape: biconcave, saddle concave-convex, and saddle convex-concave. The selected sculptured surfaces are described by a radius of curvature radius ρ parameter (the inverse of the curve curvature) in the feed direction ρ_1 and in the direction perpendicular to the feed ρ_2, respectively. A negative sign was assumed for the radius of convex curvature and a positive sign for the radius of concave curvature, as illustrated in Figure 3.

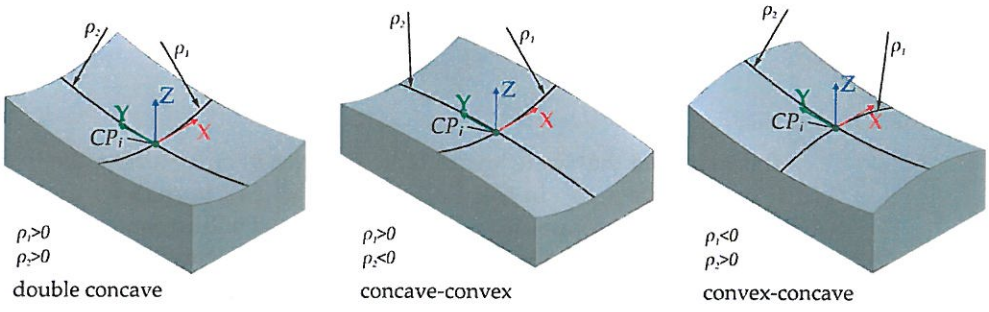

Figure 3. Types of sculptured surfaces.

A sphere of radius R was used to determine the position of the tool in a way that excludes the possibility of the torus undercutting the machined surface. This method was first defined by Marciniak [36]. The common part of the sphere and the torus is the contact diameter, and the local position of the tool determines the contact between the torus and the machined surface at the CP_i contact point, as shown in Figure 4. The inclination angle δ of the tool axis is defined relatively to the nornal vector $n(CP_i)$ of the machined surface at the contact point CP_i. In generalizing the problem, the machined surface was assumed to be a strictly tangential plane. This plane, in turn, is a simplified model of any type of sculptured surface at the contact point between the torus and the machined surface.

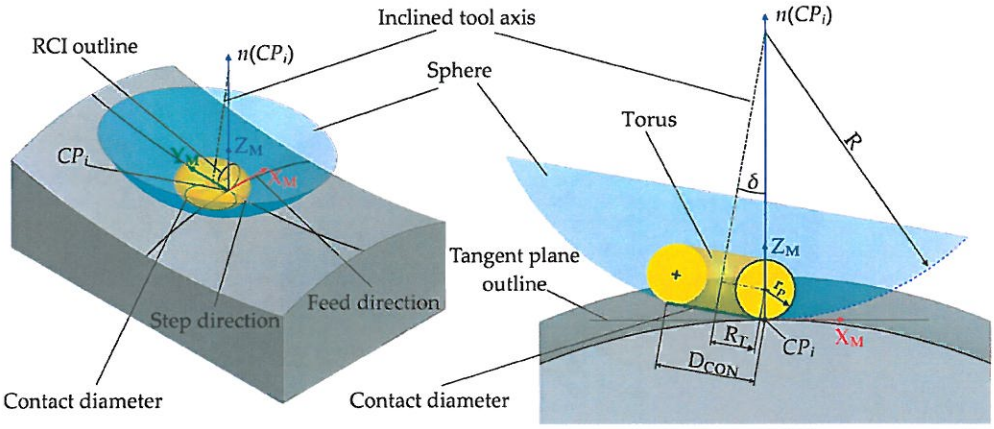

Figure 4. Method of detecting undercutting of the machined surface by the torus of the cutter.

The radius of sphere R can be determined using Equation (3).

$$R = \frac{R_T}{\sin(\delta)} + r_p, \tag{3}$$

where R_T is the radius of the torus milling cutter (the tool rotation axis of distance of the torus from the center of the RCI outline defining it); δ is the inclination angle; r_p is the radius of the round cutting insert (the circle defining the torus).

The undercutting of the machined surface by the torus does not occur when Equation (4) is fulfilled.

$$R \leq \rho_1, \rho_2, \tag{4}$$

where ρ_1 is the smallest radius of concave curvature in the feed direction; ρ_1 is the smallest radius of concave curvature in the step direction.

The above condition must be met for concave contours (for which the curvature has a positive sign). For convex contours, for $\delta \geq 0°$, undercutting does not occur.

Hence, Equation (5) applies to calculate the minimum inclination angle δ_{min}, depending on the nominal diameter.

$$\delta_{min} = \sin^{-1}\left(\frac{R_T}{\rho - r_p}\right), \tag{5}$$

It is assumed that there are no large changes in curvature in the immediate vicinity of the contact point CP_i in the CWE that could lead to undercutting. Therefore, once calculated, the δ_{min} parameter is used as a constant value along the entire contour of the machined surface, and the tool axis is oriented in the Cartesian space relative to the normal vector $n(CP_i)$ of the machined contour.

2.4. Active Cutting Edge Segment and Active Cutting Belt

Basically, the inclination angle δ is spread and determined in a plane perpendicular to the cutting speed vector v_c and passing through the contact point CP_i in the CWE, which is the common point of the outline of the machined surface and the cutting edge of the tool blade. The geometry of the cut layer is considered in the same plane. The geometrical parameters of the cut layer have a significant influence on the physical and technological effects of the cutting process, especially multi-axis milling.

During multi-axis TPL-type milling using the torus milling cutter, the geometry of the cut layer has a characteristic shape, where, due to the kinematic-geometric system, the thickness of the cut layer h varies along the cutting edge, as shown in Figure 5a. The geometry of the cut layer is influenced by the radius of the round cutting insert r_p, the feed per tooth f_z, and the depth of cut a_p.

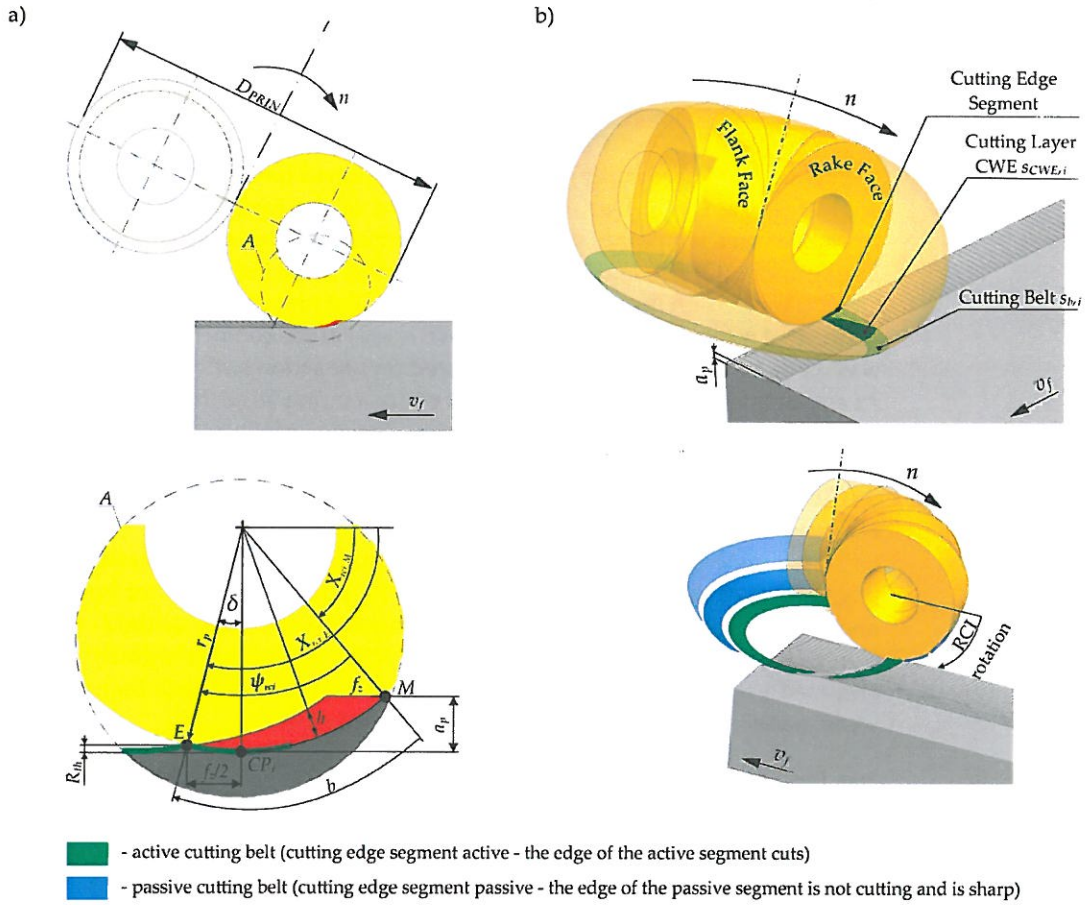

Figure 5. Multi-axis milling using the torus milling cutter: (**a**) cut layer geometry; (**b**) active cutting edge segment and active cutting belt.

By considering the contact conditions in the CWE at the CP_i contact point, the angles X_{rci_M}, X_{rci_E}, and ψ_{rci} were determined to determine the maximum cross-sectional limits of the cut layer.

Angle X_{rci_M}—the angle defining the origin of the cross-section of the cut layer, as described in Equation (6).

$$X_{rci_M} = \sin^{-1}\left(1 - \frac{a_p}{r_p}\right), \tag{6}$$

Angle X_{rci_E}—the angle defining the end of the cross-section of the cut layer, as described in Equation (7).

$$X_{rci_E} = \frac{\pi}{2} + \sin^{-1}\left(\frac{f_z}{2r_p}\right), \tag{7}$$

Angle ψ_{rci}—working angle of the torus milling cutter, considered in the base plane of the round cutting insert at the CP_i contact point, as described in Equation (8).

$$\psi_{rci} = \left[\frac{\pi}{2} + \sin^{-1}\left(\frac{f_z}{2r_p}\right) - \sin^{-1}\left(1 - \frac{a_p}{r_p}\right)\right], \tag{8}$$

Equation (8) is an important and rarely analyzed relationship in the literature. It acquires particular importance, especially under the conditions of finish machining, which takes place at very small values of depth of cut a_p and feed per tooth f_z. Under these cutting conditions, the number of involved cutting blades (active blades) of the tool in the cutting process is $z_c \leq 1$ [37]. Knowing the value of the angle ψ_{rci} and having the given radius r_p of the round cutting insert, the length of the active segment of the cutting edge b can be calculated using Equation (9).

$$b = \psi_{rci} r_p, \tag{9}$$

Thus, the active cutting belt can be determined (see Figure 5b) for a given inclination angle δ in the CWE. During the movement of the tool, the tool is in contact with the workpiece on a temporary patch of the machined surface, which is called Cutter-Workpiece Engagement (CWE), and the material removed is the cut layer in the form of a chip. The CWE is located on the torus action surface of the tool within the adopted depth of cut a_p. As the tool rotates about its axis, the CWE $s_{CWE,i}$ at the contact point forms a belt $s_{b,i}$, which was named the cutting belt, and is located on the action surface of the torus milling cutter. At any moment of cutting, the segment on the cutting edge that is inside the CWE is called the active segment of the cutting edge, i.e., the edge of the active segment is cutting at that moment. In addition, segments that are outside the CWE have been identified that are passive cutting edge segments, where the edge of the passive segment does not cut and is sharp.

The angle parameter ψ_{rci} in this work is used as the main parameter for the angular positioning of the round cutting insert in the torus milling cutter body, which is a new and original solution and the basis of the angular positioning method of the round cutting insert. In order to know after what time an active cutting edge segment is unusable (for an assumed *VB* criterion) and what the nature of the wear is at each time interval, both a tool wear model and a tool life model must be developed.

2.5. The Torus Milling Cutter Wear and Life Model

The wear rate of a torus milling cutter reflects the wear rate at any point on the active cutting edge, which is a part in common with the torus action surface and depends on the inclination angle. Importantly, it changes during machining. Figure 6 shows a typical tool wear curve as a function of the cutting time at a certain constant cutting speed. It presents a classic three-phase course. During phase I—the initial phase—tool wear increases dramatically and reaches its baseline value in a short period of time. In phase II, wear and tear of a quasi-linear and difficult-to-predict nature can be observed. Phase III is characterized by accelerated wear until a critical value associated with blade failure is reached.

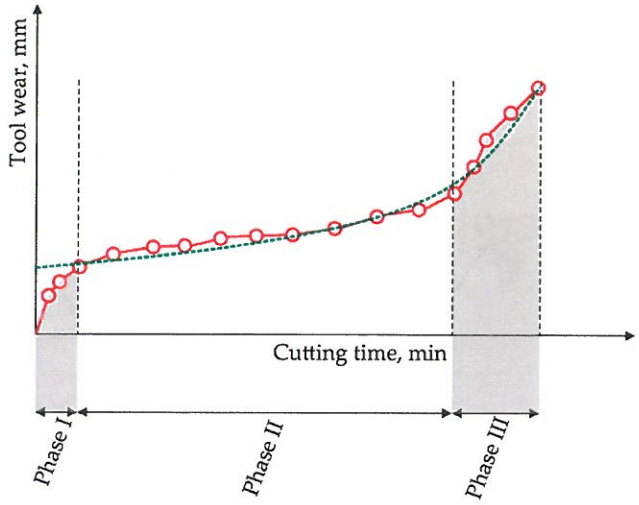

Figure 6. Typical tool wear rate at a constant cutting speed.

Furthermore, for wear modeling (dotted green line), i.e., using regression analysis [38–40], phase I can be neglected, and the tool wear at any cutting point on the torus action surface can be considered as a variable over time (such as in accelerated motion) and described by the model of an exponential function, which is expressed by Equation (10).

$$VB_{Bmax} = b_0 \cdot b_1^{t_c}, \tag{10}$$

where VB_{Bmax}—maximum abrasion width, an important indicator in multi-axis finish milling; b_0 and b_1—coefficients determined for a given material pair, i.e., round cutting insert—workpiece, and machining conditions; t_c—cutting time. The b_0 and b_1 coefficients are constituted on the basis of machinability tests and non-linear estimation analysis.

The tool is used for machining with the declared fixed machining parameters until the tool wear reaches the adopted critical value VB_{Blim} at time T_t. The value of time T_t, i.e., the tool life, is expressed by Equation (11):

$$T_t = C_t \cdot v_c^p \cdot f^q, \tag{11}$$

where T_t—the tool life; v_c—the cutting speed at the selecting cutting point; and f is the feed rate. C_t, p, and q are certain constants for a given material pair, i.e., the material of the round cutting insert material of the workpiece. These constants are constituted on the basis of calibrated machinability tests. On this basis, the tool life is determined from which the C_t, p, and q factors are calculated.

When milling with a torus milling cutter, with the spindle speed set to an arbitrary and constant value, the cutting speed varies along the cutting edge from the cutter tip point (TCP) towards the tool attachment point in the spindle. The cutting speed $v_{c,g}$ at a point with height g from the apex of the TCP torus milling cutter is expressed by Equation (12):

$$v_{c,g} = \frac{2\pi n\left(R_T + \sqrt{2r_p g - g^2}\right)}{1000}, \tag{12}$$

where n is the spindle speed; R_T is the radius from the rotational axis of the tool to the center point of the round cutting insert; and r_p is the radius of the round cutting insert. As shown in Figure 7, the cutting speed varies significantly given the parameter g along the torus milling cutter axis. The cutting speed values $v_{c,g}$ in this case were simulated for a cutting angle in the range $0° \leq \psi_{rci} \leq 23.4411°$ in the tool base plane coinciding with the tool's feed speed plane v_f.

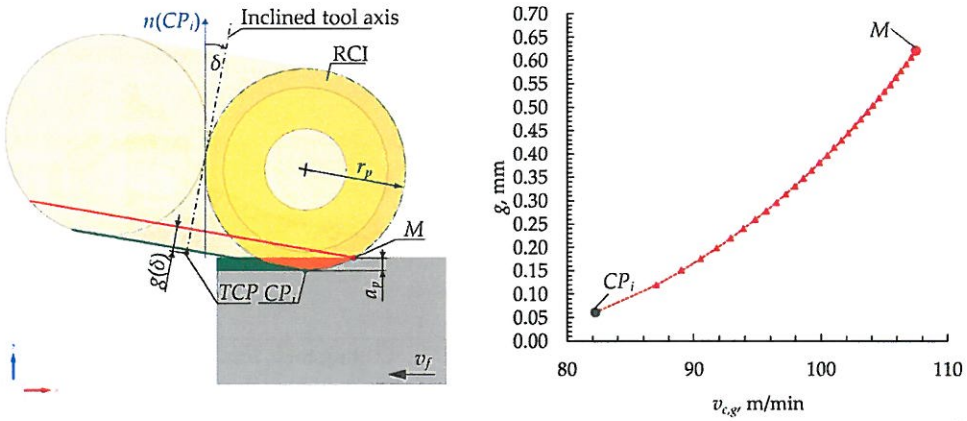

Figure 7. Cutting speed variation along the tool axis for torus milling cutter (tool diameter: 16 mm; round cutting insert radius: 4 mm; spindle speed: 2786 rpm; inclination angle: 10°).

Note that, assuming that both feed rate and the spindle speed are constant, the cutting speed $v_{c,g}$ depends only on the latitude g of the adopted cutting point, e.g., the contact point CP_i that falls within the length of the active cutting edge segment b. The latitude g is described in Equation (13).

$$g = r_p\left[1 - \cos\left(\frac{\pi}{2} - \sin^{-1}\left(1 - \frac{a_p}{r_p}\right)\right) + \delta\right], \tag{13}$$

where r_p is the radius of the round cutting insert; a_p is the depth of cut; and δ is the inclination angle.

For further considerations, the symbol $T_{c,g}$ is adopted to denote the tool wear rate of any point in the length of the active cutting edge segment b (i.e., in the active cutting strip $s_{b,i}$) at latitude g, as expressed by Equation (14) [11].

$$T_{c,g} = C_t\left(\frac{2\pi n\left(R_T + \sqrt{2r_p g - g^2}\right)}{1000}\right)^p f^q, \tag{14}$$

3. Machining and Measurement Conditions

3.1. Materials, Tools, and Machining Station

The Ni-based superalloy Inconel 718 was selected for machining tests. The TPL machining process was carried out using steel torus milling cutter body R300-016A20L-08L, dedicated to round cutting inserts R300-0828E-PL. The torus milling cutter as a tool assembly has a neutral geometry. The replaceable round cutting inserts are made of fine-grain carbide and coated with TiAlN anti-wear PVD technology. Round cutting inserts with a diameter of 8 mm were fitted into a tool body with a diameter of 16 mm at an overhang of 65 mm.

The machining station with experimental set-up is shown in Figure 8. A 5-axis CNC vertical machining center, model DMU 100 MonoBLOCK, was used to carry out machinability tests in the multi-axis TPL milling process. The tool life was determined by the wear VB_{Bmax} located on the lateral surface of the cutting edge until the adopted maximum value of the wear criterion VB_{Blim} was reached. The machining process was interrupted at specific intervals to collect data for modeling and wear calibration. Measurements were carried out using a DinoLite 7000 CE workshop microscope. The above-mentioned experimental workstation is at the equipment of the Department of Manufacturing Technics and Automation, seated in Rzeszów.

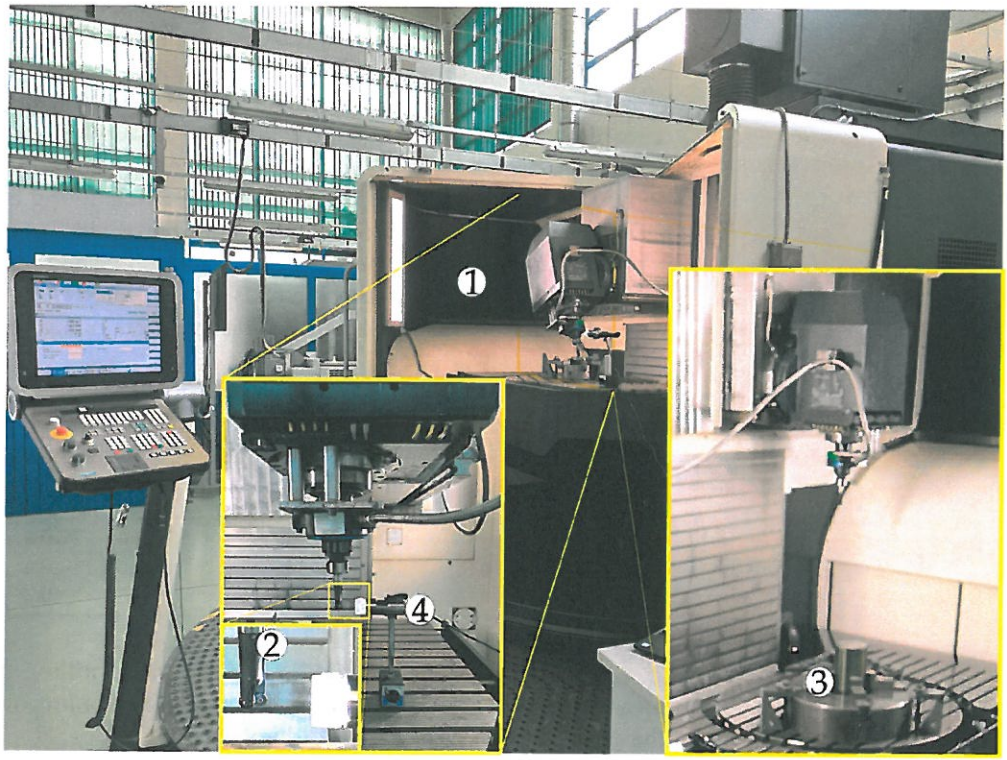

Figure 8. Experimental test bench (1. Machining tool, 2. Torus milling cutter, 3. Workpiece, 4. Dino-Lite 7000 CE series digital workshop microscope).

3.2. Tool Wear Modeling and Calibration

The research on tool wear and tool life, to develop a model and calibrate tool wear, involved a series of passes in a multi-axis milling process with a torus milling cutter, whose axis was deflected with respect to the normal vector of the machined surface in the feed direction by the inclination angle parameter δ (see Figure 1).

The experimental tests were carried out in two main stages. Flood cooling was used in all cutting tests. The cutting conditions were chosen on the basis of our own preliminary research and works [10,11,13,40]. The ambient temperature was 21°.

In the first stage, by carrying out machinability tests, data were obtained to develop a wear model using a non-linear estimation method. Cutting tests were carried out under HSM (High-Speed Machining). A constant cutting speed of v_c = 140 m/min was determined at the principal diameter of the torus D_{PRIN} (see Figure 5). The inclination angle was determined to be constant throughout the machining and was δ = 1.10946°. This angle ensured that the surface machining process was carried out with the greatest efficiency. Consequently, the real cutting speed v_c at the CP_i contact point of the shaping of the machined surface was 71 m/min. In addition, two criteria were used as follows: uniformly distributed roughness $Rth = R_{thvf}$ (i.e., the theoretical roughness has the same value in the feed direction as in the direction perpendicular to it), and a wear limit criterion of VB_{Blim} = 0.2 mm was adopted. The machining parameters for this stage are shown in Table 1.

Table 1. Cutting conditions for the first stage of the research.

Inclination Angle δ [°]	Work Angle of Cutting Blade ψ_{r_rci} [°]	Distance Between Toolpaths b_r [mm]	Axial Depth of Cut a_p [mm]	Feed per Tooth f_z [mm/z]	Cutting Speed (at p. CP_i) v_c [m/min]	Criterion $Rth = R_{thvf}$ [mm]	Criterion VB_{Blim} [mm]
1.10946	23.4411	1.6	0.3	0.1549	71	0.0015	0.2

In order to obtain more accurate test results, the second stage of the model tests, i.e., wear calibration, was carried out. A relationship was established between the maximum allowable cutting time (MACT) at the CP_i contact point of the cutter and its axial distance from the *TCP* vertex. The relationship was established with constant machining parameters (spindle speed and feed rate) in relation to a fixed tool wear threshold, VB_{Blim} = 0.2 mm. For the calibration test, the method described by Altintas [40] was adopted, and Figure 7 shows a simple test setup; by continuously machining at a constant angle δ until tool wear reached a threshold of 0.2 mm, MACT was obtained for a cutter axis orientation of 1.10946°. The machining parameters for the calibration test are shown in Table 2. Each of the machinability and calibration tests was repeated three times, after which the average was calculated. On the basis of the data thus obtained, a tool life model was determined.

Table 2. Cutting conditions for tool wear calibration.

Test No.	Cutting Speed (at p. CP_i) v_c [m/min]	Feed Rate f [mm/rev]	Measured Tool Life T_c [min]
1	40	0.4	84
2	140	0.4	0.97
3	140	0.2	3.7

Tool wear values are similar for the same milling parameters. In each iteration, measurements were carried out at the same fixed points on the time axis. At these points, the differences in wear values did not exceed 10%.

3.3. Measuring and Auxiliary Equipment

In the conception of the proposed solution, in addition to the development of wear and tool life models, it is also necessary to establish a measurement reference on the circular cutting insert and, relative to it, to make the necessary measurements of the angular position using the cutting blade work angle parameter. In addition, the measurement systems and strategies used should allow for the assessment of blade wear.

The xTool F1 laser system on the equipment of the Department of Industrial Engineering and Informatics seated in Prešov was used to determine the measurement reference on the round cutting insert, as shown in Figure 9.

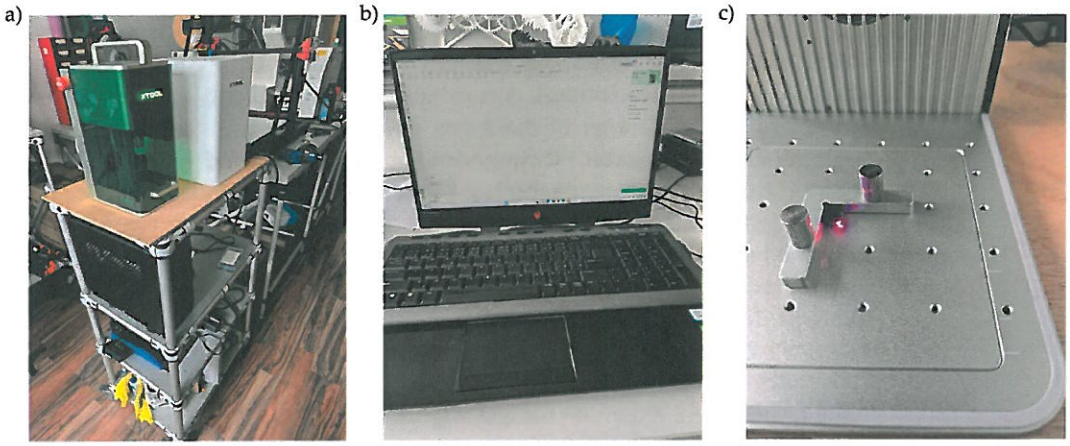

Figure 9. Laser engraving workstation: (**a**) xTool F1 machine; (**b**) PC workstation with xTool Creative Space software (v2.2.23); (**c**) working space with fixed round cutting insert visible laser dot.

It is a system that ensures the engraving of any curve by the action of a laser beam on any part geometry made of any material. The beam movement is programmed in the planar

module of the dedicated xTool Creative Space software. The most important parameters of the reference line application are shown in Table 3.

Table 3. Laser setting parameters.

Laser Set	Movement Accuracy [mm]	Repeat Positioning Accuracy [mm]	Up to Working Speed [mm/s]
2 W 1064 nm	0.00199	0.000248	84

The xTool F1 laser was used to apply an engraving of a line passing through the center of the round cutting insert. A coordinate system was established in the center of the insert based on automatically determined edge outlines. The line itself in the subsequent measurement steps on the microscope served as a reference for measuring the working angle of the blade and the angular positioning in the torus cutter body. The positioning error of the laser spot is 0.000248 mm—therefore negligible in the further stages of testing and positioning.

The proper setting of the round cutting insert in the torus milling cutter body and its subsequent angular positioning after reaching the VB_{Blim} threshold, according to the prepared models, was performed using a KEYENCE VHX 7000 digital microscope (Keyence International, Mechelen, Belgium), which is equipped by the Department of Automobile and Manufacturing Technologies seated in Prešov, as shown in Figure 10. The measurement parameters are shown in Table 4.



Figure 10. Digital 3D microscope used for angular positioning and evaluation of the cutting blade wear.

Table 4. Measurement equipment and parameters.

Microscope	Keyence VHX 7000
Lens	ZS-20 with 20–200× zoom
Shooting mode	4K 3D HDR scanning mode with glare reduction
Magnification	merging images at 100× zoom
Room temperature	22 °C
Humidity	55%

The wear measurements of VB_B along a segment of the active cutting edge were started by determining the outline of this edge. First, the plane tangent to the uppermost

outline of the round cutting insert was determined. From this, the center point that lies in the axis of the insert hole was determined. The error in the displacement of the reference line traced by the laser beam relative to the designated point was then checked. This error did not exceed 0.02 mm. This value did not exceed the minimum threshold of the measure values for tool wear and the work angle of the cutting blade.

4. Results and Discussion

4.1. Procedure for Angular Positioning of the RCI of the Torus Milling Cutter

In order to be able to carry out angular positioning of the RCI of the torus milling cutter, a procedure for the proposed solution was developed, as shown in Figure 11. This procedure takes into account the basic restriction of tool wear and is dedicated to the multi-axis milling process.

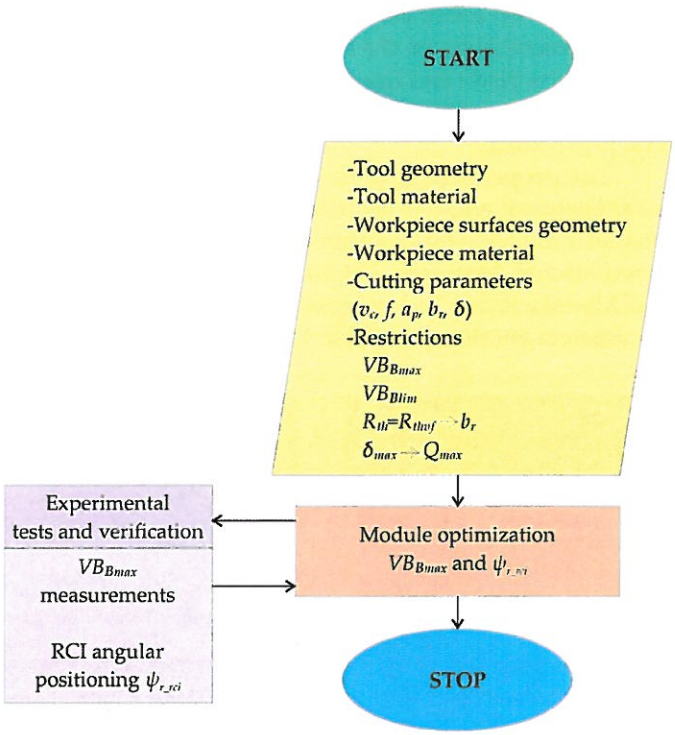

Figure 11. General procedure for the angular positioning of the RCI.

In terms of multi-axis machining, this procedure aims to maximize the volumetric efficiency of the cutting process while fully exploiting the cutting capacity of the tool over its lifetime, as described by the wear parameter. This makes it possible, on the one hand, to use cutting parameters in the HSM range and, on the other, to use the cutting edge length on the periphery of the insert in a controlled and complete manner. This makes the overall tool life significantly longer.

4.2. Tool Wear and Tool Life Models

The development of a concept for an angular positioning method for the round cutting insert of a torus milling cutter begins the wear modeling stage. When modeling tool wear, all three phases of the wear curve were taken into account. This is evident from the resulting classic three-phase wear curve that was obtained for the adopted machining conditions, as shown in Figure 12a. To clarify, it should be mentioned that this drawing shows the first of the three machining tests carried out. The higher number of tests performed is due to the generally accepted principles of statistical analysis and to increase the accuracy of the final model.

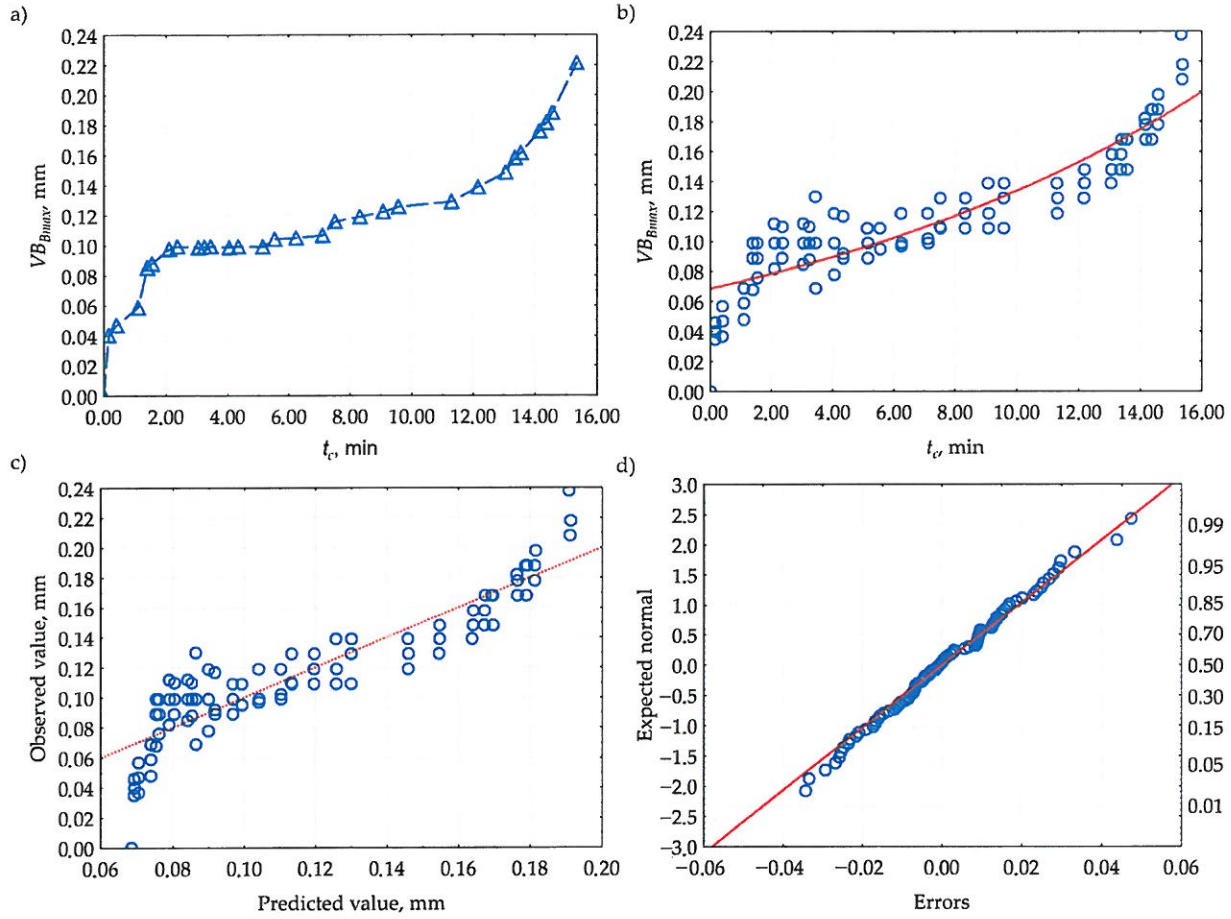

Figure 12. Results of non-linear estimation: (**a**) wear curve; (**b**) fitted model function and observed values; (**c**) scatter plot; (**d**) error normality chart.

As mentioned, wear modeling was carried out using an advanced non-linear ANOVA estimation, as the data obtained cannot be transformed into a linear model. Non-linear estimation involves calculating the relationship between a set of independent variables (i.e., cutting time t_c) and the dependent variable (i.e., tool wear VB_{Bmax}). It was assumed that the wear was evenly distributed over the individual cutting blades, i.e., only one cutting blade is active in the individual feed motion sequences, as also observed by Kita [41].

Analyzing the resulting data set, it was found that it could be approximated by an exponential function model, as described by Equation (10). This is an assumed estimated function. The Least-Squares Method (LSM) was adopted as the loss function, while the Levenberg–Marquardt algorithm was used as the estimation method. The method solves a system of linear equations in each iteration to calculate the gradient. A maximum number of iterations of 6000 was adopted, with a convergence criterion of six decimal places. Based on the above, a model relationship was obtained, which is described by Equation (15).

$$VB_{Bmax} = 0.0685797 \cdot 1.06903^{t_c}, \quad (15)$$

Table 5 shows the estimation statistics and results of the ANOVA analysis of variance.

Table 5. Estimation statistics and results of ANOVA analysis of variance.

	Sum of Squares	Degrees of Freedom	Mean Square	*F*-Value	*p*-Value	*R*
Regression	1.3271	2.0	0.6635	1867.4383	0.0000	0.90
Residual	0.0305	86	0.0003			
Total	1.3577	88				
Adjusted grand total	0.1675	87				
Regression of the adjusted total	1.3271	2.0	0.6635	344.5687	0.0000	

However, Figure 12b–d show the fitted model function and the observed values, a scatter plot of the observed values against the predicted values, and a probability normality plot, respectively.

Based on the results obtained and the analysis of variance, it was concluded that, within the assumed range of variables under study, the developed model is adequate (F = 344.5687) and approximates the predictor variable, i.e., tool wear during cutting, with an accuracy of 90%. This is evidenced by a determination coefficient of R = 0.90. Furthermore, in the scatter plot (Figure 12c), the points lay along a straight line, indicating that the model is appropriate and that the residuals (i.e., errors) are subject to a normal distribution, which, in turn, is illustrated in Figure 12d.

Subsequently, a tool life model was developed for HSM machining, that is, in the range adopted in this work according to Table 2. As a result of the machining tests, the so-called calibration, and after performing the necessary calculations, the tool life is described by Equation (16).

$$T_{c,0.00075} = 4.2 \cdot 10^{6,2} \left(\frac{2\pi n \left(R_T + \sqrt{2 r_p g - g^2} \right)}{1000} \right)^{3.561149} f^{1.931468}, \quad (16)$$

Again, an adequate model was obtained, since for an assumed threshold of VB_{Blim} = 0.2 mm, the lifetime T_c for the CP_i point (g = 0.00075 mm) is 16.353177 min.

4.3. Measurements and APofRCI

The next stage in the development of the concept for the angular positioning method of a circular cutting insert (APofRCI) torus cutter was the measurements.

In order to be able to carry out an angle measurement, i.e., measure the angle of the blade in the base plane under given machining conditions, a reference line must first be marked. This line is applied to a round cutting insert. It passes through the center point of the RCI. In this way, when assembling the tool set (body with inserts), it is possible to position the insert for the first time in such a way that the reference line is parallel from the tool's axis of rotation, as shown in Figure 13. As can be observed in Figure 13b, the marked trace of the cross-sectional effect of the cut layer on the cutting blade is completely within the limits of the cutting blade working angle.

Subsequently, each successive angular positioning of the RCI was realized according to the model dependencies once the limit value VB_{Blim} was reached. Machining tests, together with angular positioning, were repeated two more times, obtaining three active segments worn on the cutting edge, as illustrated in Figure 14.

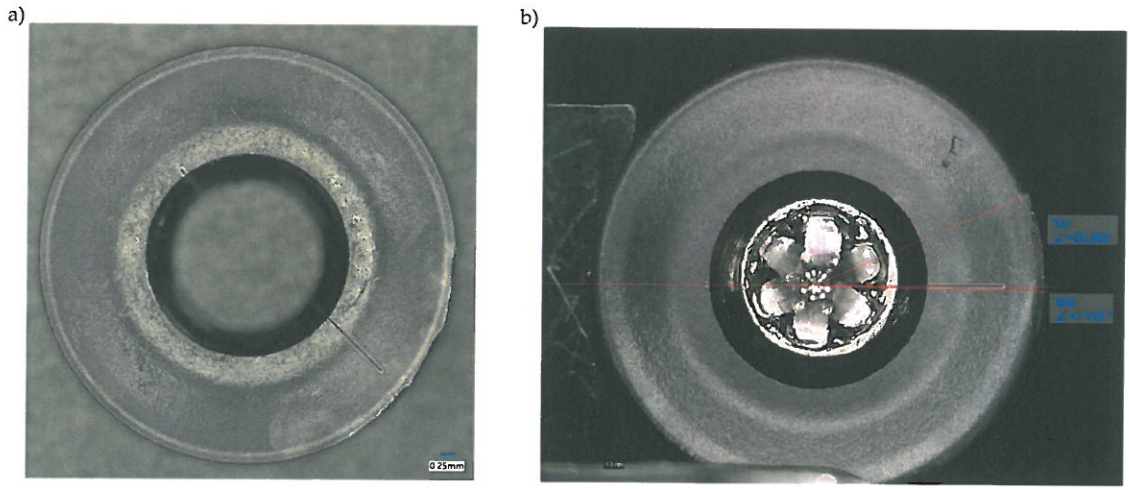

Figure 13. Round cutting insert: (**a**) after laser marking; (**b**) assembled in the cutter body and subjected to a first measurement verification after the first 20 s of operation.

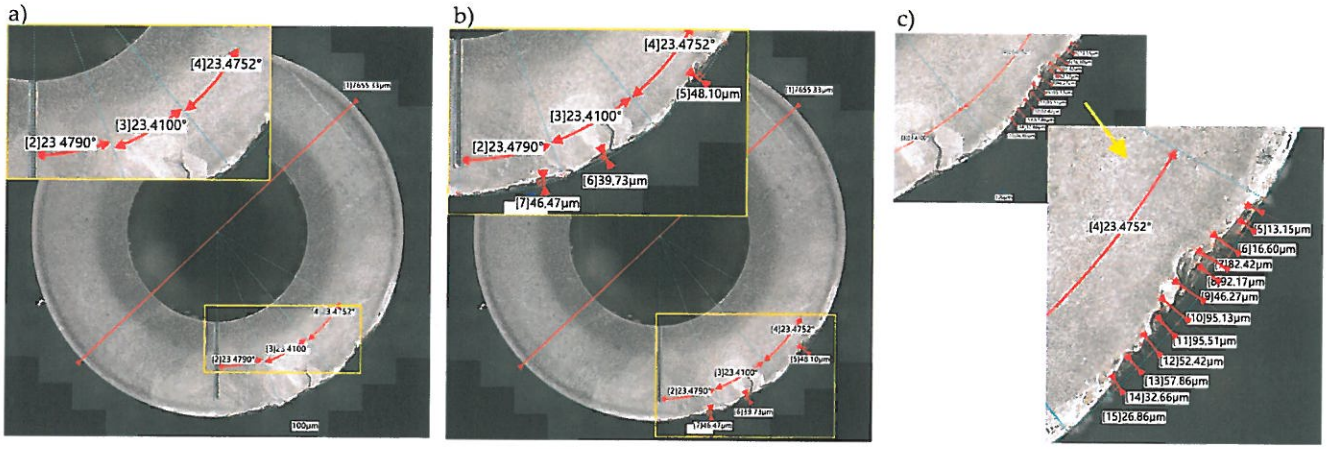

Figure 14. Measurement results: (**a**) correctness of angular positioning; (**b**) maximum defect values for the segments obtained; (**c**) distribution of defect values along the worn active cutting edge.

Analyzing the results obtained from the digital microscope measurement, it was found that all worn segments were within the cutting blade working angle (Figure 14a). This demonstrates the correctness of both the models developed and the procedure together with the measurement techniques used. These techniques made it possible to measure the maximum defect, that is, the abrasion of the blade material, as shown in Figure 14b. It was found that there were differences in the value of the maximum abrasion between the segments, which may be due to the radial runout of the cutting blade. In this case, further research and clarification of the proposed solution should be carried out. In addition, it was also possible to measure the distribution of clash variation relative to the nominal RCI outline, which, in turn, is shown in Figure 14c. Maximum abrasion values were obtained in the zone of maximum thickness of the cut layer acting on the cutting blade. And, in this case, further research is needed. In conclusion, it can be said that the proposed solution works well not only for angular positioning of the RCI but also for carrying out analysis on wear mechanisms.

5. Conclusions

This paper proposes a method for angular positioning of a round cutting insert in a torus cutter body. The method is dedicated to the process of multi-axis milling of sculptured surfaces, but it can also be successfully adopted for other variants of milling as well as

turning using the round cutting insert. The topic addressed in this paper is new and, according to the current state of knowledge, is being tackled for the first time.

The novelty of this work, in addition to the method of angular positioning of the round cutting insert, is above all the comprehensive approach in terms of machinability and tool wear, so that the presented procedure can be used for any workpiece–tool materials pair. In addition, the proposed solution allows the full cutting capability of the entire edge length of the round cutting insert to be fully and predictably over time. The solution is essentially based on the tool wear model developed as part of this work, the tool life model, the way round cutting inserts are labeled and assembled, and the wear measurement methodology.

Taking the above into account, a procedure was developed for the angular positioning of the round cutting insert in a torus cutter body. Based on the results obtained and the analyses carried out, the following key conclusions were drawn:

- The adopted function for approximating tool wear over its lifetime is adequate and provides 90% prediction accuracy;
- The tool life model developed is essentially based on the cutting blade working angle parameter. This makes it possible to predict tool life for different machining conditions and for individual instantaneous positions of the cutting edge in relation to the workpiece surface (3D analysis), which is the subject of further work;
- The developed procedure for angular positioning and measurement enables the entire cutting edge of the blade to be fully utilized, so that the total lifespan of the tool as an assembly is significantly extended;
- The proposed solution also allows measurement and analysis of wear mechanisms, which significantly extends the possibilities of angular positioning of the RCI, taking into account its macro- and micro-geometric characteristics.
- The method proposed in this paper was developed for a specific pair of materials, while the method procedure can be successfully applied to any other pair of workpiece–tool material pair.

The results obtained allowed us to direct further research in the area of tool wear and, more specifically, the prediction of 'notching' wear, which in this work was identified as the highest value of the defect between the worn edge and the nominal outline of the RCI from the measurements.

The research leading to these results was carried out within the framework of international cooperation and Michał Gdula's research internship abroad.

Author Contributions: Conceptualization. M.G. and J.H.; methodology. M.G.; measurements. M.G. and R.V.; modeling and validation. M.G.; formal analysis. M.G.; investigation. M.G., J.H. and R.V.; resources. M.G., L.K. and J.H.; data curation. M.G. and J.H.; writing—original draft preparation. M.G.; writing—review and editing. L.K. and J.H.; visualization. M.G.; supervision. L.K.; project administration. M.G.; funding acquisition. M.G. and L.K. All authors have read and agreed to the published version of the manuscript.

Funding: This research received no external funding.

Institutional Review Board Statement: Not applicable.

Informed Consent Statement: Not applicable.

Data Availability Statement: The original contributions presented in the study are included in the article, further inquiries can be directed to the corresponding author.

Conflicts of Interest: The authors declare no conflicts of interest.

References

1. Escudero, G.G.; Bo, P.; González-Barrio, H.; Calleja-Ochoa, A.; Bartoň, M.; De Lacalle, L.N.L. 5-Axis Double-Flank CNC Machining of Spiral Bevel Gears via Custom-Shaped Tools—Part II: Physical Validations and Experiments. *Int. J. Adv. Manuf. Technol.* **2022**, *119*, 1647–1658. [CrossRef]
2. Bo, P.; González, H.; Calleja, A.; De Lacalle, L.N.L.; Bartoň, M. 5-Axis Double-Flank CNC Machining of Spiral Bevel Gears via Custom-Shaped Milling Tools—Part I: Modeling and Simulation. *Precis. Eng.* **2020**, *62*, 204–212. [CrossRef]
3. González, H.; Calleja, A.; Pereira, O.; Ortega, N.; Norberto López de Lacalle, L.; Barton, M. Super Abrasive Machining of Integral Rotary Components Using Grinding Flank Tools. *Metals* **2018**, *8*, 24. [CrossRef]
4. González, H.; Pereira, O.; Fernández-Valdivielso, A.; López De Lacalle, L.; Calleja, A. Comparison of Flank Super Abrasive Machining vs. Flank Milling on Inconel® 718 Surfaces. *Materials* **2018**, *11*, 1638. [CrossRef]
5. Sliusarenko, O.; Escudero, G.G.; González, H.; Calleja, A.; Bartoň, M.; Ortega, N.; De Lacalle, L.N.L. Constant Probe Orientation for Fast Contact-Based Inspection of 3D Free-Form Surfaces Using (3+2)-Axis Inspection Machines. *Precis. Eng.* **2023**, *84*, 37–44. [CrossRef]
6. Wang, J.; Luo, M.; Xu, K.; Tang, K. Generation of Tool-Life-Prolonging and Chatter-Free Efficient Toolpath for Five-Axis Milling of Freeform Surfaces. *J. Manuf. Sci. Eng.* **2019**, *141*, 031001. [CrossRef]
7. Zeng, H.; Yan, R.; Du, P.; Zhang, M.; Peng, F. Notch Wear Prediction Model in High Speed Milling of AerMet100 Steel with Bull-Nose Tool Considering the Influence of Stress Concentration. *Wear* **2018**, *408–409*, 228–237. [CrossRef]
8. An, Q.; Cai, C.; Zou, F.; Liang, X.; Chen, M. Tool Wear and Machined Surface Characteristics in Side Milling Ti6Al4V under Dry and Supercritical CO_2 with MQL Conditions. *Tribol. Int.* **2020**, *151*, 106511. [CrossRef]
9. Ni, C.; Wang, X.; Zhu, L.; Liu, D.; Wang, Y.; Zheng, Z.; Zhang, P. Machining Performance and Wear Mechanism of PVD TiAlN/AlCrN Coated Carbide Tool in Precision Machining of Selective Laser Melted Ti6Al4V Alloys under Dry and MQL Conditions. *J. Manuf. Process.* **2022**, *79*, 975–989. [CrossRef]
10. Gdula, M.; Mrówka-Nowotnik, G. Analysis of Tool Wear, Chip and Machined Surface Morphology in Multi-Axis Milling Process of Ni-Based Superalloy Using the Torus Milling Cutter. *Wear* **2023**, *520–521*, 204652. [CrossRef]
11. Luo, M.; Luo, H.; Zhang, D.; Tang, K. Improving Tool Life in Multi-Axis Milling of Ni-Based Superalloy with Ball-End Cutter Based on the Active Cutting Edge Shift Strategy. *J. Mater. Process. Technol.* **2018**, *252*, 105–115. [CrossRef]
12. Cao, L.-X.; Gong, H.; Liu, J. The Offset Approach of Machining Free Form Surface. *J. Mater. Process. Technol.* **2007**, *184*, 6–11. [CrossRef]
13. Musfirah, A.H.; Ghani, J.A.; Haron, C.H.C. Tool Wear and Surface Integrity of Inconel 718 in Dry and Cryogenic Coolant at High Cutting Speed. *Wear* **2017**, *376–377*, 125–133. [CrossRef]
14. Zhu, Z.; Peng, F.; Yan, R.; Li, Z.; Wu, J.; Tang, X.; Chen, C. Influence Mechanism of Machining Angles on Force Induced Error and Their Selection in Five Axis Bullnose End Milling. *Chin. J. Aeronaut.* **2020**, *33*, 3447–3459. [CrossRef]
15. Chang, Z.; Qian, J.; Chen, Z.C.; Wan, N.; Zhang, D. Geometrical Theory of Cutting Stock with Torus End Mills in Five-Axis CNC Machining and Its Applications in Machining Simulation. *Int. J. Adv. Manuf. Technol.* **2019**, *105*, 27–46. [CrossRef]
16. Gao, W.; Kim, S.W.; Bosse, H.; Haitjema, H.; Chen, Y.L.; Lu, X.D.; Knapp, W.; Weckenmann, A.; Estler, W.T.; Kunzmann, H. Measurement Technologies for Precision Positioning. *CIRP Ann.* **2015**, *64*, 773–796. [CrossRef]
17. Ivanov, V.; Botko, F.; Dehtiarov, I.; Kočiško, M.; Evtuhov, A.; Pavlenko, I.; Trojanowska, J. Development of Flexible Fixtures with Incomplete Locating: Connecting Rods Machining Case Study. *Machines* **2022**, *10*, 493. [CrossRef]
18. Brillinger, M.; Wuwer, M.; Abdul Hadi, M.; Haas, F. Energy Prediction for CNC Machining with Machine Learning. *CIRP J. Manuf. Sci. Technol.* **2021**, *35*, 715–723. [CrossRef]
19. Ramos-Fernández, J.C.; López-Morales, V.; Márquez-Vera, M.A.; Pérez, J.M.X.; Suarez-Cansino, J. Neuro-Fuzzy Modelling and Stable PD Controller for Angular Position in Steering Systems. *Int. J. Automot. Technol.* **2021**, *22*, 1495–1503. [CrossRef]
20. Kaščak, J.; Gašpár, Š.; Paško, J.; Husár, J.; Knapčíková, L. Polylactic Acid and Its Cellulose Based Composite as a Significant Tool for the Production of Optimized Models Modified for Additive Manufacturing. *Sustainability* **2021**, *13*, 1256. [CrossRef]
21. Abdul Hadi, M.; Brillinger, M.; Wuwer, M.; Schmid, J.; Trabesinger, S.; Jäger, M.; Haas, F. Sustainable Peak Power Smoothing and Energy-Efficient Machining Process Thorough Analysis of High-Frequency Data. *J. Clean. Prod.* **2021**, *318*, 128548. [CrossRef]
22. Abdul Hadi, M.; Kraus, D.; Kajmakovic, A.; Suschnigg, J.; Guiza, O.; Gashi, M.; Sopidis, G.; Vukovic, M.; Milenkovic, K.; Haslgruebler, M.; et al. Towards Flexible and Cognitive Production—Addressing the Production Challenges. *Appl. Sci.* **2022**, *12*, 8696. [CrossRef]
23. Visan, D.A.; Lita, I.; Cioc, I.B. Wireless Control System for Angular Positioning Applications. In Proceedings of the 2013 IEEE 19th International Symposium for Design and Technology in Electronic Packaging (SIITME), Galati, Romania, 24–27 October 2013; pp. 103–106.
24. Adamczak, M.; Kolinski, A.; Trojanowska, J.; Husár, J. Digitalization Trend and Its Influence on the Development of the Operational Process in Production Companies. *Appl. Sci.* **2023**, *13*, 1393. [CrossRef]
25. Hrehova, S. Description of Using Different Software Tools to Analyze the Selected Process. In Proceedings of the 2019 20th International Carpathian Control Conference (ICCC), Krakow-Wieliczka, Poland, 26–29 May 2019; pp. 1–5.
26. Coranic, T.; Mascenik, J. Experimental Measurement of Dynamic Characteristics of Structural Units. *Processes* **2023**, *11*, 3333. [CrossRef]

27. Jurko, J.; Miškiv-Pavlík, M.; Hladký, V.; Lazorík, P.; Michalík, P.; Petruška, I. Measurement of the Machined Surface Diameter by a Laser Triangulation Sensor and Optimalization of Turning Conditions Based on the Diameter Deviation and Tool Wear by GRA and ANOVA. *Appl. Sci.* **2022**, *12*, 5266. [CrossRef]
28. Jurko, J.; Miškiv-Pavlík, M.; Husár, J.; Michalik, P. Turned Surface Monitoring Using a Confocal Sensor and the Tool Wear Process Optimization. *Processes* **2022**, *10*, 2599. [CrossRef]
29. Tran, C.-S.; Hsieh, T.-H.; Jywe, W.-Y. Laser R-Test for Angular Positioning Calibration and Compensation of the Five-Axis Machine Tools. *Appl. Sci.* **2021**, *11*, 9507. [CrossRef]
30. Yi-Tsung, L.; Kuang-Chao, F. A Novel Method of Angular Positioning Error Analysis of Rotary Stages Based on the Abbe Principle. *Proc. Inst. Mech. Eng. Part B J. Eng. Manuf.* **2018**, *232*, 1885–1892. [CrossRef]
31. Kanno, Y.; Sato, Y. Linear and Angular Position Sensing for Two- Degrees-of-Freedom Motor. *Int. J. Smart Sens. Intell. Syst.* **2014**, *7*, 1–6. [CrossRef]
32. Chen, H.; Jiang, B.; Lin, H.; Zhang, S.; Shi, Z.; Song, H.; Sun, Y. Calibration Method for Angular Positioning Deviation of a High-Precision Rotary Table Based on the Laser Tracer Multi-Station Measurement System. *Appl. Sci.* **2019**, *9*, 3417. [CrossRef]
33. Gietler, H.; Stetco, C.; Zangl, H. Scalable Retrofit Angular Position Sensor System. In Proceedings of the 2020 IEEE International Instrumentation and Measurement Technology Conference (I2MTC), Dubrovnik, Croatia, 25–28 May 2020; pp. 1–6.
34. Sridharan, M.; Dhandapani, S. Real Time Embedded System Development for Missile Angular Position Acquisition through Image Processing. *CSIT* **2020**, *8*, 257–261. [CrossRef]
35. Diakov, D.; Komarski, D. Micro-Positioning Module for Angular Orientation Position of the Axis of Rotation Analysis. In Proceedings of the 2021 XXXI International Scientific Symposium Metrology and Metrology Assurance (MMA), Sozopol, Bulgaria, 7–11 September 2021; pp. 1–6.
36. Marciniak, K. Influence of Surface Shape on Admissible Tool Positions in 5-Axis Face Milling. *Comput. Aided Des.* **1987**, *19*, 233–236. [CrossRef]
37. Lazoglu, I.; Liang, S.Y. Modeling of Ball-End Milling Forces With Cutter Axis Inclination. *J. Manuf. Sci. Eng.* **2000**, *122*, 3–11. [CrossRef]
38. Knapčíková, L.; Dupláková, D.; Radchenko, S.; Hatala, M. Rheological Behavior Modelling of Composite Materials Used in Engineering Industry. *TEM J.* **2017**, *6*, 242–245. [CrossRef]
39. Pavlenko, I.; Piteľ, J.; Ivanov, V.; Berladir, K.; Mižáková, J.; Kolos, V.; Trojanowska, J. Using Regression Analysis for Automated Material Selection in Smart Manufacturing. *Mathematics* **2022**, *10*, 1888. [CrossRef]
40. Altintas, Y. *Manufacturing Automation. Metal Cutting Mechanics, Machine Tool Vibrations, and CNC Design*, 2nd ed.; Cambridge University Press: New York, NY, USA, 2012; ISBN 978-0-521-17247-9.
41. Kita, Y.; Furuike, H.; Kakino, Y.; Nakagawa, H.; Hirogaki, T. Basic Study of Ball End Milling on Hardened Steel. *J. Mater. Process. Technol.* **2001**, *111*, 240–243. [CrossRef]

Disclaimer/Publisher's Note: The statements, opinions and data contained in all publications are solely those of the individual author(s) and contributor(s) and not of MDPI and/or the editor(s). MDPI and/or the editor(s) disclaim responsibility for any injury to people or property resulting from any ideas, methods, instructions or products referred to in the content.

ARTYKUŁ

A6

dr inż. Michał Gdula
Politechnika Rzeszowska im. I. Łukasiewicza
Wydział Budowy Maszyn i Lotnictwa
Katedra Technik Wytwarzania i Automatyzacji

Rzeszów, dn. 23.04.2025 r.

OŚWIADCZENIE AUTORA

Oświadczam, że w pracy:

lp.: ..A6.....

Gdula M.: *Determination and Analysis of Working Diameters and Working Angle of the Torus Cutter Blade in Multi-axis Machining in the Aspect of Tool Wear.* International Journal of Mechanical Enginerring and Robotics Research, Vol. 13, No. 5 (2024). IF -.-, MNiSW 20 pkt.;

mój wkład w powstanie tej pracy polegał na: kompletnym opracowaniu manuskryptu obejmującym analizę aktualnego stanu wiedzy w zakresie tematu pracy, opracowaniu zależności matematycznych opisujących średnicę kontaktu oraz średnicę efektywną dla różnych wariantów kinematycznych frezowania wieloosiowego, opracowaniu zależności matematycznych opisujących graniczne punkty zarysu przekroju warstwy skrawanej i w tym także kąta pracy ostrza frezu, opracowanie zależności matematycznych opisujących szerokość frezowania dla wariantu kinematycznego typu przyciąganie narzędzia, opracowaniu metodyki badań, przeprowadzeniu badań symulacyjnych i eksperymentalnych, przeprowadzeniu analizy i interpretacji otrzymanych wyników, opracowaniu wniosków, wykonaniu wykresów, rysunków oraz tabel, koordynowaniu procesu wydawniczego.

Gdula Michał
.....
Podpis
dr inż. Michał Gdula

Determination and Analysis of Working Diameters and Working Angle of the Torus Cutter Blade in Multi-axis Machining in the Aspect of Tool Wear

Michał Gdula

Department of Manufacturing Techniques and Automation, Faculty of Mechanical Engineering and Aeronautics, Rzeszow University of Technology, 35-959 Rzeszow, al. Powstańców Warszawy 12, Poland
Email: gdulam@prz.edu.pl

***Abstract*—The aim of this study is to provide a theoretical and experimental analysis of the multi-axis milling process by the torus milling cutter of nickel-based superalloy parts in terms of surface quality and tool wear. In the analytical part, using, among other things, matrix calculus and trigonometric relationships, mathematical models were developed to describe the relationships between the tool axis orientation and the geometric parameters of the cutting layer at the contact point. On this basis, mathematical relationships for contact diameter and effective diameter were derived. The basis for these considerations is the very rarely considered working angle of the cutter blade. In part of the experimental study, machining tests were carried out for selected kinematic variants of multi-axis cutting. Based on the results obtained, it was found that as the tool axis inclination angle increases, the contact diameter increases. The effective diameter at the upper characteristic point of the cutting layer increases up to a certain angle of inclination, after which it begins to decrease. The rotational angle of the tool axis does not affect any of the diameters, but it does affect the displacement of the contact point, the values of the working angle of the tool blade and the feed-related component decrease. The result of this displacement is a change from climb milling to conventional milling, which has significantly degraded surface quality and tool life. The best results of the machining test were obtained when only the angle of inclination of the tool axis was used. It was concluded that the parameter tool blade working angle can be a control variable in a multi-axis milling process and has a major impact on the physical aspects of the cutting process.**

***Keywords*—torus milling cutter, effective diameter, contact diameter, multi-axis machining, cutter blade working angle, tool wear, surface roughness**

I. Introduction

Multi-axis torus milling cutter machining of sculptured surfaces parts made of Ni-based superalloy is one of the increasingly used technologies for precision finishing. This is primarily due to the advantages that the torus geometry has. It enables the milling width to be significantly increased, making the machining process more efficient while maintaining the required quality indicators of the machined surface. In addition, zero-speed cutting does not occur with a torus milling cutter geometry, which is the case with a ball-end milling cutter geometry [1–6]. Essentially, the cutter rotates around its axis and moves to shape the surface by following a movement trajectory programmed in the Computer-Aided Design/Computer-Aided Manufacturing (CAD/CAM) system at a specific speed (feed rate, v_f) and finally moves away and u-turns or departs.

In the case of multi-axis milling of sculptured surfaces using a torus milling cutter (as well as using a ball-end milling cutter, which is the subject of the vast majority of the research work in the theme of this paper), the surface quality indicators depend on several factors and parameters, such as: essential diameter, effective diameter, contact diameter, cutting parameters, cutting blade and workpiece materials, machined surface geometry, toolpath, kinematic variant of multi-axis cutting process, etc. The parameter that links all of the above with surface quality indicators is tool wear.

Regarding the essential diameter and effective diameter of the tool, Fan [7] conducted a study on the effect of variations in cutting speed on the quality of the machined surface. He also noted that cutting speed is a significant factor in tool wear. On the other hand, de Souza *et al.* [8] carried out a study of the influence of effective diameter on surface roughness and selected mechanics of the cutting process, i.e., chip formation, curl and breakage, and cutting forces. He indicated that an increase in the cutting speed results in a decrease in the value of the surface roughness parameters. Wojciechowski *et al.* [9] analysed the milling process using the ball-end mill cutter of planar surfaces inclined at different angles, resulting in different effective diameters. They indicated that the larger the effective diameter, the lower the surface roughness, while an increase in the cutting speed results in a decrease in the value of the surface roughness parameters. In addition,

Manuscript received February 26, 2024; revised April 6, 2024; accepted May 28, 2024; published October 17, 2024.

Wojciechowski *et al.* in their work [10, 11] extended the scope of the study to include the determination of geometrical parameters of the machined layer in different phases of blade operation, indicating their influence on the components of the cutting force taking into account tool wear. In turn Mikó *et al.* [12] and Mgherony *et al.* [13], they presented the geometrical basis of the 3-axis milling process with a spherical milling cutter for free-form surfaces. Based on the results of research, they formulated assumptions for a ball-end milling strategy that minimises changes in instantaneous effective diameter values.

Regarding tool material, workpiece, and cutting kinematics, Vopát *et al.* [14] conducted a study of the influence of tool material and milling direction on quality indicators of machined surface and tool wear. They indicated that the solid carbide cutter provides better surface roughness and blade life than the HSS mill. Furthermore, for both tool materials, milling in the kinematic variant push the tool provides better surface roughness. In the works of Wojciechowski *et al.* [9–11], a similar kinematic range of milling was performed and the workpiece material was hardened steel. The kinematics of multi-axis cutting is closely related to the inclination parameter of the tool axis or machined surface, so Vyboishchik [15] described a geometric model of the topology of a flat surface and a convex and concave curvilinear surface. On this basis, he assessed that the angle of inclination of the surface at the local contact point plays an important role in the milling process of free-form surfaces.

Regarding milling strategies and parameters, Beno *et al.* [16] conducted a study of milling strategy selection based on the analysis of complex surface features. He noted that cutting speed has a major impact on the quality indicators of the machined surface. Pena *et al.* [17] conducted a study of different milling strategies in terms of the surface roughness achieved. Due to the different roughness values obtained, they introduced a correction factor that modifies the feed rate to ensure better surface quality indicators. On the other hand, Pena [18] also analysed different milling strategies, found that the calculated roughness height was smaller than its actual value, and proposed a correction factor to modify the cutting width. Redonnet *et al.* [19] carried out an optimisation of a milling strategy for free-form surfaces using a torus cutter, minimising machining time using a kinematic roughness height criterion. Zhang *et al.* [20] developed a geometric model of the topography of a surface machined using a ball-end mill. They performed the optimisation by taking into account the effect of the feed rate on the tooth and the cutting width.

The process of simultaneous multi-axis milling can solve an existing problem in optimising tool life extension, resulting, among other things, from the occurrence of variable effective diameters and therefore cutting speeds during machining. As pointed out by Zhang *et al.* [1], cutting speed has a major impact on tool wear. By combining the simultaneous multi-axis milling technique with the 3+2 milling technique while introducing the technique of segmenting the machined surface and/or cutting edge by varying the inclination of the tool axis, this problem can be largely overcome. Liu *et al.* [21] developed a workpiece surface segmentation method to identify regions for a 3+2-axis milling strategy. They pointed out that this technique, due to the static axis of the tool in three-dimensional space, allows for increased feed rates. On the other hand, Gdula *et al.* [22] determined the basic kinematics variants of multi-axis cutting in terms of segmentation of the cutting edge of a torus cutter. They conducted a series of milling tests for different tool axis inclinations, determining their effect on tool wear and the morphology of the chip and machined surface. This work provides a starting point for the research within this thesis.

In summary, the surface quality according to the geometric model depends on the diameter of the tool, the cutting width, and the tool axis inclination of the tool axis, as well as on the cutting parameters such as feed and cutting speed. When sculptured surfaces, the effective diameter of the cutting tool changes, and thus the cutting speed also changes. In turn, the cutting speed determines the minimum value of the chip thickness.

This paper emphasises engineering aspects in the context of CAD/CAM programming support, taking into account the tool wear parameter. As can be seen from the analysis of the literature, the cutting speed has a significant effect on the wear of the tool and thus on surface roughness. In the case of multi-axis torus milling cutter machining, the effective diameter is a key research parameter. In addition, the novelty of this work is the inclusion of the diameter at the point of contact (contact diameter), as that which shapes the machined surface through the direct cutting edge-machined surface contact. Furthermore, this work is distinguished by its geometric-kinematic approach to the description of the aforementioned diameters and other related parameters. The mathematical model developed describes the multi-axis milling of a surface using the torus milling cutter with a variable inclination of its axis, where the tool paths are parallel to each other. The machined surface is a tangent plane, which is a simplified model of a sculptured surface at the contact point between the torus and the machined surface, as shown in Fig. 1. The necessary simulations were performed on the developed model relationships and the discrete direct CAD method in the CAD/CAM environment.

This study is an extension of the geometrical approach used for 3-axis ball-end milling process [12, 13, 23–26]. Among other things, the novelty of this work is the consideration of the kinematics of the 5-axis milling process at the contact point between the tool and the machined surface, by introducing a working angle of the blade parameter. This parameter was used to determine the effective and contact diameters, which, according to the literature analysis, is the first of its kind given the modelling of the multi-axis milling process. In addition, the milling cutter working angle blade parameter was used as a control variable when programming the milling

cutter axis inclination angle as well as during the implementation of the experimental tests. All tests and analyses were carried out for the torus milling cutter, for which there are no studies in the above area.

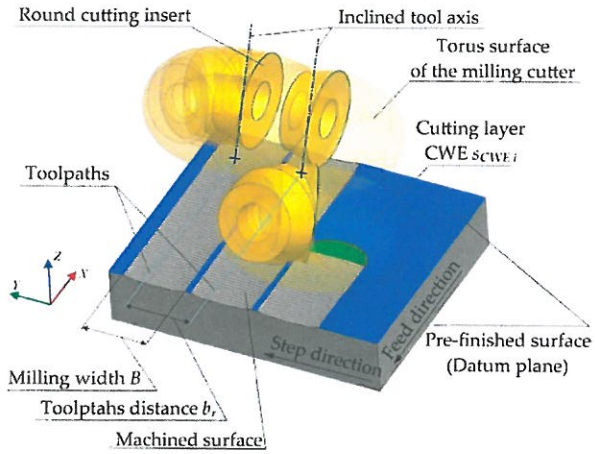

Fig. 1. Milling of the plane surface with inclined torus milling cutter axis.

II. Contact and Effective Diameters

Let the reference coordinate system (X_{ci}, Y_{ci}, Z_{ci}) be located at point O_{ci} of the circular outline centre of the cutting edge of the cutting insert and the coordinate system (X_{CPi}, Y_{CPi}, Z_{CPi}) at the contact point CP_i. The Z_{ci} axis is constant in terms of direction and the turn of the axis, and is parallel to the normal vector N of the machined surface. The parameter D_{PRIN} indicates the tool's principal diameter. Furthermore, let the angle δ be the angle of inclination of the tool axis and let the angle θ be the angle of rotational of the tool axis, relative to the normal vector N at the CP_i contact point. The parameters δ and θ are the spherical coordinates of the tool axis, as shown in Fig. 2.

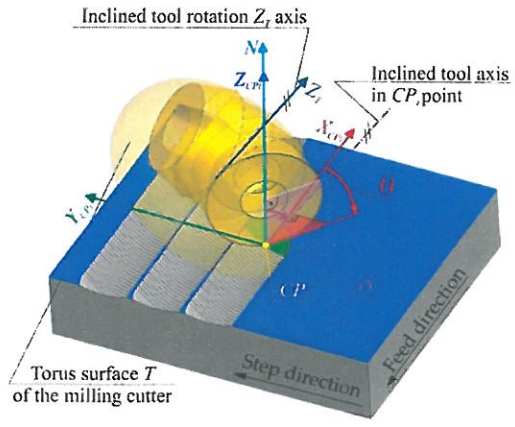

Fig. 2. Directional versor k of the torus milling cutter axis and its spherical coordinates: inclination angle δ and rotational angle θ at the CP_i contact point.

A. Contact Diameter

1) Case I: $\delta=0°$ and $\theta=0°$

If R_T is the radius of the torus milling cutter (the Z_T rotation axis of distance of the torus from the centre of the circle defining it), the contact diameter at the contact point CP_i is described by Eq. (1) (see Fig. 3(a)):

$$D_{CON\,I} = 2R_T \tag{1}$$

2) Case II: $\delta>0°$ and $\theta=0°$ or $-90°<\theta<90°$

However, in addition, if r_p is the radius of the circular cutting insert (the circle defining the torus) and R_T, δ and θ as described above, the contact diameter at the CP_i contact point is described by Eq. (2) (see Fig. 3(b)):

$$D_{CON_{II}} = 2\left(R_T + r_p \sin(\delta)\right) \tag{2}$$

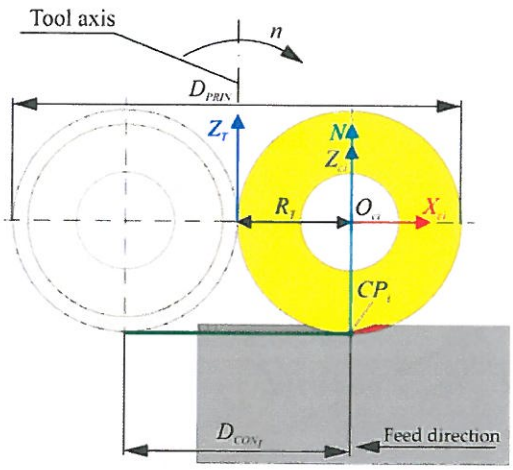

(a)

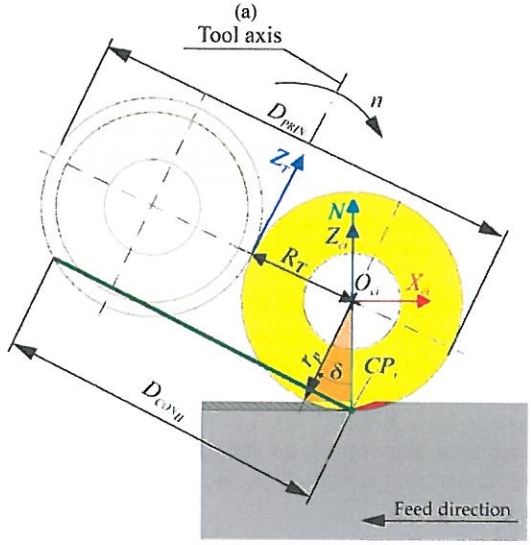

(b)

Fig. 3. Definition of the contact diameter in the $X_{ci}Z_{ci}$ plane: (a) case I: $\delta=0°$ and $\theta=0°$, (b) case II: $\delta\neq0°$ and $\theta=0°$ or $\theta\neq0°$.

B. Effective Diameter

1) Specific case: The cutting edge tangential to the machined surface at the contact point CP_i

In the multi-axis cutting process with the torus milling cutter used, the cutting speed v_c depends not only on the spindle rotation speed n and the principal diameter D_{PRIN}, but also on the axial depth of cut a_p, the inclination angle

δ and the rotational angle θ of the tool axis. The cutting speed will reach its maximum value when, in a given kinematic variant of multi-axis cutting, the active cutting edge is tangential to the contour of the machined surface (generalising: machined plane) at the contact point CP_i. In this particular position of the geometrical-kinematic tool-workpiece relationship (CWE), due to the maximum value of the axial depth of cut a_{p_max}, the effective diameter also has a maximum value.

To calculate the maximum value of the cutting speed, Eq. (3) applies:

$$v_{c_max} = \frac{\pi \cdot D_{eff_max} \cdot n}{1000} \tag{3}$$

In Eq. (3), D_{eff_max} denotes the maximum effective diameter of the tool (considered in the base plane P_r in the tool layout), as shown in Fig. 4.

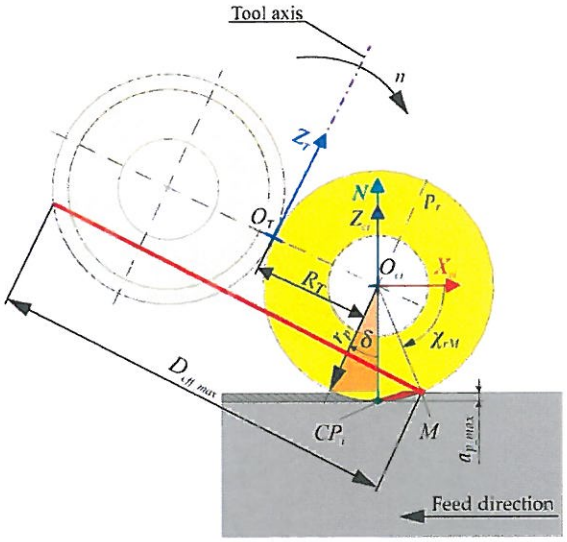

Fig. 4. Definition of the maximal effective diameter in the multi-axis milling process using the torus milling cutter.

In order to determine the equation of the maximum effective diameter D_{eff_max}, assumptions were made as described above. The components in the direction of the X_{ci} and Z_{ci} axes of the adopted reference coordinate system (O_{ci}, X_{ci}, Y_{ci}, Z_{ci}), i.e. the cutting blade system, were then determined, as shown in Fig. 5. The x and y components are described by the system of Eq. (4):

$$\begin{cases} x = r_p \cos(\chi_{rM}) \\ y = r_p \sin(\chi_{rM}) \end{cases} \tag{4}$$

Due to the inclination of the torus cutter axis by an angle δ, the components of the system of Eq. (4) were transformed, that is, rotation by an angle δ. Therefore, in the next step of the calculation another counterclockwise rotation of these components by angle δ was performed. This is to bring the components from the cutting tool system to the cutting blade system.

Therefore, the rotation matrix takes the form in Eq. (5):

$$R(-\delta) = \begin{bmatrix} \cos(-\delta) & -\sin(-\delta) \\ \sin(-\delta) & \cos(-\delta) \end{bmatrix} \tag{5}$$

This matrix rotates the column vectors according to Eq. (6):

$$\begin{bmatrix} x' \\ y' \end{bmatrix} = \begin{bmatrix} \cos(-\delta) & -\sin(-\delta) \\ \sin(-\delta) & \cos(-\delta) \end{bmatrix} \cdot \begin{bmatrix} x \\ y \end{bmatrix} \tag{6}$$

Hence, the x' and y' components, when transformed, take the form of a system of Eq. (7):

$$\begin{cases} x' = r_p \cos(\chi_{rM}) \cos(-\delta) - r_p \sin(\chi_{rM}) \sin(-\delta) \\ y' = r_p \cos(\chi_{rM}) \sin(-\delta) - r_p \sin(\chi_{rM}) \cos(-\delta) \end{cases} \tag{7}$$

The component in the direction of the X_{ci}, axis is important in this case, so ultimately the formula for the maximum effective diameter, taking into account the axis inclination of the torus milling cutter and the axial depth of cut, takes the form in Eq. (8):

$$D_{eff_max} = 2\left[R_T + \begin{pmatrix} r_p \cos(\chi_{rM}) \cos(-\delta) - \\ -r_p \sin(\chi_{rM}) \sin(-\delta) \end{pmatrix} \right] \tag{8}$$

In Eqs. (4), (7) and (8), the symbol χ_{rM} denotes the final position angle of the boundary point M of the cutting layer cross-section at the cutting edge relative to the X_{ci} axis in the cutting blade coordinate system.

2) Cutting blade work angle

Due to the shape of the cutting edge of the torus milling cutter, the value of the cutting speed varies along the length of its active segment of the cutting edge. During multi-axis milling (all kinematic cases for combinations when $\delta > 0°$ and $\theta = 0°$ or $\theta \neq 0°$), the cutting speed varies from a certain minimum value at point E to a certain maximum value at point M. As can be seen from the kinematics of the multi-axis milling of the torus milling cutter, in the range of the cutting blade work angle $\psi_r(\Omega)$, point M moves along the active segment of the cutting edge, moving away from or closer to the point E (see Fig. 5).

Points E and M are the boundary points of the cross-section of the CWE $s_{cwe,i}$ cut layer. In addition, these points, together with the O_{ci} point of the adopted reference coordinate system, form the outline of the circle cutout $O_{ci}EM$ in the base plane P_r of the round cutting insert of torus T. The circle cutout angle $O_{ci}EM$ is the cutting blade work angle in the base plane P_r, which depends on the tool rotation angle Ω, which is denoted by $\psi_r(\Omega)$. In order to determine the cutting blade work angle, the angles describing the position of the boundary points of the cross-section of the cut layer relative to the X_{ci} axis of the adopted reference coordinate system were determined.

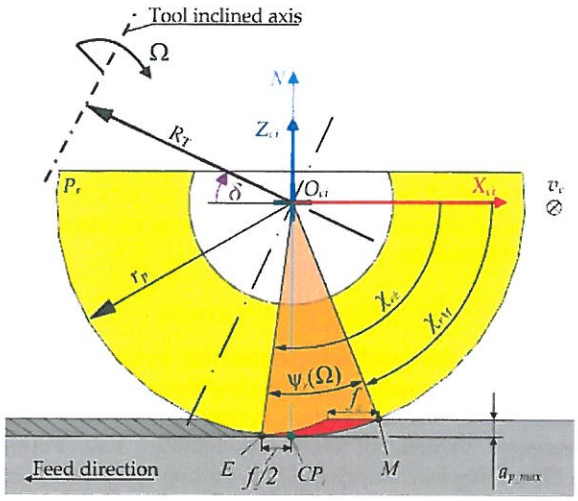

Fig. 5. Geometry of the cutting layer CWE $s_{cwe,i}$ along the cutting edge.

Based on the trigonometric relationships shown in Fig. 5, the value of the angle χ_{rM} of the position of the boundary point M is described by Eq. (9):

$$\chi_{rM} = \arcsin\left(1 - \frac{a_{p_max}}{r_p}\right) \tag{9}$$

In turn, the value of the angle χ_{rE} of the position of the boundary point E is described by Eq. (10):

$$\chi_{rE} = \frac{\pi}{2} + \arcsin\left(\frac{f_z \sin\theta}{2r_p}\right) \tag{10}$$

Hence, the value of the cutting blade working angle $\psi_r(\Omega)$ in the base plane P_r, which depends on the tool rotation angle Ω, is expressed by Eq. (11):

$$\psi_r(\Omega) = \left(\frac{\pi}{2} + \arcsin\left(\frac{f_z \sin\theta}{2r_p}\right) - \arcsin\left(1 - \frac{a_{p_max}}{r_p}\right)\right) \tag{11}$$

For further considerations, the assumption is made that the angle Ω of tool rotation assumes the value $\Omega=0°$, i.e., the outline of the cutting edge is tangent to the outline of the machined surface at the contact point CP_i. Hence, due to the parameter a_{p_max}, the value of the cutting blade work angle $\psi_r(\Omega)$ is the maximum value in this particular case under consideration, and will be denoted as ψ_{r_max} for further consideration.

In conclusion of this section, it should be mentioned that the spherical coordinate in the form of the angle of rotation θ does not affect the value of the contact diameter and the effective diameter, but rather its position in Euclidean space, where the common point of each position of these diameters is the contact point CP_i and the boundary point M, respectively. Hence, on the basis of this kinematic property, the distance between the extreme points of the contact curve was determined in the next step.

In Fig. 6, a general example of the considerations to date is shown. The actual effective diameter is the distance between the centre of the torus and the circle of contact. This distance depends on the kinematic variant of multi-axis cutting and the direction of milling.

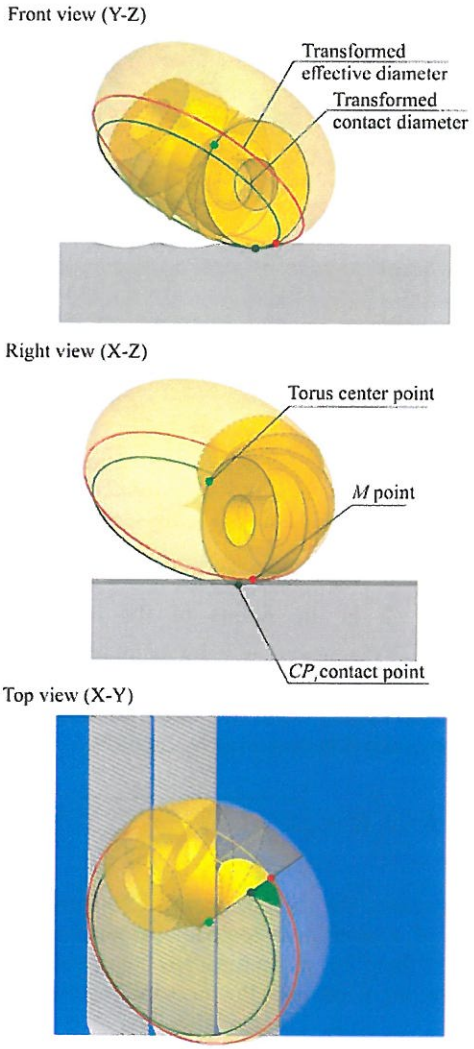

Fig. 6. An example: 3 projected views of the torus milling cutter and the transformed diameters.

III. Determining Distance between the Intersection Points of Contact Curve and Pre-finished Surface

In the transformed contact circle (contact diameter), using analytical geometry and trigonometric relationships, in the Y-Z plane, the length of the chord defined by the points t_1 and t_2 can be calculated, as shown in Fig. 7. These are the points of intersection of the contact circle with the machined surface (assumed plane). In the geometrical-kinematic system adopted, there are only two such points. Given the parameters δ and θ, three cases should be considered.

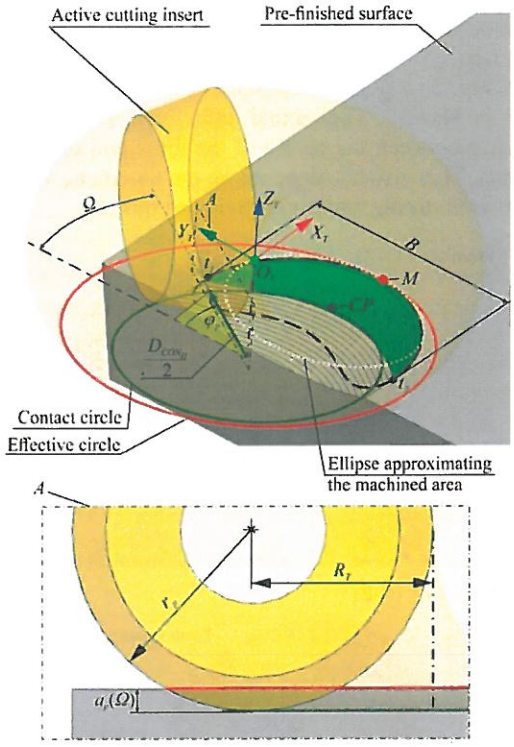

Fig. 7. Determination of milling width B.

A. Case I: $\delta=0°$ and $\theta=0°$

If $D_{CON_{II}}/2$ is the radius of the contact circle, $a_{p_max}=a_p(\Omega)$ is the maximum axial depth of cut, the R_T is the radius of the torus milling cutter, and if r_p is the radius of the circular cutting insert (the circle defining the torus), the milling width B is described by Eq. (12):

$$B = 2\left(R_T + \sqrt{2r_p a_{p_max} - (a_{p_max})^2} \right) \tag{12}$$

In this case, the contact point CP_i moves in the direction of a rectilinear toolpath perpendicular to the segment defined by the points t_1t_2, thus obtaining the greatest milling width used the torus milling cutter.

B. Case II: $0°<\delta<\left[90-\left(\frac{90-\chi_{rM}}{2}\right)\right]°$ and $\theta\neq0°$

If $D_{CON_{II}}/2$ is the radius of the contact circle, $a_p(\Omega)$ is the the axial instantaneous depth of cut dependent on the angle of rotation of the tool, r_p is the radius of the circular cutting insert (the circle defining the torus), and the φ_p is the cut initial working angle of the torus milling cutter, the milling width B is described by Eq. (13):

$$B = 2\left[\frac{D_{CON_{II}}}{2} \cdot \cos(\varphi_p) + \left(\sqrt{2r_p a_p(\Omega) - a_p(\Omega)^2} \right) \cos(\varphi_p) \right] \tag{13}$$

The values of the parameters $a_p(\Omega)$ and φ_p, for a given angle δ of the cutter axis within the given range, are determined using the discrete direct CAD method.

In the third case, i.e. when also $\theta>0°$ (*DP TPL-diagonally positive tool pull*) or $\theta<0°$ (*DN TPL-diagonally negative tool pull*), the determination of the milling width B is carried out in a similar way as above, with the additional reliance on an ellipse approximating the machined area.

IV. Research Conditions

Based on the developed geometrical-kinematic model, this section presents adopted conditions of simulation studies and experimental investigations for three kinematic variants of multi-axis cutting: Tool Pulling (TPL), Diagonal Positive Tool Pulling (DP-TPL) and Diagonal Negative Tool Pulling (DN-TPL). Simulation studies were carried out in a CAD/CAM environment using the discrete direct method.

A. Changing Contact Diameter, Effective Diameter and Cutting Speed

Tests in stage one shows the change of values in contact diameter, effective diameter, and cutting speed. In the case shown, the tool's principal diameter D_{PRIN} is 16 mm, the radius of the round cutting insert is 4 mm, and the depth of cut is 0.5 mm. The spindle speed n was 1989.43678 1/min, making the cutting speed at the periphery of the principal diameter v_{c_PRIN} equal 100 m/min. In order to avoid the influence of the toolpath distance b_r on the character of the time courses of the tested output quantities, the values of the milling width B were smaller than b_r (see Fig. 1). The variable parameters were the inclination angle δ and the rotational angle θ of the tool axis. A detailed summary of the quantities studied in this phase of the research is shown in Tables I and II.

TABLE I. Machining Simulation Parameters, Case $\delta\geq0°$ and $\theta=0°$

Inclination angle δ [°]	Rotational angle θ [°]	Cutting speed v_{c_PRIN} [m/min]	Feed per tooth f_z [mm/z]	Depth of cut a_{p_max} [mm]
$\Delta=0$ as long as $\delta<90$ perform $\delta=\delta+$	0	100	0.25	0.5

TABLE II. Machining Simulation Parameters, Case $\delta=10°$ and $-90°\leq\theta\leq90°$

Inclination angle δ [°]	Rotational mangle θ [°]	Cutting speed v_{c_PRIN} [m/min]	Feed per tooth f_z [mm/z]	Depth of cut a_{p_max} [mm]
10	$\Theta=-90$ as long as $\theta<90$ perform $\theta=\theta+5$	100	0.25	0.5

B. Changing the Working Angle of the Tool Blade

On the next hand, in the second stage, the study shows, in the first case, the variation of the tool blade working angle ψ_r as a function of the depth of cut and feed per

blade for the kinematic variant of *TPL*-type multi-axis cutting, and as a function of the rotational angle θ of the tool axis for the kinematic variants of *DP-TPL* and *DN-TPL* multi-axis cutting in the second case. To carry out this simulation study, analogous assumptions and values of the variables under study were used as in stage one. A detailed summary of the quantities studied in this phase of the research is shown in Tables III and IV.

TABLE III. MACHINING SIMULATION PARAMETERS, FIRST CASE

Inclination angle δ [°]	Rotational angle θ [°]	Cutting speed v_{c_PRIN} [m/min]	Feed per tooth f_z [mm/z]	Depth of cut a_{p_max} [mm]
10	0	100	0.25	0.3 0.4 0.5
10	0	100	0.15 0.20 0.25	0.5

TABLE IV. MACHINING SIMULATION PARAMETERS, SECOND CASE

Inclination angle δ [°]	Rotational mangle θ [°]	Cutting speed v_{c_PRIN} [m/min]	Feed per tooth f_z [mm/z]	Depth of cut a_{p_max} [mm]
10	θ=15 as long as θ<165 perform θ=θ+5	100	0.25	0.5

C. *Experimental Investigation of the Multi-axis Milling Process Using the Torus Milling Cutter*

The experimental set-up is shown in Fig. 8. A vertical 5-axis CNC machining centre (DMU 100 MonoBLOCK) is used to conduct the multi-axis milling tests. Test material is Ni-based superalloy Inconel 718.

The multi-axis milling process was conducted by applying steel torus milling cutter body R300-016A20L-08L for indexable round cutting inserts R300-0828E-PL. The body of the torus milling cutter has a neutral geometry. Round cutting inserts are made of S30T cemented carbide grade. Grade S30T has fine-grain cemented carbide and a TiAlN Physical Vapor Deposition (PVD) coating. The round cutting inserts used in the tests have the following parameters: the rake angle is 20°, the relief angle (or else clearance) is 15° and the insert radius is 4 mm.

Furthermore, the cutting insert does not have a typical roundness radius r_ε of the cutting edge, but an asymmetrical chamfer with the following dimensions: length 0.1 mm measured along the line of intersection of the reference plane and orthogonal plane, and an angle of 15° measured in the orthogonal plane between the edge of the chamfer and the line of intersection of the reference plane and orthogonal plane in the Orthogonal Rake System (ORS) of the tool geometry. These 8 mm diameter round cutting inserts was attached in to a 16 mm diameter tool body at an overhang measuring 65 mm.

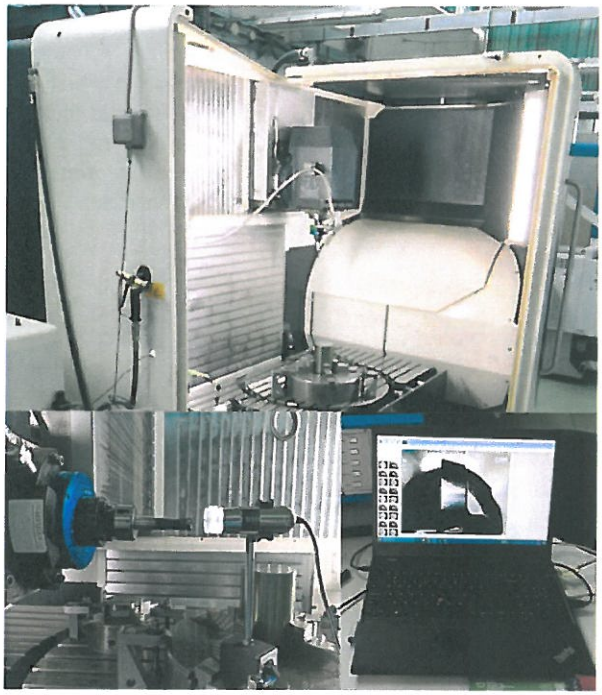

Fig. 8. Experimental test bench.

Multi-axis milling parameters are presented in Table V. In this parameters consist of: the cutting parameters and the tool axis orientation parameters. The cutting parameters were assumed to be constant and invariant for each experiment. Their values were chosen based on recommendations from the tool manufacturer and the aerospace industry. Hence, it was decided to keep the cutting speed values within the speed range for High Speed Machining (HSM) cutting with regard to Ni-based superalloys. The input variables were the tool axis orientation parameters, i.e., inclination angle δ and rotational angle θ. Flood cooling was used in each experiment, and starting each new experiment, the round cutting inserts were replaced with a new set. The tool life was determined on the basis of the localized flank wear (VB_{max}), until it reached 0.3 mm. This was to avoid the effect of excessive tool wear on the workpiece surface due to the higher temperature. The multi-axis milling process was interrupted at specific intervals to identify the wear patterns and measure the wear rate by using a Dino-Lite 7000 CE series digital workshop microscope. Selected 2D and 3D roughness paramaters of the shaped surfaces at the CP_i contact points were measured non-contact using Alicon's InfiniteFocus optical microscope.

TABLE V. MULTI-AXIS MILLING PARAMETERS

Experiment No.	Inclination angle δ [°]	Rotational angle θ [°]	Cutting speed v_{c_PRIN} [m/min]	Feed per tooth f_z [mm/z]	Depth of cut a_{p_max} [mm]	Milling width B [mm]	Toolpaths distance b_r [mm]
1	21.26157	−63.05383				5.3587	5.8
2	21.26157	63.05383	100	0.25	0.5	5.3587	5.8
3	10.00000	0.00000				9.1191	9.3

V. Result and Discussion

A. Changing Contact Diameter, Effective Diameter and Cutting Speed

1) Case, $\delta \geq 0°$ and $\theta = 0°$

A study was first carried out for the case in which the machining parameters, i.e. rotation speed and cutting speed, were set relative to the principal diameter D_{PRIN}. Fig. 9 illustrates the variations in contact diameter, effective diameter, and cutting speed for this case.

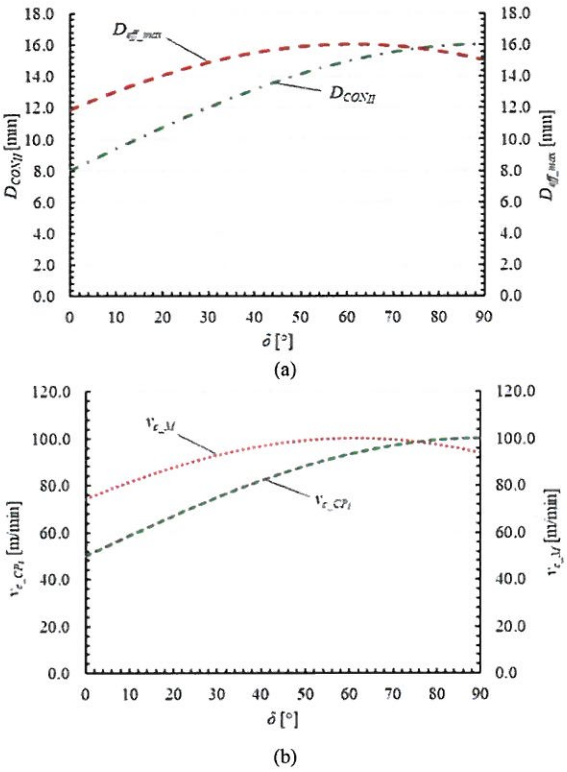

Fig. 9. The changing of: (a) the contact and effective diameters, (b) the cutting speed, in the function of inclination angle δ.

As the value of the angle δ of the torus cutter axis in the feed direction increases, the value of the contact diameter $D_{CON_{II}}$ also increases. The same is true for the cutting speed v_{c_CPi} at the contact point. The minimum values of these parameters are obtained for δ=0°, and the maximum values for δ = 90°. Whereas, as the value of the angle δ in the feed direction increases, the value of the effective diameter D_{eff_max} and the cutting speed v_{c_M}, also increase, before reaching a maximum and these values decrease. This is due to the geometry of the torus. In doing so, two important aspects should be noted. Firstly, the actual cutting speed is always lower than the programmed one because both the contact and effective diameters are smaller than the principal diameter, therefore, for example, for δ=10° instead of 100 m/min a speed of v_{c_Cpi} = 58.68241 m/min and v_{c_M} = 81.43551 m/min is realized. In this case, the difference is 29%, and over the entire δ angle range from 0% to 67%. Secondly, for the torus geometry, there is a special case for which the difference in the values of the tested parameters is 0%. In the machining example being considered, this is the setting for which the angle δ = 75.52249°, and it depends on the radius of the round cutting insert of the torus and the depth of cut. In this case, the contact and effective diameters are equal. On this basis, it can be assumed that the milling will be more beneficial with the smaller the differences between these diameters.

Tests were then carried out for the case in which the machining parameters were set relative to the contact diameter $D_{CON_{II}}$, and therefore directly affect the cutting conditions in the CWE at the CP_i contact point and thus the topography of the shaped surface. Firstly, the courses of: the cutting speed at point M and at point CP_i as a function of inclination angle δ are collated. These courses are illustrated in Fig. 10. From this graph, it was found that by setting the same value of cutting speed at the contact point (100 m/min) for each new angle value, the cutting speed at the limit point M of the cut layer cross section decreases.

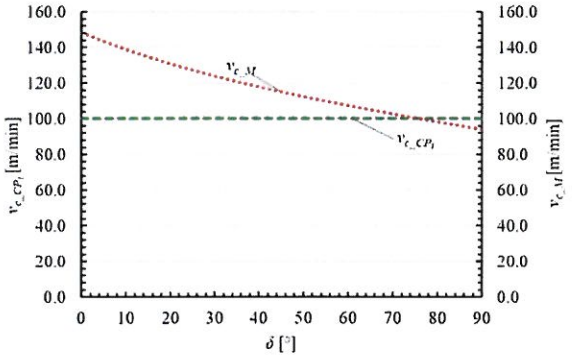

Fig. 10. The changing of the cutting speed at point M and point CP_i in CWE in the function of inclination angle δ.

Furthermore, it should be noted that the cutting speed v_{c_M} occurs in the zone of maximum thickness of the cut layer. Thus, it can be concluded that a decrease in the value of the cutting speed at point M of the cut layer cross-section can significantly increase tool life and reduce the formation of notching wear.

Based on the above, secondly compares the courses of the cutting speed v_{c_CPi} and the feed rate v_f as a function of the inclination angle δ, for machining parameters related to the principal diameter and then the contact diameter. These courses are illustrated in Fig. 11.

From these graphs, it was found that when the machining parameters are fixed with respect to the principal diameter, the cutting speed at the contact point increases as the angle of inclination increases, and the feed rate does not change (top graph). However, when the machining parameters are fixed with respect to the contact diameter, the cutting speed at the contact point does not change and the feed rate (also the spindle speed) decreases (bottom graph). Note that for small inclination angles, the feed rate in the second case is almost twice as high as the feed rate in the first case. This can have a negative impact on the tool life. However, it should be denoted that the cutting speed is the parameter that most

influences the wear of the tool. Higher feed rates, on the other hand, undoubtedly increase the efficiency of the machining process.

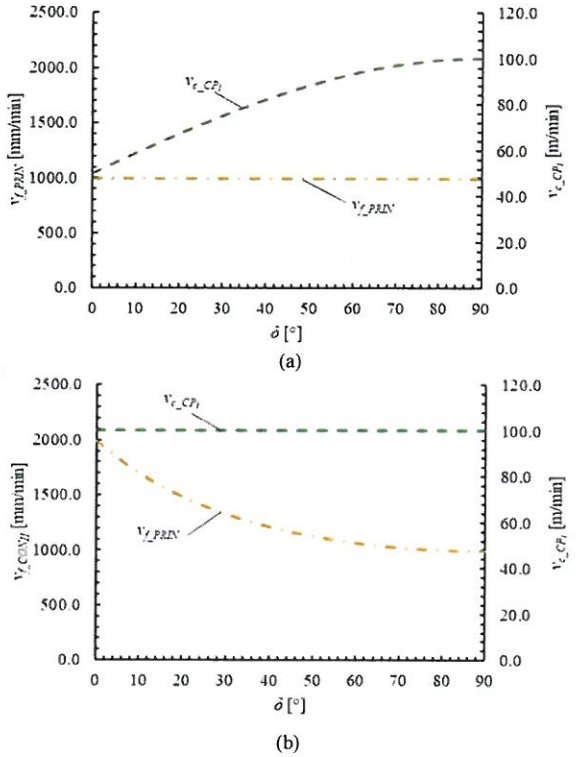

Fig. 11. The changing of: (a) the cutting speed at point CP_i, (b) the feed rate v_{f_PRIN} in CWE, in the function of inclination angle δ.

2) Case, $\delta \geq 0°$ and $0° \leq \theta \leq 90°$

In the next step, the effect of the rotational angle θ of the torus milling cutter axis on the change in contact diameter and effective diameter was investigated. The courses obtained are shown in Fig. 12 for the *DP-TPL*, and Fig. 13 for the *DN-TPL* kinematic variant, respectively.

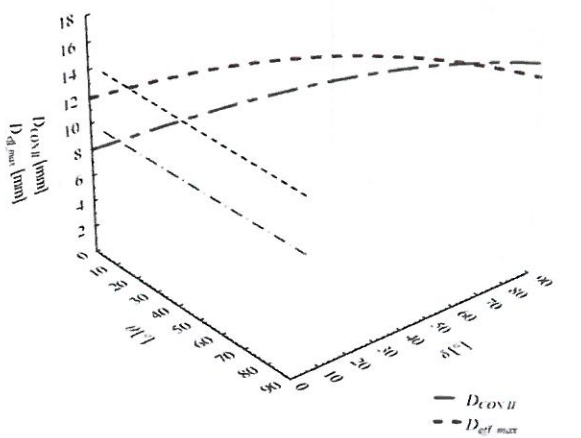

Fig. 12. The changing of the contact and effective diameters in the function of rotational angle in the *DP-TPL* kinematic cutting variant.

Analysing the graphs obtained for both kinematic variants, it was found that the rotational angle of the tool axis has no effect on either changes in contact diameter or changes in effective diameter. At this stage of the research, it can be concluded that the variations in these diameters will generally be influenced by the geometry of the tool used for machining, the curvature of the machined sculptured surface and the uneven distribution of the machining allowance, which translates into variations in depth of cut values along the tool path.

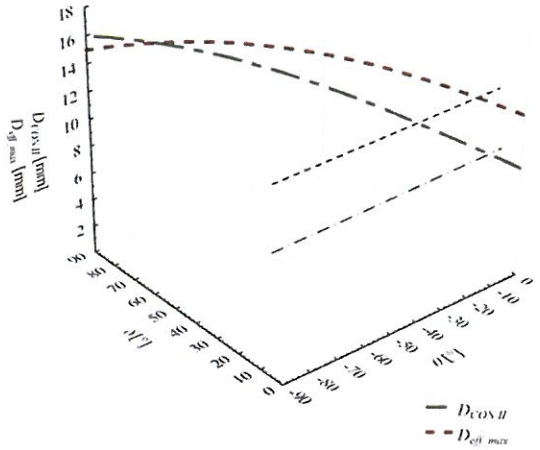

Fig. 13. The changing of the contact and effective diameters in the function of rotational angle in the *DN-TPL* kinematic cutting variant.

B. Changing the Working Angle of the Tool Blade

Fig. 14 illustrates the changes of the work angle ψ_r of the cutter blade as a function of the maximum depth of cut a_{p_max} occurring at the CP_i contact point, whereas Fig. 15 illustrates the changes of the cutter blade work angle ψ_r as a function of the feed per tooth f_z.

By analysing the graphs obtained, it was found that both with an increase in the value of the maximum depth of cut at the contact point and the feed per tooth, the cutter blade work angle increases. This results in an extension of the active cutting edge segment.

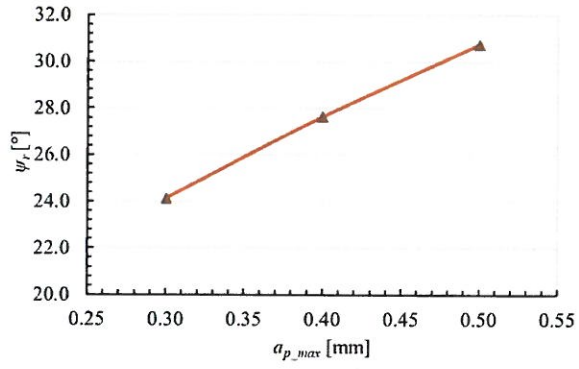

Fig. 14. The changing of the cutting blade work angle in the function of maximal depth of cut.

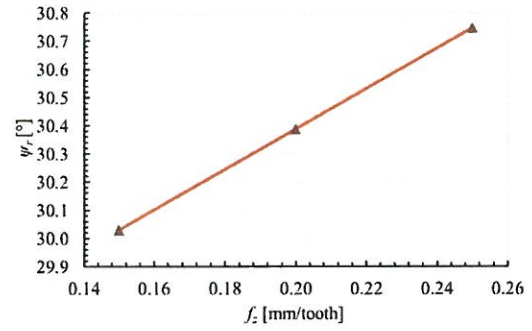

Fig. 15. The changing of the cutting blade work angle in the function of feed per tooth.

Figs. 16 and 17, in turn, illustrate the changes in the cutter blade work angle ψ_r as a function of the rotational angle θ of the tool axis with respect to the contact point CP_i, respectively for the multi-axis kinematic variants *DP-TPL* and *DN-TPL*. The kinematic variant of *TPL* is illustrated in the graphs by the rotational angle θ=90°.

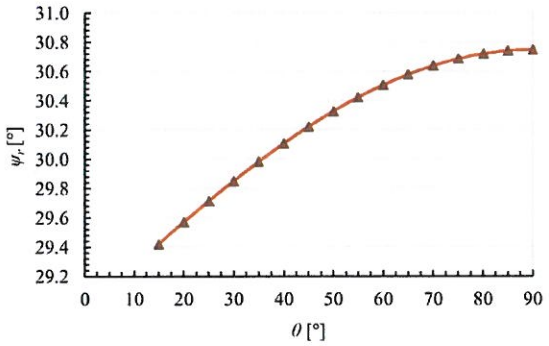

Fig. 16. The changing of the cutting blade work angle in the function of maximal depth of cut.

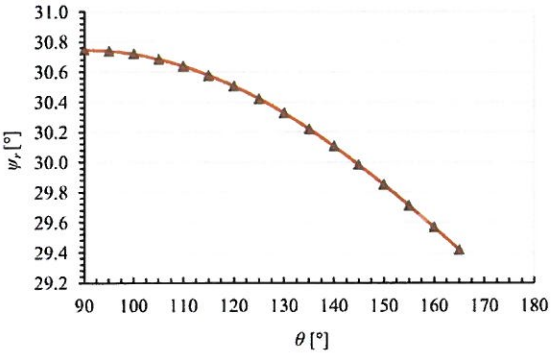

Fig. 17. The changing of the cutting blade work angle in the function of maximal depth of cut.

From the analysis of the graphs above, it can be seen that the rotational angle affects changes in the cutter blade work angle, and thus the length of the active cutting edge segment. The highest value of the cutter blade work angle at the contact point was obtained for the *TPL* variant. The change in the working angle of the cutter blade as a function of the rotational angle of the tool axis is related in this case to a change in the parameter $f_z/2$. This change takes place as a function of the rotational angle in the area defined by the $O_{ci}CP_iE$ points (see Fig. 5). In this area, the cutting edge shapes the part of the roughness profile downstream of the contact point, and this can be important in terms of the minimum thickness of the cut layer. Taking this into account, graphs were developed showing the differences between the maximum value of the parameter $f_z/2$, and the values resulting from the introduction of the rotational angle of the tool axis, i.e., $f_z/2\sin(\theta)$. The graphs are illustrated in Figs. 18 and 19.

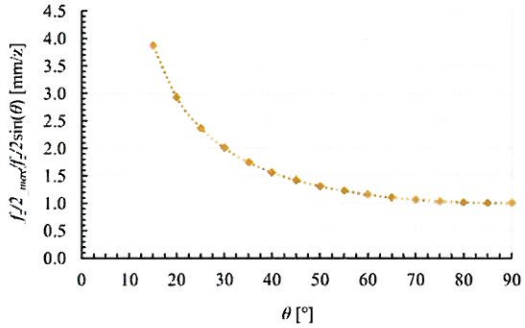

Fig. 18. Course of variation of the ratio $(f_z/2)$ / $(f_z/2\sin(\theta))$ as a function of the rotational angle θ for the *DP-TPL* variant.

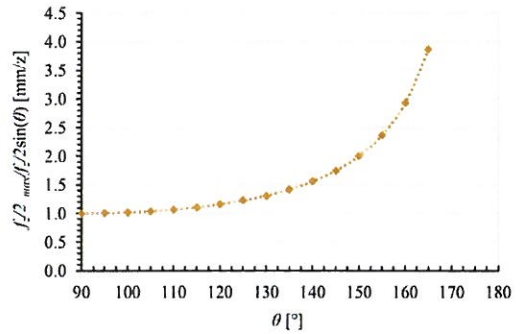

Fig. 19. Course of variation of the ratio $(f_z/2)$ / $(f_z/2\sin(\theta))$ as a function of the rotational angle θ for the *DN-TPL* variant.

Figs. 18 and 19 show that the differences between the maximum value of the parameter $f_z/2$, and the values resulting from the introduction of the rotational angle of the tool axis, i.e., $f_z/2\sin(\theta)$, are almost four times, in the range of large values of the rotational angle θ. Whereas, in the kinematic variant of *TPL* multi-axis cutting, the ratio is 1. An increase in the angle θ, whether in the negative or positive direction, results in an increase in the ratio $(f_z/2)/(f_z/2\sin(\theta))$.

C. Surface Roughness

Histograms of selected 3D surface roughness parameters are illustrated in Fig. 20. Whereas, Fig. 21 illustrates images of machined surfaces and texture images of these surfaces.

From the analysis of the measurement results obtained, it can be seen that in terms of the physical and functional properties of the surfaces obtained, those shaped with the *TPL* kinematic variant are the best.

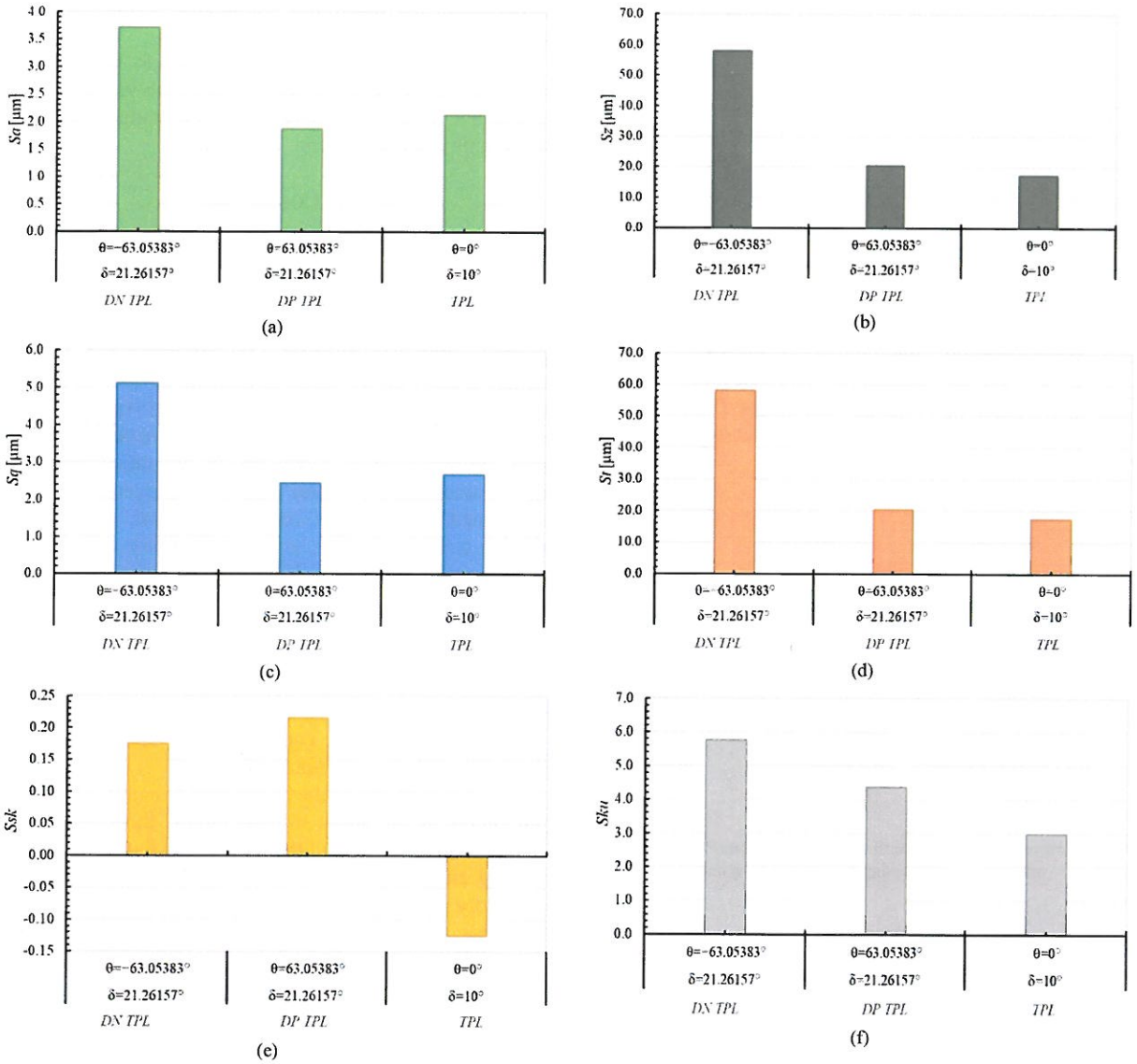

Fig. 20. Histograms of the 3D (area) surface roughness parameters after multi-axis milling using the torus milling cutter with a different kinematic variants cutting: (a) Sa: arithmetical mean height, (b) Sz: maximum hight, (c) Sq: root mean square hight, (d) St: maximum peak hight, (e) Ssk: skewness, (f) Sku: kurtosis.

Surfaces after multi-axis milling with the *TPL* variant are characterised by low roughness, which contributes to fatigue strength. As $Sa = 2.12$ µm, the effect of roughness on fatigue strength is comparable to that of residual stress and microstructure of the material. This is evidenced, among other things, by the parameter $Sku = 3$, which means that the machined surface is characterised by a Gaussian distribution of the shape of the grooves of the surface profile and thus a favourable stress concentration. In addition, the resulting lower surface roughness increases the corrosion resistance of this surface. The structure of these surfaces is characterised by anisotropy, which also makes them more resistant to corrosion. On the other hand, for consumption of $VB = 0$ mm parameter $Ssk = -0.008$, for $VB = 0.15$ mm $Ssk = -0.12$, and beyond $VB = 0.3$ mm $Ssk = 0.14$. This shows that the surface obtained by multi-axis *TPL* milling is flat, has an overall symmetrical height distribution, and contains small indentations. Thus, tool wear also has a strong influence on the physical and functional characteristics of the surfaces manufactured with the *TPL* variant.

D. Tool Wear

As shown in Fig. 22, for the adopted wear criterion of VB=0.3 mm, the tool life was 1.33; 1.83 and 3.33 min for the kinematic variant of *DN-TPL*; *TPL* and *DP-TPL* multi-axis cutting, respectively. It can therefore be seen that the change in tribological conditions in CWE resulting from the geometrical-kinematic relationships of multi-axis milling results in an increase in tool life.

By analysing the wear curves, it can be seen that they present a classic three-phase course.

During the inception phase, the wear rate is relatively high, and wear reaches a baseline in a short time. In the middle phase, uniform wear and tear of a quasi-linear and predictable nature can be observed. The final phase is

characterised by accelerated wear until a critical value associated with cutting blade failure is reached.

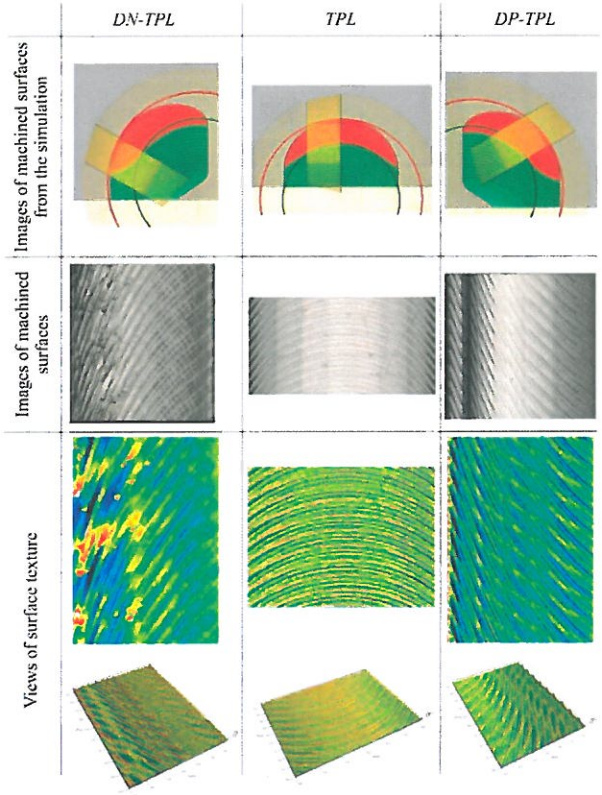

Fig. 21. Images of machined surfaces and views of surface texture after multi-axis milling using the torus milling cutter.

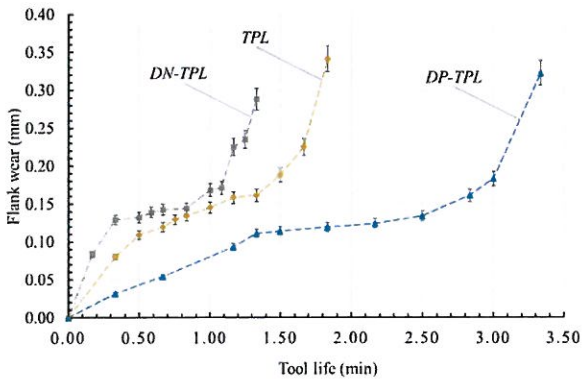

Fig. 22. Change of the wear indicator *VB* on the flank surface of the round cutting insert for multi-axis milling *DN-TPL*, *TPL* and *DP-TPL*.

The contact diameter and effective diameter of the torus milling cutter change continuously when milling sculptured surfaces. Consequently, the actual position of the contact point on the cutting edge of the cutter also changes. Along with this parameter, the cross section of the cut layer, the cutting speed, and the tool life in the CWE also change. It also fundamentally affects surface integrity. To minimise this impact, it is worth considering keeping the contact and effective diameters constant or very slightly varying during toolpath planning and determining the machining parameters in relation to the contact point.

In order to do this, it is necessary to carry out the necessary calculations at any point in the toolpath on the workpiece surface as early as the planning stage of the multi-axis milling process.

VI. Conclusion

This work presents selected the theoretical and experimental issues of the process of multi-axis milling of the surface of Ni-based superalloy Inconel 718 parts used the torus milling cutter in a kinematic variants of the: tool pulling, diagonal positive tool pulling, and diagonal negative tool pulling types, in terms of surface quality and tool wear. Since cutting speed during high-speed finishing milling is the parameter that has the greatest impact on tool life and surface roughness, mathematical models of the contact diameter and effective diameter were first developed. Simulations and experiments of multi-axis milling were carried out, and the necessary analyses were performed. It is worth highlighting that the theoretical and experimental research was based on the parameter of the working angle of the tool blade in the basic plane, which is very rarely taken into account. This is a novelty in the geometric-kinematic approach to determining technological, geometric, and physical parameters within of the cutting layer. The following conclusions were drawn from the results obtained.

The value of the contact diameter basically depends on the radius of the torus milling cutter, the radius of the round cutting insert, and the inclination angle of the torus milling cutter axis. The contact curve is also part of the trajectory of the contact point within the cutting layer. Whereas, the value of the effective diameter depends essentially on the radius of the torus cutter, the radius of the round cutting insert, the angle of inclination of the torus cutter axis and the boundary angle of the intersection point of the cutting edge outline with the pre-finished surface outline. In the CWE area, there are significant changes in the cutting speed values.

It was found that when the machining parameters are fixed with respect to the principal diameter, the cutting speed at the contact point increases as the angle of inclination increases and the feed rate does not change. However, when the machining parameters are fixed with respect to the contact diameter, the cutting speed at the contact point does not change and the feed rate (also the spindle speed) decreases with an increase in the inclination angle.

In addition, it was found that the rotational angle of the tool axis affects changes in the tool blade working angle, and thus the length of the active cutting edge segment. The change in the working angle of the tool blade as a function of the rotational angle of the tool axis is related to a change in the parameter $f_z/2$. Hence, climb milling was obtained for the variants tool pulling and diagonal positive tool pulling, whereas for the variant diagonal negative tool pulling conventional milling was obtained.

The best results of machining tests, taking into account the obtained values of surface roughness and tool life

parameters, were obtained for the variant tool pulling, and thus this kinematic variant of the multi-axis milling requires conducting further research in the field of physical and technological aspects of cutting.

CONFLICT OF INTEREST

The author declares no conflict of interest.

ACKNOWLEDGMENT

I would like to thank Anna Bazan for her help in surface roughness measured of the research objects.

REFERENCES

[1] C. Zhang, S. Guo, H. Zhang, and L. Zhou, "Modeling and predicting for surface topography considering tool wear in milling process," *Int. J. Adv. Manuf. Technol.*, vol. 68, no. 9–12, pp. 2849–2860, Oct. 2013.

[2] L.-X. Cao, H. Gong, and J. Liu, "The offset approach of machining free form surface," *Journal of Materials Processing Technology*, vol. 184, no. 1–3, pp. 6–11, Apr. 2007.

[3] M. Gdula, "Empirical models for surface roughness and topography in 5-axis milling based on analysis of lead angle and curvature radius of sculptured surfaces," *Metals*, vol. 10, no. 7, 932, Jul. 2020.

[4] M. Gdula and J. Burek, "Cutting layer and cutting forces in a 5-axis milling of sculptured surfaces using the toroidal cutter," *Journal of Machine Engineering*, vol. 4, no. 17, pp. 98–122, Dec. 2017.

[5] Z. Chang, J. Qian, Z. C. Chen, N. Wan, and D. Zhang, "Geometrical theory of cutting stock with torus end mills in five-axis CNC machining and its applications in machining simulation," *Int. J. Adv. Manuf. Technol.*, vol. 105, no. 1–4, pp. 27–46, Nov. 2019.

[6] Z. Zhu, F. Peng, R. Yan, Z. Li, J. Wu, X. Tang, and C. Chen, "Influence mechanism of machining angles on force induced error and their selection in five axis bullnose end milling," *Chinese Journal of Aeronautics*, vol. 33, no. 12, pp. 3447–3459, Dec. 2020.

[7] J. Fan, "Cutting speed modelling in ball nose milling applications," *Int. J. Adv. Manuf. Technol.*, vol. 73, no. 1–4, pp. 161–171, Jul. 2014.

[8] A. F. De Souza, A. E. Diniz, A. R. Rodrigues, and R. T. Coelho, "Investigating the cutting phenomena in free-form milling using a ball-end cutting tool for die and mold manufacturing," *Int. J. Adv. Manuf. Technol.*, vol. 71, no. 9–12, pp. 1565–1577, Apr. 2014.

[9] S. Wojciechowski, P. Twardowski, and M. Wieczorowski, "Surface texture analysis after ball End milling with various surface inclination of hardened steel," *Metrology and Measurement Systems*, vol. 21, no. 1, pp. 145–156, Mar. 2014.

[10] S. Wojciechowski and P. Twardowski, "The influence of tool wear on the vibrations during ball end milling of hardened steel," *Procedia CIRP*, vol. 14, pp. 587–592, 2014.

[11] S. Wojciechowski and P. Twardowski, "Tool life and process dynamics in high speed ball end milling of hardened steel," *Procedia CIRP*, vol. 1, pp. 289–294, 2012.

[12] B. Mikó and P. Zentay, "A geometric approach of working tool diameter in 3-axis ball-end milling," *Int. J. Adv. Manuf. Technol.*, vol. 104, no. 1–4, pp. 1497–1507, Sep. 2019.

[13] A. Mgherony and B. Mikó, "Simulation of the working diameter in 3-axis ball-end milling of free form surface," *Teh. Vjesn.*, vol. 29, no. 4, Aug. 2022.

[14] T. Vopát, J. Peterka, V. Šimna, and M. Kuruc, "The influence of different types of copy milling on the surface roughness and tool life of end mills," *Procedia Engineering*, vol. 100, pp. 868–876, 2015.

[15] A. V. Vyboishchik, "Modelling topology of freeform surfaces with ball-end milling," *Procedia Engineering*, vol. 150, pp. 761–767, 2016.

[16] J. Beňo, I. Maňková, P. Ižol, and M. Vrabel', "An approach to the evaluation of multivariate data during ball end milling free-form surface fragments," *Measurement*, vol. 84, pp. 7–20, Apr. 2016.

[17] A. E. Pena, F. D. Anania, and M. Zapciu, "Research concerning optimum cutting parameters according with tool path strategy for finishing procedures," *IOP Conf. Ser.: Mater. Sci. Eng.*, vol. 95, 012020, Nov. 2015.

[18] Pena, "Method for optimum calculus of machining parameters according to tool trajectories type based on milling process simulation," *Teh. Vjesn.*, vol. 24, no. 2, Apr. 2017.

[19] J.-M. Redonnet, A. G. Vázquez, A. T. Michel, and S. Segonds, "Optimization of free-form surface machining using parallel planes strategy and torus milling cutter," in *Proc. the Institution of Mechanical Engineers, Part B: Journal of Engineering Manufacture*, Jan. 2018, vol. 232, no. 2, pp. 240–250.

[20] Q. Zhang, S. Zhang, and W. Shi, "Modeling of surface topography based on relationship between feed per tooth and radial depth of cut in ball-end milling of AISI H13 steel," *Int. J. Adv. Manuf. Technol.*, vol. 95, no. 9–12, pp. 4199–4209, Apr. 2018.

[21] X. Liu, Y. Li, and Q. Li, "A region-based 3 + 2-axis machining toolpath generation method for freeform surface," *Int. J. Adv. Manuf. Technol.*, vol. 97, no. 1–4, pp. 1149–1163, Jul. 2018.

[22] M. Gdula and G. Mrówka-Nowotnik, "Analysis of tool wear, chip and machined surface morphology in multi-axis milling process of Ni-based superalloy using the torus milling cutter," *Wear*, vol. 520–521, 204652, May 2023.

[23] A. Mgherony and B. Mikó, "Controlling the spindle speed when milling free-form surfaces using ball-end milling cutter," *Acta Polytech Hung*, vol. 20, no. 6, pp. 135–149, 2023.

[24] A. Mgherony and B. Mikó, "The effect of the cutting speed on the surface roughness when ball-end milling," *Hung. J. Ind. Chem.*, vol. 49, no. 2, pp. 9–13, 2021.

[25] A. Mgherony and B. Mikó, "The effect of the spindle speed control when milling free-form surfaces," *Int. J. Adv. Manuf. Technol.*, vol. 130, no. 3–4, pp. 1439–1449, Jan. 2024.

[26] A. Mgherony and B. Mikó, "Tool path planning of ball-end milling of free-form surfaces as a search algorithm," *Acta Tech. Jaurinensis*, Mar. 2024.

Copyright © 2024 by the authors. This is an open access article distributed under the Creative Commons Attribution License (CC BY-NC-ND 4.0), which permits use, distribution and reproduction in any medium, provided that the article is properly cited, the use is non-commercial and no modifications or adaptations are made.

ARTYKUŁ
A7

dr inż. Michał Gdula
Politechnika Rzeszowska im. I. Łukasiewicza
Wydział Budowy Maszyn i Lotnictwa
Katedra Technik Wytwarzania i Automatyzacji

Rzeszów, dn. 23.04.2025 r.

OŚWIADCZENIE WSPÓŁAUTORA

Oświadczam, że w pracy:

lp.: A4

Gdula M., Mrówka-Nowotnik G.: *Analysis of tool wear, chip and machined surface morphology in multi-axis milling process of Ni-based superalloy using the torus milling cutter.* WEAR, Vol. 520-521 (2023) 204652. IF 5.3, MNiSW 200 pkt.;

mój wkład w powstanie tej pracy polegał na: analizie aktualnego stanu wiedzy w zakresie tematu pracy, opracowaniu metodyki badań, przeprowadzeniu badań eksperymentalnych, przeprowadzeniu analizy trwałości narzędzia dla różnych wariantów kinematycznych frezowania wieloosiowego, opracowaniu krzywych zużycia, analizy mechanizmów zużycia dla różnych wariantów kinematycznych frezowania wieloosiowego, opracowaniu i interpretacji wyników pomiarów sił skrawania, analizy morfologii wiórów oraz obrobionych powierzchni, opracowaniu wniosków, wykonaniu wykresów, rysunków oraz tabel, współudziale w opracowaniu manuskryptu, koordynowaniu procesu wydawniczego.

Gdula Michał

Podpis
dr inż. Michał Gdula

dr hab. inż. Grażyna Mrówka-Nowotnik, prof. PRz
Politechnika Rzeszowska im. I. Łukasiewicza
Wydział Budowy Maszyn i Lotnictwa
Katedra Nauki o Materiałach

Rzeszów, dn. 23.04.2025 r.

OŚWIADCZENIE WSPÓŁAUTORA

Oświadczam, że w pracy:

lp.: A4

Gdula M., Mrówka-Nowotnik G.: *Analysis of tool wear, chip and machined surface morphology in multi-axis milling process of Ni-based superalloy using the torus milling cutter*. WEAR, Vol. 520-521 (2023) 204652. IF 5.3, MNiSW 200 pkt.;

mój wkład w powstanie tej pracy polegał na: przeprowadzeniu obserwacji i wykonaniu mikrofotografii powierzchni przyłożenia i natarcia zużytych ostrzy skrawających, wiórów oraz obrobionych powierzchni z zastosowaniem mikroskopu skaningowego (SEM) wyposażonego w układy EDS i WDS do analizy składu chemicznego oraz układ EBSD umożliwiający wyznaczenie tekstury materiałów oraz identyfikację składników fazowych, współudziale w opracowaniu korekty wersji roboczej manuskryptu.

.....
Podpis
dr hab. inż. Grażyna Mrówka-Nowotnik, prof. PRz

Wear 520–521 (2023) 204652

Contents lists available at ScienceDirect

Wear

journal homepage: www.elsevier.com/locate/wear

Analysis of tool wear, chip and machined surface morphology in multi-axis milling process of Ni-based superalloy using the torus milling cutter

M. Gdula [a,*], G. Mrówka-Nowotnik [b]

[a] Department of Manufacturing Techniques and Automation, Rzeszow University of Technology, al. Powstańców Warszawy 12, 35-959, Rzeszow, Poland
[b] Department of Materials Science, Rzeszow University of Technology, al. Powstańców Warszawy 12, 35-959, Rzeszow, Poland

ARTICLE INFO

Keywords:
Tool wear
Chip morphology
Machined surface characetristics
Multi-axis milling
Torus milling cutter
Inconel 718

ABSTRACT

This article presents an investigation into the life of the torus milling cutter with round cutting inserts when multi-axis milling process in high-speed cutting conditions of Inconel 718 under various of kinematic variants of multi-axis machining. The experiments were performed at varying tool axis orientation parameters of; lead angle: 1.37–20° and tilt angle: −18.86–20°. A new research approach was introduced to evaluate the possibility of extending the life of the torus milling cutter by changing the tool axis orientation in multi-axis machining. The analysis performed includes the tool life, tool wear patterns, and mechanisms as well as its relationship with the chip and machined surface morphology and kinematics variants of multi-axis cutting. The experimental results showed that tool wear has begun with smooth abrasion and chipping around the depth of cut line, which then progressed into flank wear and finally notching and flaking via mechanisms of abrasive and adhesive wears. However, for each of the analyzed kinematic variants of multi-axis cutting, the above processes proceeded in a completely different way. Thus, by changing the tool axis orientation in a controlled manner, it is possible to influence the cutting conditions in the tool-chip and chip-workpiece interfaces; hence, efficiently displace the point of contact and thus offset the negative impact of the concentration of tribological interactions at that point. Consequently, it was possible to slow down the tool wear development and prolong the torus milling cutter life to a maximum 78%. There was also a strong influence of multi-axis cutting conditions and tool wear patterns on the morphology of the chip and the machined surface. In conclusion, the kinematic variant of multi-axis cutting (i.e. axis orientation) using the torus milling cutter of Ni-based superalloys plays an important role in the possibility of extending tool life.

1. Introduction

Continuous advances in aviation engine and energy turbine technology and innovative material technologies determine the increasingly widespread use of difficult-to-cut materials in new design solutions of the turbine. This entails an increased demand for alternative machining methods, particularly including various variants of multi-axis milling of difficult-to-cut materials, e.g. Ni-based superalloys. Ni-based superalloys, which Inconel 718 is the main representative, are an unusual class of metallic materials with an exceptional combination of high temperature strength, toughness, and resistance to degradation in corrosive or oxidizing environments. Therefore are widely used in the jet engine parts and/or energy turbine, such as turbine disc, turbine blades and other parts working in the high temperature [1–4]. This material also characterized by low thermal conductivity, and severe work-hardening which mainly makes it difficult to be machined, particularly at high cutting speed [5,6].

One parameter that has a disruptive effect on the machining process of difficult-to-cut materials is tool wear, and more precising the wear length *VB* [1]. Tool wear is considered to be a result of mechanical (abrasion) and chemical (diffusion) interactions between the tool and workpiece. In addition, the tool mechanical wear, adhesive wear, diffusion wear and oxidation wear become more definitely serious in the machining of Ni-based superalloys, wchich resulting in significant short tool life [3,4]. Hence, the consequences of tool wear are: high values of cutting force components and value of temperature in the workpiece-tool engagement zone, deviations in part quality, i.e. an increase in the values of surface roughness 2D and 3D parameters and dimensional-shape inaccuracies [7,8].

When milling Ni-based superalloy, rapid tool wear has always been a

* Corresponding author.
E-mail address: gdulam@prz.edu.pl (M. Gdula).

https://doi.org/10.1016/j.wear.2023.204652
Received 2 November 2022; Received in revised form 25 January 2023; Accepted 5 February 2023
Available online 11 February 2023
0043-1648/© 2023 Elsevier B.V. All rights reserved.

one on the major concern and is now one of the key challenges in precision machining, especially multi-axis. In some cases, a milling cutter can only be used for a dozen of minutes before its damage [9,10]. As mentioned above, tool wear seriously affects the geometrical/dimensional accuracy and surface quality for many types of complex parts (e.g., turbine blade) where machining accuracy and surface integrity are paramount for their performance, e.g., aerodynamics performance. Aerodynamic performance in this case is achieved by using in CAD/CAM design of these parts of functional sculptured surfaces [11]. These surfaces are most often machined by three- or multi-axis milling used a ball-end cutter, especially on the finishing cutting stage, which is supported by selected publications [10,12–16]. On the other hand for the machining of these surfaces, it is becoming increasingly common in industrial practice is being used the torus milling cutter, especially at the stage of precision final cutting. These cutters allow for better surface quality by eliminating machining at zero cutting speed. Furthermore, the machining with the torus milling cutter is much more performance thanks to the possibility of increasing the cutting speed, width of cut and feed rate [17-22].

Zhu et al. in their work [1] showed that there are a considerable amount of studies on how to control and monitoring the tool wear and prolong the tool life. Based on this work, Luo et al. [10] found that in order to improve tool wear, the commonly used approaches include the following three issues: choosing better cutting parameters, improving cooling and lubrication for difficult-to- cut materials and adopting tool coating techniques. In addition, to understand tool wear behavior in the machining process, as a fourth issue tool wear monitoring methods/systems have also been developed [23].

Cutting parameters have a significant impact on tool wear in a machining process, and their unsuitable selection can lead to fast and catastrophic wear of the cutting tool. Sharman et al. [12] presented experimental studies of the machining of the workpiece made by Inconel 718 with surfaces inclined toward the machine tool table by 45° and 60°. They used a ball-end mill cutter for the tests. Machining process was carried out under HSM conditions. They showed that the higher the cutting speed, the shorter the life of the milling cutter. In addition, the cutting process is significantly influenced by the type of protective coating of the cutting blade. In the case of machining Inconel 718 superalloy, as indicated by Ng et al. at work [24], the tool life can be extended by up to 120% when machining at cutting speeds greater than 90 m/min with high pressure flood coolant supply (70 bar, 26 L/min) compared to the other cutting environments. On the other hand, Krain et al. at work [25] found that an increase in the immersion ratio would cause an overall reduction of tool life measured as time in cut. Altin et al. at work [26], have attempted to determine the effects of cutting speed on tool wear and tool life when machining Inconel 718. They experiment results show that flank and notch wear are dominant in round type inserts. Minimum flank wear occurs at high cutting speeds. Wan et al. in the paper [27] are presents cutting forces in various cutting conditions as well as tool wear patterns in five-axis milling GH2132 superalloy with Bull-nose End Mill, which is corresponding to torus milling cutter. Results of the experimental studies in their work proved that tool wear played affected cutting forces outstandingly.

As Ni-based superalloys have low thermal conductivity and high hardenability, this makes it difficult to be machined at high cutting speeds particularly in conditions of dry cutting. As noted in the paper [3], high cutting temperature is one of the primary sources of rapid tool wear when cutting Inconel 718 at high speeds. At the same time, the presence of abrasive particles in these superalloys generates severe thermo-mechanical contact between them and the tools [6]. These factors accelerate tool wear through induced heat mechanisms, such as adhesion, diffusion and oxidation [1,16]. To solve the aforementioned problems, cooling/lubrication techniques are often applied in the processing of Ni-based superalloys. The most common technique is flood cooling (wet cutting). Unfortunately, his technique does not respond to current assumptions about sustainable production of machine parts [28]. In order to achieve cleaner machining, eco-friendly cooling/lubrication techniques are being implemented, such as minimum quantity lubrication (MQL) and cryogenic cooling, as well as a combination of both, known as cryogenic MQL (CMQL) [3,6,29,30]. However, based on a comparison studys by Pereira et al. [29], it is evident that the flood cooling outperformed other conditions in terms of tool life when compared with dry, cryogenic, MQL and cryoMQL cutting conditions.

In addition to reducing tool wear, especially in milling of difficult-to-cut materials, coated monolithic milling cutters and indexable cutting inserts are widely used to improve the chip formation and workpiece surface finish. Thus, for example Bhatt et al. at work [31] found that triple layers (TiCN/Al2O3/TiN) CVD coated tools exhibited the highest wear resistance at high cutting speeds and low feeds ($v_c = 50$ m/min) in machining of Inconel 718, while tools with single-layer (TiAlN) PVD coating outperformed the other tools at the mean cutting speed of $v_c =$ 75 m/min.

In order to understand the relevant factors of tool wear in the machining process, methods and systems have also been developed for monitoring tool wear [23]. Cutting force components [32] signals are usually used to monitoring the tool wear. Girardin et al. at work [33] have attempted to detect the tool wear by monitoring the variation in rotational frequencies on different cutting blade of the tool. Liu et al. [34] and Twardowski et al. [35] monitored the tool wear by using the cutting sound acoustic spectrum; their experimental results show that there are clear characteristic components in the milling sound signal related to tool wear. In addition, in the paper [35], machine learning methods were used to assess the wear rate of the cutter based on AE signals. Grzesik et al. [32] used a CCD camera to acquire wear images for turning insert blade and to estimate the tool wear. Nevertheless, most of these tool wear monitoring methods/systems are cutting condition dependent and cannot be used in typical machining condition. An attempt to solve this problem was made by Nouri et al. [36]. They estimated the tool wear by monitoring the force model coefficients in real time during the cutting and introduced an overall tool wear parameter.

Notwithstanding the various studies and approaches described above proposed therein in terms of tool wear, none of them pertains to the kinematic-geometric aspects of multi-axis machining using the torus milling cutter. The idea of improving tool wear in multi-axis milling by varying tool axis orientation (i.e., its lead and tilt angle), which was proposed by Uchikata et al. [37] and Luo et al. [10] in two different approaches, is a very good idea, but requires extensive analysis. In particular, analyses of the issues of multi-axis cutting process mechanics and kinematic-geometric changes taking place in the contact zone of the cutter-workpiece engagement in multi-axis milling. Clearly, by carefully varying the inclination angle of the tool axis during the multi-axis milling process, the active cutting edges of the tool can be shifted. However, each such change in the tool axis orientation changes the kinematic-geometric system of cutting, also indirectly affecting the contact conditions, and therefore tool wear. The motivation to undertake research and analysis in the scope defined by the topic of this paper is the following problem of multi-axis milling of torus milling cutter: having a surface and a generated group of tool trajectories on this surface, how the selected axis orientation affects the torus milling cutter wear and life, chip morphology, machined surface morphology, and topography before the specified wear-out threshold (e.g., 0.3 mm) is reached at any contact point. Since milling using the torus milling cutter is a highly efficient type of milling of difficult-to-cut materials, including parts with high requirements for geometric accuracy and surface quality, the rational of the work is well founded.

2. Multi-axis milling process experiment of Ni-based superalloy inconel 718

2.1. Tool axis orientation

The torus milling cutter is widely used in multi-axis machining of elements with sculptured surfaces with a curved line contour. For the same tool path, can often choose a variety of tool axis orientations due to its geometrical features as well as the geometrical features of the machined surface. In this paper, two input variables for the machining process under investigation were adopted: the rotational angle and the inclination angle to determine the tool axis orientation for the convenience of description and analysis. The lead angle and the tilt angle are often used to determine the tool axis orientation during CAD/CAM programming and post-processing and in direct CNC programming. Fig. 1 describes the analytical diagram for tool axis orientation, and the conversion relationship between two sets of angles is as follows:

$$\delta = \arccos(\cos(a) \bullet \cos(\beta)) \tag{1}$$

$$\theta = arccos\left(\frac{cos\ (\alpha) \bullet sin\ (\beta))}{sin\ (\delta)}\right) \tag{2}$$

hence:

$$\beta = arcsin\left(sin\ (\delta) \bullet \frac{cos\ (\theta)}{\sqrt{sin^2(\delta) \bullet cos^2(\theta) + cos^2(\delta)}}\right) \tag{3}$$

$$\alpha = arccos\left(\sqrt{sin^2(\delta) \bullet cos^2(\theta) + cos^2(\delta)}\right) \tag{4}$$

Where: θ: the rotational angle; δ: the inclination angle; β: the lead angle; α: the tilt angle.

Taking into account the parameters described above for positioning the tool axis, for multi-axis machining centers, there are infinitely many different kinematics of the cut. However, each time, they can be approximated by one of the eight cases. Possible cases are presented in Fig. 2.

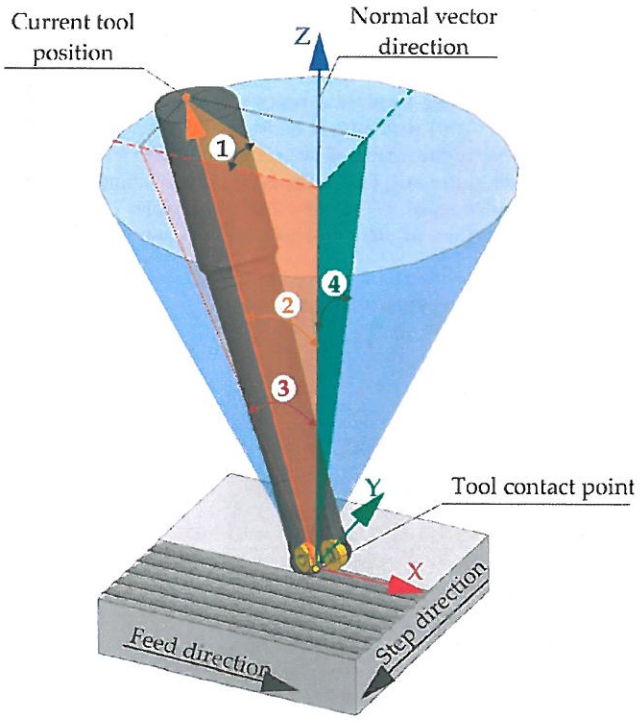

Fig. 1. Torus milling cutter axis orientation analytical scheme adopted for research: 1 - the rotational angle, 2 - the inclination angle, 3 - the lead angle, 4 - the tilt angle.

It is easy to see, that the different inclination angle can have a significant effect on the tool contact position. The factor influencing cutting contact position not only has the inclination angle but also the rotational angle. During a cutter motion, they determine the contact zone, where the cutter is in contact with the workpiece over an instanteneous surface patch, which is called the cutter-workpiece engagement (CWE). Changing the tool contact position in the cutting zone can cause a change in the cutting conditions and therefore can significantly affect tool wear, chip morphology and machined surface.

2.2. Materials and tools

Test material is Ni-based superalloy Inconel 718, the chemical composition and the main mechanical and physical properties at roomtemperature are shown in Table 1 and Table 2 respectively.

The multi-axis milling process was conducted by applying steel torus milling cutter body R300-016A20L-08L for indexable round cutting inserts R300-0828E-PL. The body of the torus milling cutter has a neutral geometry. Round cutting inserts are made of S30T cemented carbide grade. Grade S30T has fine-grain cemented carbide and a TiAlN PVD coating. The round cutting inserts used in the tests have the following parameters: the rake angle is 20°, the relief angle (or else clearance) is 15° and the insert radius is 4 mm. Furthermore, the cutting insert does not have a typical roundness radius r_ε of the cutting edge, but an asymmetrical chamfer with the following dimensions: length 0.1 mm measured along the line of intersection of the reference plane and orthogonal plane, and an angle of 15° measured in the orthogonal plane between the edge of the chamfer and the line of intersection of the reference plane and orthogonal plane in the Orthogonal Rake System (ORS) of the tool geometry. These 8 mm diameter round cutting inserts was attached in to a 16 mm diameter tool body at an overhang measuring 65 mm, as shown in Fig. 3.

2.3. Methodology

The experimental set-up is shown in Fig. 3. A vertical 5-axis CNC machining centre (DMU 100 MonoBLOCK) is used to conduct the multi-axis milling tests. The 4-component piezoelectric rotary dynamometer (Kistler 9123C), with 4-channel charge amplifier (Kistler 5223B) and data acquisition system (guickDAQ software and KUSB-3100 measuring card) is utilized for acquisition of cutting force. The acquisition frequency is 10 kHz. The focus was only on the forces induced by the representation of the blades in the workpiece material, i.e. those resulting from the kinematics of the process, taking into account wear and the phenomenon of radial run-out of the cutting blades. Therefore, in order to eliminate other factors that influence the measured forces the recorded signals were filtered through an in-house algorithm and programme developed in MatLab. Low-pass (DP) Chebyshev filters were used. Low-pass Chebyshev filters were used, while a fast Fourier Transform (FFT) was applied for frequency analysis. Due to the attachment of the force gauge directly in the spindle of the multi-axis milling centre, the measured force signal consists exclusively of components related to the kinematics of the process. The components related to process kinematics are described using the frequencies: spindle speed, spindle speed multiplied by the number of cutting blades, and harmonics. The frequency f_o of the spindle speed n is expressed by the following equation:

$$f_o = \frac{n}{60} \tag{5}$$

While the frequency of the spindle speed multiplied by the number of cutting blades z can be expressed by the equation:

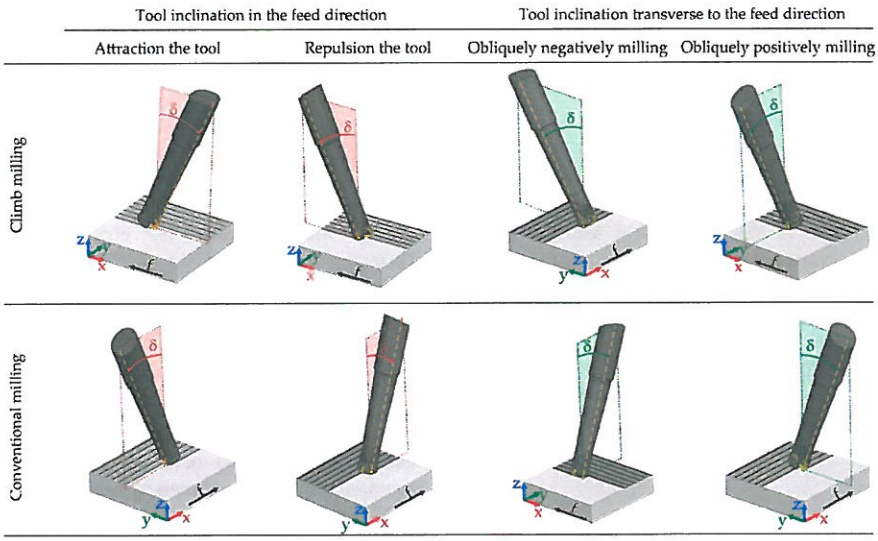

Fig. 2. Fundamental variants of cutting kinematics in multi-axis machining (own elaboration).

Table 1
Chemical composition of Ni-based superalloy Inconel718.

Material chemical composition (% wt.)				
Ni: 53.0	Cr: 18.30	Fe: 18.7	Nb: 5.05	Cu: 0.04
Al: 0.49	B: 0.004	C: 0.051	Co: 0.3	P: <0.005
Mo: 3.05	Ti: 1.05	Mn: 0.23	Si: 0.08	S: <0.002

Table 2
Main mechanical and physical propetries of Ni-based superalloy Inconel 718.

Tensile Strength (MPa)	Yield Strength (MPa)	Elongation (GPa)	Elongation (%)	Density (g/cm^3)
1330	1120	220	23	8.2

$$f_{zo} = z \bullet f_o \tag{6}$$

In order to take into account the kinematics of the process for each of the measured signals, the cut-off frequency fodc was determined according to the following relationship:

$$f_{odc} = 2 \bullet f_{zo} + 10\% \tag{7}$$

The filtered signals were used to determine the maximum forces per cutting blade (F_{cN}, F_c, F_p). These values were calculated based on equations:

$$F_{cNmax} = \frac{\sum_{j=1}^{J} F_{cNj_{max}}}{J}$$

$$F_{cmax} = \frac{\sum_{j=1}^{J} F_{cj_{max}}}{J} \tag{8}$$

$$F_{pmax} = \frac{\sum_{j=1}^{J} F_{pj_{max}}}{J}$$

where: F_{cNjmax}, F_{cjmax}, F_{pjmax} - maximum value of force per j'th mapping of the cutting blade, J - number of instantaneous force amplitudes during measurement.

Experimental testing involved a series of passes in a symmetrical milling process [38,39] with a torus milling cutter inclined relative to the normal vector of the machined surface (see Fig. 1). To achieve the inclination of the cutter axis, the headstock of the machining centre was inclined by a value equal to the delta and theta angles (according to Table 3). Furthermore, in order to avoid the influence of the rowing

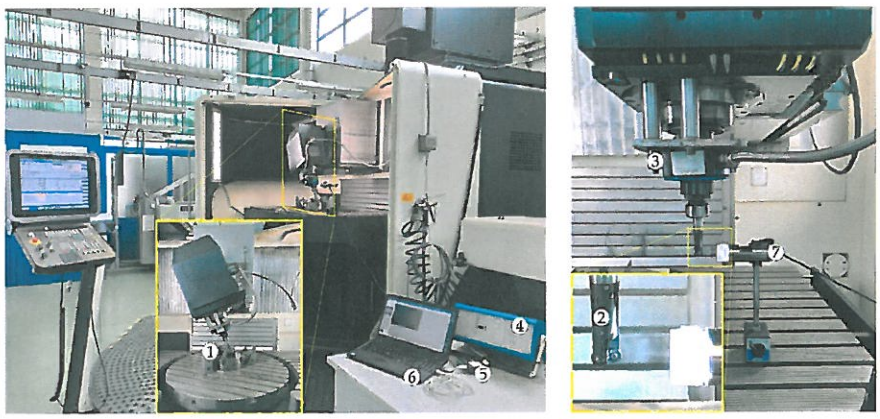

Fig. 3. Experimental test bench (1. Workpiece, 2. Torus milling cutter, 3. Four-component piezoelectric rotary dynamometer, 4. Four-channel signal amplifier, 5. KUSB KEITHLEY 3100 measuring card, 6. Computer with software for viewing, recording and analysis of measuring signals, 7. Dino-Lite 7000 CE series digital workshop microscope).

distance br on the nature of the time domain of the measured cutting force components, and thus to be able to measure the signals of the force components directly related to the process kinematics and the radial run-out phenomenon, the selected values of the milling width B were smaller than b_r, as described in inequality (9) and shown in Fig. 4.

$$B < b_r \tag{9}$$

Multi-axis milling parameters are presented in Table 3. In this parameters consist of: the cutting parameters and the tool axis orientation parameters. The cutting parameters were assumed to be constant and invariant for each experiment. Their values were chosen based on recommendations from the tool manufacturer and the aerospace industry. Hence, it was decided to keep the cutting speed values within the speed range for HSM cutting with regard to Ni-based superalloys [40]. The input variables were the tool axis orientation parameters. The range of variation in their values was determined by the value of the boundary parameter of the torus cutter geometry, that is, the rake angle. It was assumed that the combination of the tool axis orientation parameters (lead angle and tilt angle) should not exceed the value of the assumed boundary parameter, which could negatively affect the cutting conditions. It should be mentioned that the lead and tilt angles are only a reference for selecting the limits mentioned above of the tool axis orientation, as these angles only function in the planes of feed direction (lead angle) and perpendicular to the feed direction (tilt angle). This approach allows the tool axis orientation parameters to be related to the tool geometry parameters defined in the reference and orthogonal planes in the Orthogonal Rake System (ORS) of the tool geometry. For further considerations, the combinations of lead and tilt angles were calculated on the rotational and inclination angles system acting fully in the tool system. Another assumption is that the kinematic variant of tool repulsion is omitted at this stage of the research, as this requires a detailed analysis of the cutting conditions. The experimental tests, and thus the combination of input variable values, was designed based on the RSM *(Response Surface Method)* method as one of the main statistical tools. Statistica software was used for this purpose. Flood cooling was used in each experiment, and starting each new experiment, the round cutting inserts were replaced with a new set. The tool life was determined on the basis of the localized flank wear (VB_{max}), until it reached 0.3 mm. This was to avoid the effect of excessive tool wear on the workpiece surface due to the higher temperature. The multi-axis milling process was interrupted at specific intervals to identify the wear patterns and measure the wear rate by using a Dino-Lite 7000 CE series digital workshop microscope. Photographs of the worn areas were also captured using a Dino-Lite 7000 CE series microscope with DinoCapture 2.0 software. In order to determine the wear mechanisms of the torus milling cutter, the worn round cutting inserts were then thoroughly investigated using a Scanning Electron Microscope (SEM) (model HITACHI S–3400 N). This microscope is equipped with EDS and WDS systems for chemical composition analysis and an EBSD system for determining the texture of the materials and identifying phase components. Similarly, surfaces after treatment were investigated using the aforementioned Scanning Electron Microscope (SEM) for investigation on machined surface morphology. In addition, after each pass interval, the chips were collected for more in-depth investigation on chips morphology.

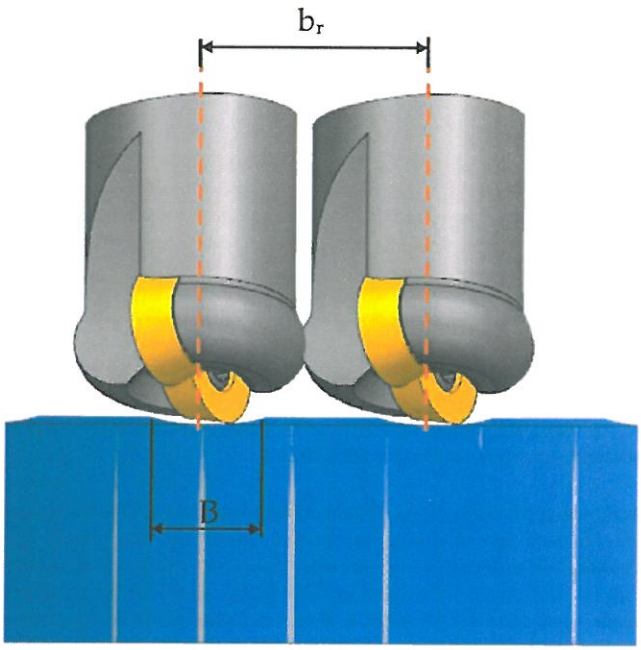

Fig. 4. Scheme for selecting the value of the rowing distance *br*.

3. Results and discussion

3.1. Torus milling cutter life in different variants of cutting kinematics in multi-axis machining

Fig. 5 illustrates the torus milling cutter life comparison between multi-axis cutting kinematics variants (see Fig. 2) and their combinations from all experiments conducted (see Table 3). The results show that for each tool axis orientation setting of the test plan, a different tool life was obtained. Analysing the results obtained, especially the values of the tool axis orientation parameters after compiled with the tool life values, it can be seen that three groups of axis orientation settings emerged for which the tool life is significantly different. It would be respectively: group I (exp. nr 1, 3 and 7), group II (exp. nr 2, 4 and 8) and group III (exp. nr 5, 6, 9 and 10).

One of the shortest life of the torus milling cutter was obtained for experiments from group I. The tool life between experiments in this

Table 3
Multi-axis milling parameters.

Experiment No.	Inclination angle δ [°]	Rotational angle θ [°]	Lead angle β [°]	Tilt angle α [°]	Cutting speed v_c [m/min]	Feed per tooth f_t [mm/t]	Axial depth of cut a_p [mm]	Milling width B [mm]	Toolpaths distance b_r [mm]
1	15.51234	−75.40782	4	−15				5.1254	6
2	20.38000	79.15058	4	20				4.5298	4.8
3	24.81422	−38.07625	20	−15				6.3299	6.5
4	27.99089	46.78082	20	20				5.8165	6
5	1.37000	0.00000	1.37	0	100	0.25	0.5	11.5147	11.7
6	18.62000	0.00000	18.62	0				7.6752	8
7	21.26157	−63.05383	10	−18.86				5.3587	5.8
8	21.26157	63.05383	10	18.86				5.3587	5.8
9(C)	10.00000	0.00000	10	0				9.1191	9.3
10(C)	10.00000	0.00000	10	0				9.1191	9.3

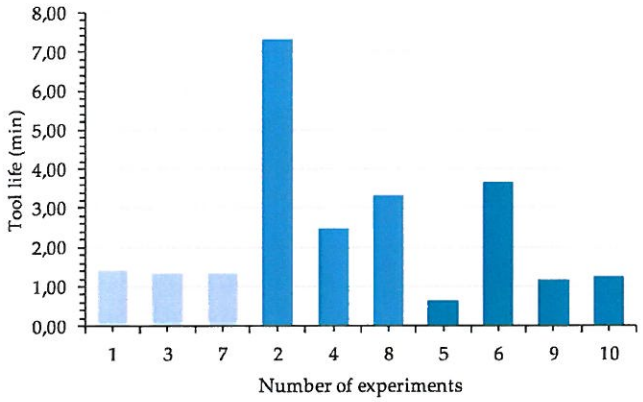

Fig. 5. Torus milling cutter life comparison between the different cutting kinematics variants in multi-axis machining.

group ranged from 1.33 to 1.42 min. Interestingly, the differences in tool life for each test in this group do not exceed 0.1 min, despite the considerable differences in cutter axis orientation settings. Such a short tool life was mostly influenced by the negative values of the rotational angle θ and thus the tilt angle a. Negative values of these angles have resulted in the occurrence of conventional obliquely negative milling, which adversely affected the multi-axis cutting conditions of the Ni-based superalloy. It is worth noting here that climb milling was used in all experiments. In the analyzed Group I, conventional negative oblique milling has a dominant character, so the influence of the leading angle β on the tool life is negligible in this case. Comparing the tool life obtained between Experiments 7 and 8, it can be clearly seen that the obliquely negative conventional milling has an adverse effect on the multi-axis cutting conditions, by which the life of the torus milling cutter reduced by more than 60%. In turn, comparable values of the tool life in the discussed group result from the comparable values obtained of the milling width B, and the milling width depends on the axis orientation parameters of the torus milling cutter. The milling width B between experiments in group I ranged from 5.1254 to 6.3299 mm, and the difference between them did not exceed 1.2045 mm.

The longest torus milling cutter life was obtained for experiments in Group II. In this group, a combination of variants was tested: tool attraction and obliquely positive milling. Both variants in the climb milling kinematics. The tool life between experiments in this group ranged from 2.5 to 7.33 min. It was found that as the angle of inclination δ increases, the life of the tool decreases. It is noted that in the above-mentioned combination of multi-axis machining variants, obliquely positively milling can positively and simultaneously negatively affect the multi-axis machining process. The positive aspect is the improvement in cutting conditions, which translates into a significant increase in tool life. In the other hand, with increasing of the inclination angle value 3 increases also the milling width (and also, one can assume, the wrap angle), which manifests itself as a reduction in the service life of the torus cutter. As noted, in the analyzed variant of multiaxis machining, a completely disparate effect of inclination angle was obtained on tool life compared to even if the results were obtained in group III.

The results of the research in Group III are also interesting. The tool life between experiments in this group ranged from 0.66 (exp. nr 5) to 3.66 min (exp. nr 6). Tool life slightly below the average in this range was recorded for Experiments Nos. 9 and 10 (the so-called centre). In this group, only the inclination angle δ was an input variable, while the rotation angle θ did not change and was $\theta = 0°$. It was found that as the value of the angle of inclination δ increases, the value of the milling width B decreases, so that the tool wrap angle should also decrease. Consequently, the shelf-life of the torus milling cutter is extended. It should be noted that the tool life obtained in Experiments 9 and 10 is comparable to that obtained in Group I experiments.

One very interesting aspect that arises from the research is worth noting. Milling width B is the smallest for experiment No. 2, this might imply that the uncut chip cross-section is the smallest in this case. This, in turn, will influence the thermos-mechanical loads on the cutting edge and should result in the lowest tool wear. However, in opposition to this, we have the results of experiments No. 7 and No. 8. The milling width B for these experiments is identical (5.3587 mm) and only 0.8289 mm wider than in experiment No. 2. For experiment No. 7, the tool life was 1.37 min, while for experiment No. 8 it was 3.35 min. Interestingly, the experiments differed only in the multi-axis cutting kinematic variant used. In the case of experiment no. 7, it was the attraction of the tool together with the obliquely negative milling, while in the case of experiment no. 8 it was the attraction of the tool together with the obliquely positively milling (similar as in experiment no. 2). As can clearly be seen, the multi-axis cutting kinematic variant used in terms of tool life is of paramount importance, and even more so the selection of appropriate values of the angular parameters of the axis orientation of the torus milling cutter.

The tool wear patterns and chip morphology, with respect to the progress of maximum flank wear and cutting time observed in selected variants of cutting kinematics in multi-axis machining, are illustrated in Fig. 6, Fig. 7 and Fig. 8 respectively. When analysing the wear curves, it can be seen that they present a three-phase course of wear, namely an early stage where the flank wear rapidly increased reaching a baseline value, a stable stage where uniform the exploitation flank wear of a quasi-linear nature can be observed, leading to the formation of notch wear and flaking near the depth of cut (DOC) line, and the final stage where the notch wear and flaking rose sharply until the critical value associated with cutting blade failure is reached.

As shown in Figs. 6, Figs. 7 and 8, tool flank wear in the form of abrasive wear grew rapidly and evenly distributed near the DOC line in the early wear stage. It was also noted that already in the early wear stage in the case of multi-axis machining in a combination of: tool attraction and oblique negative milling (see Fig. 6) numerous chipping have occurred along the cutting edges. This is due to the negative effect of the conventional milling kinematics in this multi-axis combination, i. e. the cyclic and simultaneously high load on the cutting edge when exiting the workpiece material; in addition, the cutting edge cuts into the material by rubbing it and crushing, resulting in high friction. In this multi-axis machining combination some instances of the built-up edge (BUE) being adjacent to the DOC line were also noted. These were few in number as the chip caused immediate chipping of the cutting edge. The BUE is the adhesion of chips that flow on the tool rake face during the cutting process. As shown in Fig. 6, the phase of stable wear stage the flank wear is characterized by a significant flattening of the wear curve, which results from the occurrence of only cutting edge chipping. At the moment of the appearance of notching and flaking and, therefore, a significant weakening of the cutting edge, the flank wear increases sharply, reaching a critical value.

In the other two multi-axis machining combinations, i.e., tool attraction and oblique positive milling, and only in the tool attraction variant, very similar wear course were observed (see Figs. 7 and 8). In the second stage of wear, the depth of the flank wear was shown to gradually increase with respect to the cutting time. At the same time, numerous chipping was observed along the cutting edge. This phenomenon occurred due to the repetitive cyclic load of intermittent milling cutting, which caused the tool to experience a mechanical shock. The adhered BUE in the discussed machining cases was repetitively present in almost all cutting intervals. The built-up edge (BUE) was also observed adhering to the DOC line. It was found that some cutting spacing did not increase the flank wear rate. Instead, a widened width of wear was observed, which directly influenced the prolonged the cutting time. Moreover, in the stable wear stage phase, both in experiment no. 2 and in experiment no. 6, a sudden increase in the flank wear rate was observed, which stabilized after several intervals. This is due to the fact that, as the cutting process resumed, the gradual increase flank wear

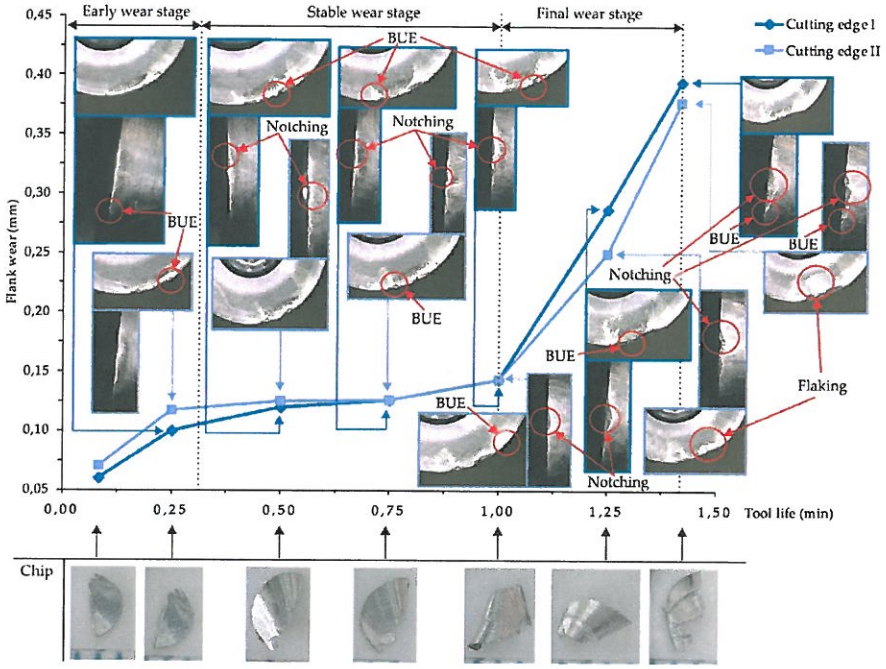

Fig. 6. Tool wear progress and chip morphology under tool attraction and obliquely negative multi-axis milling at tool flank and rake faces from experiment 1.

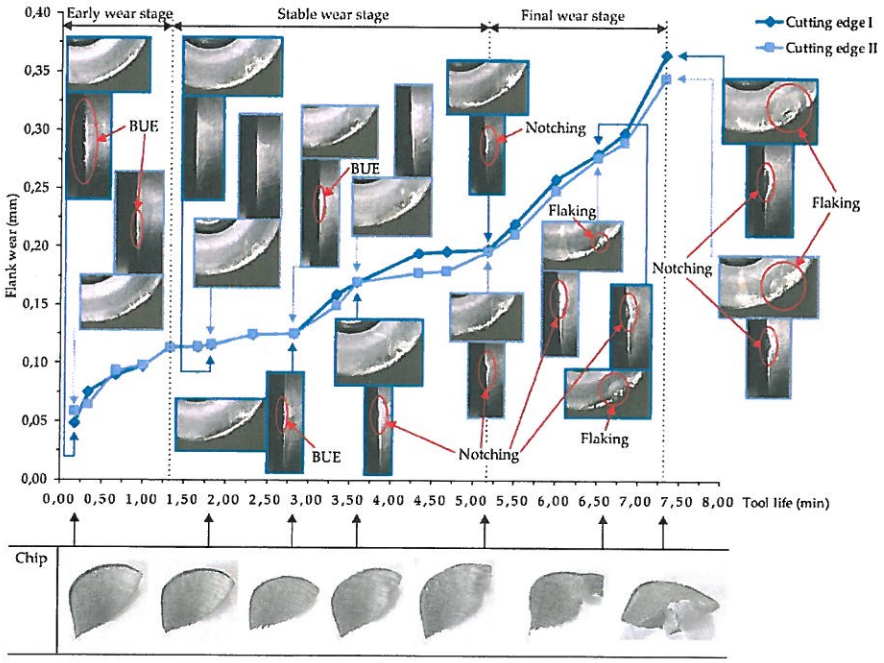

Fig. 7. Tool wear progress and chip morphology under tool attraction and obliquely positive multi-axis milling at tool flank and rake faces from experiment 2.

(VB) slowly formed a localized flank wear (VB_{max}), located near the DOC line. This is a wear mechanism, also known as DOC notching. At the same time, the repetitive load from the milling process also increased the size of flaking on the rake face. The worn torus milling cutter enters the final stage with rapid notch wear progress and widening of flaking on the rake's face.

During the study implementation stage, it was decided that wear curves would be made for both cutting edges of the torus milling cutter. As shown in Figs. 6, Figs. 7 and 8, the wear curves for each cutting edge are comparable. It is noted that there are intervals in a given experiment in which the flank wear is almost identical and those in which the difference between the flank wear of each cuttin edge individually reaches 0.025 mm. This can be caused, among other things, by the run-out of the cutting blades. In this case, the run-out was created by shifting the axis of the round cutting insert from the rotation axis of the cutter, resulting in different values for the active length of the cutting edge L of the torus milling cutter, as shown in Fig. 9. Thus, for example, for the first measurement point from experiment No. 6, a value of L = 2.348 mm was obtained for cutting blade No. 1 and L = 2.184 mm for cutting blade No. 2, respectively. The longer active cutting edge of the cutting blade No. 1

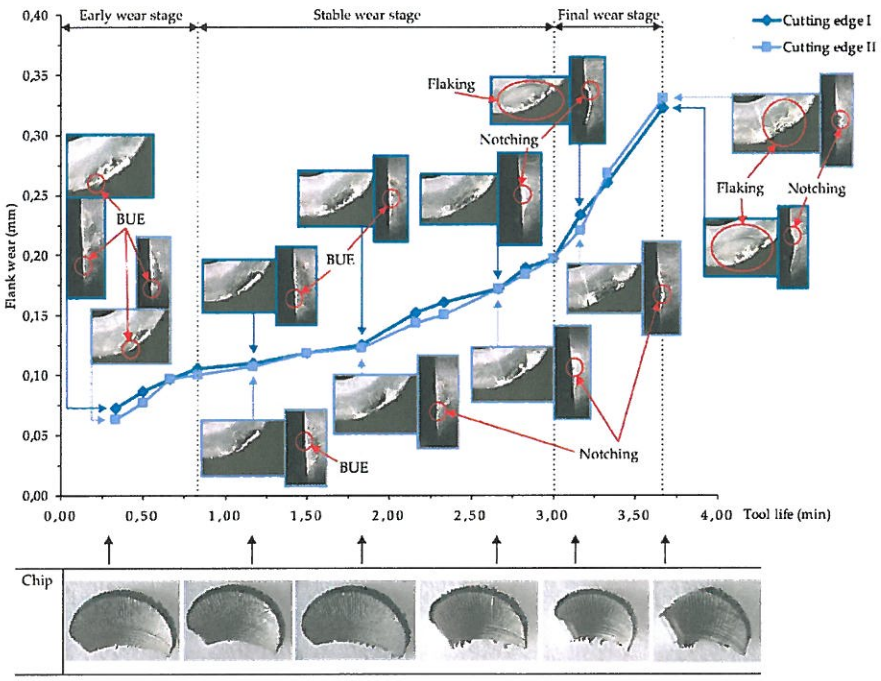

Fig. 8. Tool wear progress and chip morphology under tool attraction of multi-axis milling at tool flank and rake faces from experiment 6.

means a higher value of the cross sectional area of the cut layer accruing on this cutting blade, and thus a higher dynamic load and abrasion of the flank surface than for blade No. 2, as can be observed in Fig. 7.

In the initial wear phase, the differences in the wear values of each blade individually can be clearly seen, after which the differences disappear. This indicates that the cutting blades are being 'running in' and a greater degree of wear is observed on a blade whose active cutting edge length is longer. Further differences in the degree of wear of the individual cutting blades appear in the middle of the stable wear stage. Again, increased wear rates are observed on the cutting blade whose active cutting edge length was longer. This may be due to the greater degree of clashing on the flank and rake faces of this cutting edge, and thus the large and unfavourable changes in the geometric values of this cutting blade, which subjects it to greater cyclic dynamic loads derived from the milling process than the other cutting blade. These and the factors mentioned above could be observed in the component courses of the cutting force.

3.2. *Cutting force components in different variants of cutting kinematics in multi-axis machining*

Force analysis in the multi-axis milling process provides information concerning the mechanics of the cutting process, taking into consideration the properties of the workpiece material, kinematic and technological aspects and tool geometry. In Fig. 10 shows histograms presenting the results of measurements of the cutting force components, respectively, for experiments no 1, 2 and 6, in the adopted intervals of the torus milling cutter lifetime. For the normal cutting force component F_{cN}, in none of the cases of kinematic variants of multi-axis milling considered, azone associated with tool lapping and accelerated wear after the life criterion can be distinguished. In the case of experiment No. 2, a steady increase in this force component can be seen until a maximum value is reached. On the other hand, in the case of experiments 1 and 6, an increased intensity of the normal force increase is seen until the maximum value is reached in the final wear phase, after which the value of the component decreases. This is due to the significant breakout of the cutting edge, which was observed in the microscopic studies (see Figs. 6 and 8). In the uniform wear range, the increase in the normal component of the cutting force does not exceed 18% for the variant of Experiment 1 and 16% for the variants of Experiments 2 and 6. In each of the cases, the wear intensity change point was reached at a different point on the time axis, which results from the influence of the kinematic multi-axis milling variant on the life of the torus milling cutter. The analysis of the passive component F_p of the cutting force is very similar. In this case, the lowest values of the passive force component were obtained in experiment 6, and the increase in this force did not exceed 30%.

The components of the cutting force analyzed above were most influenced by the kinematic variant of multi-axis milling and the related tool wear. The differences in the limit value of the normal cutting force component for the similar largest width of the wear band VB_{Bmax} exceeded 50%, and in the case for the limit value of the passive cutting force component, they even exceeded 100%.

The kinematic variant of multi-axis milling and tool wear had the least impact on the tangential component of the cutting force. The maximum values of this force in the phase of uniform tool wear generally did not exceed 500 N.

Just as in the case of the wear curves and the differences revealed, such and it can be seen in the obtained courses of the component cutting forces that the values of the forces attributable to individual cutting edge are vary. This can also be seen in the recorded forces signals in both the time and frequency domains (determined based on the fast Fourier transform - FFT), as shown in Fig. 11. Fig. 10 in part a shows the filtered signal of the F_{cN} cutting force component in the time domain. It can be clearly seen that the tool goes into vibration in two main phases of work: at the moment when the maximum value of the force F_{cN} is reached, which also indicates that the maximum value of the cross-sectional area of the cut layer per cutting blade has been reached and that the cutting blade-workpiece kinematic system has changed due to the momentary angle of rotation of the tool, and in the phase when no cutting blade is in contact with the workpiece. On the other hand, Fig. 10 in part b shows the filtered signal of the cutting force component F_{cN} in the frequency domain. The frequencies of the F_{cN} component of the cutting force associated with the kinematics of the process (spindle speed, see Eq. (5),

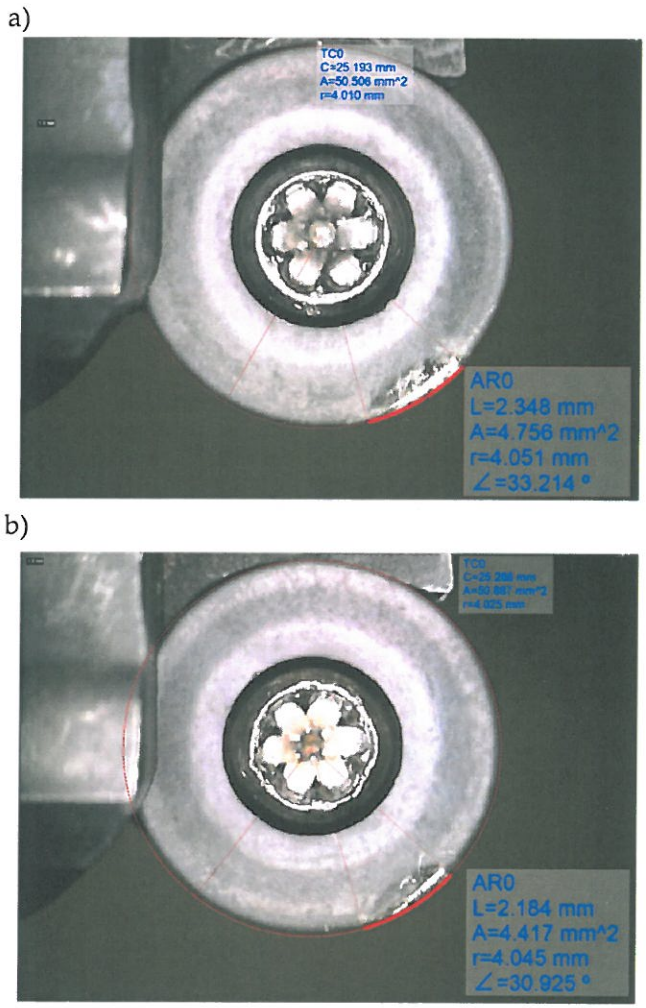

Fig. 9. The active length of the cutting edge for measuring point 1 of experiment 6: a) cutting blade I, b) cutting blade II.

and spindle speed multiplied by the number of cutting blades, see Eq. (6)) shown therein confirm the occurrence of the phenomenon of radial run-out of the cutting blades during the early wear stage. As mentioned above, this has a significant impact on the different nature of the wear of each cutting blade. In addition, in the case of experiment 1 in the tool-workpiece system, in the recorded force signals there were evident vibrations from the first second onward. This confirms the adverse effect of the cutting kinematics type of tool attraction and obliquely negative milling variant on the cutting conditions, and thus on the wear of the torus milling cutter.

3.3. *Wear mechanisms of coated carbide round cutting inserts of the torus milling cutter in multi-axs machining*

Based on the SEM images, abrasion and adhesion were the tool wear mechanisms observed on the tool's rake and flank faces, as shown in Fig. 12 and Fig. 13. These mechanisms are the result of mechanical shock that developed abrasion, chipping, fracturing, notching, and flaking, and chemical interactions at the tool-workpiece and tool-chip interfaces that caused adhesion. The continuous sliding of the hard carbide particles contained in the workpiece material and chips over the surfaces of the circular cutting insert causes friction and leaves abrasion marks along the all-active length of the cutting edge. This abrasive wear mechanism was observed from the initial seconds of the cutting process in every multi-axis machining variant studied. The intensification of this mechanism was most noticeable for the variant in experiment no. 1 and during the early wear stage in all the multi-axis machining variants studied, particularly at the edge of the cutting blade, which shows a higher radial run-out value. It has been observed that the NbC carbide particles present in Inconel 718 cause grooves to form on the tool rake face, which can also be seen in Fig. 12. In the case of the study in this work, the abrasive wear mechanism caused the coating of the round cutting insert to delaminate, exposing the base material of the cutting blade. In addition, it was observed that, depending on the kinematic variant of multiaxial cutting used, different shapes of gouge outlines were obtained on the flank surface, which may indicate a different location of the point of concentration of tribological interactions in the cutting zone and of the cutting forces. This may be simultaneously due to the different degrees of weakening of the structure of the individual cutting edges as a result of radial run-out and lapping in the early wear stage.

The direct sliding contact between the flow of chips and the tools' base material caused the adhesion wear as shown in Fig. 14, Fig. 15 and Fig. 16. The spectrum EDS analysis confirmed the adherence of the workpiece elements on the worn tool area (Ni element). The smallest amount of adhering workpiece particles was observed in the worn-out area of the cutting blades for machining with the kinematic variant of experiment no 1, while adhering whole strands of workpiece material occurred for machining with the kinematic variant of experiment no. 2. Also it can be clearly seen that the coating layer of TiAlN were removed from the tool surface, where the identified elements represent the base materials of the uncoated tool (W elements). Without the coated layer, the notch wear progressed rapidly and the flaking on the rake's face was enlarged.

It was found that continuous mechanical shock and thermal fluctuation due to intermittent milling process led to the enlargement of flaking at the rake face (see Fig. 12) and flank wear at the flank face (see Fig. 13). Meanwhile, cracks at the flank face subsequently covered by the thin layers of wear debris. The falling off of wear debris caused cavitation and fracture at the flank face, which then accelerated notching (see Fig. 13). The case of experiment no. 2 is very interesting in this respect. Despite the accelerated notching, the torus milling cutter in this kinematic variant of multi-axis machining had the longest life. This can be explained by the fact that the adhesion of the extensive patches of workpiece material (Ni elements on the EDS analysis, see Fig. 15 - experiment no. 2) provided a protective coating, so to speak, which may have directly contributed to the extended life of the cutting blades. In addition, the favourable cutting conditions resulting from the kinematic variant of tool attraction and positive oblique milling may have contributed to this, resulting in general climbing milling in these configurations, which is recommended for the machining of Ni-based superalloys.

3.4. *Characteristics of chip morphology*

In the multi-axis milling process studied, using the torus milling cutter with round cutting inserts, in each kinematic variant analyzed, obtained a chip which is concave in shape with trailing effect at its end, as shown in Fig. 16. Fig. 16 a, b and c show the free surfaces of the chip respectively obtained in the individual experiments analyzed. The basic features of the back surface can be identified by its smooth and shiny appearance due to high contact pressure, frictional forces, and contact temperature developed when the chip slides over the tool rake face during cutting (by way of example, see Fig. 5). The free surface of the chip showed a serrated and rough appearance, attributed to the shearing actions, causing a large plastic deformation on the surface. The lamella structure on the free surface can be separated into a main area and a corner area. At the main area (see Fig. 16 area A), the structure is uniform, with relatively consistent shape and thickness, and varying according to the kinematic variant of multi-axis cutting. This area was

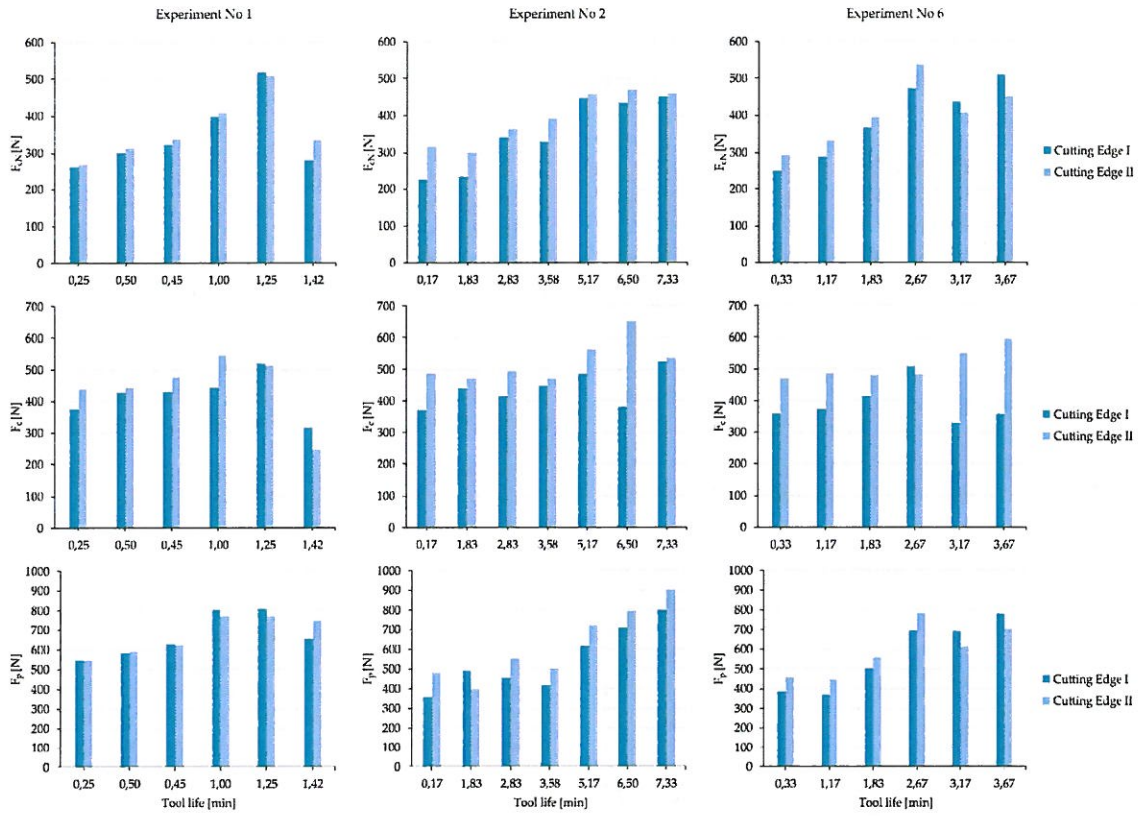

Fig. 10. Changes in force components: F_{cN} (normal cutting force), F_c (tangential cutting force) and F_p (passive cutting force) as a result of tool wear during the cutting of the Inconel 718 alloy for the kinematic variants adopted of multi-axis milling, respectively, in experiments no 1, 2 and 6.

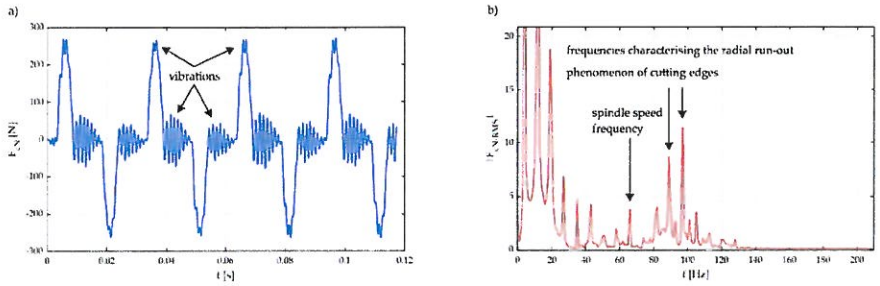

Fig. 11. The filtered signal of the F_{cN} component after 15 s of work in the a) time domain and b) frequency domain.

sheared by the tool side edge. At the corner area (see Fig. 16 area B), it can be seen that the lamella is sheared by the tool nose edge, thus its inclination to have a trailing effect at the end of the chip, which can be attributed to the geometry of the round cutting insert. The end of the chip also touches and slides on the uncut workpiece surface. Thus, its shape can also be affected by the rubbing action, thermal effects and cutting condition of multi-axis milling induced at the interface cutting edge-machined surface (see Fig. 17).

3.5. *The effect of torus milling cutter wear and kinematics variant of multi-axis machining on the chip morphology*

The morphology of chips was analyzed to determine its correlation with the tool flank wear rate and variant of multi-axis cutting kinematics, as shown in Figs. 6, Figs. 7 and 8 for variants from experiments 1, 2 and 6 respectively. Generaly, in the milling process, the chip is formed as the cutting edge rotates around the rotational axis of the cutter body and one complete rotation of cutting tool produces one complete segment of a chip. In the early stages of wear, cutting with a new set of round cutting inserts produces a chip in single element. However, under the cutting conditions obtained for multi-axis machining in experiment no 1, chip cracking was observed in the corner area propagated from the trailing effect as it was subjected to the unfavourable conditions of obliquely negative (conventional milling) cutting and the resulting thermal effects of high friction temperature, especially when the blade exited the cutting zone.

As the cutting process entered the stable wear stage, it was found that the chip was still represented by a single element, at the same time, the cracking of the cracking of the chip in the corner area increased in each of the cases analyzed. This form of chip was believed to have been affected by the worn tool geometry at the cutting edges, as it appeared parallel to the gradual deepening and widening of flank wear and flaking at the rake face, as can be seen in Figs. 6, Figs. 7 and 8. In the final phase of the stable wear stage, it was observed that the cracking of the chip had

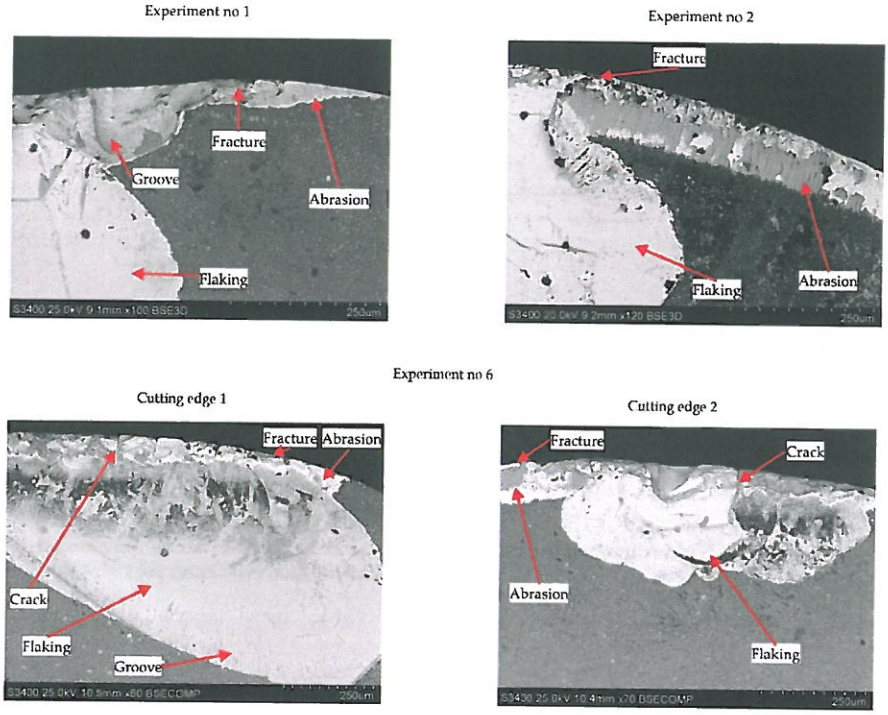

Fig. 12. SEM images of the worn area on the rake face of the round cutting inserts.

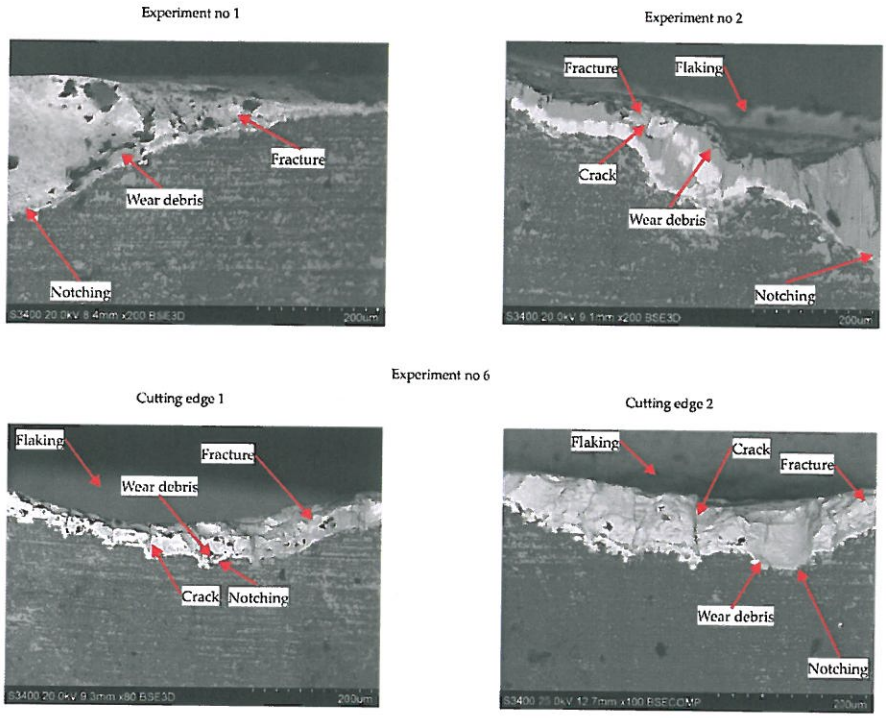

Fig. 13. SEM images of the worn area on the flank face of the round cutting inserts.

moved into its main area, which was obtained for the multiaxis machining variant of experiment no 2. And for the multi-axis machining variant of experiment no 6, a chip curl phenomenon was observed in the zone where the cutting edge enters the workpiece material. This is due to the torus milling cutter axis orientation and thus the multi-axis machining conditions in the analyzed kinematic cases. In the case of the kinematic variant from experiment no. 2, the contact point of the cutting edge with the machined surface is located in the main area of the chip. At this point, the highest values of the tribological interactions and the cutting force components are concentrated. The wear of the cutting blade progresses most rapidly within the contact point mentioned above. Similarly, chip deformation. This is confirmed by the SEM images

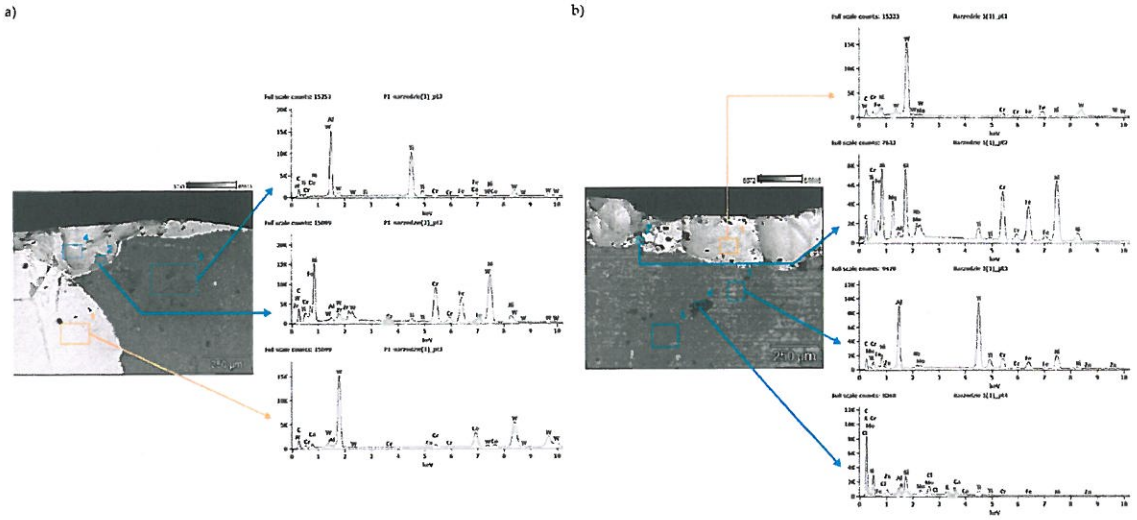

Fig. 14. SEM image and analysis of spectrum EDS which show: the deposit of Inconel 718 on the tool surface, Inconel 718 elements, tool base elements and coating elements on the: a) rake face, b) flank face of the torus milling cutter after multi-axis machining form experiment no. 1 kinematic variant.

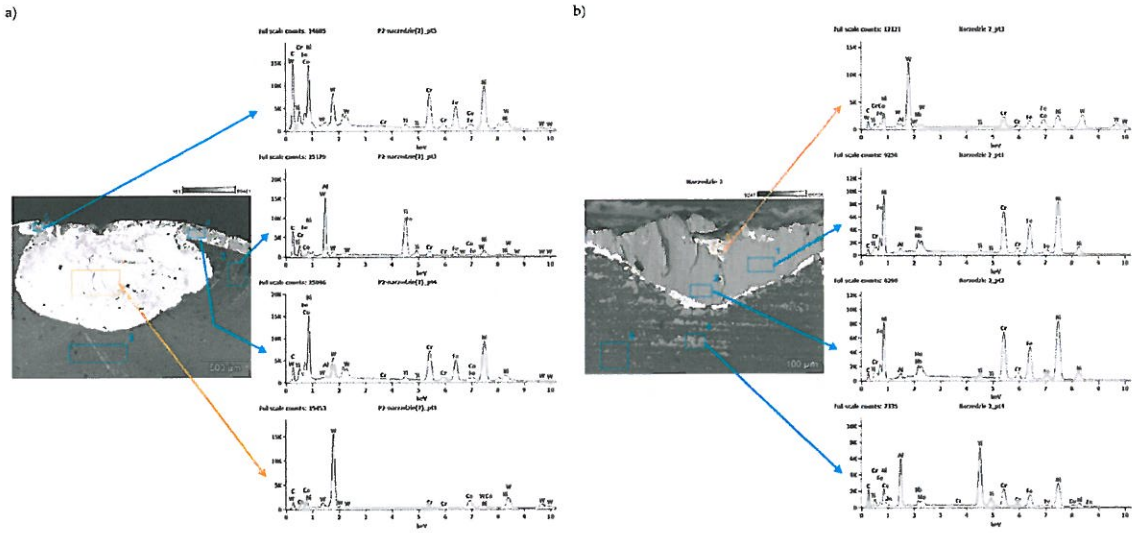

Fig. 15. SEM image and analysis of spectrum EDS which show: the deposit of Inconel 718 on the tool surface, Inconel 718 elements, tool base elements and coating elements on the: a) rake face, b) flank face of the torus milling cutter after multi-axis machining form experiment no. 2 kinematic variant.

of the rake and the flank surfaces of the cutting edge, shown in Figs. 12 and 13, and the chip morphology shown in Fig. 7. However, in the case of the kinematic variant of experiment no. 6, the contact point of the cutting edge with the machined surface is located in the transition edge zone between the corner and the main chip area. Hence, due to the location of the contact point, uniform wear of the rake and flank surfaces was observed in the central active zone of the cutting edge length, which is confirmed by the SEM images shown in Figs. 12 and 13. No significant chip deformation was observed in these areas and subsequent its curl phenomenon is due to the change in the cutting blade geometry as a result of wear and indicates the need for more cutting power.

Further observations revealed different values of the tool axis orientation produced different chips morphology and with different sizes of chips. The milling width *(B)* seemed to provide significant influence on the length of chips since it increased with the increase of *B*. This was caused by the changing of the torus milling cutter axis orientation and therefore the contact conditions during cutting.

3.6. Characteristics of machined surface morphology

SEM micrographs of machined surfaces morphology are shown in Fig. 18. Scratches along the cutting edge mapping curves are observed irrespective of the kinematic variant of multi-axis cutting, which result from microchipping and chip sticking of the cutting edge. The feed marks are only observed on the machined surface for the kinematic variant from experiments no. 2 and no. 6. The distance between two adjacent torus milling cutter marks in the early wear stage is *Ntft (Nt* is the number of teeth, *ft* is the feed per tooth) instead of *ft*, which is caused by the tool runout. In the stable wear stage the distance between to adjacent tool marks is *ft*. In variant of multi-axis cutting kinematics from experiment no. 1, vibration marks of the tool are observed. They are particularly evident in zone *B* and at the exit of the blade from the machining zone, as evidenced by the cutting forces courses. Besides, adhesive chips are mainly found in a variant of multi-axis cutting kinematics from experiment no. 2. They are observed in the 2/3 area of the machined belt from the stable wear stage. This is because the friction of

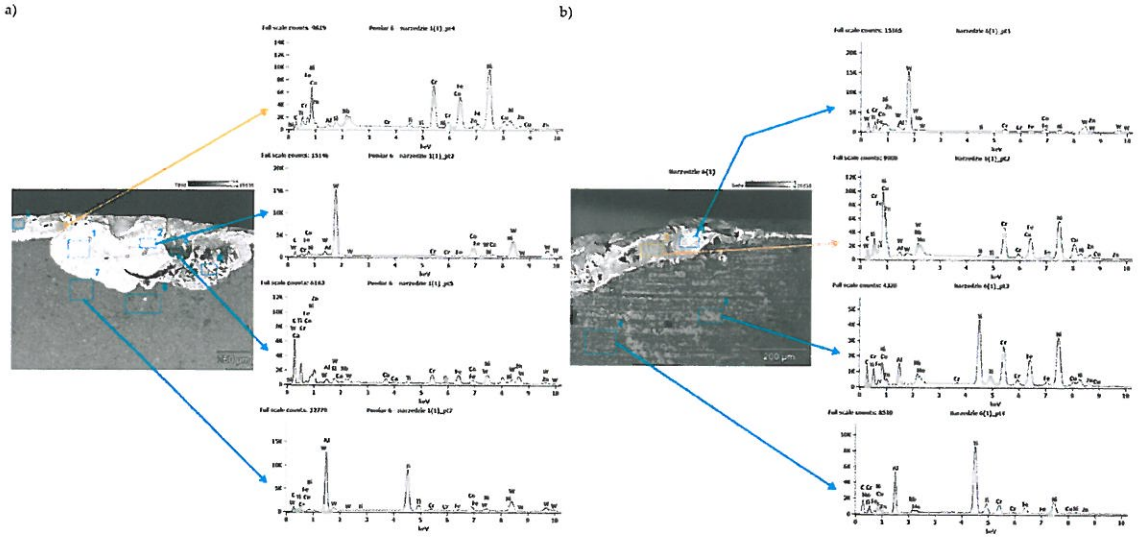

Fig. 16. SEM image and analysis of spectrum EDS which show: the deposit of Inconel 718 on the tool surface, Inconel 718 elements, tool base elements and coating elements on the: a) rake face, b) flank face of the torus milling cutter after multi-axis machining form experiment no. 6 kinematic variant.

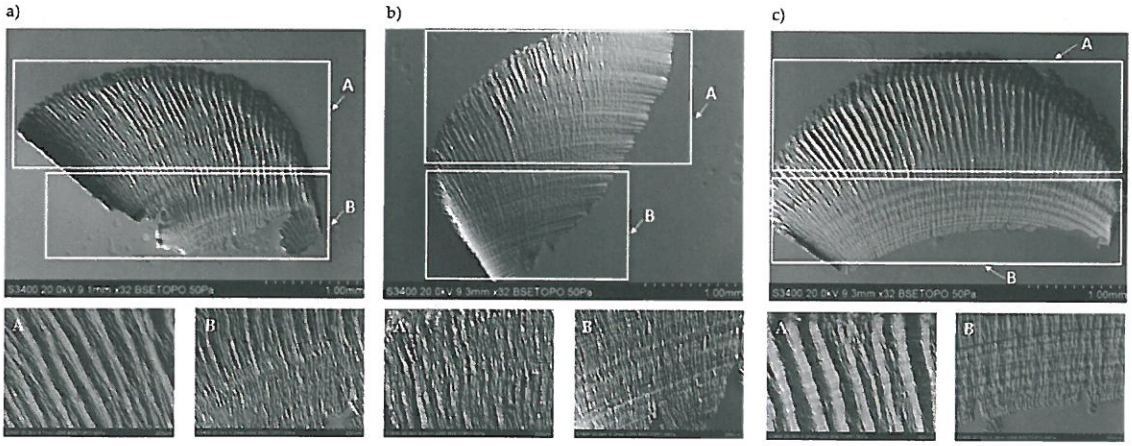

Fig. 17. Free surface chip characteristics from experiment: a) no. 1, b) no. 2, c) no. 6 (A-lamella structure at main area: and B-lamella structure at contact point motion area).

the tool-chip interface is aggravates and chips are easy to weld and adhere to the machined surface under condition of the kinematics variant of the tool attraction and obliquely positive milling. This also confirms the observation in subsection 3.3 about chip flakes welded to the base material of the cutting edge, which can provide a protective layer for the carbide and affect the tool life. In experiment no. 6, only a few chip fragments remain on the surface, resulting in a higher surface finish.

4. Conclusion

The effects of nine different settings of torus milling cutter axis orientations in multi-axis machining were experimentally investigated, from which the three cases (variants of multi-axis cutting kinematics) with the longest tool life obtained during high-speed milling of Inconel 718 were selected for in-depth analysis. The following conclusions were drawn.

- It was found that the tool life extension in the multi axis machining process of Ni-based superalloys is significantly affected by the applied kinematic variant of multi axis cutting (i.e., the cutter axis orientation parameters).
- By changing the orientation of the tool axis in a controlled manner, it is possible to influence the cutting conditions at the tool-workpiece interfaces; hence, efficiently displace the contact point in the cutting blade-machined surface engagement and thus displace the effect of concentrated tribological interactions on the unworn segments of the active cutting edge of the torus milling cutter.
- By machining with the multiaxis variants: tool attraction or tool attraction together with obliquely positive milling, it is possible to extend the life of the torus milling cutter by even 78% as compared to the variant: tool attraction together with obliquely negative milling.
- Approximately, similar tool wear patterns were observed under kinematics variants: tool attraction, tool attraction together with obliquely positive milling, and tool attraction together with obliquely negative milling of multi-axis cutting, where their progress began with a smooth abrasion and chipping around the depth of cut line, then progressed to flank wear, and finally flaking and notching at the rake and flank faces respectively. However, the kinematics variant of tool attraction together with obliquely negative milling

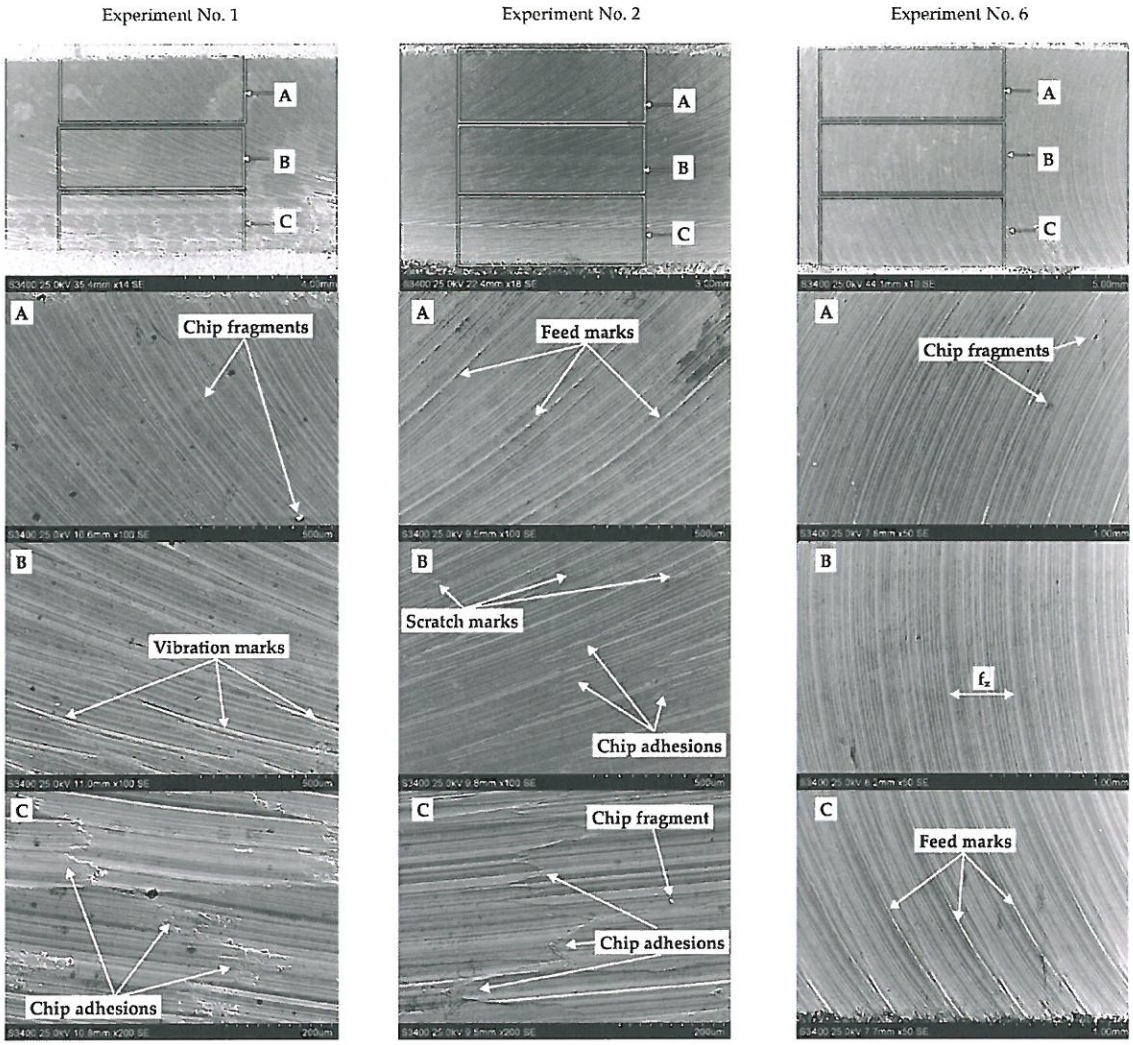

Fig. 18. SEM micrographs of machined surfaces obtained at a tool wear of approximately VB_{max} = 0.15 mm.

generated severe and frequent BUEs, which widened the flaking and accelerated the notching.

- SEM and spectrum EDS analyses confirmed abrasive and adhesive wear as the mechanisms causing the observed tool wear. The intensity and location of their occurrence depended on the kinematic variant of multi-axis cutting used, hence; the cutting conditions associated with the displacement of the contact point. Consequently, the concentration of tribological interactions in the cutting zone was also variable. The varying intensity of these phenomena and wear mechanisms was also a consequence of the uneven degree of individual cutting edge wear, to which run-out of the round cutting inserts, especially in the early stages of wear, also contributed.
- There was a strong influence by cutting conditions and tool wear patterns in multi-axis machining process on the chips morphology, which can be used to envisage the torus milling cutter wear condition when milling Ni-based superalloys at high cutting speeds.

Author statement

Michał Gdula: Conceptualization, Methodology, Resources, Supervision, Visualization, Writing-original draft preparation, Investigation. Grażyna Mrówka-Nowotnik: Investigation, Writing-review and editing.

Declaration of competing interest

The authors declare that they have no known competing financial interests or personal relationships that could have appeared to influence the work reported in this paper.

Data availability

No data was used for the research described in the article.

Acknowledgment

The authors would like to thank the editors and anonymous reviewers for providing insightful suggestions and comments to improve the quality of research paper.

References

[1] D. Zhu, X. Zhang, H. Ding, Tool wear characteristics in machining of nickel-based superalloys 64 60-77. doi: 10.1016/j.ijmachtools.2012.08.001. URL: https://linkinghub.elsevier.com/retrieve/pii/S0890695512001575.

[2] F. Guo, Z. Yin, D. Hong, K. Yu, J. Yuan, Cutting performance of a new spark plasma sintered SiAlON ceramic tool for high-speed milling of inconel 718 119 (11) 7327-7338. doi: 10.1007/s00170-022-08702-6. URL: https://link.springer.com/10.1007/s00170-0 22-08702-6.

[3] N. Halim, C. Haron, J. Ghani, M. Azhar, Tool wear and chip morphology in high-speed milling of hardened inconel 718 under dry and cryogenic CO2 conditions 426-427 1683-1690. doi: 10.1016/j.wear.2019.01.095. URL: https://linkinghub.elsevier.com/retrieve/pii/S0043164819302698.

[4] E. Ezugwu, Key improvements in the machining of difficult- to-cut aerospace superalloys 45 (12) 1353-1367. doi: 10.1016/j.ijmachtools.2005.02.003. URL: https://linkinghub.elsevier.com/retrieve/pii/S0890695505000544.

[5] F. Molaiekiya, A. Aliakbari Khoei, M. Aramesh, S.C. Veldhuis, Machined surface integrity of inconel 718 in high-speed dry milling using SiAlON ceramic tools 112 (7) 1941-1950. doi: 10.1007/s00170-020-06471-8. URL: http://link.springer.com/10.1007/s00170-020-06471-8.

[6] A. Musfirah, J. Ghani, C.C. Haron, Tool wear and surface integrity of inconel 718 in dry and cryogenic coolant at high cutting speed 376-377 125-133. doi: 10.1016/j.wear.2017.01.031. URL: https://linkinghub.elsevier.com/retrieve/pii/S0043164817301060.

[7] W. Grzesik, C. van Luttervelt, An investigation of the thermal effects in orthogonal cutting associated with Multilayer coatings 50 (1) 53-56. doi: 10.1016/S0007-8506(07)62069-1. URL: https://www.sciencedirect.com/science/article/abs/pii/S0007850607620691.

[8] A. Moufki, G. Le Coz, D. Dudzinski, End-milling of Inconel 718 Superalloy - an Analytical Modelling 58 358-363. doi: 10.1016/j.procir.2017.03.330. URL: https://linkinghub.elsevier.com/retrieve/pii/S2212827117306169.

[9] R. M'Saoubi, D. Axinte, S.L. Soo, C. Nobel, H. Attia, G. Kappmeyer, S. Engin, W.M. Sim, High performance cutting of advanced aerospace alloys and composite materials 64 (2) 557-580. doi: 10.1016/j.cirp.2015.05.002. URL: https://linkinghub.elsevier.com/retrieve/pii/S0007850615001419.

[10] M. Luo, H. Luo, D. Zhang, K. Tang, Improving tool life in multiaxis milling of ni-based superalloy with ball-end cutter based on the active cutting edge shift strategy 252 105-115. doi: 10.1016/j.jmatprotec.2017.09.010. URL: https://linkinghub.elsevier.com/retrieve/pii/S0924013617304090.

[11] B.K. Choi, R.B. Jerard, Sculptured surface machining, springer US. doi: 10.1007/978-1-4615-5283-3. URL: http://link.springer.com/10.1007/978-1-4615-5283-3.

[12] A. Sharman, R.C. Dewes, D.K. Aspinwall, Tool Life when High Speed Ball Nose End Milling Inconel 718 (TM), J. Mater. Process. Technol. 118 (1) 29–35, doi:10.1016/S0924-0136(01)00855-X.

[13] P. Yang, C. Yao, S. Xie, D. Zhang, D.X. Tang, Effect of tool orientation on surface integrity during ball end milling of titanium alloy TC17 56 143-148. doi: 10.1016/j.procir.2016.10.044. URL: https://linkinghub.elsevier.com/retrieve/pii/S2212827116310368.

[14] M. Kasim, M. Hafiz, J. Ghani, C. Haron, R. Izamshah, S. Sundi, S. Mohamed, I. Othman, Investigation of surface topology in ball nose end milling process of inconel 718 426-427 1318-1326. doi: 10.1016/j.wear.2018.12.076. URL: https://linkinghub.elsevier.com/retrieve/pii/S0043164818316879.

[15] M. Boujelbene, M. Mhamdi, B. Ayadi, H. Singh, Tool wear analysis of ball nose end mill in the finish machining of free form surfaces Mater, Today 26 (2020) 1289–1292, https://doi.org/10.1016/j.matpr.2020.02.257. URL: https://linkinghub.elsevier.com/retrieve/pii/S2214785320310105.

[16] M. Kasim, C. Che Haron, J. Ghani, M. Sulaiman, M. Yazid, Wear mechanism and notch wear location prediction model in ball nose end milling of inconel 718, Wear 302 (1) (2013) 1171–1179, https://doi.org/10.1016/j.wear.2012.12.040. URL: https://linkinghub.elsevier.com/retrieve/pii/S0043164812004681.

[17] A. Warkentin, F. Ismail, S. Bedi, Multi-point tool positioning strategy for 5-axis mashining of sculptured surfaces 17 (1) 83-100. doi: 10.1016/S0167-8396(99)00040-0. URL: https://linkinghub.elsevier.com/retrieve/pii/S0167839699000400.

[18] L.X. Cao, H. Gong, J. Liu, The offset approach of machining free form surface 184 (1) 6-11. doi: 10.1016/j.jmatprotec.2006.10.048. URL: https://linkinghub.elsevier.com/retrieve/pii/S0924013606009034.

[19] M. Gdula, J. Burek, Cutting layer and cutting forces in a 5-axis milling of sculptured surfaces using the toroidal cutter 17 (4) 25. doi: 10.5604/01.3001.0010.7009. URL: https://jme.publisherspanel.com/resources/html/article/details?id=157385&language=en.

[20] M. Gdula, Adaptive method of 5-axis milling of sculptured surfaces elements with a curved line contour 33 (6) 2863-2872. doi: 10.1007/s12206-019-0534-4. URL: http://link.springer.com/10.1007/s12206-019-0534-4.

[21] M. Gdula, Empirical models for surface roughness and topography in 5-axis milling based on analysis of lead angle and curvature radius of sculptured surfaces 10 (7) 932. doi: 10.3390/met10070932. URL: https://www.mdpi.com/2075-4701/10/7/932.

[22] Z. Zhu, F. Peng, R. Yan, Z. Li, J. Wu, X. Tang, C. Chen, Influence mechanism of machining angles on force induced error and their selection in five axis bullnose end milling 33 (12) 3447-3459. doi: 10.1016/j.cja.2019.12.019. URL: https://linkinghub.elsevier.com/retrieve/pii/S1000936120300765.

[23] S. Choudhury, S. Rath, In-process tool wear estimation in milling using cutting force model 99 (1) 113-119. doi: 10.1016/S0924-0136(99)00396-9. URL: https://linkinghub.elsevier.com/retrieve/pii/S0924013699003969.

[24] E.G. Ng, D.W. Lee, A.R.C. Sharman, R.C. Dewes, D.K. Aspinwal, High speed ball nose end milling of inconel 718, CIRP Ann. 49 (1) 41–46, doi:10.1016/S0007-8506(07)62892-3.

[25] H. Krain, A. Sharman, K. Ridgway, Optimisation of tool life and productivity when end milling inconel 718tm 189 (1) 153-161. doi: 10.1016/j.jmatprotec.2007.01.017. URL: https://linkinghub.elsevier.com/retrieve/pii/S0924013607000374.

[26] A. Altin, M. Nalbant, A. Taskesen, The effects of cutting speed on tool wear and tool life when machining inconel 718 with ceramic tools 28 (9) 2518-2522. doi: 10.1016/j.matdes.2006.09.004. URL: https://linkinghub.elsevier.com/retrieve/pii/S0261306906002561.

[27] Y. Wan, Z.Q. Liu, X. Ai, Cutting forces and tool wear patterns in five- axis milling fe-based super alloy with bull-nose end mill 97-101 2049-2052. doi: 10.4028/www.scientific.net/AMR.97-101.2049. URL: https://www.scientific.net/AMR.97-101.2049.

[28] G. Krolczyk, R. Maruda, J. Krolczyk, S. Wojciechowski, M. Mia, P. Nieslony, G. Budzik, Ecological trends in machining as a key factor in sustainable production - a review 218 601-615. doi: 10.1016/j.jclepro.2019.02.017. URL: https://linkinghub.elsevier.com/retrieve/pii/S0959652619303968.

[29] O. Pereira, A. Rodrfguez, J. Barreiro, A.I. Fernandez-Abia, L.N.L. de Lacalle, Nozzle design for combined use of MQL and cryogenic gas in machining 4 (1) 87-95. doi: 10.1007/s40684-017-0012-3. URL: http://link.springer.com/10.1007/s40684-017-0012-3.

[30] Q. An, C. Cai, F. Zou, X. Liang, M. Chen, Tool wear and machined surface characteristics in side milling ti6al4v under dry and supercritical CO2 with MQL conditions 151 106511. doi: 10.1016/j.triboint.2020.106511. URL: https://linkinghub.elsevier.com/retrieve/pii/S0301679X20303431.

[31] A. Bhatt, H. Attia, R. Vargas, V. Thomson, Wear mechanisms of WC coated and uncoated tools in finish turning of inconel 718 43 (5) 1113-1121. doi: 10.1016/j.triboint.2009.12.053. URL: https://linkinghub.elsevier.com/retrieve/pii/S0301679X09003909.

[32] W. Grzesik, P. Nieslony, W. Habrat, J. Sieniawski, P. Laskowski, Investigation of tool wear in the turning of inconel 718 superalloy in terms of process performance and productivity enhancement, Tribol. Int. 118 (2018) 337–346, https://doi.org/10.1016/j.triboint.2017.10.005. URL: https://linkinghub.elsevier.com/retrieve/pii/S0301679X17304656.

[33] F. Girardin, D. Remond, J.F. Rigal, A New Method for Detecting Tool Wear and Breakage in Milling 3 463-466. doi: 10.1007/s12289-010-0807-z. URL: http://link.springer.com/10.1007/s12289-010-0807-z.

[34] M.K. Liu, Y.H. Tseng, M.Q. Tran, Tool wear monitoring and prediction based on sound signal 103 (9) 3361-3373. doi: 10.1007/s00170-019-03686-2. URL: http://link.springer.com/10.1007/s00170-019-03686-2.

[35] P. Twardowski, M. Tabaszewski, M. Wiciak - Pikula, A. Felusiak- Czyryca, Identification of Tool Wear Using Acoustic Emission Signal and Machine Learning Methods 72 738-744. doi: 10.1016/j.precisioneng.2021.07.019. URL: https://linkinghub.elsevier.com/retrieve/pii/S0141635921001884.

[36] M. Nouri, B.K. Fussell, B.L. Ziniti, E. Linder, Real-time tool wear monitoring in milling using a cutting condition independent method 89 1-13. doi: 10.1016/j.ijmachtools.2014.10.011. URL: https://linkinghub.elsevier.com/retrieve/pii/S0890695514000014.

[37] S. Uchikata, A. Beaucamp, Y. Takeuchi, 5-axis control finishing for decreased tool wear 63 313-317. doi: 10.1016/j.procir.2017.03.320. URL: https://linkinghub.elsevier.com/retrieve/pii/S2212827117305085.

[38] S. Wojciechowski, P. Twardowski, The influence of tool wear on the vibrations during ball end milling of hardened steel 14 587-592. doi: 10.1016/j.procir.2014.03.108. URL: https://linkinghub.elsevier.com/retrieve/pii/S2212827114002510.

[39] S. Wojciechowski, The Estimation of Cutting Forces and Specific Force Coefficients during Finishing Ball End Milling of Inclined Surfaces 89 110-123. doi: 10.1016/j.ijmachtools.2014.10.006. URL: https://linkinghub.elsevier.com/retrieve/pii/S0890695514000099.

[40] G. Byrne, D. Dornfeld, B. Denkena, Advancing cutting technology 52 (2) 483-507. doi: 10.1016/S0007-8506(07)60200-5. URL: https://linkinghub.elsevier.com/retrieve/pii/S0007850607602005.

ARTYKUŁ

A8

dr inż. Michał Gdula
Politechnika Rzeszowska im. I. Łukasiewicza
Wydział Budowy Maszyn i Lotnictwa
Katedra Technik Wytwarzania i Automatyzacji

Rzeszów, dn. 23.04.2025 r.

OŚWIADCZENIE AUTORA

Oświadczam, że w pracy:

lp.: A8

Gdula M.: *Empirical Models for Surface Roughness and Topography in 5-Axis Milling Based on Analysis of Lead Angle and Curvature Radius of Sculptured Surfaces*. Metals, (2020) 10, 932. IF 2.351, MNiSW 70 pkt.;

mój wkład w powstanie tej pracy polegał na: kompletnym opracowaniu manuskryptu obejmującym analizę aktualnego stanu wiedzy w zakresie tematu pracy, opracowaniu modelu obiektu badań eksperymentalnych, opracowaniu metodyki badań, przeprowadzeniu badań eksperymentalnych, przeprowadzeniu pomiarów wybranych parametrów 2D i 3D chropowatości powierzchni, opracowaniu empirycznych zależności modelowych, przeprowadzeniu analizy i interpretacji otrzymanych wyników, opracowaniu wniosków, wykonaniu wykresów, rysunków oraz tabel, koordynowaniu procesu wydawniczego.

Gdula Michał

Podpis
dr inż. Michał Gdula

metals

MDPI

Article

Empirical Models for Surface Roughness and Topography in 5-Axis Milling Based on Analysis of Lead Angle and Curvature Radius of Sculptured Surfaces

Michał Gdula

Department of Manufacturing Techniques and Automation, The Rzeszow University of Technology, 35-959 Rzeszów, Poland; gdulam@prz.edu.pl; Tel.: +48-17-865-13-72

Received: 25 June 2020; Accepted: 9 July 2020; Published: 10 July 2020



Abstract: The orientation of the tool axis and the variable curvature of the machined profile of a sculptured surface have a significant impact on the roughness and topography of the surface in the process of 5-axis milling by means of a toroidal milling cutter. The selection of the orientation of the toroidal milling cutter axis relative to the radius of curvature of the machined surface profile is very important as it can provide a better surface quality and an even distribution of roughness parameters. In this paper, an attempt to carry out model tests to obtain mathematical relationships was made. These relationships were to determine the impact of the tool axis orientation and the variable curvature radius of the machined profile on the surface roughness and its topography in the 5-axis milling process of sculptured surfaces. The tests were conducted on an example of a turbine blade made of Inconel 718 alloy. A measurable effect of the work undertaken was the development of model relationships that can be applied in specialized modules of CAM (Computer Aided Manufacturing) systems supporting the programming of 5-axis machining of sculptured surfaces. The models developed will also make it possible to obtain an evenly distributed roughness on the machined sculptured surface, especially on the surface of the turbine blades of the Inconel 718 alloy, as indicated by the results of the tests carried out.

Keywords: surface roughness; 5-axis milling; sculptured surfaces; curvature radius; turbine blade; toroidal cutter; Inconel 718

1. Introduction

Sculptured surfaces are currently widely used for the design of complex elements, mainly turbine blades, especially in the aviation and energy industries. The surfaces in these types of elements are characterized by a variable radius of a curved line contour along the machined profile. Due to the complexity of the shape of these surfaces, 5-axis milling is used for their machining.

The 5-axis trajectory of the tool movement is generated in a CAM (Computer Aided Manufacturing) system, which offers different algorithms of the tool positioning and the machining strategies, depending on the geometry of the surface to be treated. One of the main adjustable parameters of 5-axis milling is the lead and tilt angle. The above considerations are shown schematically in Figure 1.

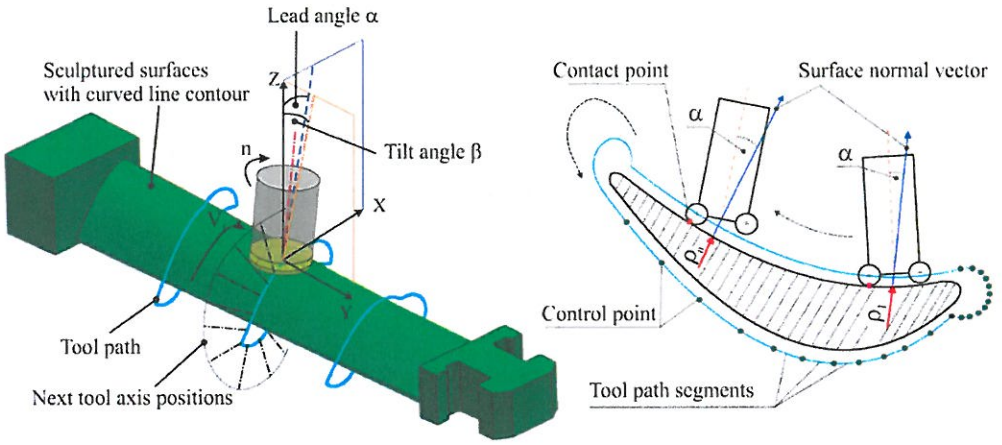

Figure 1. Five-axis milling of sculptured surfaces elements with a curved line contour.

In [1], the authors stated that the machined surface quality resulted from the choice of the strategy and the corresponding cutting parameters. According to this statement, they developed a predicting model of the surface roughness of the sculptured surface after 5-axis milling. However, the researchers did not include the variable radius of the surface profile curvature and different lead angle values in the studies, and used a toroidal cutter for the research. When analyzing the results obtained by them, it can be stated that the roughness of the curvilinear surface after 5-axis milling was characterized by an uneven distribution of roughness parameters. This may be due to the variable curvature radius along the surface profile being machined. Similar conclusions were obtained after analyzing the results of the research shown in [2]. Uneven distribution of roughness parameters, especially on the surfaces of turbine blades, resulted in a decrease in the efficiency of the rotor machine. Particular attention was paid to this in [3], which is shown in Figure 2, according to the study [3].

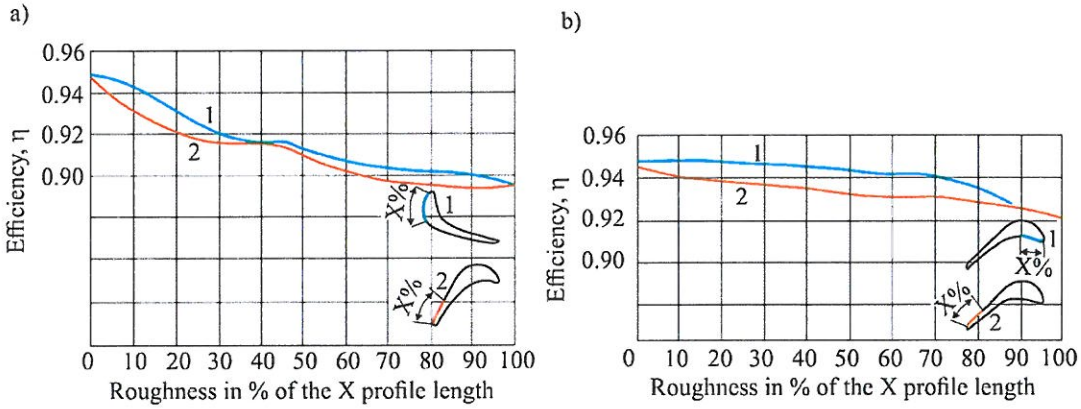

Figure 2. Effect of unevenly distributed roughness: (**a**) roughness builds up from the inlet side, (**b**) roughness builds up from the outlet side.

The first attempts of fundamental research in the field of uneven distribution of the roughness parameters were undertaken in [4,5]. Cao et al. [4] attempted to determine the effect of the curvature radius of a sculptured surface on the selection of the 5-axis tool path whereas Yao et al. [5] tried to determine the impact of tool orientation and surface curvature on the surface integrity in TC17 alloy milling with a ball end milling cutter. In both of these works, there were a lot of cognitive data, but there were no models linking the geometrical parameters of the surface with the kinematic parameters of the 5-axis milling process. Such an attempt, as the first to date, will be made in this work.

Various studies on the influences of tool axis orientation on the surface roughness and topography during 5-axis milling of sculptured surfaces were conducted. Toh in his work [6] focused on the 5-axis high-speed milling and reported that the minimum surface roughness was obtained when a positive lead angle was used. Chen et al. in [7,8] made an attempt to investigate the 5-axis milling theory and revealed the effects of various tool orientations on the surface roughness. In turn, Ko et al. [9] focused on the lead and tilt angle and cutter path by considering, among others, the surface roughness in their research where the results indicated that a 15° inclination angle was optimal. The work of Cao et al. [4] attempted to investigate the effect of the radius of curvature of sculptured surfaces on tool path selection in 3-axis milling. For the tool path selection, the method of constant scallop height based on high productivity was used. Kalvoda et al. [10] indicated that they obtained the best surface roughness when the lead and tilt angles were negative, and the worst surface roughness was when there was no inclination. Lim et al. [2] paid attention to the high-speed finish machining of sculptured surfaces of a blade and investigated the effects of four different cutter path orientations on the surface roughness and surface morphology. The results of their research indicated that the distribution of roughness parameters was uneven. Hendriko [11] developed a model to calculate the scallop height of a toroidal cutter in 5-axis milling. His research shed new light on the problem of roughness in 5-axis milling, but also showed no correlation between kinematic and geometric parameters, which was similar in the work of Segonds et al. [12].

A sculptured curvilinear surface is usually composed of many curved surface patches with different curvatures/radii of curvature. As these surfaces are widely used in various fields, the 5-axis milling process has stringent requirements to obtain a high accurate shape and the required surface roughness and topography. The lead angle of the tool axis changes during the sculptured surface milling process due to changes in the surface normal vector, thus affecting the surface quality.

In machining a sculptured surface, recent studies have mainly focused on the cutter path generation method with tool axis orientation for a curved surface [13,14] and the engagement of a tool and machining surface [15]. However, these studies did not consider the variable radii of the curvature of the machined surface, which could result in being able to use the processing experience or the test results to evaluate the sculptured surface machining strategies or tool axis orientation in the actual machining.

Various studies on the surface roughness and topography during 5-axis milling of sculptured surfaces that considered different cutter path orientations and tool axis orientation were conducted. In [16], the researchers described the generation of cutter paths, the identification and effects of tool orientations on the milling process, and the selection of tool parameters. They discussed the problems that occurred during sculptured surface (especially curvilinear) machining and future research directions. Xie et al. [17] proposed a curvature distribution value to evaluate the 5-axis machining efficiency and machining accuracy, and verified the validity by conducting experiments and analyses. This proposal may also apply to the assessment of surface quality in the 5-axis machining of sculptured surfaces. Duan et al. [18] analyzed the tool orientation when 5-axis machining 300M steel and summarized the surface roughness after machining planes with different angles. Cao et al. [4] analyzed the effect of the curvature radius of the sculptured surface on finish 5-axis milling tool path selection. They stated that curvature radius, especially the normal curvature radius that is parallel to the feeding direction, had an obvious effect on machining productivity and quality.

In conclusion, one of the groups of research has focused on the influences of tool axis orientation on surface roughness and topography in a 5-axis milling process of sculptured surfaces and have obtained numerous research findings from the perspective of theory and experimentation. In the case of the radii of the curvature of sculptured surfaces, which are used for profiling turbine blades, Cao et al. [4] investigated the effect of the curvature radius of the sculptured surface on finish milling tool path selection, and Yao et al. [5] and Yang et al. [19] studied the effects of tool orientation and surface curvature on surface integrity in ball end milling. However, their studies did not bind the lead angle with the radius of curvature to the mathematical model, and did not determine their effect on the

surface roughness and topography. In this paper, the effects of lead angle and radii of curvature on surface roughness and topography during the 5-axis milling of Inconell 718 nickel alloy using the toroidal cutter were studied, and different forms of surface structures were taken based on the turbine blade. The results can provide new guidance for the 5-axis machining of sculptured surface parts of Inconel 718 nickel alloy to obtain good surface roughness and topography.

2. Five-Axis Milling Process of Sculptured Surfaces

2.1. Definition of Tool Axis Orientation and Experimental Model of Sculptured Surfaces with Variable Radii of Curvature

A toroidal cutter is increasingly used to manufacture sculptured surfaces, and there are various possible tool axis orientations while maintaining maximum performance and good surface roughness due to its geometrical features. The lead angle and the tilt angle are often used to describe the tool axis orientation during the real CAM/CNC (Computerized Numerical Control) programming and post-processing. This paper adopted the lead angle to describe the tool axis orientation for the convenience of description and analysis. Figure 3a presents the analytical diagram of the tool axis orientation, and the relationship between the existing sets of angles is as follows:

$$\alpha = \arcsin\left(\sin(\theta)\cdot\frac{\cos(\zeta)}{\sqrt{\sin(\theta)^2\cdot\cos(\zeta)^2+\cos(\theta)^2}}\right) \quad (1)$$

$$\beta = \arccos\left(\sqrt{\sin(\theta)^2\cdot\cos(\zeta)^2+\cos(\theta)^2}\right) \quad (2)$$

where α is the lead angle; β is the tilt angle; θ is the inclination angle; and ζ is the rotational angle.

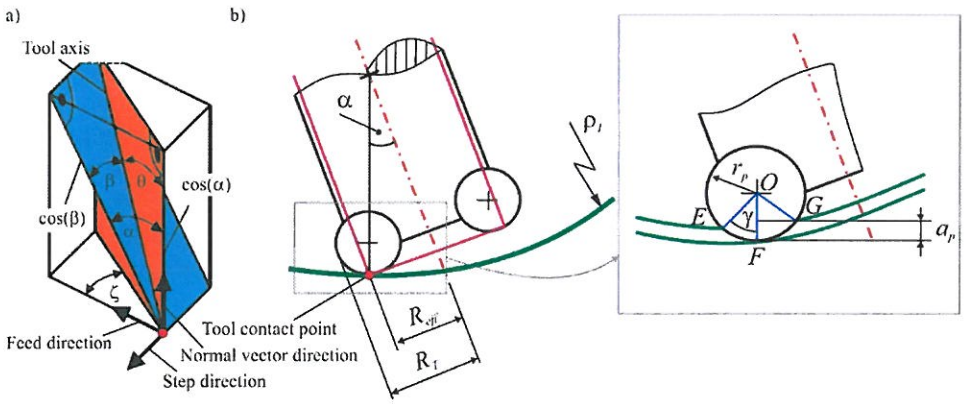

Figure 3. Analytical diagrams of tool orientation and tool contact position. **(a)** Tool orientation, **(b)** tool contact position.

Variation in the lead angle can have a significant effect on the toroidal cutter contact point position; a schematic view is shown in Figure 3b. Parameter r_p represents the radius of the round cutting insert of the toroidal milling cutter, α denotes the lead angle, a_p is the cutting depth, and γ is the normal angle between the toroidal cutter contact point boundary (E) and the cutting plane point (F). The value of γ can be calculated by solving Equation (3):

$$\gamma = \arccos\left(\frac{r_p - a_p}{r_p}\right) \quad (3)$$

It can clearly be seen that the point with the highest cutting speed (v_c) is clockwise to the side edge of the toroidal milling cutter. When analyzing geometrical relationships, the following conclusions can be obtained: at any point on the cutting edge, the cutting speed is always greater than 0 ($v_c > 0$) and the tool center does not participate in the milling process; when the material is on the left side of the round cutting insert, the maximum cutting speed $v_{cE} = v_{cmax} \cdot \sin(\alpha + \eta)$ (point E); when the material is on the right side of the round cutting insert, the minimum cutting speed $v_{cG} = v_{cmax} \cdot \sin(\alpha - \eta)$ (point G); and the cutting speed of the maximum cutting depth $v_{cF} = v_{cmax} \cdot \sin\alpha$ (point F). The effective radius of the toroidal milling cutter passes through point F, which can be calculated from Equation (4):

$$R_{eff} = R_T - r_p(1 - \sin(\alpha)) \quad (4)$$

Sculptured surfaces can be divided into convex, concave, biconvex, and biconcave surfaces according to their characteristic parameters in the form of curvatures/radii of curvature. The turbine blade surface consists of the suction surface (convex), the pressure surface (concave), and the leading and trailing edge surfaces. To simulate features such as the suction surface and the pressure surface, their geometry is based on different radii of curvature, which show continuous variability of value in the direction of the tool feed. A three-dimensional model of the research turbine blade is shown in Figure 4.

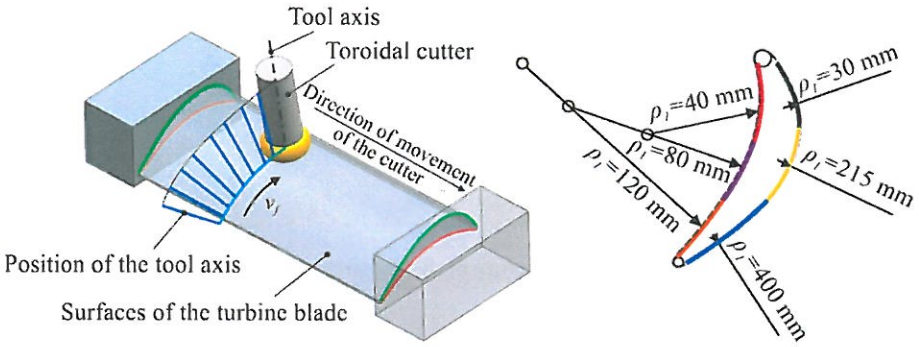

Figure 4. Research 3D-CAD model of the turbine blade.

In the machining process of sculptured surfaces, variation in the normal vector (as a result of changes in the radius of curvature) leads to the variation of the tool axis orientation, which in turn affects the surface roughness and topography. The experimental and empirical studies of characteristic surfaces of the turbine blade were carried out according to the 3D-CAD models and the model of the research object.

2.2. *Materials and Tools*

The workpiece material used was the Inconell 718 nickel alloy; its chemical composition and the main mechanical and physical properties at room temperature are given in Tables 1 and 2, respectively. The shape of the blank for the toroidal milling cutter axis orientation experiments was a rectangular block. The sculptured surfaces had the same shapes as those in the 3D-CAD models presented above.

Table 1. Chemical composition of the Inconel 718 alloy in% of elements.

	Fe	Cr	Co	Mo	W	Nb	Al	Ti	C	B	Zr	Ni
IN718	18.	19	-	3	-	5.1	0.5	0.95	0.05	0.04	-	525

Table 2. Main mechanical and physical properties of Inconel 718 nickel alloy.

Tensile Strength (MPa)	Yield Strength (MPa)	Elastic Modulus (GPa)	Elongation (%)	Density (g/cm^3)
1330	1120	220	23%	8.2

A toroidal milling cutter R300-016B20L-08L Sandvik Coromant and round inserts R300-0828E-PL made of S30T carbide were used for the experiment and empirical tests.

2.3. Experimental and Empirical Procedure and Research Technology

The purpose of the experiments was to study the effects of different axis orientations of the toroidal milling cutter and variability of the radius of curvature on surface roughness and topography. The two-factor test was used for the experiments, and the lead angle and the radii of curvature were changed to explore the effect of each on the surface roughness and topography. The tests were conducted based on the study object, which is presented in Figure 5.

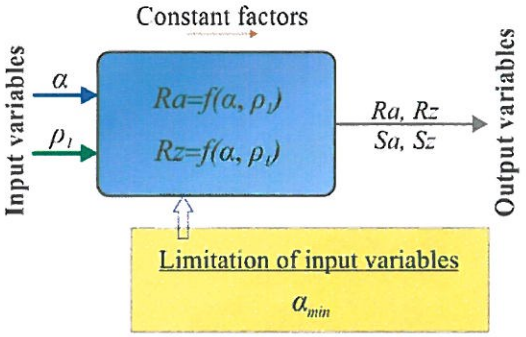

Figure 5. Structure of the research object.

The features of the research object are presented in Table 3.

Table 3. Dimensions characteristic for the test object.

		Description
Input variables	X_1	Lead angle α
	X_2	Curvature radius ρ_1
Output variables	Y_1	2D and 3D surface roughness parameters
Constant factors	C_1	Machine tool
	C_2	Material
	C_3	Toroidal cutter
Limitation	O_1	Minimum lead angle α_{min}

The input variables of the test object (i.e., the angle α and the curvature radius ρ) as well as the limitations for carrying out experimental tests were selected after taking into account the conclusions of the simulation tests conducted by the author at work [2]. When the diameter D and the radius of the round cutting insert r_p of the toroidal cutter are known as well as the radius of curvature ρ_1 of the currently processed surface profile, it is possible to determine the value of the minimal lead angle α_{min} from relation (2), where the undercutting will not occur:

$$\alpha_{min} = \arcsin\left(\frac{\frac{D}{2} - r_p}{\rho_1 - r_p}\right) \quad (5)$$

The convex surface and concave surface were divided into test areas according to the variable values of the curvature radius ρ_1 and the lead angle α, as shown in Figure 6.

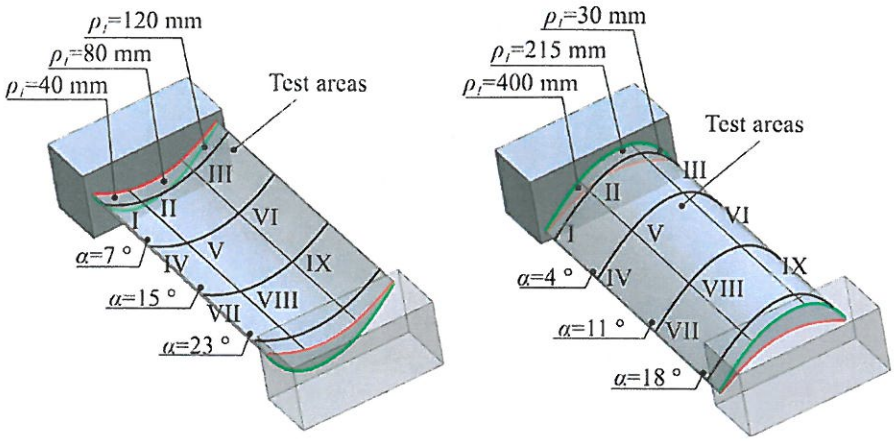

Figure 6. Test areas depending on the curvature radius ρ_1 and the lead angle α.

Table 4 shows the machining parameters for the concave surface and convex surface of the turbine blade. For each of the processing steps, the fixed parameters were: axial infeed a_p; radial infeed a_e; feed per tooth f_z; toroidal cutter diameter D = 16 mm; and the radius of the round cutting insert r_p = 4 mm. In addition, in order to avoid undercutting of the concave surface, the limit value of the lead angle was calculated (α_{min} = 7°) for the radius ρ_1 = 40 mm of this surface.

Table 4. Machining conditions.

No.	Parameters	Convex Surface Machining	Concave Surface Machining
1.	a_p [mm]	0.25	0.25
2.	a_e [mm]	1.5	1.5
3.	f_z [mm/tooth]	0.26	0.26
4.	v_c [m/min]	40	40
5.	ρ_1 [mm]	$\rho_1 \in$ <30 ÷ 400>	$\rho_1 \in$ <40 ÷ 120>
6.	α [°]	$\alpha \in$ <4 ÷ 18>	$\alpha \in$ <7 ÷ 23>

The test stand was built on the basis of the DMG DMU 100 MonoBlock 5-axis milling center, which is shown in Figure 7.

The machine was equipped with NC (Numerical Control) dividing heads and tools for roughing and finishing machining of the test object. The DMU 100 MonoBlock machine tool has a milling head with a built-in spindle with a maximum rotational speed of n = 24,000 1/min (axis B), enabling the setting of the tilt angle β. The head is equipped with the HSK-A63 chuck, intended for fixing the holder together with the toroidal cutter. In addition, equipping the machine tool with NC subdivision heads (dividing heads, axis A) enables the setting of the lead angle α. The SINUMERIK 840Di control system enables the realization of simultaneous 5-axis machining. The movement in the Z axis is carried out by the machine table, while the movement in the X and Y axes is carried out by the milling head.



Figure 7. Test stand.

To measure the 2D surface roughness and 3D topography parameters, a MAHR MarSurf GD 120 profilograph was used, which is shown in Figure 8. The measurement was done with the MFW 250 × 2.0:1 head with the measuring tip MFW Tastarm 90st/2µm_6851877, with the rounding radius of 2 µm.

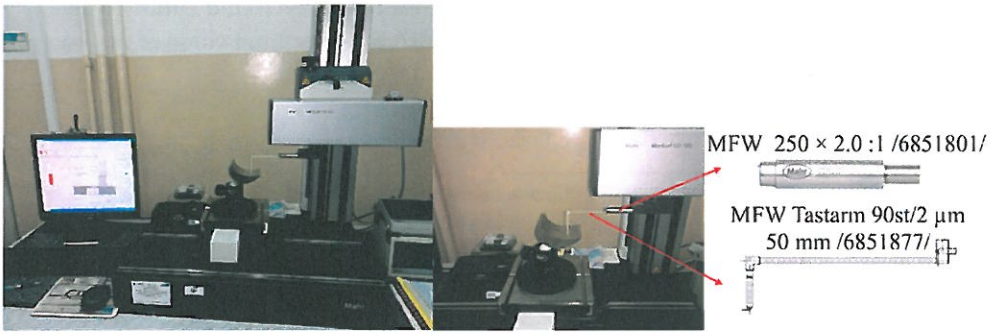

Figure 8. 3D profilograph MarSurf GD 120.

The measurements were conducted by means of the contact method using MarWin software version 6268201 Mahr firm. This software allowed for the determination of the value of the selected 2D and 3D surface roughness parameters. The 2D roughness measurement was carried out in the feed direction of the toroidal milling cutter with the measurement being repeated three times, then the average values were calculated. The measurements were done along the measuring tracks, which were defined in the MarWin program as the upper profile line (red line), lower profile line (blue line), and middle profile line (green line). The measurement method is shown in Figure 9. Then, the 3D roughness parameters were measured. Therefore, the 2D roughness parameters in the perpendicular direction to the feed were not analyzed. The estimation of 3D topography parameters was made by scanning the area of the measured surface (the green surface area in Figure 9). The dimensions of the scanning surface area were 2.5 mm × 4 mm in the x and y axes, respectively. The measuring speed was 0.5 mm/s. The displacements during sampling were equal in the x direction: $\Delta x = 0.5$ µm and in the y direction: $\Delta y = 19.4$ µm.

Model studies were carried out using a three-level complete static plan PS/DK 3^n, with the number of repetitions r = 3 and the assumed significance level $\tau = 0.05$. The matrix of the study plan is shown in Table 5. This plan allows the empirical mathematical model of the investigated process to be obtained in the form of a polynomial function convenient for a mathematical analysis and model tests. In addition, this plan takes into account the interactions between the factors studied.

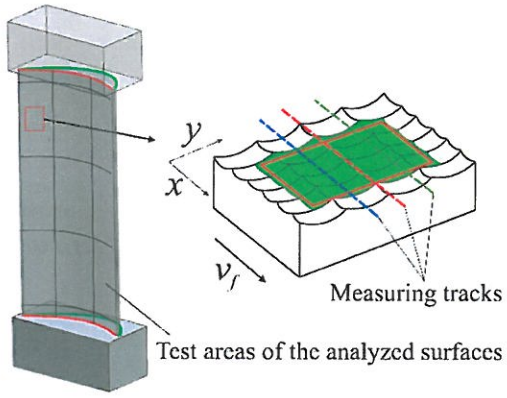

Figure 9. Methodology for measuring surface roughness and topography.

Table 5. Studies' plan matrix PS/DK 3^2.

Test Number	Standardized Variables			Squares		Interactions
	x_0	x_1	x_2	${x_1}^2$	${x_2}^2$	$x_{1\times 2}$
1	+	+	+	+	+	+
2	+	+	0	+	0	0
3	+	+	-	+	+	-
4	+	0	+	0	+	0
5	+	0	0	0	0	0
6	+	0	-	0	+	0
7	+	-	+	+	+	-
8	+	-	0	+	0	0
9	+	-	-	+	+	+

Table 6 shows the ranges of the analyzed values parameters of the lead angle α and the curvature radius ρ_1 for individual test areas.

Table 6. Studies' plan for the convex and concave surface of the turbine blade.

Test Number	Convex Surface		Concave Surface	
	$x_1(\alpha)$	$x_2(\rho_1)$	$x_1(\alpha)$	$x_2(\rho_1)$
1	18	400	23	120
2	18	215	23	80
3	18	30	23	40
4	11	400	15	120
5	11	215	15	80
6	11	30	15	40
7	4	400	7	120
8	4	215	7	80
9	4	30	7	40

3. Results and Discussion

In industrial practice, in the field of mechanical engineering, mainly the parameters *Ra*, *Rz*, *Sa*, and *Sz* are used, which on their basis the surface roughness class is determined. Therefore, these

parameters were analyzed in this study. In addition, these parameters are the easiest to adopt in a CAM system.

3.1. Surface Roughness

3.1.1. *Ra* Roughness Parameter

The relationship between surface roughness (*Ra* parameter, arithmetical mean height) and the lead angle and the curvature radius of the convex and concave surface are shown in Figure 10.

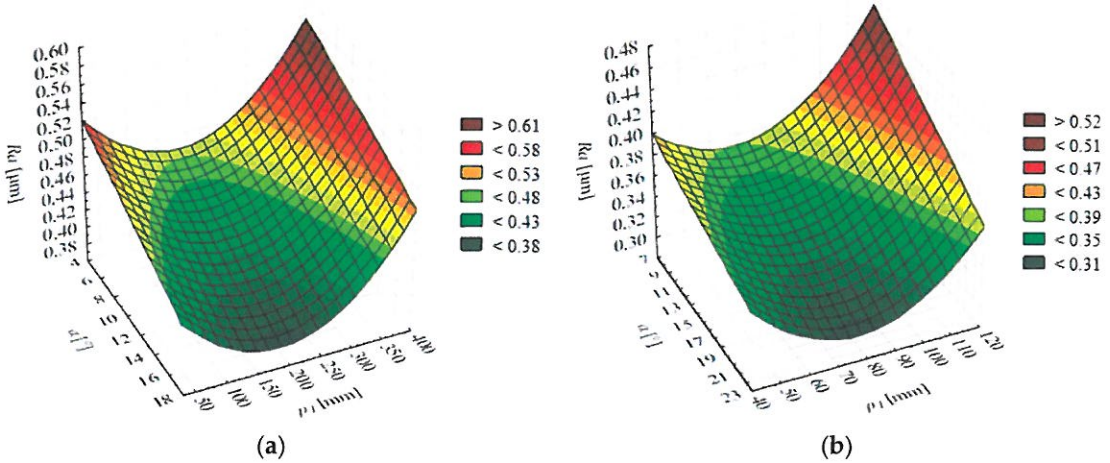

(**a**) (**b**)

Figure 10. Influence of the lead angle α and radius of curvature ρ_1 on the *Ra* roughness parameter of the convex (**a**) and concave (**b**) surface.

Based on the results of the studies, it was found that both in the machining of the convex and concave surface of the turbine blade, the maximum values of the *Ra* roughness parameter were obtained for the upper level (ρ_1 = 400 mm and ρ_1 = 120 mm, respectively) of the tested curvature radius. The lowest values of the *Ra* parameter were obtained for the middle level (ρ_1 = 215 mm and ρ_1 = 80 mm, respectively). It was noted that with an increase of the lead angle α, the Ra parameter decreased by about 20% for both the convex and concave surface. For the machining of the convex surface, the maximum value of 0.5 µm of the *Ra* parameter was noted in the first test area, while in the machining of the concave surface in III area, it reached a value of about 0.4 µm.

In the next step for the measured values of the *Ra* roughness parameter, the calculations were made according to the adopted test plan. As a result of the calculations, model functions of the test object were obtained, which showed the course of the *Ra* parameter in the machining of the convex (6) and the concave surface (6) of the turbine blade within the established range of the tested parameters ρ_1 and α:

$$Ra = 0.556 - 0.0057\alpha - 0.00085\rho_1 + 0.0000023{\rho_1}^2 \quad (6)$$

$$Ra = 0.1986 + 0.0428\alpha - 0.0008\rho_1 - 0.00008\alpha^2 + 0.00001{\rho_1}^2 \quad (7)$$

The courses of the models' dependences that describe changes of the *Ra* roughness parameter values in machining the convex and concave surface of turbine blade as a function of the radius of curvature ρ_1 and the lead angle α are shown in Figures 11–14, respectively.

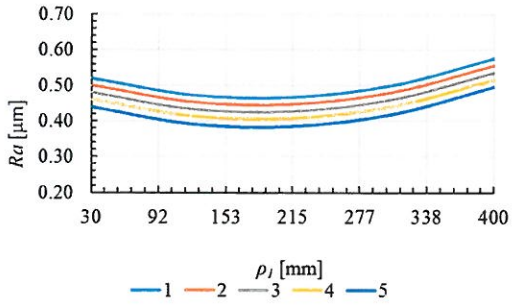

Figure 11. Effect of the curvature radius ρ_1 on the *Ra* roughness parameter in the machining of the convex surface: (1) $\alpha = 4°$, (2) $\alpha = 7.5°$, (3) $\alpha = 11°$, (4) $\alpha = 14.5°$, (5) $\alpha = 18°$.

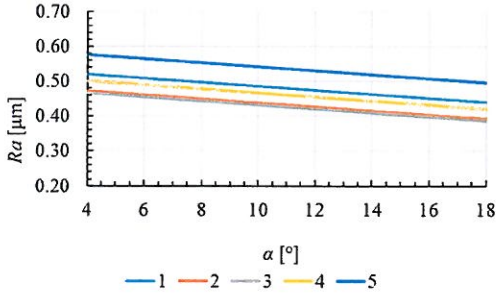

Figure 12. Effect of the lead angle α on the *Ra* roughness parameter in the machining of the convex surface: (1) $\rho_1 = 30$ mm, (2) $\rho_1 = 122.5$ mm, (3) $\rho_1 = 215$ mm, (4) $\rho_1 = 307.5$ mm, (5) $\rho_1 = 400$ mm.

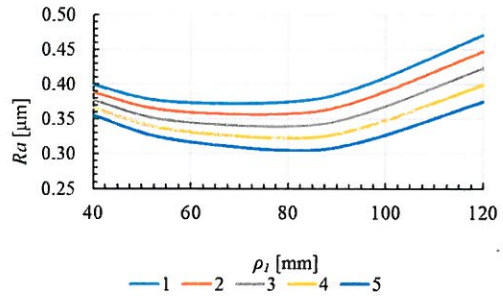

Figure 13. Effect of the curvature radius ρ_1 on the *Ra* roughness parameter in the machining of the concave surface: (1) $\alpha = 7°$, (2) $\alpha = 11°$, (3) $\alpha = 15°$, (4) $\alpha = 19°$, (5) $\alpha = 23°$.

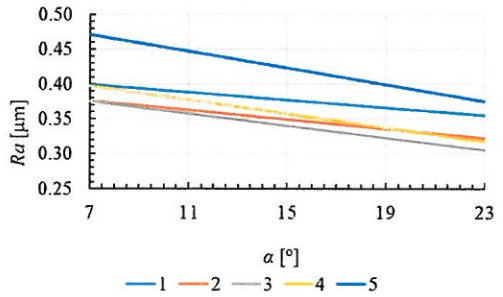

Figure 14. Effect of the lead angle α on the *Ra* roughness parameter in the machining of the concave surface: (1) $\rho_1 = 40$ mm, (2) $\rho_1 = 55$ mm, (3) $\rho_1 = 80$ mm, (4) $\rho_1 = 95$ mm, (5) $\rho_1 = 120$ mm.

As shown in the graphs, in the case of the convex surface within a scope of the radius of curvature $\rho_1 = 30 \div 175$ mm, there was a slight decrease in the value of the *Ra* roughness parameter as the parameter ρ_1 increased. Whereas, above the value of about 175 mm of radius ρ_1, along with the increase of this parameter, the *Ra* parameter also increased. In the case of a concave surface, the value

of the *Ra* parameter also slightly decreased with an increase in the radius of curvature ρ_1 to about 80 mm. Above this value, the *Ra* roughness parameter increased, together with a growth of parameter ρ_1. This is due to the change on the contact zone and the elongation of the toroidal cutter cutting edge contact line with the machined surface. The highest values of the *Ra* parameter were obtained in surface machining with a fixed angle $\alpha = 4°$, and the lowest in machining with a fixed angle $\alpha = 18°$. The highest values of the *Ra* parameter in the concave surface machining were obtained for the lead angle $\alpha = 7°$, and the smallest for the angle $\alpha = 23°$. The highest values of the *Ra* parameter in the concave surface machining were obtained for the lead angle $\alpha = 7°$, while the smallest values were obtained for the angle $\alpha = 23°$.

3.1.2. *Rz* Roughness Parameter

The relationship between surface roughness (*Rz* parameter–maximum height of profile) and the lead angle and the curvature radius of the convex and concave surface are shown in Figure 15.

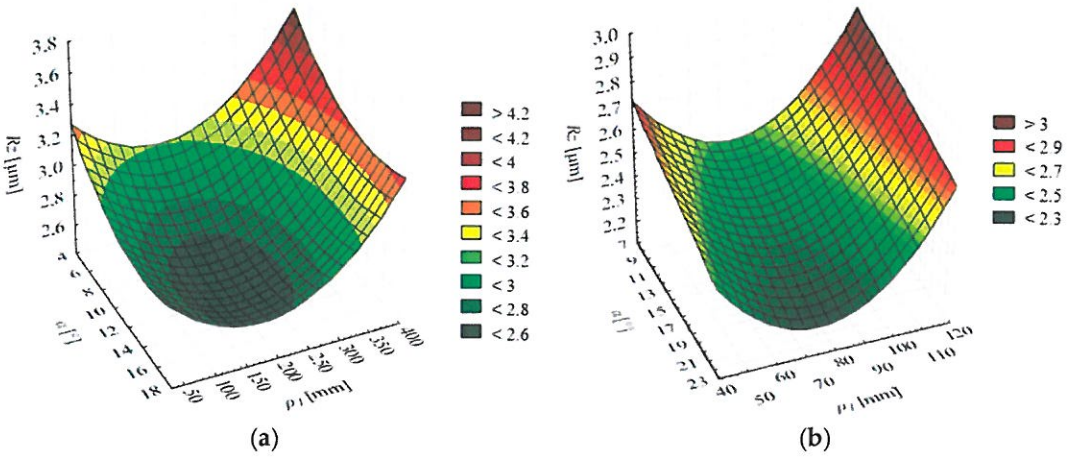

Figure 15. Influence of the lead angle α and radius of curvature ρ_1 on the *Rz* roughness parameter of the convex (**a**) and concave (**b**) surface.

Based on the results from the measurement of the *Rz* parameter values, it was found that the maximum values of this roughness parameter were obtained for the upper level ($\rho_1 = 400$ mm and $\rho_1 = 120$ mm, respectively) of the tested radius of curvature ρ_1, while the lowest values of the *Rz* parameter were obtained for the middle level ($\rho_1 = 215$ mm and $\rho_1 = 80$ mm, respectively). This was observed in the entire investigated range of the radius of curvature ρ_1 of the convex and concave surface subject of the research. An increase in the value of the lead angle α caused a decrease in the *Rz* parameter value of about 10%. The maximum value of *Rz* parameter of about 3.5 µm was measured in the first test area of the convex surface, and in the sixth area of the concave surface where *Rz* was about 2.5 µm.

Then, for the measured values of the *Rz* roughness parameter, some calculations were made according to the adopted test plan. As a result of the calculations, model functions of the test object were obtained that showed the course of the *Rz* parameter in the machining of the convex (8) and the concave surface (9) of the turbine blade within the established range of the tested parameters ρ_1 and α:

$$Rz = 4.26 - 0.15\alpha - 0.0068\rho_1 + 0.0038\alpha^2 + 0.000013{\rho_1}^2 \quad (8)$$

$$Rz = 3.165 - 0.03\alpha - 0.0385\rho_1 + 0.000022{\rho_1}^2 \quad (9)$$

The courses of the models' dependences that describe the changes of the *Rz* roughness parameter values in machining the convex and concave surface of the turbine blade as a function of the curvature radius ρ_1 and the lead angle α are shown in Figures 16–19, respectively.

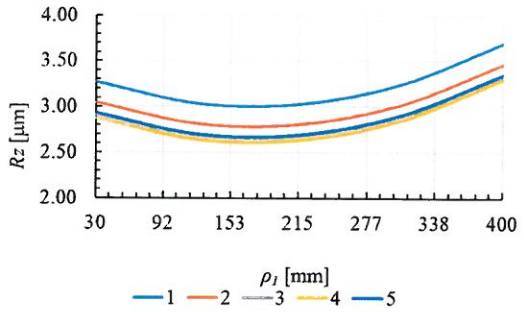

Figure 16. Effect of the curvature radius ρ_1 on the *Rz* roughness parameter in the machining of the convex surface: (1) $\alpha = 4°$, (2) $\alpha = 7{,}5°$, (3) $\alpha = 11°$, (4) $\alpha = 14{,}5°$, (5) $\alpha = 18°$.

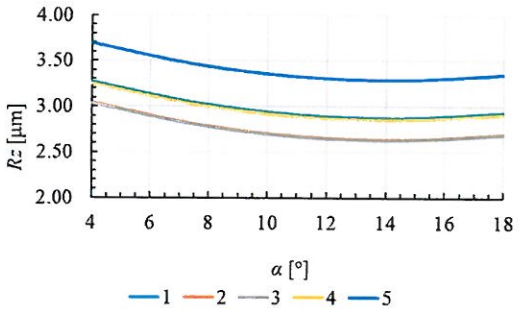

Figure 17. Effect of the lead angle α on the *Rz* roughness parameter in the machining of the convex surface: (1) $\rho_1 = 30$ mm, (2) $\rho_1 = 122.5$ mm, (3) $\rho_1 = 215$ mm, (4) $\rho_1 = 307.5$ mm, (5) $\rho_1 = 400$ mm.

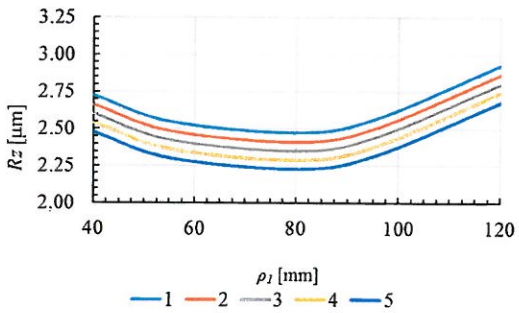

Figure 18. Effect of the curvature radius ρ_1 on the *Rz* roughness parameter in the machining of the concave surface: (1) $\alpha = 7°$, (2) $\alpha = 11°$, (3) $\alpha = 15°$, (4) $\alpha = 19°$, (5) $\alpha = 23°$.

As shown in the graphs, along with an increase in the curvature radius ρ_1 to the value of about 215 mm for the convex surface, the value of the *Rz* parameter decreased. Above the value of ρ_1 of approximately 215 mm, the *Rz* parameter increased again. However, in the whole tested range of the lead angle α, from the value of the parameter $\rho_1 = 40$ mm to about $\rho_1 = 80$ mm of the concave surface, the *Rz* roughness parameter decreased., whereas in the range of parameter ρ_1 from about 80 mm to about 120 mm, the value of the *Rz* roughness parameter increased again. In this case, it may be due to the increase in the height of the tops and the depth of the roughness grooves. This was the result of the change in the contact zone and the elongation of the toroidal cutter's cutting edge contact line with the machined surface. It was also found that as the value of the angle α increased, the value of the *Rz* parameter in machining the convex surface decreased. The exception was the radius of curvature ρ_1 in

the range of about 300÷400 mm, where the value of this parameter grew slightly. On the other hand, as the angle α increased, the *Rz* value of the concave surface roughness decreased over the entire range of the values for the curvature radius ρ_1 tested.

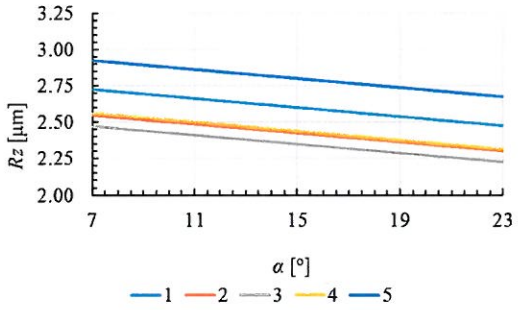

Figure 19. Effect of the lead angle α on the *Rz* roughness parameter in the machining of the concave surface: (1) ρ_1 = 40 mm, (2) ρ_1 = 55 mm, (3) ρ_1 = 80 mm, (4) ρ_1 = 95 mm, (5) ρ_1 = 120 mm.

3.2. Surface Topography

The next stage of the research was to carry out measurements of 3D surface geometry in selected places of the convex and concave surface of the turbine blade. Histograms of the values of the selected 3D parameters obtained from measurement in individual areas of the analyzed surfaces are shown in Figures 20–23.

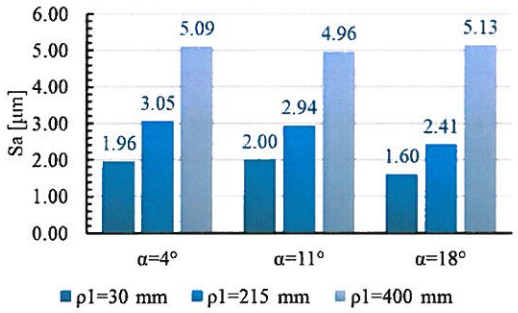

Figure 20. Statement of the measurement results of the parameter *Sa* of the convex surface of the turbine blade.

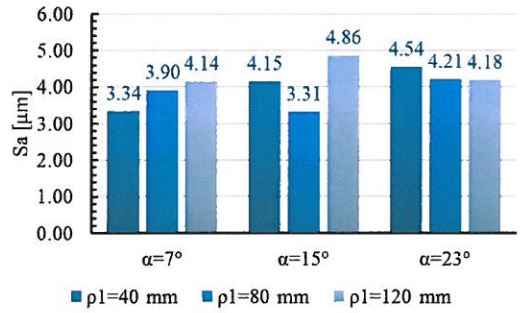

Figure 21. Statement of the measurement results of the parameter *Sa* of the concave surface of the turbine blade.

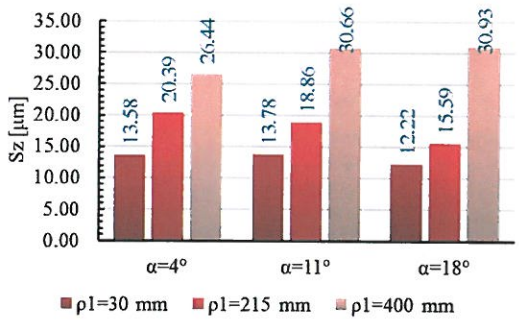

Figure 22. Statement of the measurement results of the parameter *Sz* of the convex surface of the turbine blade.

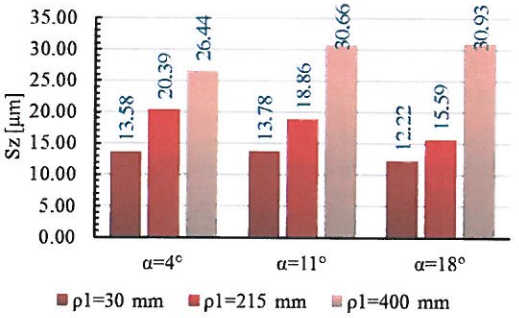

Figure 23. Statement of the measurement results of the parameter *Sz* of the concave surface of the turbine blade.

When analyzing the results of measuring parameters *Sa* (arithmetic deviation of the surface) and *Sz* (maximum height of the surface) of the convex surface, it was found that the values of these parameters went up with an increase in the curvature radius ρ_1. However, in the case of the concave surface, it was observed that for the value of the angle $\alpha = 7°$, along with the increase in the value of the radius ρ_1, there was a slight increase in the values of parameters *Sa* and *Sz*. For the angle $\alpha = 15°$, the smallest values of parameters *Sa* and *Sz* were obtained for the radius $\rho_1 = 80$mm, while the largest was obtained for the radius $\rho_1 = 120$ mm. For the angle $\alpha = 23°$, a slight decrease in the value of the analyzed parameters along with an increase in parameter ρ_1 was observed.

The topography images of the convex and concave surface of the turbine blade in individual test areas after machining are shown in Figures 24–29.

When analyzing the presented images of the topography of the convex and concave surface, it was observed that in the structures of these surfaces, there was periodicity in the *x*-axis and *y*-axis direction. This was due to the machining marks created as a result of feed on the tooth of the toroidal cutter in a specific longitudinal direction (x-axis) and cross direction (y-axis). A mutual overlapping of traces (grooves) of adjacent transitions (rows) of the toroidal milling cutter was observed. It was also noted that along with the increase in value of the lead angle α, both in the machining of the convex and concave surface, extended grooves of the profile in the feed direction were obtained correspondingly. This indicates the extension of the active length of the cutting edge of the toroidal milling cutter. In addition, it was observed that as the value of this angle increased, higher profile tops were obtained correspondingly. This may indicate the residual material on the machined surface. These residues result from the reduced contact area between the tool and the machined surface due to the inclining of the mill axis in the feed direction. As a result of these residues, higher values of the parameter *Sa* of both analyzed surfaces were obtained after machining with larger settings of the lead angle α.

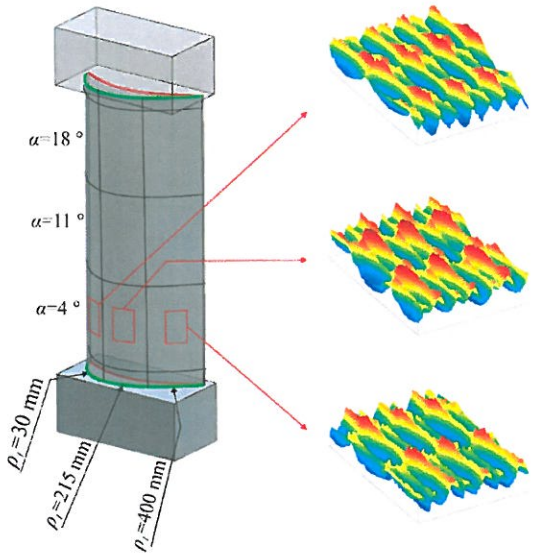

Figure 24. Topography of the convex surface when changing the curvature radius for the lead angle $\alpha = 4°$.

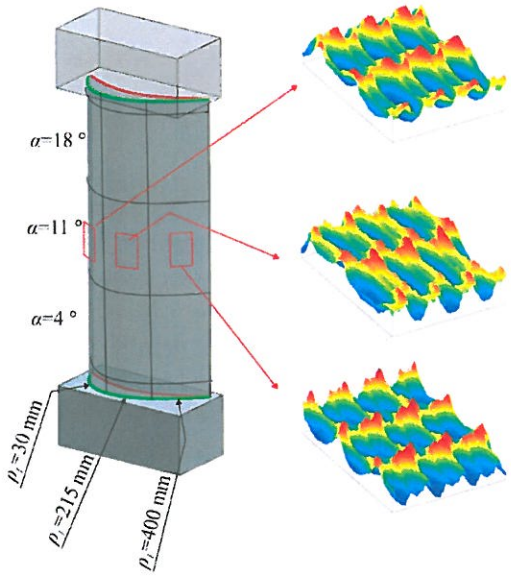

Figure 25. Topography of the convex surface when changing the curvature radius for the lead angle $\alpha = 11°$.

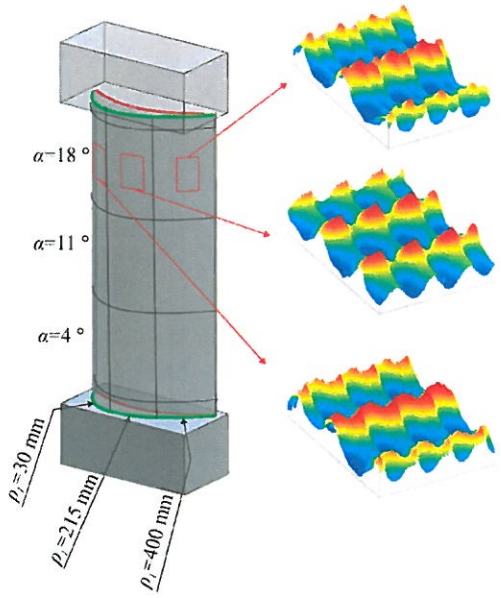

Figure 26. Topography of the convex surface when changing the curvature radius for the lead angle $\alpha = 18°$.

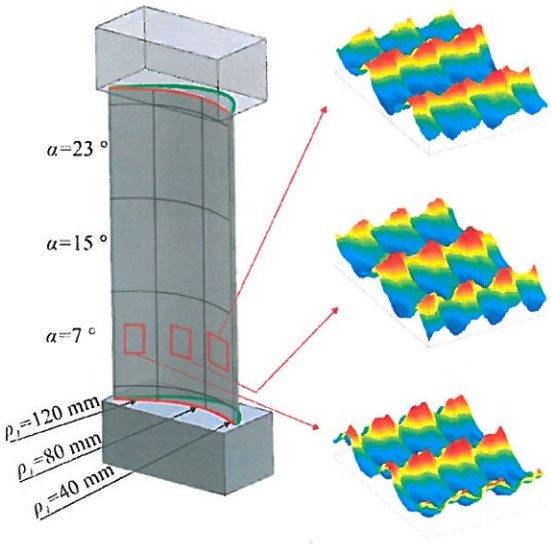

Figure 27. Topography of the concave surface when changing the curvature radius for the lead angle $\alpha = 7°$.

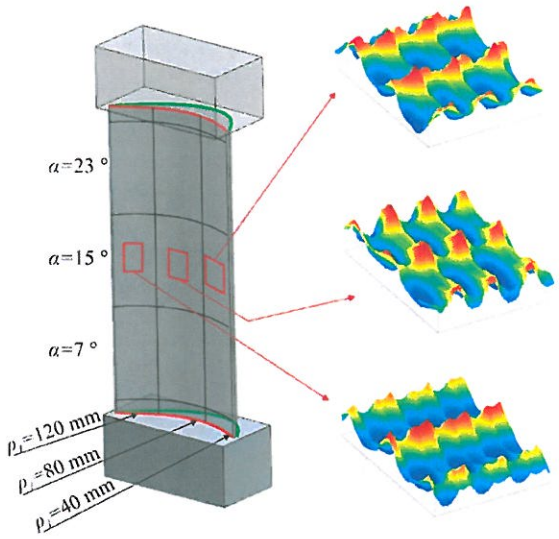

Figure 28. Topography of the concave surface when changing the curvature radius for the lead angle $\alpha = 15°$.

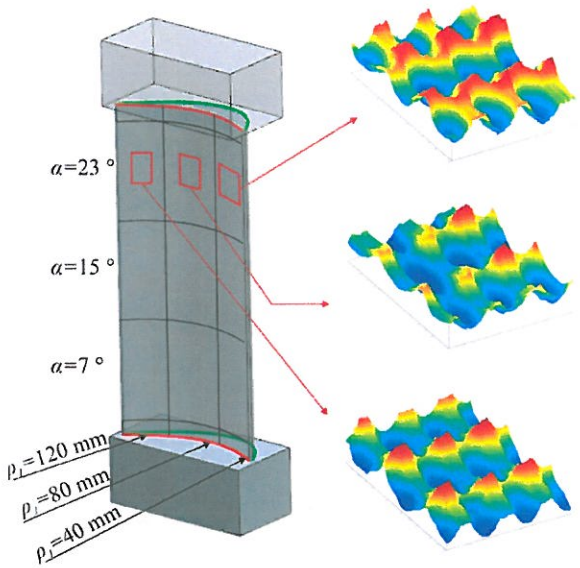

Figure 29. Topography of the concave surface when changing the curvature radius for the lead angle $\alpha = 23°$.

In addition, it was found that the resulting convex surfaces with a profile radius $\rho_1 = 30$ mm and $\rho_1 = 215$ mm after milling with a specified lead angle $\alpha = 4°$ and $\alpha = 11°$ had plateau-shaped tops. In other cases, the areas of the convex and concave surfaces had sharpened tops. Based on the analysis carried out, it was found that the surfaces obtained as a result of the machining were of an anisotropic mixed periodic nature.

4. Summary

This article focused on the 5-axis milling process of the sculptured surface of a turbine blade with a curved line contour and studied the influence of toroidal cutter axis orientation and curvature radius on surface roughness and topography for a curved surface. On this basis, the conclusion was applied

to the turbine blade sculptured surface machining process, and the tool axis orientation and variable radius of curvature were studied simultaneously. The results can be summarized as follows:

1) Both the curvature radius ρ_1 and the lead angle α affected the surface roughness and topography of the convex and concave surface of the turbine blade. An increase in the value of the lead angle α across the entire established range caused the reduction in the roughness *Ra* and *Rz* parameters in both cases of the analyzed surfaces.
2) It was shown that the nature of the changes in the *Ra* and *Rz* parameters of the convex and concave surface roughness was nonlinear with an upward trend with an increase in the radius of curvature ρ_1. The largest growth in the value of these parameters occurred above the radius values $\rho_1 = 175$ mm for a convex surface and $\rho_1 = 80$ mm for a concave surface.
3) Within the range of the tested values of the angle α and the curvature radius ρ_1, the geometrical structure (topography) of the convex and concave surface was characterized by periodicity in the feed direction of the tool, and in the transverse feed direction of the tool. It was found that the periodicity of these surfaces mainly depended on the kinematic and geometric mapping of the round cutting insert of the toroidal cutter on the machined surface.
4) It was found that the values of the *Sa* and *Sz* parameters of both analyzed surfaces increased with a growth in the radius of curvature ρ_1. In these cases, no significant influence of the α angle on the above parameters was found.
5) It was also found that within the lower and middle level of the lead angle α values tested, the obtained surfaces had plate-shaped hills, while within the middle and upper level of the angle α parameter, these surfaces had sharpened hills.
6) It was observed that as the value of the lead angle α increased, the active cutting edge length of the toroidal cutter was lengthened and the roughness profile grooves were lengthened in the direction of feed.

To sum up, it can be stated that the values of the lead angle α in the machining of the turbine blade surfaces with a variable profile curvature should be appropriately changed in a continuous way along with the change in the curvature radius ρ_1 of a machined profile. A continuous change of the lead angle α can be carried out adaptively in CAM systems using the models developed in this paper, which is the subject of the author's further research. The proposed adaptive method, after entering the criteria of the permissible parameter *Ra* and *Rz* of the surface roughness and *Sa* and *Sz* parameters of the topography, can allow for an adaption of the lead angle α of the toroidal cutter axis to the current value of the radius of curvature ρ_1 of the sculptured surface during machining.

Author Contributions: Conceptualization, methodology, formal analysis, investigation, resources, data curation, writing—original draft preparation, writing—review and editing, visualization, M.G. All authors have read and agreed to the published version of the manuscript.

Funding: This research received no external funding.

Conflicts of Interest: The author declares no conflict of interest.

References

1. Lavernhe, S.; Quinsat, Y.; Lartigue, C. Model for the prediction of 3D surface topography in 5-axis milling. *Int J. Adv. Manuf. Technol.* **2010**, *51*, 915–924. [CrossRef]
2. Lim, T.-S.; Lee, C.-M.; Kim, S.-W.; Lee, D.-W. Evaluation of cutter orientations in 5-axis high speed milling of turbine blade. *J. Mater. Process. Technol.* **2002**, *130–131*, 401–406. [CrossRef]
3. Wieczorek, B. *Technologia Turbin Parowych*, 1st ed.; Państwowe Wydawnictwa Techniczne: Warszawa, Rzeczpospolita Polska, 1961.
4. Cao, Q.Y.; Zhao, J.; Zhu, L. The effect of curvature radius of sculptured surface on finish milling tool path selection. *Int J. Adv. Manuf. Technol.* **2017**, *89*, 3349–3357. [CrossRef]
5. Yao, C.; Tan, L.; Yang, P.; Zhang, D. Effects of tool orientation and surface curvature on surface integrity in ball end milling of TC17. *Int. J. Adv. Manuf. Technol.* **2018**, *94*, 1699–1710. [CrossRef]

6. Toh, C.K. Cutter path orientations when high-speed finish milling inclined hardened steel. *Int J. Adv. Manuf. Technol.* **2006**, *27*, 473–480. [CrossRef]
7. Chen, X.; Zhao, J.; Dong, Y.; Han, S.; Li, A.; Wang, D. Effects of inclination angles on geometrical features of machined surface in five-axis milling. *Int. J. Adv. Manuf. Technol.* **2013**, *65*, 1721–1733. [CrossRef]
8. Chen, X.; Zhao, J.; Dong, Y.; Li, A.; Wang, D. Research on the machined surface integrity under combination of various inclination angles in multi-axis ball end milling. *Proc. Inst. Mech. Eng. Part. B J. Eng. Manuf.* **2014**, *228*, 31–50. [CrossRef]
9. Ko, T.J.; Kim, H.S.; Lee, S.S. Selection of the Machining Inclination Angle in High-Speed Ball End Milling. *Int J. Adv. Manuf. Technol.* **2001**, *17*, 163–170. [CrossRef]
10. Kalvoda, T.; Hwang, Y.-R. Impact of various ball cutter tool positions on the surface integrity of low carbon steel. *Mater. Des.* **2009**, *30*, 3360–3366. [CrossRef]
11. Hendriko, H. Mathematical Model for Calculating Scallop Height of Toroidal Cutter in Five-Axis Milling. *J. Eng. Appl. Sci.* **2017**, *12*, 5.
12. Segonds, S.; Seitier, P.; Bordreuil, C.; Bugarin, F.; Rubio, W.; Redonnet, J.-M. An analytical model taking feed rate effect into consideration for scallop height calculation in milling with torus-end cutter. *J. Intell. Manuf.* **2019**, *30*, 1881–1893. [CrossRef]
13. Erdim, H.; Lazoglu, I.; Ozturk, B. Feedrate scheduling strategies for free-form surfaces. *Int. J. Mach. Tools Manuf.* **2006**, *46*, 747–757. [CrossRef]
14. Manav, C.; Bank, H.S.; Lazoglu, I. Intelligent toolpath selection via multi-criteria optimization in complex sculptured surface milling. *J. Intell. Manuf.* **2013**, *24*, 349–355. [CrossRef]
15. Rao, A.; Sarma, R. On local gouging in five-axis sculptured surface machining using flat-end tools. *Comput. Aided Des.* **2000**, *32*, 409–420. [CrossRef]
16. Chen, T.; Li, C.; Wang, H. Tool path generation for five-axis sculptured surface machining with a toroidal cutter. *Int. J. Mach. Mach. Mater.* **2010**, *8*, 372. [CrossRef]
17. Xie, J.; Zou, M.; Cui, X. Effect of curvature distribution feature o complex freeform surface on cnc milling performance. *J. Mech. Eng.* **2009**, *45*, 158–162. [CrossRef] [PubMed]
18. Duan, X.; Yu, S.; Peng, F.; Jiang, G. Study of the Effect of Tool Orientation on Surface Roughness in Five-Axis Milling of 300M Steel. *IOP Conf. Ser. Mater. Sci. Eng.* **2018**, *382*, 022087. [CrossRef]
19. Yang, P.; Yao, C.; Xie, S.; Zhang, D.; Tang, D.X. Effect of Tool Orientation on Surface Integrity During Ball End Milling of Titanium Alloy TC17. *Procedia CIRP* **2016**, *56*, 143–148. [CrossRef]



© 2020 by the author. Licensee MDPI, Basel, Switzerland. This article is an open access article distributed under the terms and conditions of the Creative Commons Attribution (CC BY) license (http://creativecommons.org/licenses/by/4.0/).